

AFWAL-TR-88-3038

ACTIVE CONTROL TECHNIQUE EVALUATION FOR SPACECRAFT (ACES)

Principal Investigator:
Dr. Henry B. Waites, NASA/MSFC
Contributing Authors:
Dr. R. Dennis Irwin
Ms. Victoria Jones
Mrs. Sally Curtis Rice
Dr. Sherman M. Seltzer
Mr. Danny K. Tollison

Control Dynamics Company
600 Boulevard South, Suite 304
Office Park South
Huntsville, Alabama 35802

June 1988

Final Report for Period August 1986 to July 1987

Approved for public release; distribution is unlimited.

20100730 274

FLIGHT DYNAMICS LABORATORY
AIR FORCE WRIGHT AERONAUTICAL LABORATORIES
AIR FORCE SYSTEMS COMMAND
WRIGHT-PATTERSON AIR FORCE BASE, OHIO 45433-6553

NOTICE

When Government drawings, specifications, or other data are used for any purpose other than in connection with a definitely related Government procurement operation, the United States Government thereby incurs no responsibility nor any obligation whatsoever; and the fact that the government may have formulated, furnished, or in any way supplied the said drawings, specifications, or other data, is not to be regarded by implication or otherwise as in any manner licensing the holder or any other person or corporation, or conveying any rights or permission to manufacture use, or sell any patented invention that may in any way be related thereto.

This report has been reviewed by the Office of Public Affairs (ASD/PA) and is releasable to the National Technical Information Service (NTIS). At NTIS, it will be available to the general public, including foreign nations.

This technical report has been reviewed and is approved for publication.

Wayne Yuen

WAYNE YUEN, Project Engineer
Vibration Group

Al M. Janiszewski

AL M. JANISZEWSKI, Maj, USAF
Chief, Vibration Group

FOR THE COMMANDER

Jerome Pearson

JEROME PEARSON
Chief, Structural Dynamics Branch

"If your address has changed, if you wish to be removed from our mailing list, or if the addressee is no longer employed by your organization please notify AFWAL/FDSGC *W-PAFB, OH 45433 to help us maintain a current mailing list".*

Copies of this report should not be returned unless return is required by security considerations, contractual obligations, or notice on a specific document.

UNCLASSIFIED

SECURITY CLASSIFICATION OF THIS PAGE

REPORT DOCUMENTATION PAGE

Form Approved OMB No. 0704-0188

1a. REPORT SECURITY CLASSIFICATION: Unclassified

1b. RESTRICTIVE MARKINGS:

2a. SECURITY CLASSIFICATION AUTHORITY:

2b. DECLASSIFICATION/DOWNGRADING SCHEDULE:

3. DISTRIBUTION/AVAILABILITY OF REPORT: Approved for public release; distribution is unlimited.

4. PERFORMING ORGANIZATION REPORT NUMBER(S):

5. MONITORING ORGANIZATION REPORT NUMBER(S): AFWAL-TR-88-3038

6a. NAME OF PERFORMING ORGANIZATION: Control Dynamics Company

6b. OFFICE SYMBOL (If applicable):

7a. NAME OF MONITORING ORGANIZATION: Flight Dynamics Lab (AFWAL/FDSGC) AF Wright Aeronautical Labs

6c. ADDRESS (City, State, and ZIP Code): 600 Boulevard South, Suite 304 Huntsville, Alabama 35802

7b. ADDRESS (City, State, and ZIP Code): Wright-Patterson AFB OH 45433-6553

8a. NAME OF FUNDING/SPONSORING ORGN.:

8b. OFFICE SYMBOL:

9. PROCUREMENT INSTRUMENT IDENTIFICATION NUMBER: F33615-86-C-3225

8c. ADDRESS (City, State, and ZIP Code):

10. SOURCE OF FUNDING NUMBERS

PROGRAM ELEMENT NO.	PROJECT NO.	TASK NO	WORK UNIT ACCESSION NO.
62201F	2401	04	36

11. TITLE (Include Security Classification): Active Control Technique Evaluation for Spacecraft (ACES)

12. PERSONAL AUTHOR(S): R. D. Irwin; V. L. Jones; S. A. Rice; D. K. Tollison; S. M. Seltzer

13a. TYPE OF REPORT	13b. TIME COVERED	14. DATE OF REPORT (Year, Month, Day)	15. PAGE COUNT
FINAL	FROM 15AUG86 TO 30JUL87	880616	240

16. SUPPLEMENTARY NOTATION:

17. COSATI CODES			18. SUBJECT TERMS (Continue on reverse if necessary and identify by block number)
FIELD	GROUP	SUB-GROUP	
22	02		
14	02		

19. ABSTRACT (Continue on reverse if necessary and identify by block number)

This report describes the Active Control Technique Evaluation for Spacecraft (ACES) Program. Three LSS control design techniques, developed under the Active Control of Space Structures (ACOSS) Program, were compared. The three techniques included Filter Accommodated Model Error Sensitivity Suppression (FAMESS),High Authority Control/Low Authority Control (HAC/LAC), and Positivity. The comparison was accomplished both analytically and experimentally. Each controller was implemented and tested at the NASA/MSFC Large Space Structure Ground Test Facility on the ACES test article. The design and implementation of each controller were performed under identical conditions, The identical control model, sensor/actuator complement, computer, disturbances, and performance criteria were applied to each control design/evaluation. Topics discussed in the report include the test article and laboratory, modeling and dynamic testing, simulation, control design, implementation, test results, and controller evaluation.

20. DISTRIBUTION/AVAILABILITY OF ABSTRACT: ☐ UNCLASSIFIED/UNLIMITED ☐ SAME AS RPT. ☒ DTIC USERS

21. ABSTRACT SECURITY CLASSIFICATION: Unclassified

22a. NAME OF RESPONSIBLE INDIVIDUAL: WAYNE YUEN

22b. TELEPHONE (Include Area Code): (513)255-5236

22c. OFFICE SYMBOL: AFWAL/FDSGC

DD Form 1473, JUN 86 *Previous editions are obsolete.*

SECURITY CLASSIFICATION OF THIS PAGE

UNCLASSIFIED

ACKNOWLEDGEMENTS

The Principal Investigator is Dr. Henry B. Waites (NASA/MSFC), the Program Manager is Dr. George B. Doane III, and the Project Leader is Dr. R. Dennis Irwin. Primary contributors to the accomplishment of the work and the preparation of this report are:

Control System Design:
- Dr. R. Dennis Irwin
- Mr. Danny K. Tollison
- Mr. Jeffery Lucas

Control Software Development:
- Mr. Marlin Williamson
- Dr. R. Dennis Irwin
- Mr. James E. King
- Mr. Jeffery Lucas
- Mr. Danny K. Tollison

Dynamic Modeling:
- Mrs. Sally Curtis Rice

Dynamic Testing:
- Mr. Archie D. Coleman, NASA/MSFC
- Mr. Charles D. Seal, NASA/MSFC
- Ms. Victoria L. Jones
- Mr. Patrick A. Tobbe

Simulation:
- Ms. Victoria L. Jones
- Mr. James E. King

Implementation/Testing:
- Ms. Victoria L. Jones
- Mr. Alan F. Patterson, NASA/MSFC
- Mr. Michael J. Dendy

Facility Modifications:
- Mr. Walter R. McIntosh, NASA/MSFC
- Mr. Lewis J. Cook, NASA/MSFC
- Ms. Victoria L. Jones
- Mr. Alan F. Patterson, NASA/MSFC
- Mr. Ralph R. Kissel, NASA/MSFC

Final Report Preparation:
- Ms. Mozelle F. Roberts

TABLE OF CONTENTS

1.0	Introduction	
	1.1 History	1-1
	1.2 Facility	1-3
	1.3 Intent of ACES Program	1-3
2.0	Problem Statement	2-1
	2.1 Facility Description	2-1
	2.2 Control Problem Definition	2-15
	2.2.1 Testing Procedures	2-15
	2.2.2 Disturbances	2-18
	2.2.3 Sensors and Actuators	2-24
	2.2.4 Performance Measures	2-24
3.0	Model	3-1
	3.1 Approach	3-1
	3.2 Verification by Modal Survey	3-5
	3.3 Verification by Transfer Function Testing	3-5
	3.4 Modification Due to Test Results	3-9
	3.5 Representative Data	3-11
	3.6 Control Model	3-21
4.0	Simulation	4-1
5.0	HAC/LAC	5-1
	5.1 Theory	5-1
	5.1.1 HAC Theory	5-1
	5.1.2 LAC Theory	5-4
	5.1.3 HAC/LAC Combined Control	5-6
	5.1.4 HAC/LAC Applied to ACES	5-7
	5.2 Model Selection and Reduction	5-8
	5.2.1 HAC Model Selection	5-8
	5.2.2 LAC Model Selection	5-14
	5.3 Design Process	5-18
	5.3.1 HAC Design	5-18
	5.3.2 LAC Design	5-27
	5.4 Observation	5-39
	5.5 Test Results	5-39
	5.6 Conclusions	5-50
6.0	Positivity	6-1
	6.1 Theory	6-1
	6.2 Model Selection and Reduction	6-9
	6.3 Design Process	6-9
	6.4 Test Results	6-17
	6.5 Conclusions	6-31

7.0 FAMESS 7-1
7.1 Theory 7-1
7.1.1 Continuous-Time Theory 7-2
7.1.2 Discrete-Time Theory 7-12
7.2 Model Selection and Reduction 7-17
7.2.1 Decentralized Approach 7-17
7.2.2 IMC Design Model 7-18
7.3 Design Process and Simulation Results 7-20
7.3.1 Original IMC Design 7-20
7.3.2 MAST Controller Design Process 7-25
7.3.2.1 Original MAST Controller Design 7-25
7.3.2.2 Final MAST Controller Design 7-33
7.4 Test Results 7-38
7.5 Conclusions 7-64
7.5.1 Observations and Critical Issues 7-64
7.5.2 Recommendations 7-66

8.0 Meetings with Developers of ACES Techniques 8-1

9.0 Conclusions 9-1
9.1 Technique Theory 9-1
9.2 Software 9-2
9.3 Model Fidelity 9-2
9.4 Technique Applicability 9-2
9.5 Design Process Complexity 9-3
9.6 Hardware Limitations 9-3
9.7 Summary 9-4

References R-1

Acronyms R-2

LIST OF FIGURES

Figure 2.1-1	LSS GTF Laboratory	2-2
Figure 2.1-2	Cruciform and Antenna Appendages	2-4
Figure 2.1-3	LSS GTF Experiment	2-5
Figure 2.1-4	Linear Momentum Exchange Devices	2-8
Figure 2.2-1a	Crew and RCS Force Profiles	2-19
Figure 2.2-1b	Crew and RCS Position Profiles	2-20
Figure 2.2-2	Riverside Disturbance PSD	2-21
Figure 2.2-3	Force Position Profiles of Demonstration Disturbance	2-22
Figure 2.2-4	Disturbance Interfaces	2-23
Figure 2.2-5	ACES Configuration Sensor Complement	2-25
Figure 2.2-6	ACES Configuration Actuator Complement	2-26
Figure 3.0-1	Configuration History	3-2
Figure 3.1-1	LSS GTF Experiment	3-3
Figure 3.3-1	Transfer Function Excitation	3-9
Figure 3.5-1A	Experimental Mode, 0.637 Hz	3-13
Figure 3.5-1B	Analytical Mode 4, 0.53 Hz	3-14
Figure 3.5-2A	Experimental Mode, 1.042 Hz	3-15
Figure 3.5-2B	Analytical Mode 14, 1.00 Hz	3-16
Figure 3.5-3A	Experimental Mode, 2.000 Hz	3-17
Figure 3.5-3B	Analytical Mode 23, 2.20 Hz	3-18
Figure 3.5-4	Transfer Function AGS Y to Base Gyro Y	3-19
Figure 3.5-5	Transfer Function AGS Y to LMED-1 X	3-20
Figure 3.6-1	LOS Geometry	3-22
Figure 4.0-1	LSS GTF Experiment	4-2
Figure 4.0-2	LSS Simulation Block Diagram	4-4
Figure 4.0-3	Crew and RCS Force Profiles	4-6
Figure 4.0-4	Riverside Disturbance PSD	4-7
Figure 4.0-5	Simulate Tip, Base Sensors	4-11
Figure 5.2-1a	Frequency Response from Pointing Gimbal Y to LOS X	5-10
Figure 5.2-1b	Frequency Response from Pointing Gimbal X to LOS Y	5-10
Figure 5.2-1c	Frequency Response from Pointing Gimbal X to LOS X	5-11
Figure 5.2-1d	Frequency Response from Pointing Gimbal Y to LOS Y	5-11
Figure 5.2-2a	Frequency Response from Pointing Gimbal Y to LOS X (HAC Model)	5-12
Figure 5.2-2b	Frequency Response from Pointing Gimbal X to LOS Y (HAC Model)	5-12
Figure 5.2-2c	Frequency Response from Pointing Gimbal X to LOS X (HAC Model)	5-13
Figure 5.2-2d	Frequency Response from Pointing Gimbal Y to LOS Y (HAC Model)	5-13
Figure 5.2-3a	Frequency Response from Gimbal X to Faceplate Gyro X	5-15
Figure 5.2-3b	Frequency Response from Gimbal Y to Faceplate Gyro Y	5-15
Figure 5.2-3c	Frequency Response from Gimbal Z to Faceplate Gyro Z	5-16
Figure 5.2-4	Typical LMED Frequency Response from LMED to LMED Accelerometer	5-17
Figure 5.3-1	Discrete HAC Design Model	5-19
Figure 5.3-2	Closed Loop HAC System with Set Point Inputs	5-21

Figure 5.3-3	IMC System Step Responses from Design Plant	5-26
Figure 5.3-4	IMC System Step Responses from Full Order Plant	5-26
Figure 5.3-5a	LAC Controller Faceplate Rate Responses to Step Inputs (X and Y Axes)	5-35
Figure 5.3-5b	LAC Controller Faceplate Rate Response to Step Inputs (Z-Axis)	5-36
Figure 5.3-6a	Open Loop Plant Faceplate Rate Responses to Step Inputs (X and Y Axes)	5-37
Figure 5.3-6b	Open Loop Faceplate Rate Response to Step Inputs (Z-Axis)	5-38
Figure 5.5-1	Open Loop Faceplate Gyro Rate Response due to the RCS Disturbance	5-40
Figure 5.5-2	Closed Loop Faceplate Gyro Response due to the RCS Disturbance	5-40
Figure 5.5-3	Open Loop Detector Response due to the RCS Disturbance	5-41
Figure 5.5-4	Closed Loop Detector Response due to the RCS Disturbance	5-41
Figure 5.5-5	Open Loop Faceplate Gyro Response due to the Crew Motion Disturbance	5-45
Figure 5.5-6	Closed Loop Faceplate Gyro Response due to the Crew Motion Disturbance	5-45
Figure 5.5-7	Open Loop Detector Response due to the Crew Motion Disturbance	5-46
Figure 5.5-8	Closed Loop Detector Response due to the Crew Motion Disturbance	5-46
Figure 5.5-9	Open Loop Detector Response due to the Riverside Disturbance	5-47
Figure 5.5-10	Closed Loop Detector Response due to the Riverside Disturbance	5-47
Figure 5.5-11	Open Loop Faceplate Gyro Response due to the Riverside Disturbance	5-48
Figure 5.5-12	Closed Loop Faceplate Gyro Response due to the Riverside Disturbance	5-48
Figure 5.5-13	Open Loop Faceplate Gyro Response due to the Demonstration Disturbance	5-49
Figure 5.5-14	Closed Loop Faceplate Gyro Response due to the Demonstration Disturbance	5-49
Figure 6.1-1	Block Diagram Representation Used to Illustrate Positivity	6-2
Figure 6.1-2	Operator Embedding Block Diagram	6-5
Figure 6.3-1	Positivity Controller Configuration	6-10
Figure 6.3-2	Transfer Function from LMED1 Force Input to LMED1 Accelerometer Output	6-13
Figure 6.3-3	Compensated LMED Transfer Function	6-13
Figure 6.3-4	Magnitude and Phase of a Representative Plant Characteristic Locus (Compensated)	6-15
Figure 6.3-5	Element of Characteristic Vector	6-15
Figure 6.3-6	Transfer Function from Gimbal Torque X to Faceplate Gyro X	6-18
Figure 6.3-7	Transfer Function from Gimbal Torque Y to Faceplate Gyro Y	6-18
Figure 6.3-8	Frequency Response IMC X	6-19
Figure 6.3-9	Frequency Response IMC Y	6-19

Figure 6.3-10	High Fidelity Simulation Response at Detector due to the RCS Disturbance (Open Loop)	6-20
Figure 6.3-11	High Fidelity Simulation Response at Detector due to the RCS Disturbance (Closed Loop)	6-20
Figure 6.4-1	Open Loop Faceplate Angular Rate Response due to the RCS Disturbance	6-22
Figure 6.4-2	Closed Loop Faceplate Angular Rate Response due to the RCS Disturbance	6-22
Figure 6.4-3	Open Loop Faceplate Angular Rate Response due to the Crew Motion Disturbance	6-23
Figure 6.4-4	Closed Loop Faceplate Angular Rate Response due to the Crew Motion Disturbance	6-23
Figure 6.4-5	Open Loop Detector Response due to the Crew Motion Disturbance	6-24
Figure 6.4-6	Closed Loop Detector Response due to the Crew Motion Disturbance	6-24
Figure 6.4-7	Open Loop Faceplate Angular Rate Response due to the Riverside Disturbance	6-27
Figure 6.4-8	Closed Loop Faceplate Angular Rate Response due to the Riverside Disturbance	6-27
Figure 6.4-9	Open Loop Detector Response due to the Riverside Disturbance	6-28
Figure 6.4-10	Closed Loop Detector Response due to the Riverside Disturbance	6-28
Figure 6.4-11	Open Loop Faceplate Angular Rate Response due to the Demonstration Disturbance	6-29
Figure 6.4-12	Closed Loop Faceplate Angular Rate Response due to the Demonstration Disturbance	6-29
Figure 7.1-1	Design Model for Filter Accommodation Regulator Design	7-8
Figure 7.3-1	Detector Response with Final IMC Controller to Simulated RCS Disturbance	7-24
Figure 7.3-2	Detector Error Response for the Combined IMC/MAST Controller (Original MAST Controller)	7-32
Figure 7.3-3	Detector Error Response for the Combined IMC/MAST Controller (Final MAST Controller)	7-37
Figure 7.4-1	Detector Error Offset Response with FAMESS IMC Controller Only	7-39
Figure 7.4-2	Detector Error Response with FAMESS IMC Controller Only (Gains Reduced by 6dB)	7-40
Figure 7.4-3	Open Loop Response at the Faceplate Gyros due to the Crew Motion Disturbance	7-41
Figure 7.4-4	Open Loop Detector Response due to the Crew Motion Disturbance	7-42
Figure 7.4-5	Closed Loop Faceplate Gyro Response due to the Crew Motion Disturbance	7-44
Figure 7.4-6	Closed Loop Detector Response due to Crew Motion Disturbance	7-45
Figure 7.4-7	Closed Loop Detector Error Response due to Crew Motion Disturbance (Pointing Gimbal Gains Reduced)	7-46
Figure 7.4-8	Open Loop Gyro Response due to the RCS Disturbance	7-47
Figure 7.4-9	Open Loop Detector Response due to the RCS Disturbance	7-48

Figure 7.4-10	Closed Loop Faceplate Gyro Response due to the RCS Disturbance	7-49
Figure 7.4-11	Closed Loop Detector Response due to the RCS Disturbance	7-50
Figure 7.4-12	Open Loop Gyro Response due to the Riverside Disturbance	7-51
Figure 7.4-13	Open Loop Detector Response due to the Riverside Disturbance	7-52
Figure 7.4-14	Closed Loop Gyro Response due to the Riverside Disturbance	7-56
Figure 7.4-15	Closed Loop Detector Response due to the Riverside Disturbance	7-57
Figure 7.4-16	Open Loop Gyro Response due to the Demonstration Disturbance	7-58
Figure 7.4-17	Open Loop Detector Response due to the Demonstration Disturbance	7-59
Figure 7.4-18	Open Loop Laser Beam Detector Presence due to the Demonstration Disturbance	7-60
Figure 7.4-19	Closed Loop Gyro Response due to the Demonstration Disturbance	7-61
Figure 7.4-20	Closed Loop Detector Response due to the Demonstration Disturbance	7-62
Figure 7.4-21	Closed Loop Laser Beam Presence due to the Demonstration Disturbance	7-63

LIST OF TABLES

Table 3.2-1	Summary of Modal Test Results	3-6
Table 3.3-1	Transfer Functions with Unlocked LMEDs	3-7
Table 3.3-2	Transfer Functions with Locked LMEDs	3-8
Table 3.5-1	Tuned Preliminary Model Mode Descriptions	3-9
Table 3.6-1	Final ACES Model	
Table 5.3-1	LAC Controller Design Desired Root Shifts and Weights	5-27
Table 5.3-2	Poles of Continuous LAC Plant Closed with LAC Controller	5-29
Table 5.3-3	Poles of Continuous Full Order Plant Closed with LAC Controller	5-30
Table 5.3-4	Poles of Digital Full Order Plant Closed with LAC Controller and Computational delay	5-32
Table 5.5-1	Summary of Test Results for HAC/LAC Controller	5-44
Table 6.3-1	Product of V(s) A at s = j 2.0	6-16
Table 6.4-1	Summary of Test Results for Positivity Controller	6-30
Table 7.3-1	Final IMC Controller Design Parameters	7-23
Table 7.3-2	Design Parameters for the Original Mast Controller Design (Q_R, R_R)	7-29
Table 7.3-3	Design Parameters for the Original Mast Controller Design (Q_o, R_o)	7-30
Table 7.3-4	Design Parameters for the Original Mast Controller Design (Q_{rs}, Q_{os}, α_c, α_e)	7-31
Table 7.3-5	Attributes of the Combined IMC/MAST Controller	7-31
Table 7.3-6	Design Parameters for the Final Mast Controller Design	7-35
Table 7.3-7	Attributes of the Combined IMC/MAST Controller (Final Mast Design)	7-36
Table 7.4-1	Summary of Test Results for the FAMESS Controller	7-55

1.0 INTRODUCTION

1.1 History.

The ACES Program has its historical roots in the DARPA ACOSS (Active Control of Space Structures) Program begun in 1978 and concluded in 1984. During those six pre-SDI years, the DARPA ACOSS Program was the most instrumental driver in the U. S. to controls techniques that could be applied to Large Space Structures (LSS). This broad multi-million dollar Government program funded efforts primarily from the following members of U. S. industry:

Control Dynamics Co: Dynamic modeling and digital control system design.

Convair/General Dynamics: Development of an LSS controls technique termed FAMESS (Filter Accommodated Model Error Sensitivity Suppression). Built a hardware "plate" to emulate some LSS characteristics.

Draper Lab: Control system development and disturbance characterization.

Honeywell: System Identification & Singular Values

Hughes: Preliminary control system development and electronic damping. Built a hollow cylinder to emulate some LSS characteristics.

Lockheed: Development of an LSS controls technique termed HAC/LAC (High Authority Control / Low Authority Control). Also built and tested a number of structures emulating various characteristics of LSS.

TRW: Development of an LSS controls technique that ensures stability -- often termed "Positivity" after its origins. Built and tested a plate structure to study some LSS characteristics.

In addition, Control Dynamics and Draper furnished DARPA with two experienced controls consultants -- Dr. Sherman M. Seltzer and Mr. Robert Strunce -- to aid the Program Manager (LTC Allan Herzberg) in his technical direction of this multi-faceted program.

In the 1983-84 time frame, it became apparent that three of the so-called modern controls techniques -- FAMESS (General Dynamics), HAC/LAC (Lockheed), and Positivity (TRW) -- would dominate the efforts performed at that time. It also had become evident that a truly high-fidelity LSS hardware test facility was beyond the funding constraints of DARPA and individual company IRAD programs. The Air Force Wright Aeronautical Laboratory (AFWAL) was brought into conference with DARPA and Rome Air Development Center (RADC) to begin a program to investigate the feasibility of implementing some of the ACOSS controls developments. The first phase of this program, termed VCOSS (Vibration Control of Space Structures) - I, was awarded competitively in two parallel contracts to Lockheed and TRW. When VCOSS-I was nearly completed, the caucus was held at Control Dynamics Co. between the ACOSS Program Manager (LTC Herzberg), the VCOSS Program Manager (Mr. Jerome Pearson), the RADC ACOSS Manager (Mr. Richard Carman), the NASA/MSFC LSS Program Manager (Dr. Henry Waites), and Control Dynamics representatives (Dr. Worley and Dr. Seltzer). During that important caucus it was determined that an agreement between NASA and USAF must be reached to develop jointly a program to investigate the realities of controlling LSS's. It was determined to utilize the NASA/MSFC LSS Ground Test Facility as the test-bed. The winner (ultimately TRW) of the VCOSS-II competition would implement their techniques on this test-bed with the assistance of Control Dynamics Co. It also was determined that a larger scale program should be embarked upon to study the most promising LSS controls techniques emerging from national studies underway. This, of course, ultimately led to the present ACES Program.

As an excursion into determining if a practical digital controller could be designed as simply as possible, the ASCOT Program was initiated at a meeting between the U. S. Air Force Weapons Lab (AFWL) at Albuquerque and Control Dynamics in December 1984. This led to a DARPA contract to Control Dynamics Co. to implement the ASCOT (Advanced Structural Control Techniques)Program.

This contract was completed in February 1985 with the development of a digital controller that would be relatively (as compared to the complex ACOSS approaches) easy to implement.

1.2 Facility.

In the early 1980's, NASA's Marshall Space Flight Center began the development of an LSS Ground Test Facility. The three-fold purpose of this facility was (and still is)

- to provide a means for testing, assessing, and verifying dynamics and controls concepts;
- to incorporate LSS pathologies; and
- to be sufficiently versatile so that numerous LSS configurations and/or controls techniques could be incorporated

Largely through the efforts and direction of Dr. Henry Waites of MSFC, this versatile facility has been assembled at a minimum cost to the Government. The evolution of the facility is portrayed graphically in Figure 1.2-1.

1.3 Intent of ACES Program.

The specific intent of the ACES Program is to investigate the implementation of the three primary ACOSS LSS controls techniques: FAMESS, HAC/LAC, and Positivity. Their relative effectiveness as structural vibration suppressors will also be investigated.

2.0 PROBLEM STATEMENT

2.1 Facility Description.

MSFC and Control Dynamics have successfully developed the present LSS GTF, which consists of the LSS SSC Laboratory located in the Test Laboratory, Building 4619 Load Test Annex (LTA). Figure 2.1-1 depicts the basic configuration of the test facility. The subsequent configurations are structurally augmented versions of this basic form, i.e., cruciform and adaptor, antenna and counter weights, and VCOSS II momentum exchangers.

The following subsections provide detailed information on the individual components of the test facility. These components are:

- Test Article
- Computer System
- COSMEC
- Base Excitation Table (BET)
- Augmented Advanced Gimbal System (AGS)
- Kearfott Attitude Reference System (KARS)
- Apollo Telescope Mount (ATM) Rate Gyros
- Accelerometer Packages
- Linear Momentum Exchange Devices (LMEDs)
- Image Motion Compensation (IMC) System

Structure

The basic test article is a deployable, lightweight beam approximately 45 feet in length. The test article is a spare Voyager Astromast built by ASTRO Research, Inc. It was supplied to MSFC by the Jet Propulsion Laboratory (JPL). The Astromast is extremely lightweight (about 5 pounds) and is very lightly damped. It is constructed almost entirely of S-GLASS. It is the flight backup Voyager magnetometer boom.

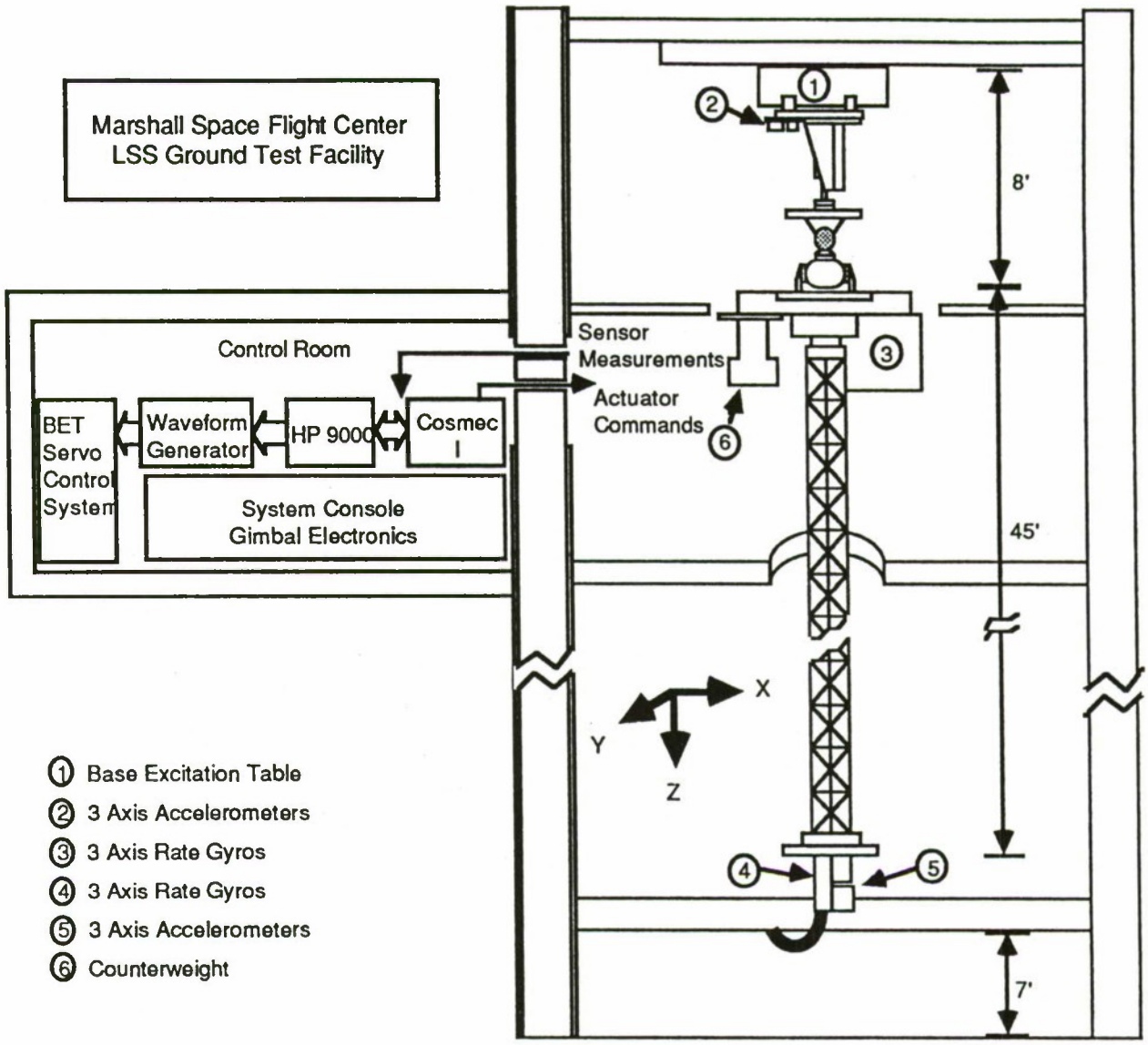


Figure 2.1-1. LSS GTF Laboratory

The Astromast is a symmetric beam which is triangular in cross section. Three longerons form the corners of the beam and extend along its full length unbroken. The cross members, which give the beam its shape, divide the beam into 91 sections each having equal length and mass and similar elastic properties. When fully deployed, the Astromast exhibits a longitudinal twist of approximately 260 degrees.

The test article can be reconfigured from this basic form to any of several different configurations. As an example, a cruciform structure was attached to the tip of the Astromast to elicit additional low frequency modes. The cruciform structure, which is made of aluminum, weighs 8 pounds (Figure 2.1-2). Another structural appendage currently in use is the antenna appendage which is shown in Figure 2.1-2. The ACES configuration (Figure 2.1-3) consists of the antenna and counterweight legs appended to the Astromast tip and the pointing gimbal arms at the Astromast base. The addition of structural appendages creates the "nested" modal frequencies characteristic of LSS.

The precise motion of the BET is obtained by supplying a commanded voltage input to the BET servo control system. The BET movements are monitored by the directional feedback electronic deflection indicators which are fed back to the servo controllers. The servo controllers compare the commanded input voltage to the electronic deflection indicators and automatically adjust the position of the BET. The closed loop controller allows any type of BET movement within the frequency limitations of the hydraulic system.

Disturbance Excitation System

The LSS GTF employs the Base Excitation Table (BET) to excite the system in order to determine the effectiveness of different control methodologies. The disturbance excitation system applies a hydraulic force disturbance to the base of the test structure. Presently, the disturbances represent either an astronaut pushoff, a Reaction Control System (RCS) thruster firing, a sinusoidal, or a Riverside disturbance. The Base Excitation Table (BET) is attached to the building support structure. It provides a means of producing such disturbance inputs. The BET is comprised of a programmable signal generator (deterministic or random noise), dc conditioning amplifiers are used to scale the signal generator while the conditioners are used to condition the electronic deflection indicator monitors for display. The oscillograph records the actual motion of the BET.

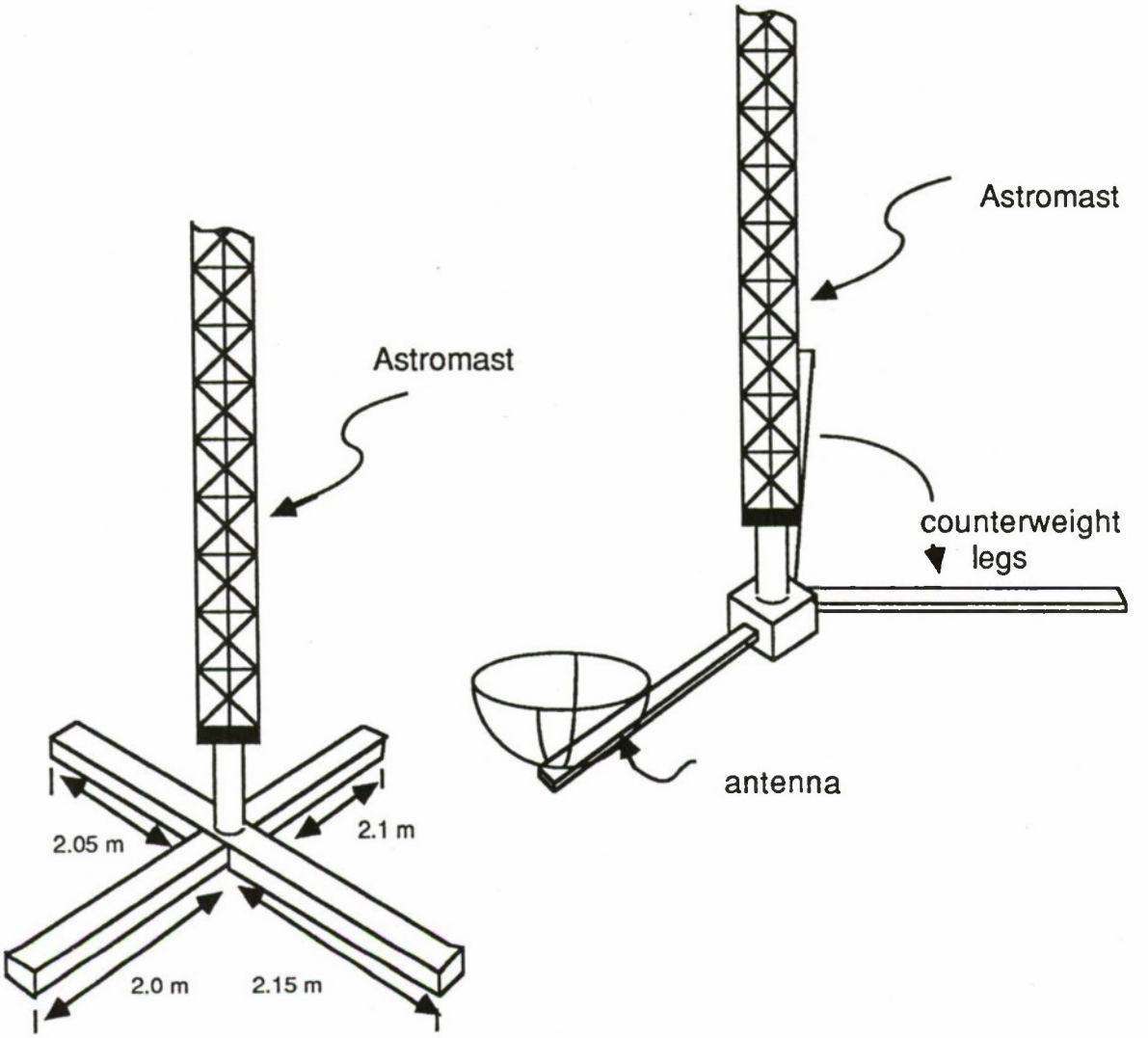


Figure 2.1-2. Cruciform and Antenna Appendages.

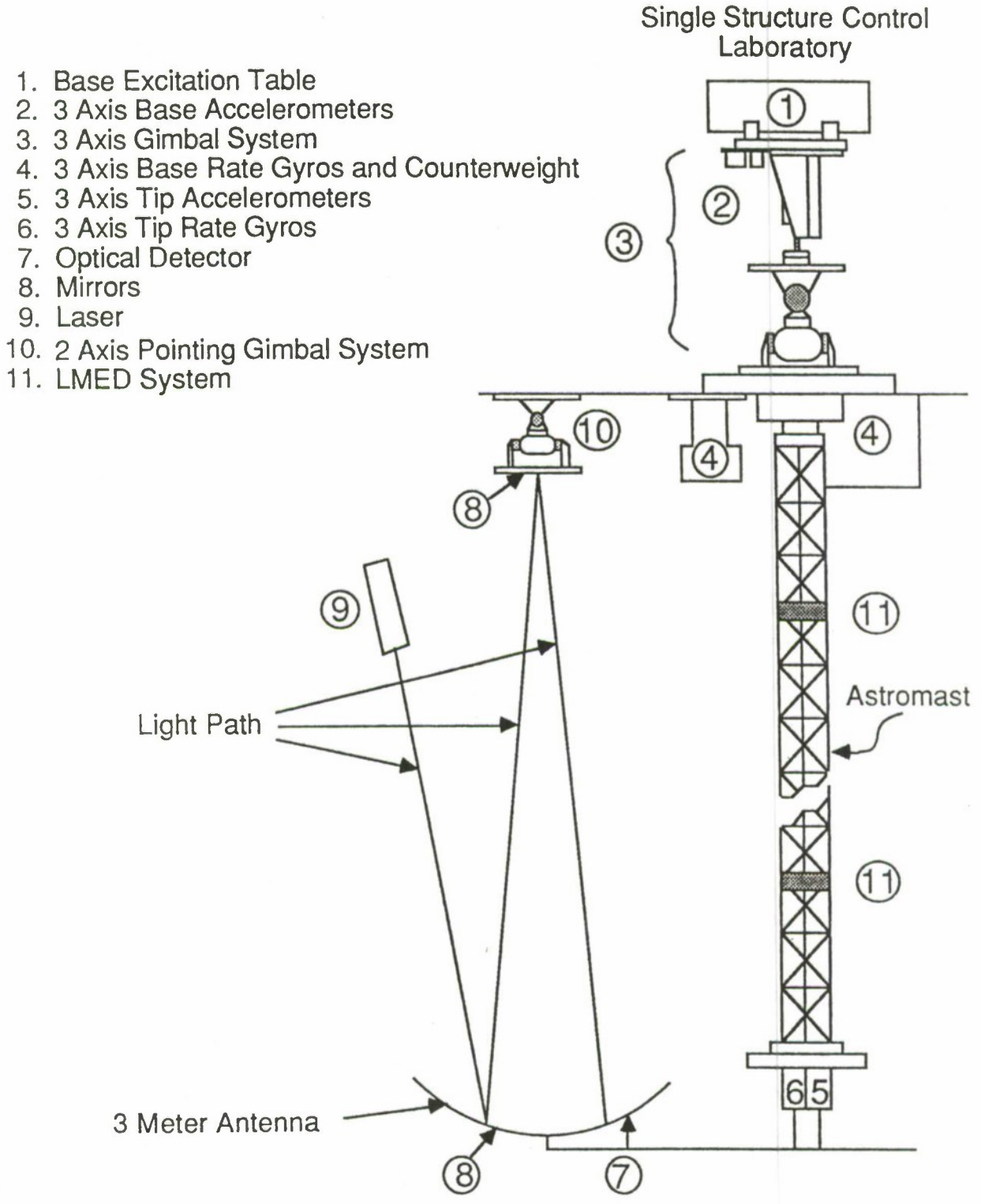


Figure 2.1-3. LSS GTF Experiment (ACES Configuration)

The precise motion of the BET is obtained by supplying a commanded voltage input to the BET servo control system. The BET movements are monitored by the directional feedback electronic deflection indicators which are fed back to the servo controllers. The servo controllers compare the commanded input voltage to the electronic deflection indicators and automatically adjust the position of the BET. The closed loop controller allows any type of BET movement within the frequency limitations of the hydraulic system.

The definition of the disturbance can be implemented either manually or via the waveform generator - HP 9000 interface. The programmable waveform generator (Wavetek) - HP 9000 interface has been established to enable time-efficient and error-free disturbance definition. The interface is time-efficient in terms of time expended to enter the disturbance by the operator and time utilized during the experimental run by both the operator and computer. In addition, the interface minimizes the errors associated with definition of a disturbance and ensures that the same disturbance is applied in repetitive tests. Several BASIC programs are available which "program" a disturbance using the HPIB (HP Interface Bus) interface from the HP 9000 to the Wavetek. The RCS, crew, and Riverside disturbance programs currently reside in the HP 9000. The interface is especially useful for disturbances which are repeatedly applied at the facility.

Actuators

The actuators described in this section include the three-axis gimbal system and the LMED system. The pointing gimbals are described in the IMC section.

Augmented Advanced Gimbal System

The Advanced Gimbal System (AGS) is a precision, two-axis gimbal system designed for high accuracy pointing applications, which has been augmented with a third gimbal in the azimuth. The gimbal system provides torque actuation at the base of the Astromast. The AGS receives commands from the control algorithm implemented on the HP 9000 via the COSMEC data acquisition system in the form of analog inputs over the range of -10 to +10 volts. This saturation represents a current

limit of 27 amps which is built into the AGS servo amplifier as a protective measure. Because the AGS servo amplifier outputs a current which causes an applied torque proportional to the current, the control algorithms used in the COSMEC I must be designed to produce torque command signals.

The AGS gimbal torquers, with the power supply and servo amplifiers used in the SSC laboratory, can generate 37.5 ft-lbs of torque over an angular range of approximately ± 30 degrees. The azimuth torquer is capable of generating 13.8 ft-lbs over an angular range of about ± 5 degrees. It can, however, be set manually to allow the ± 5 degrees of rotation at any position about the 360 degrees of azimuth freedom. This allows the test article to be rotated to any position desired without remounting.

Linear Momentum Exchange Devices (LMEDs)

The LMED provides a collocated sensor/actuator pair which applies a force and measures the resulting acceleration (Figure 2.1-4). Each LMED package contains two LMEDs having orthogonal axes, two accelerometers, and two LVDTs (Linear Variable Displacement Transducers). The two LMED packages are positioned at intermediate points along the ASTROMAST, where these points were selected to maximize the actuation capability. Each LMED package is aligned with the X and Y axes of the laboratory reference frame.

The LMED applies a force to the structure in a linear manner and measures the resulting acceleration at the actuator location. Each LMED consists of a linear permanent magnet motor whose magnet functions as a proof mass. Force is applied to the structure as a reaction against this proof mass. The magnet assembly travels along a single shaft on a pair of linear bearings. The coils of the motor consist of a hollow voice coil which extends inside the magnet assembly from one end. The magnet assembly then moves along the shaft with respect to the fixed coils. The magnet is constrained on each end by a bracket which holds the shaft and a rubber bumper in addition to a light spring which provides a small centering force to the proof mass. A linear accelerometer is mounted in line with the shaft. An LVDT is utilized to measure the position of the proof mass with respect to the LMED assembly.

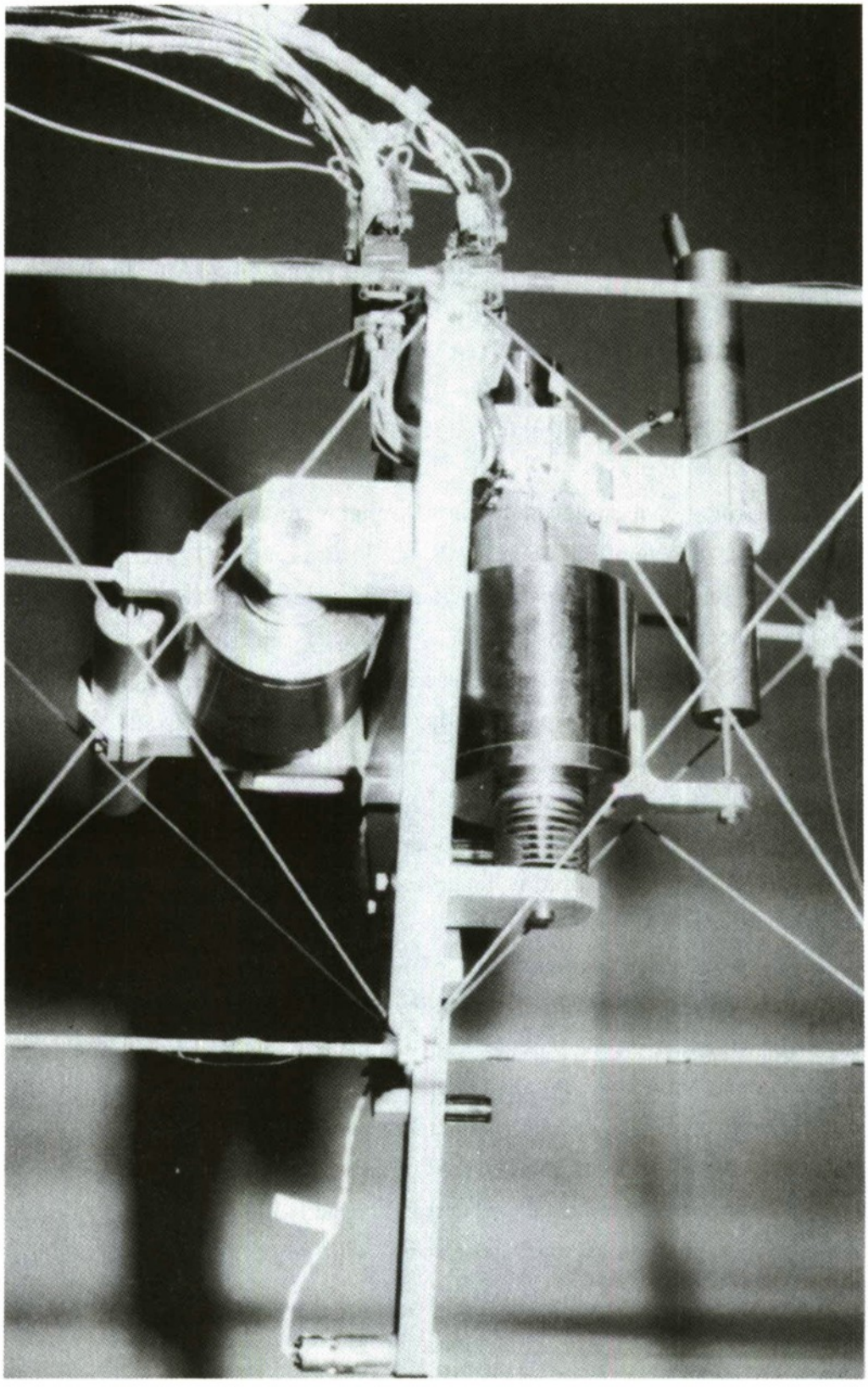


Figure 2.1-4 Linear Momentum Exchange Devices

Sensors

The measurement devices described in this section include the three-axis ratc gyros at the tip and base as well as the three-axis accelerometers at the tip and base.

Kearfott Attitude Reference System (KARS)

The KARS is used as the mast tip rotation sensor in the ground test experiment. The KARS is an attitude measurement system designed for use in the U. S. Army rcmotely pilotcd vehicle. It provides measurement resolution of 13.9 X 10-3 deg/sec in the X and Y axes and 25.0 X 10-3 deg/sec in the Z axis. The dynamic range of the ratc gyro outputs of the KARS is 40 deg/sec in the X and Y axes and 70 deg/sec in the Z axis.

Although the KARS includes accclerometers and outputs measurements of lincar acceleration, the measurements are not used because of inappropriate scaling of the instruments. The KARS outputs three digital health checks, which are monitorcd at thc system console.

The output signals of the KARS are in the form of a synchronous digital pulses which are updated at rates of 50 Hz. One signal, the change in angular position in yaw for instance, requires two channels: one for pulses representing positive rotation and the other for pulses rcpresenting negative rotation. The COSMEC I system accumulates the pulses over a 20-millisecond period to produce measurements of the angular rate and position of the Astromast tip.

Apollo Telescope Mount (ATM) Rate Gyros

The ATM rate gyro packages are mounted on the faceplate of the engineering AGS so that they can measure the rotation of the base of the test article. The ATM rate gyro packages arc designed to measure small angular rates very precisely.

The output signals of the ATM rate gyro packages are ± 45 volts analog and arc handled by the analog to digital converter card of the COSMEC I system where they

are converted to 12-bit binary words. The ATM rate gyro packages require a warmup period of approximately 40 minutes. Each package requires 1.5 amps during warmup and then 1.25 amps after stabilization; both at 28 Vdc.

Accelerometer Packages

The accelerations at the base and tip of the ASTROMAST are measured by the two identical three-axis accelerometer packages. The accelerometer outputs are input to the computer system and the strapdown algorithm derives the velocities and positions at the tip and base from the accelerations.

The accelerometers provide resolution finer than 0.0001 g and a dynamic range of ±3 g with a bandwidth of 25 to 30 Hz. They require approximately 20 minutes for warmup, during which time each package requires 1.2 amps at 28 Vdc. After warmup the power requirement reduces to about 0.9 amp per package. The accelerometer electronics are included on board the instrument package.

The signals from the accelerometers are different from either the KARS or the ATM rate gyros. As in the case of the KARS, two channels are required for each of the degrees of freedom of the accelerometer package, i.e., six channels per accelerometer package. One channel of each pair carries a 2.4-kHz square wave synchronization signal, and the other channel carries the acceleration information. Zero acceleration is represented by a signal identical to that of the synchronization channel, positive acceleration by an increase in frequency, and negative acceleration by a decrease in frequency as compared to the synchronization channel. As in the cases of the other instruments, these signals are monitored by a hardware card in the COSMEC system.

Computer System

The computer system consists of the HP 9000 digital computer interfaced with the COSMEC Input/Output system.

The computer system is responsible for inputing, scaling, processing, plotting, storing, and outputing all the LSS GTF data. The HP 9000, COSMEC, vector processor, and faster HP 9000 CPU (Central Processor Unit) should provide sufficient computing power to satisfy the SSC facility needs for the next few years.

HP 9000 Computer

The HP 9000 performs the control algorithm, data storage, real-time plotting, and the strapdown algorithm (described in the next section). The HP 9000 is a 32-bit machine with an 18-MHz clock rate. It includes an HPIB interface card, two 16-bit parallel interface cards, 512 Kbytes of extra memory, and a floppy disc drive. The benchmark test times for processing the present control and strapdown algorithms, plotting, and data storage are 10 to 13 milliseconds.

COSMEC

The COSMEC is a highly modified AIM-65 microcomputer system used for I/O processing. The primary purposes of the COSMEC are to process the sensor inputs, to provide force and torque commands for the actuators, and to off-load control and sensor data to the computer system. Currently the COSMEC performs these tasks with 25 sensor inputs and nine actuator outputs, while maintaining a 50-Hz sampling rate. The cycle time for COSMEC operation is approximately 5 milliseconds while the HP 9000 uses approximately 13 milliseconds for a total of 18 milliseconds. This provides a margin of 10 percent relative to the 20-millisecond sampling period. The margin will be substantially increased when the new HP CPU is incorporated into the computer system.

The COSMEC has the capability to manage 32 differential analog inputs and 32 8-bit digital inputs. The input time per channel is 20 ms for 16-bit parallel digital information and 80 ms for a 12-bit analog data input. The COSMEC output capability is 16 analog channels, at ±10 V, and 32 8-bit digital channels. The output time per channel is 20 ms for 16-bit parallel digital information, and 40 ms for 12-bit analog data. The RAM size for the COSMEC processor is 32 kbytes, and the clock rate is 2 MHz. The COSMEC also has an alphanumeric keyboard, a single line display, a cassette tape machine for mass storage, and a small printer. The entire system is a relatively portable package.

The COSMEC "reads" various types of sensor output signals via interface cards which are an integral part of the COSMEC system. These cards allow the COSMEC processor to interface in a similar manner (with regard to data format) with the ATM rate gyros, the KARS, the accelerometer packages, the momentum exchange devices, the AGS, the pointing gimbals, and the detector, each of which has a different type input or output signal. The COSMEC also features a real-time clock which is useful in the recording of experimental data.

The hardware cards which interface the COSMEC's processor to the measurement instruments and actuators are individual by their very nature, and some special software is required to handle each card. However, each card makes information available to the HP 9000 as digital words, which is the unifying feature of the system.

Computer Strapdown Algorithm

The purposes of the computer strapdown algorithm are to provide the sensor outputs in a common coordinate frame and to eliminate the effects of the earth.

The strapdown algorithm is necessary to process the sensor outputs to a form acceptable to the controller. The controller inputs must be in a common reference frame and must be expressed in common units. In addition, the sensor instrument biases generated by the earth must be removed. The rate gyro and accelerometer sensors at the ASTROMAST tip and base each measure the constant angular rate and acceleration effects of the earth. The strapdown algorithm also removes any

instrument biases in sensors other than those at the tip and base. The strapdown algorithm, which resides in the HP 9000, performs the following six tasks:

(1) Determines each of the sensor outputs in metric units,
(2) Removes instrument biases from sensor outputs (if necessary),
(3) Derives angular position information and transformation matrices from rate gyro outputs,
(4) Transforms the sensor outputs to a common laboratory reference frame,
(5) Removes the effects of the earth from the base and tip sensors,
(6) Derives rate and position information from base and tip accelerations.

It is important to note that the ACES program did not use the rate and position information (derived from the accelerometers). This information was not used due to the "dynamics" (or recursive) nature of parts of the strapdown algorithm.

IMC System

The Image Motion Compensation (IMC) System consists of a 5-mW laser, two 12-inch mirrors, two pointing gimbals, an analog servo controller, a four-quadrant detector and associated electronics, and two power supplies.

Figure 2.1-3 shows the location of each of the components of the IMC system. The goal of the control design is to position the laser beam in the center of the detector. The detector and pointing gimbals are each positioned on the end of a flexible appendage for the purpose of increasing the difficulty of the control problem. The lack of information about the appendage motion also adds complexity to the controller design (i.e., there is no accelerometer or gyro at the location of the gimbals or the detector).

The IMC system has several modes of operation, which are determined by the user-defined status of two switches on the servo: the open/closed loop status switch and the scan mode on/off status switch. The loop status switch determines which control loop is closed. The closed loop setting refers to the closing of the 50-Hz analog servo controller loop. The open loop setting signifies the closing of the digital control loop through the computer system. The scan mode switch determines the status of the servo scan generator.

The ability to close the digital loop requires the interface between the servo inputs and outputs and the COSMEC outputs and inputs. The detector, presence, and gimbal position measurements are inputs to the computer system. The presence signal is a two level signal which indicates whether the laser is or is not on the detector. The gimbal position is a low resolution measurement supplied by a potentiometer and is not used in the ACES designs. The detector outputs are the X and Y line of sight errors. The output of the computer system commands torques to the pointing gimbals. The bandwidth of the digital loop is obviously much less than that of the analog loop, since the sampling rate of the computer system is only 50 Hz. Development is presently underway to increase the sampling rate of the IMC digital loop to 150 Hz. This sampling rate would allow the digital controller to compete more equally with the analog controller.

The purpose of the scan mode is to reacquire the laser beam on the detector once the beam is off the detector. The scan on status prompts the servo to scan sinusoidally over the operational range of the gimbals until the beam is reacquired on the detector. The scan off status will not reposition the beam on the detector.

2.2 Control Problem Definition.

The control problem to be solved is representative of one which must be solved to design an LSS controller. The structure is very characteristic of an LSS. It is a large structure (45 feet) and is very flexible and lightly damped (0.1 percent). It contains many closely spaced, low frequency modes (43 modes under 8 Hz).

Each control design technique is applied to the same problem and is subject to the same design constraints. Each controller is implemented using an identical test regimen and identical disturbances. Each controller is designed using the same dynamic modal model and the same fixed sensor/actuator complement. The same computer resources were available for each controller. Each test is run under approximately the same environmental conditions. An identical performance criteria is used to evaluate each controller.

The goals of the controller are:

(1) to reduce the Line Of Sight (LOS) error due to the three representative disturbances
(2) to ensure that the controller has a practical size (order)
(3) to attempt to ensure that the controller is tolerant of model limitations

The primary performance criterion is the RMS (Root Mean Square) or RSS (Root Sum Square) LOS error.

2.2.1 Testing Procedures.

An identical testing procedure is applied to each controller. Averaging was utilized for each controller. The controller testing was implemented under the same environmental conditions. The initial and test conditions applied to each controller were identical. Each of these topics is discussed in the following paragraphs.

Averaging

Averaging was used to increase the reliability of the test results. Each controller disturbance test was implemented five times in order to obtain a sampled average that adequately represented the controller performance. The averaging eliminated the problems associated with basing performance on a single test.

Environment

The entire set of testing was conducted under approximately the same environmental conditions. A set of open loop disturbances tests was run immediately prior to the set of closed loop disturbances. This test procedure ensured good comparablity between the open loop and closed loop tests. This test procedure also assured that the same environmental conditions existed for the open and closed loop tests.

The relatively short testing period (3 weeks) yielded generally the same environment surrounding the experiment during the duration of the testing. For example, the testing period of 3 weeks allowed little variation in the ambient temperature range of the test area. In addition, the external lighting conditions were controlled (to the extent possible) to produce approximately the same amount of ambient light at the experimental area. The lighting is particularly important because of its effect on the detector noise level.

In order to eliminate the effects of external disturbances on the experiment, the environment surrounding the test area was examined prior to testing. The first step in the examination was a visual inspection of the test area. The second step consisted of running an open loop test with no disturbance applied to the system in order to observe the system at rest. This test run allowed the operator to examine the ambient noise levels at each of the sensors. The complement of sensing instruments detected any unusual disturbances affecting the system. The test area examination resulted in suspension of tests under three conditions. The first suspension of testing occurred during a thunderstorm. The storm introduced disturbances to the structure through the building, and the disturbances were observed by the detector. The second suspension of testing was caused by the movement of a large overhead crane

in the test area. The crane movements caused a significant disturbance to be observed at all instruments. The third testing suspension was due to the outside door (near the tip of the experiment) being opened during particularly windy days. The wind disturbance was measured by the tip instruments (gyros) and by the detector.

Initial Conditions

An identical set of initial conditions were utilized to test each controller. The initial conditions included the location of the laser, detector, mirrors, BET, gimbals, and LMEDs. The location of the laser on the detector is of critical importance. The detector error signals were utilized to examine the position of the beam on the detector. The laser and mirror alignment devices were adjusted to produce approximately zero error. This alignment procedure was particularly sensitive, and was applied at the beginning of every test. In addition, the positions of the BET, gimbals, pointing gimbals, and LMEDs were examined, and if necessary, these locations were adjusted to ensure each was at its zero position. Both the pointing gimbals and the LMEDs exhibited small stiction characteristics, and as a result, slight deviations from zero were caused. These deviations had insignificant effects on the test setup.

The results of each test are substantially affected by the "stillness" level of the experiment at the initialization of the test. For each test, the initial condition of the experiment was closely examined to ensure an acceptable level of movement. The testing of an LSS experiment was a time consuming procedure due to the extremely low frequencies inherent in an LSS. The lightly damped (1 percent), lowest frequency (0.05 Hz) mode required a settling time of approximately 15 minutes. For each test, the operator waited for the previous disturbance effects to sufficiently die down at the most sensitive instrument (detector) before proceeding to the next test.

Test Conditions

In addition to ensuring the initial conditions were the same for each test, the same test conditions were also employed. Each test was run for 30 seconds, and the disturbance was applied at approximately 3 seconds into the run. The sensor/actuator complement utilized by the controllers was fixed. The computer

system operated at 50 Hz, and 10.5 ms was available for implementation of the control algorithms.

2.2.2 Disturbances.

Three disturbances, representative of a space environment, were chosen to be applied to the structure. These disturbances included the RCS Thruster firing, Crew motion, and the Riverside disturbances. The set of disturbances was composed of three basic types of waveforms (sines, constants, and ramps), and thus, constituted a very general disturbance set.

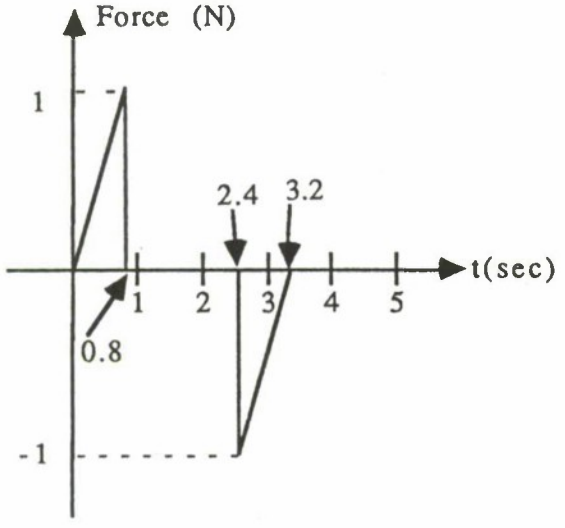
The disturbances are applied to the structure through the Base Excitation Table. These disturbances were assumed to be unmeasurable, since the base accelerometers were defined to be not available for use by the controller. The RCS disturbance was applied in the X direction, and the Crew disturbance was applied in the Y axis. The Riverside disturbance was applied in both the X and Y axes. This combination of disturbances and axes was chosen to test a representative of all possible disturbance/axis combinations.

A multiplication factor was utilized to magnify the disturbance to the largest possible value, while retaining the presence of the beam on the detector. The multiplier was determined during open loop testing. A multiplier of approximately 10 was used for the RCS disturbance, and a factor of six was applied to the Crew disturbance. The Riverside disturbance was implemented with a multiplication factor of five.

Disturbance Implementation

The crew and RCS disturbances are described by the force pulses and ramps shown in Figure 2.2-1a. An orbiter to facility mass ratio of 100 is used before implementing the disturbances. The mass ratio division causes equal accelerations to be applied to the orbiter and the test structure.

Crew Motion Disturbance



RCS Thruster Firing Disturbance

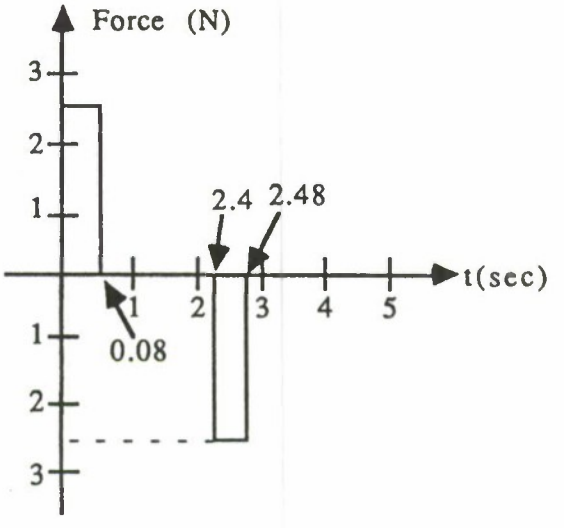


Figure 2.2-1a. Crew and RCS Force Profiles.

The disturbance forces were applied by commanding position profiles to the BET servo system. The position commands corresponding to each disturbance were derived by integrating the force profile and by dividing by the accelerating mass. The mass is approximated by the total mass of the BET, gimbals, base gyros and counterweight, and faceplate. The RCS and Crew position commands are shown in Figure 2.2-1b.

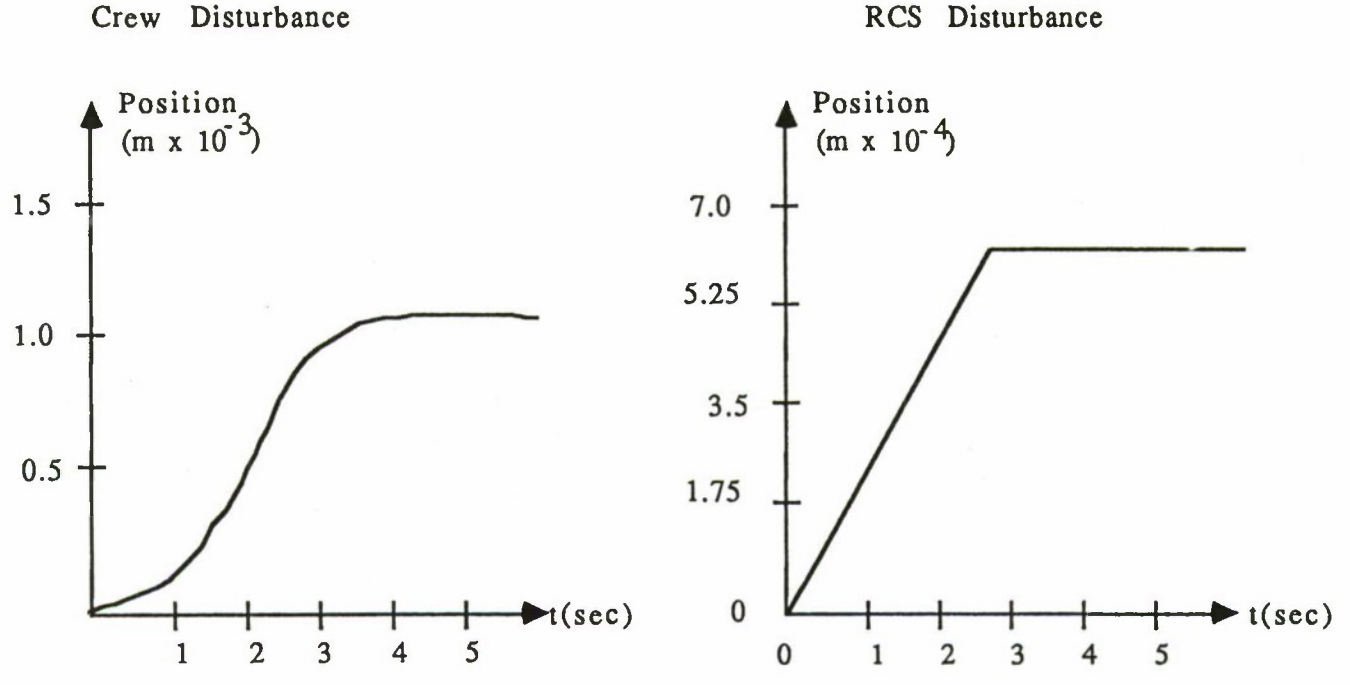


Figure 2.2-1b. Crew and RCS Position Profiles.

The Riverside disturbance is defined by the one sided PSD (Power Spectral Density) in Figure 2.2-2. The Riverside disturbance is implemented as two sinusoids of frequencies 8 and 10 Hz. The high frequency sinusoid (20 Hz) is not physically implementable by the BET, since the BET bandwidth is approximately 10 to 15 Hz. The band limited noise is simulated by the combination of BET system noise and the BET bandwidth.

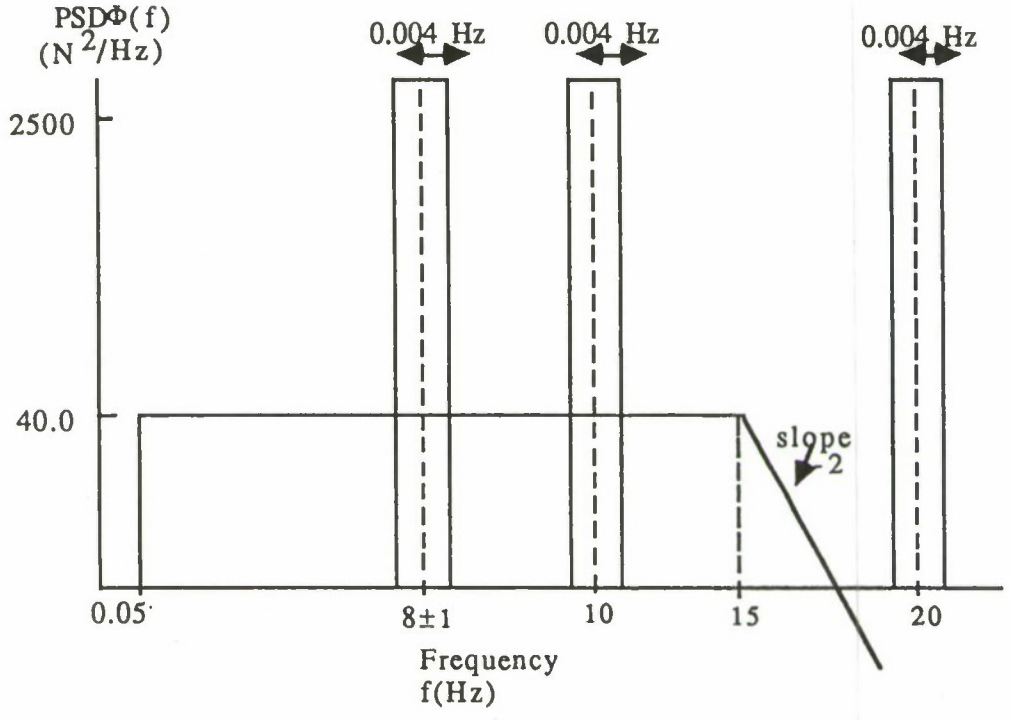


Figure 2.2-2. Riverside Disturbance PSD.

In addition to applying the required disturbances (i.e., Crew, RCS, Riverside) for experimental testing, the demonstration disturbance was also used to evaluate controller performance. The demo disturbance is usually used for purposes of demonstrating the facility and showing the ability of controllers to damp vibrations on LSS. In the ACES testing, the demo disturbance was utilized to evaluate the amount of vibration suppression on the Astromast beam portion of the experiment. The requirement to remain in the linear region of operation was satisfied for the Crew, RCS, and Riverside disturbances. The demo disturbance consists of a larger magnitude excitation, which causes the beam to miss the detector for a significant portion of the test. Thus, the beam does not operate within the linear range of the detector throughout the test. The demo allows the sensors to see a substantial signal, especially the base (i.e. faceplate) gyros. Thus, the beam controller was not limited to operation in a range with a very low SNR (as is the case with the other disturbances). Note that the pointing gimbal controller was turned off during times when the beam is not present on the detector. The detector statistics do not represent the quantity being evaluated for the demo; hence, the more meaningful variables of faceplate gyro settling time and detector percentage hits are provided. It is important to note that the demo disturbance was an additional test which was run to supplement the information with which each controller is evaluated. The results of the demo tests were calculated with only one 80-second test run; thus, the results are not as representative of the average as the test results of the other disturbances.

The demo disturbance consists of sets of force impulses and thus is an RCS-like disturbance. The force and position profiles of the demo disturbance are illustrated in Figure 2.2-3. A mass ratio of 100 is used (as is the case of the RCS disturbance).

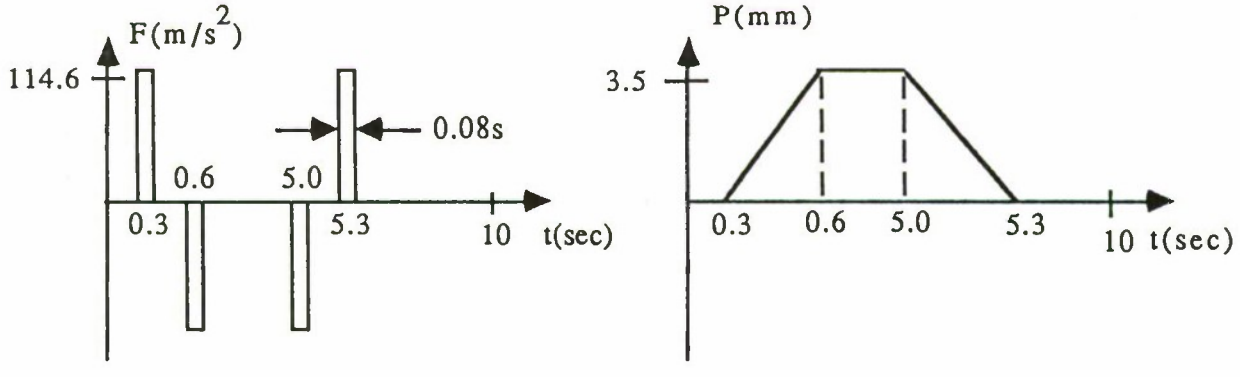


Figure 2.2-3. Force and Position Profiles of Demonstration Disturbance.

The method of disturbance implementation has been vastly improved from manual operator disturbance definition to programmable disturbance definition. The programming method is advantageous in terms of both operator time and run time. It also minimizes the operator error when entering the disturbances, and ensures repeatable error-free disturbance capability.

The HP 9000/Wavetek interface was developed to efficiently program the disturbances prior to run time. Several programs were written on the HP 9000 to "program" the disturbance into Wavetek. The program sets the waveform parameters on the Wavetek, such as time duration, maximum voltage, function definition, and waveform mode. The Crew and RCS programs allow the user the option to choose the axis (X, Y, or X & Y) and an appropriate force multiplier. The Riverside program allows the user to set the magnitude and phase of both the 8-Hz and 10-Hz sinusoids. The disturbance interfaces are described in Figure 2.2-4.

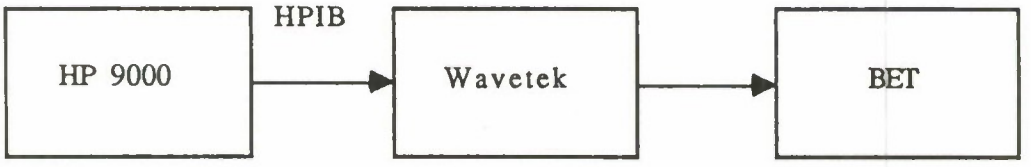


Figure 2.2-4. Disturbance Interfaces.

2.2.3 Sensors and Actuators.

The measurment devices of the ACES configuration are described in Figure 2.2-5. The characteristics of each sensor, such as the bandwidth, resolution, and dynamic range, are delineated. In addition, the purpose and measured quantity of each the sensor is listed. The control sensor complement included the faceplate gyros, LMED accelerometers, tip gyros, tip accelerometers, and the detector.

The actuation devices of the ACES configuration are characterized in Figure 2.2-6. The commanded quantity, bandwidth, and dynamic range of each actuator are described. The control actuators included the gimbals, LMEDs, and IMC pointing gimbals.

2.2.4 Performance Measures.

The performance measures used to evaluate the effectiveness of each controller include the detector response, implementation time, and the base gyro response. The primary performance design criterion was the RMS (Root Mean Square) or RSS (Root Sum Square) LOS error.

Evaluation Statistics

Several evaluation factors were calculated at the conclusion of each run. The mean and SD (Standard Deviation) of the x and y detector errors are computed. The mean and SD of the x, y, and z base angular velocities are also calculated. The sample mean and SD are calculated using the following equations.

$$\text{Mean} = \frac{1}{N}\sum_{i=1}^{N} Xi$$

$$\text{SD} = \sqrt{\left(\sum_{i=1}^{N} X_i^2 - N*\text{Mean}^2\right)/(N-1)}$$

SENSOR	MEASUREMENT	PURPOSE	BANOWIOTH	RESOLUTION	DYNAMIC RANGE
Base 2 axis accelerometers	x,y trans. acc.	excitation meas.	25-30 Hz	<.0001g	± 3g
Faceplate 3 axis gyros	x,y,z rotat. rate	control	N/A	$.5x10^{-3}$deg/sec	± 1 deg/sec
LME01 LVDT	x,y relative pos.	post analysis	200 Hz	N/A*	N/A*
LME02 LVDT	x,y relative pos.	post analysis	200 Hz	N/A*	N/A*
LME01 accelerometers	x,y trans. acc.	control	300 Hz	<5 µg	± 20g
LME02 accelerometers	x,y trans. acc.	control	300 Hz	<5 µg	± 20g
Tip 3 axis gyros	x,y,z rotat. rate	control	N/A	pitch/yaw $13.9x10^{-3}$deg roll $25x10^{-3}$deg/sec	40 deg/sec 70 deg/sec
Tip accelerometers	x,y trans. acc.	control	25-30 Hz	<.0001g	± 3g
Photodetector	x,y trans. LOS error	control	>1K Hz	N/A	N/A

*Not well defined due to linearity problems

Figure 2.2-6. ACES Configuration Actuator Complement

ACES Configuration Actuator Complement

ACTUATOR	COMMANDED QUANTITY	BANDWIDTH	DYNAMIC RANGE
Advanced Gimbal System	Torque, 3 axes at faceplate	>50 Hz >50 Hz	pitch/yaw 37 ft-lbs ± 30 deg roll 13.8 ft-lbs ± 5 deg
LMED1	Force, 2 axes	>100 Hz*	N/A*
LMED2	Force, 2 axes	>100 Hz*	N/A*
IMC Gimbal System	Torque, 2 axes at upper offset arm	>50 Hz**	N/A
Base Excitation Table	Force, 2 axes at base of AGS	N/A*	N/A*

*Not well defined due to linearity problems and the fact that the LMEDs are part of the structure and cannot be considered ideal actuators

**Associated with amplifier characteristics

Figure 2.2-5. ACES Configuration Sensor Complement

Xi = ith measurement

N = number of measurements

In addition, the percentage of hits of the beam on the detector is determined.

Phit = Number of hits/Possible Number of Hits * 100%

The statistics for the individual tests were incorporated into a single statistic for each set of five tests. This amalgamation determines a single performance measure for each statistic. The single statistic is computed from averaging the results of the five tests. In addition, the absolute average of the mean was utilized to prevent any sign difference cancellations. The absolute average mean is a more meaningful quantity than the average mean. Of course, the absolute average of the SD is not required, since the SD is always positive. For example, the absolute average mean for detector x mean is computed by

$$\text{Average Mean} = \frac{1}{5}\sum_{i=1}^{5} |(\text{Mean Det X})_i|.$$

An evaluation table was computed for each disturbance and for each controller tested. The table provides all evaluation factors and the closed loop (CL) improvements generated by the controller. The table includes the open loop (OL) and closed loop absolute average means and standard deviations. The percentage and dB improvement values are calculated to determine the degree of OL to CL improvement. The percentage improvement is calculated by

(OL statistic - CL statistic)/OL statistic * 100%.

For example, given the OL and CL detector x absolute means, the improvement factors are calculated as follows.

Mean Detx (OL) = 6.33e-4 or -63.97 dB
Mean Detx (CL) = 3.28e-5 or -89.68 dB

% improvement = (6.33e-4 - 3.28e-5)/6.33e-4 * 100% = 94.8%
dB improvement = -63.97 dB - (-89.68 dB) = 25.71 dB

Computation time

Another evaluation factor was the implementation time of each controller. The computation time was determined by the timing of repeated controller subroutine calls.

HAC/LAC	4.4 ms
Positivity	4.7 ms
FAMESS	10.2 ms

3.0 DYNAMIC MODEL

Control Dynamics has been directly involved in the modeling process of Large Space Structures (LSS) since the ground test program initiation at Marshall Space Flight Center (MSFC). The basic test article was the 13-meter Astromast (a spare Voyager Magnetometer Boom). It has since evolved through several configurations. Figure 3.0-1 depicts this evolution to the current ACES configuration. Analytical models have been developed for each configuration; good correlation exists between the analytical frequencies and modeshapes and the corresponding experimental values. The model frequencies for the ACES configuration compare well with the experimental frequencies. The analytical modeshapes follow the experimental shapes fairly well. Control Dynamics feels that the model is a valid tool and that it provides a good basis for control design

3.1 Approach.

The ACES configuration was developed through the evolution of the LSS ground test facility. Figure 3.1-1 depicts the ACES configuration in detail. The configuration was modeled using a finite element approach. The modeling of each component is discussed in this section.

The main structural component is the Astromast. It has been modeled as a series of five consistent beam elements totalling 13 meters in length and 2.27 kilograms in mass. All five elements have the same material and section properties, although the length parameters do differ from element to element. The areas, inertias, and the mass density were calculated based upon the structure itself. The moduli of elasticity and rigidity were refined to accurately reflect the stiffness characteristics by utilizing the results of the modal testing of the cantilevered Astromast. The cantilevered model yielded frequencies within 10 percent of experimental frequencies, and the modeshapes were all in agreement. This agreement established the baseline for the Astromast model for use in future configurations. Gravity has been built into all model components through geometric stiffness. This gravity "model" adds terms to the stiffness matrix based upon the applied load. However, as different loads were applied to the tip of the Astromast, it was shown that the beam bending stiffness changed with the load beyond those effects due to gravity. The

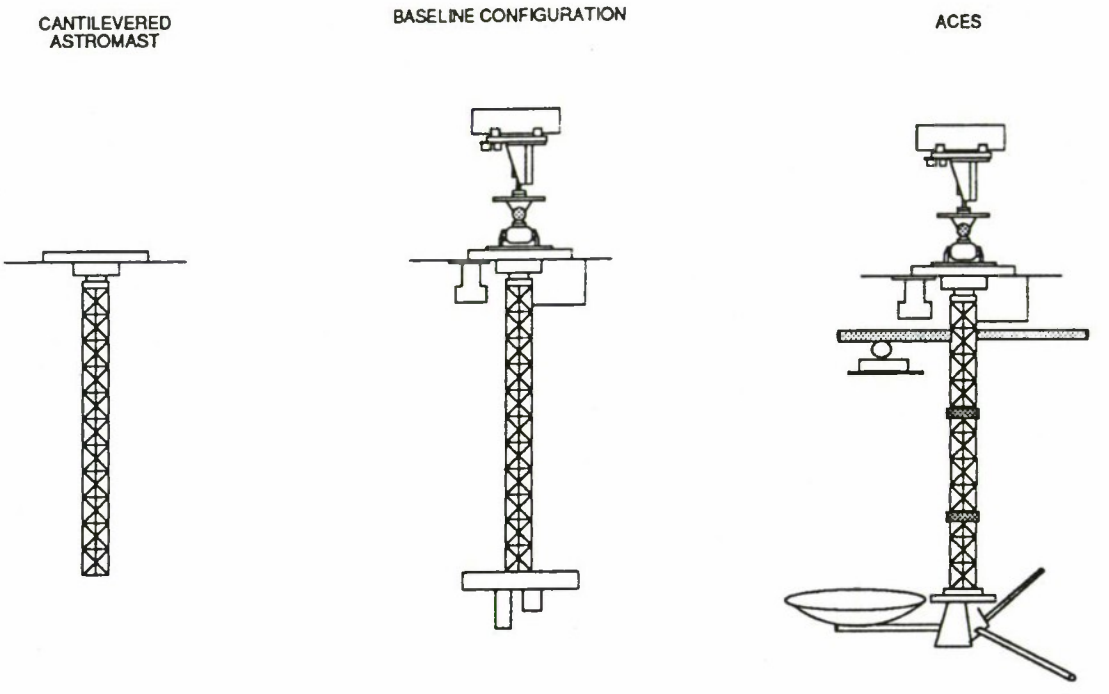


Figure 3.0-1 Configuration History

1. Base Excitation Table
2. 3 Axis Base Accelerometers
3. 3 Axis Gimbal System
4. 3 Axis Base Rate Gyros and Counterweight
5. 3 Axis Tip Accelerometers
6. 3 Axis Tip Rate Gyros
7. Optical Detector
8. Mirrors
9. Laser
10. 2 Axis Pointing Gimbal System
11. LMED System

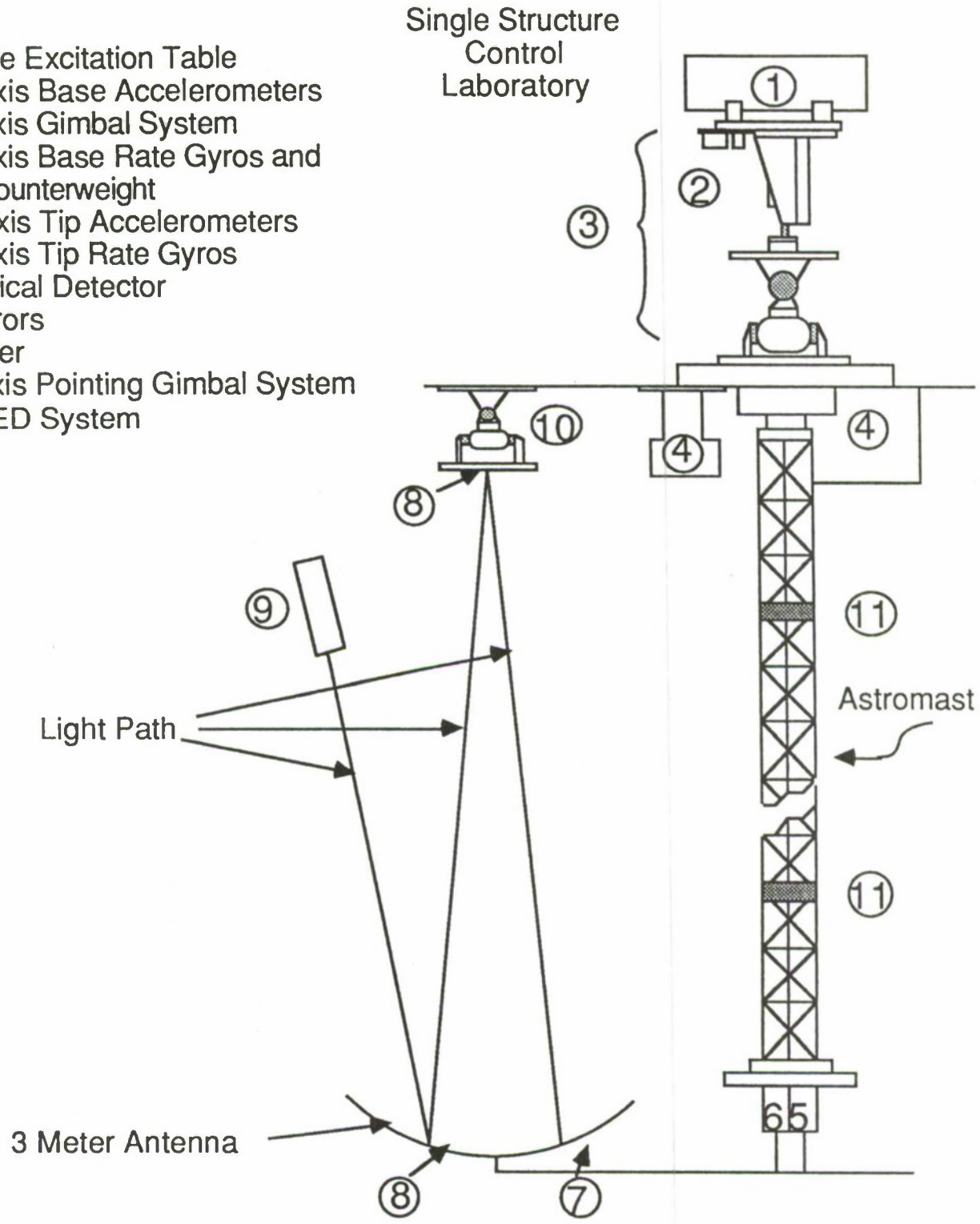


Figure 3.1-1. LSS GTF Experiment (ACES Configuration)

modified stiffness may be partially explained from the observation that as the load is increased, the Astromast joints lose their slack thereby changing the beam had significant displacements and which were aligned with the correct reference.

The baseline configuration was developed through addition of sensors and actuators to the cantilevered configuration. The following equipment was introduced: the Base Excitation Table (BET) providing translation in the X and Y directions, the augmented Advanced Gimbal System (AGS) providing rotation about all three axes, the BET accelerometers, faceplate rate gyros, tip gyros, and tip accelerometers providing measurements. The instrument characteristics used for dynamic modeling purposes are the mass and calculated rotational inertia values. The results of the baseline model generated frequencies and modeshapes comparable to the experimental values up to 10 Hz.

The preliminary ACES model was the next pertinent step in the model evolution. Additional hardware fixtures were incorporated into the baseline configuration to produce the ACES configuration: the antenna structure with associated joints, counterbalance 'legs,' and weights; the attachment bar between the antenna structure and tip instrument package; and the fixtures and counterbalances for the pointing gimbals. The preliminary model emulates the modal test configuration. During modal testing the BET and roll gimbal were turned off, the Linear Momentum Exchange Device (LMED) pairs were attached to the mast with the proof masses locked down, and hardware components were added to resemble the pointing gimbals, mirrors, and detector. The IMC system components had not been constructed at the time of the testing. For modeling purposes, it had been originally decided to eliminate the degrees of freedom for the BET and roll gimbal for the turned off condition. The control model uses the values for the actual equipment and the DOFs previously locked down in the preliminary model are freed. The unlocked LMEDs also have an effective translational stiffness between the proof mass and the Astromast which produced a 1.2-Hz mode. Since the model is linear, such things as damping and limiters are not included. These nonlinearities are accounted for in the in-house simulation.

Before the LMEDs were attached, an analysis was performed to determine a best set of locations for them on the Astromast. "Best" was defined as those locations which had significant displacements and which were aligned with the correct reference frame. From this analysis, the LMEDs are located 6.43 meters from the top and 11.43 meters from the top.

The model of the antenna was initially built up in great detail as a separate entity from the ACES models. The antenna model was considered too large to link with the remaining structural model, and a Guyan Reduction process was employed to decrease the size of the antenna model to a manageable size. The reduced mass and stiffness matrices were then incorporated into the system mass and stiffness matrices.

3.2 Verification by Modal Survey.

MSFC has conducted extensive modal tests on the preliminary ACES configuration to obtain a reliable set of test data. Single and multi-point random techniques were used to obtain the modal data. The modal data were stored and manipulated on a GenRad 2515 Structural Dynamics Analyzer, which calculated the frequencies, modeshapes, and damping values. From these tests, the frequencies and modeshape descriptions given in Table 3.2-1 were obtained. For a detailed report on the modal testing, contact ET53 at MSFC and reference report number TCP DEV-ET86-040.

3.3 Verification by Transfer Function Testing.

A second means of verifying the model was through the use of transfer function tests performed by Control Dynamics personnel. Dummy masses were still on the structure representing the pointing gimbals, mirrors, and detector. These tests had the roll gimbal operational and were performed both with and without locked LMEDS.

Most control actuator and sensor locations were utilized in the transfer function tests. Tables 3.3-1 and 3.3-2 list the possible excitation and response locations. The blocks which do not contain an 'X' had a minimal response for the associated input-output combination. The transfer functions for the boxes with an 'X' were saved on

Table 3.2-1
SUMMARY OF MODAL TEST RESULTS

TEST NO.	FREQUENCY(HZ)	DAMPING (%)	DESCRIPTION
TSS-002	0.637	1.13	2nd Bnd Y
	0.752	1.07	2nd Bnd X
	0.826	1.03	3rd Bnd Y
	1.04	0.65	3rd Bnd X
	1.405	0.68	Antenna Torsion, Upper Balance Arms Bnd
	1.702	0.36	Antenna Rocking About X, Lower Balance Arms Bnd X, Mast Bnd Y
	1.752	0.41	Antenna Torsion, and Rocking About Y, Mast Bnd X, Upper Balance Arms Bnd X, Power Balance Arms B Z
	1.92	0.51	Antenna Torsion and Rocking About X, Mast Bnd Y, Upper Balance Arms Bnd XZ, Lower Balance Arms Bnd XZ
TSS-003	2.0	0.37	Antenna Torsion, Mast Bnd XY, Upper Balance Arms Bnd X, Lower Balance Arms BndX
	2.356	0.76	Antenna Torsion, Mast Bnd XY, Upper Balance Arms Bnd X, Lower Balance Arms Bnd X) Same Motion A 2.0Hz Mode but out of Phase)
	2.494	0.63	Mast Bnd Y, Upper Balance Arms and AGS Plate Bnd Z, Antenna Rolling About Y
TSS-004	4.196	0.54	Mast Bnd XY (3rd Bnd), Antenna Rolling About Y, Lower Balance Arms Bnd Z
	7.023	1.44	AGS Adapter Plate and Upper Balance Arms Torsion
	7.261	0.91	Mast Bnd XY
TSS-005	1.36	0.2	Lower Balance Arms Bnd 2
	1.47	0.56	Antenna Torsion

NOTE: Three system modes, a first bending pair at approximately 0.14Hz and a first torsion at approximately 0.03Hz were observed in the FRF's but mode shapes were not obtainable.

TABLE 3.3-1 TRANSFER FUNCTIONS WITH UNLOCKED LMEDS

OUTPUT \ INPUT	BET x	BET y	AGS x	AGS y	ROLL z	LMED1 x	LMED1 y	LMED2 x	LMED2 y
GIMBAL ARM z									
GIMBAL ARM y									
GIMBAL ARM x									
ANTENNA BASE z									
ANTENNA BASE y									
ANTENNA BASE x									
TIP GYRO z									
TIP GYRO y			X	X			X	X	X
TIP GYRO x			X	X			X	X	X
TIP ACCEL z									
TIP ACCEL y									
TIP ACCEL x									
LMED2 y			X				X		X
LMED2 x			X	X				X	
LMED1 y			X	X					
LMED1 x			X	X		X		X	
BASE GYRO z					X				
BASE GYRO y			X	X		X			
BASE GYRO x			X	X			X		
BASE ACCEL y									
BASE ACCEL x									

TABLE3.3-2 TRANSFER FUNCTIONS WITH LOCKED LMEDS

OUTPUT \ INPUT	BET x	BET y	AGS x	AGS y	ROLL z
GIMBAL ARM z			x	x	
GIMBAL ARM y			x		
GIMBAL ARM x				x	
ANTENNA BASE z					
ANTENNA BASE y			x		
ANTENNA BASE x				x	
TIP GYRO z					
TIP GYRO y					
TIP GYRO x			x	x	
TIP ACCEL z			x	x	
TIP ACCEL y					
TIP ACCEL x					
LMED2 y			x	x	
LMED2 x			x	x	
LMED1 y				x	
LMED1 x			x	x	
BASE GYRO z					
BASE GYRO y			x	x	
BASE GYRO x			x	x	
BASE ACCEL y					
BASE ACCEL x					

tape, plotted, and used in comparison with those transfer functions from the analytical model.

The transfer functions were generated utilizing the control actuators and sensors. An input excitation was applied to the structure through each control actuator. Each output response was measured by each of the control sensors. The actuator input signal and the sensor output signal were transmitted to the HP 5423 structural analyzer to calculate the transfer function.

Judicious selection of the input excitation improves the accuracy of the transfer function over the frequency range of interest. The coherence function was examined to determine the reliability of each transfer function. Figure 3.3-1 illustrates the input excitation utilized to generate the transfer functions. The protracted pulse is of length 5 times the sample period, where the length is chosen such that its frequency response zero does not interfere with the transfer function. The amplitude of the input is maximized; this maximization is limited by sensor saturation. Ten averages were collected for each final transfer function. An 8-Hz bandwidth was used since it accommodated the significant modes and corresponded to a sampling time of close to 20 msec. An exponential window was applied to force the response to zero at the final time.

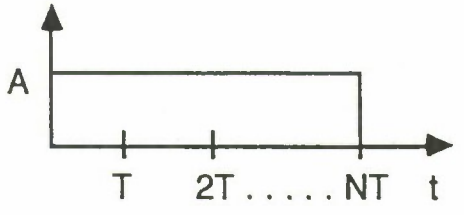


Figure 3.3-1 Transfer Function Excitation

3.4 Modifications Due to Test Results.

In comparing the preliminary analytical model with the modal test data, we saw that the antenna model contributed a significant number of frequencies in the 0 to 8-Hz range. These modes were not measured in the modal tests. We decided to simplify the antenna model to eliminate many modes localized to the antenna and to become more consistent with the actual structure. The antenna modes still did not

correspond well with the measured antenna behavior. Since these modes do not effect any sensor/actuator behavior, we decided that it was more important to tune the behavior of the Astromast, 'arms,' and 'legs' than the local antenna behavior.

During the transfer function testing it became apparent that the roll gimbal and the BET could move even when turned off. At this point it was decided to unlock the DOFs corresponding to the X and Y translations of the BET and the rotation about Z of the roll gimbal. For modeling purposes only, stiffness values were implemented to model the break-away friction for the equipment. This was done in an attempt to better match the modal test conditions. Stiffness values were chosen so that key modal frequencies matched the corresponding experimental frequencies. In the control model these DOFs are freed (i.e., no associated stiffness values) to agree with the ACES configuration which has the equipment fully operational.

The problems matching the measured torsional modes with the preliminary model were alleviated through the utilization of the torsional spring. Freeing the roll gimbal DOF and inserting the torsional spring helped immensely, as the modes could not occur with the roll gimbal locked. This allowed the shapes to match, but the frequencies were still not within an allowable range. The E (Young's Modulus) value for the 'arms' was then adjusted for stiffness purposes. It could not be adjusted dramatically as the 'arm' behavior for the bending modes would be affected. It was adjusted in coordination with the torsional spring and the Astromast G (torsional modulus) value to match the torsional frequencies and to avoid disrupting the bending frequencies.

The modal testing and transfer function testing revealed a great deal more cross coupling than seen in the model. Actual location measurements were then made on the structure and it was observed that the components were not lined up as assumed. When the misalignments were added to the model, the coupling did increase but the magnitude of the cross coupling was still below the measured behavior.

3.5 Representative Data.

Based upon the results of both the modal and transfer function testing, a tuned model was developed incorporating the updates previously discussed. The results from this tuned model and its comparison with the modal data are given in Table 3.5-1. The analytical frequencies are all within 20 percent of the experimental frequencies except for the first torsional mode. Numerical examination of this frequency reveals that it is only in error by 0.04 Hz. In the testing, this mode could be seen but is difficult to measure due to its extremely low frequency. The transfer function testing located this mode at 0.045 Hz, whereas the modal testing determined the torsional mode at 0.03 Hz.

Two modes were obtained in the modal testing which do not appear in the model. They were both obtained during the torsion testing, which had its own difficulties. As neither mode appeared in the transfer function tests and these modes did not appear from the modal testing to have a great deal of action at the sensor/actuator complement, it was decided to not try and force the model to yield these behaviors.

The remaining experimental and analytical modeshapes agree well. The basic characteristics which appeared in the modal testing appeared in the model. See Figures 3.5-1 through 3.5-3 for example modeshape comparisons. Since the model is linear and the structure is not, discrepancies are bound to occur. These differences involve 'arm' motion and some 'leg' motion. Some of the nonlinearities include non-rigid joint connections, friction, and damping.

While the modal testing helped in matching frequencies and modeshapes, the transfer function testing helped in matching the system coupling and mode dominance. Because the torsional measurements were limited by equipment and measurement locations, the transfer function results are only useful for transverse vibrations. Figures 3.5-4 and 3.5-5 depict some of the comparisons between the measured and modeled behavior. The analytical transfer functions basically have the same behavior as the experimental ones. Discrepancies between the two sets do exist however, and are listed for each transfer function. The major differences involve the magnitudes of the peaks; the model peaks are generally lower than their

Table 3.5-1 Tuned Preliminary Model Mode Descriptions

Model Frequency (Hz)	Experimental Freq. (Hz)	Percent Error	Description
.07	0.03	-133%	Torsion
.14	0.14	-	X-Bending
.14	0.14	-	Y-Bending
.53	0.637	17%	Y-Bending
.59			X + Antenna
.59			Y + Antenna
.60			Torsion + Antenna
.70			X + Legs + Ant.
.71			X + Legs + Ant.
.73	0.752	3%	X + Ant. + Arms
.95			Antenna
.95			Antenna
.95	0.826	-15%	Y + Legs + Ant.
1.00	1.042	4%	X + Legs + Ant. + Arms
1.20	1.405	15%	Torsion + Arms
1.34			Arms
	1.357		Legs
	1.466		Antenna Torsion
1.70	1.702	-	X + Y + Legs
1.73	1.752	1%	X + Y + Legs + Arms
1.84			Y + Legs + Ant.
1.92			Antenna
1.92			Antenna
2.12	1.920	-10%	Y + Antenna
2.20	2.000	-10%	X + Arms
2.53	2.356	-7%	X + Legs + Ant.
2.55	2.494	-2%	Y + Ant. + Arms
3.31			Antenna
3.31			Antenna
3.80			Torsion
4.29	4.196	-2%	X + Legs + Ant.
4.71			Antenna
4.71			Antenna
5.35			Antenna
5.45			Y + Legs + Ant.
6.73			Y + Z + Legs
6.87	7.023	2%	Torsion + Arms
6.97	7.261	4%	Torsion

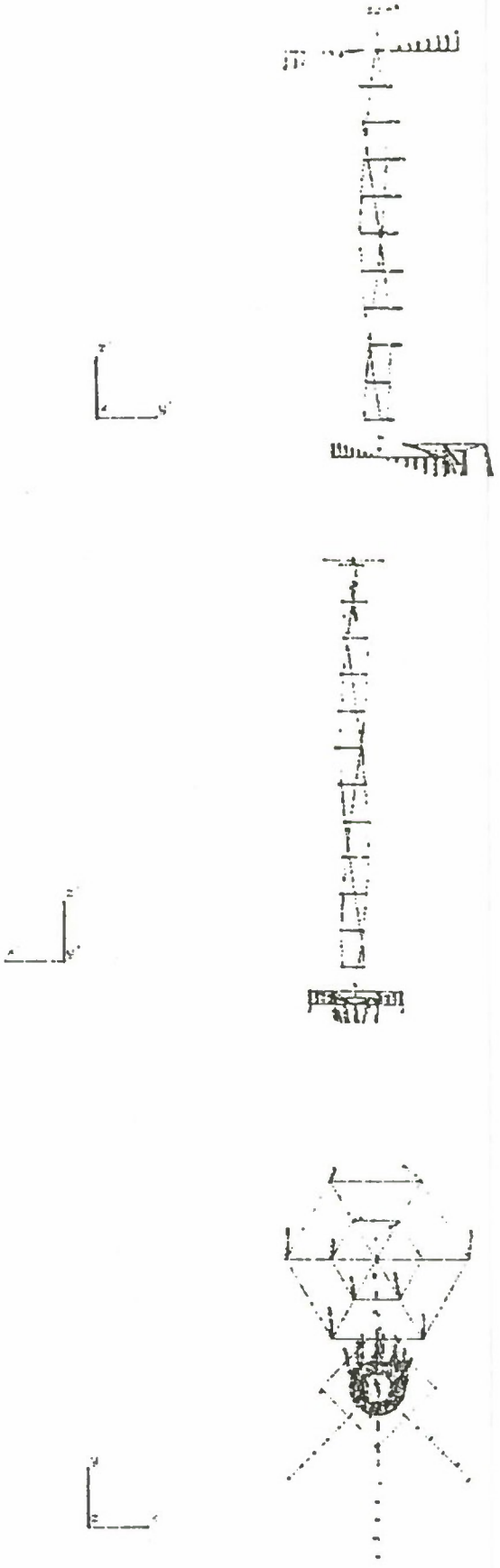


Figure 3.5-1A Experimental Mode, 0.637 Hz

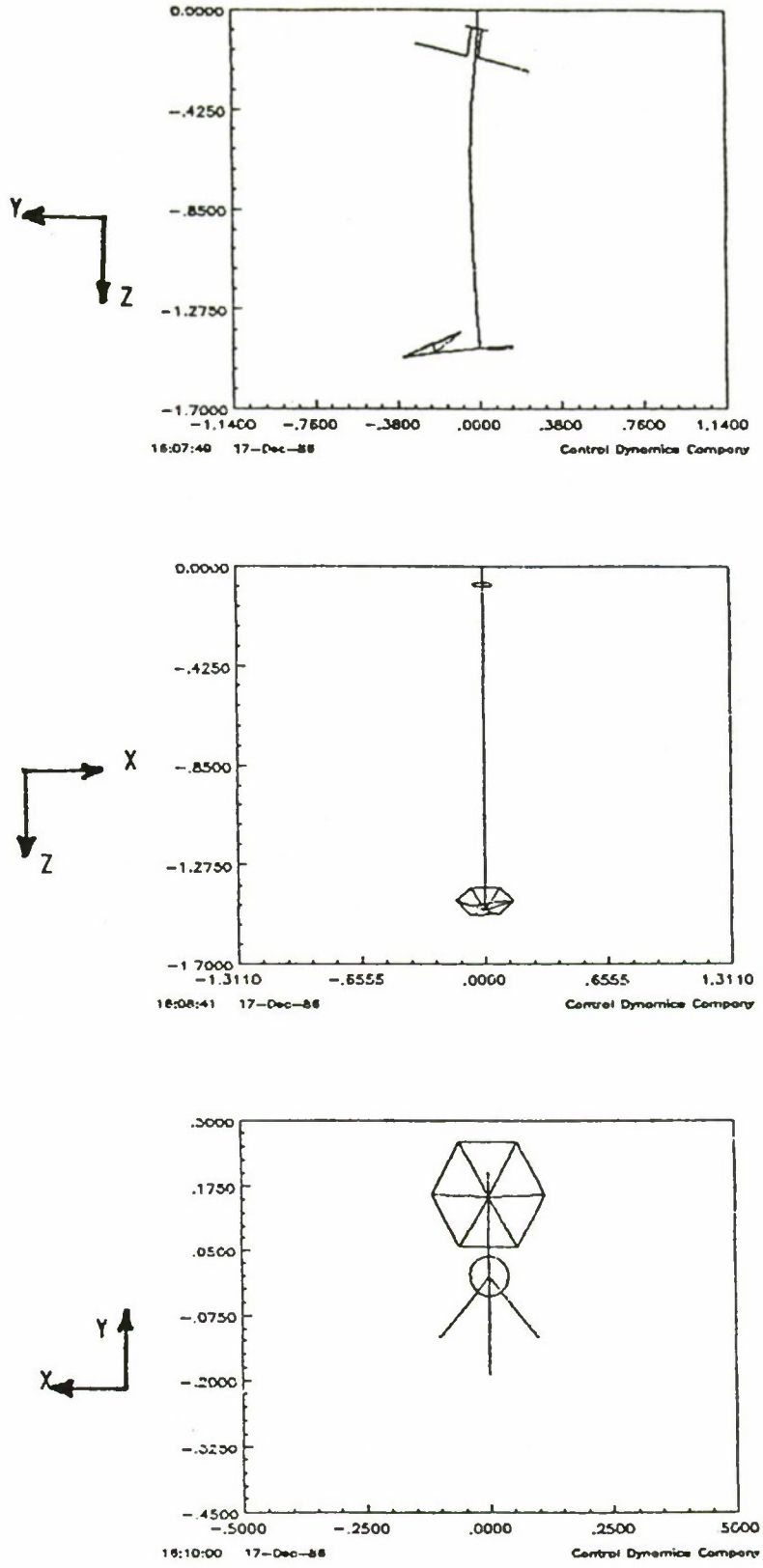


Figure 3.5-1B Analytical Mode 4, 0.53 Hz

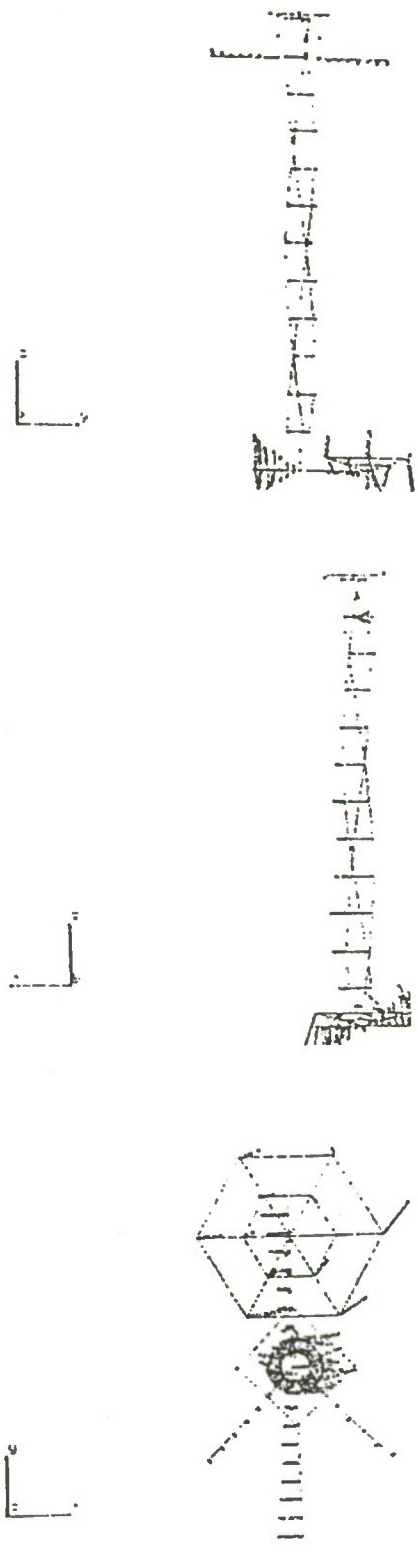
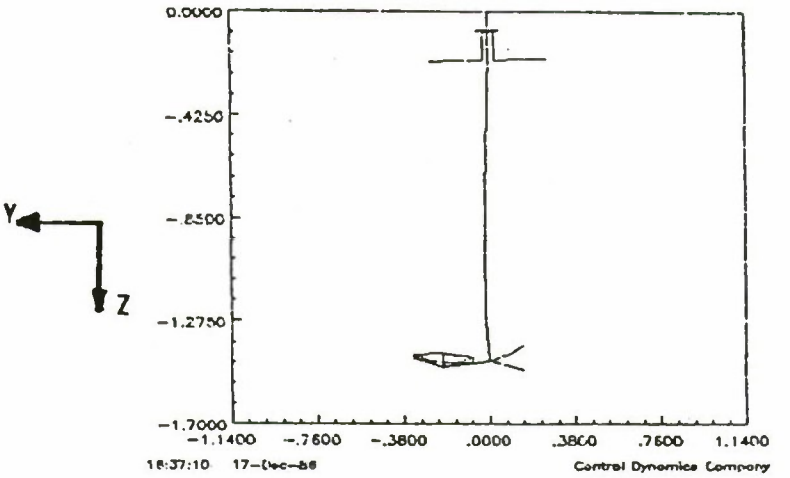
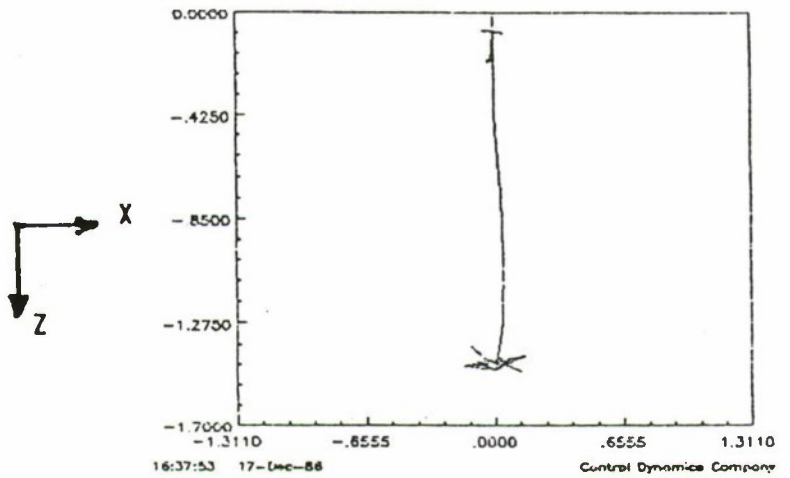


Figure 3.5-2A Experimental Mode, 1.042 Hz





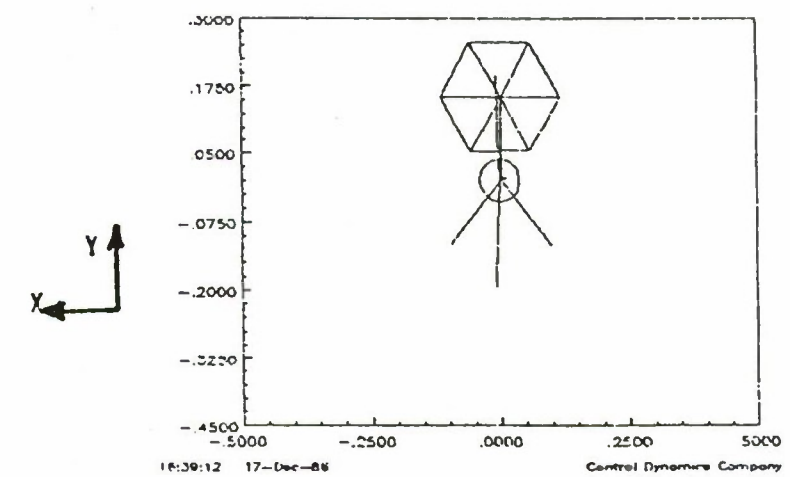


Figure 3.5-2B Analytical Mode 14, 1.00 Hz

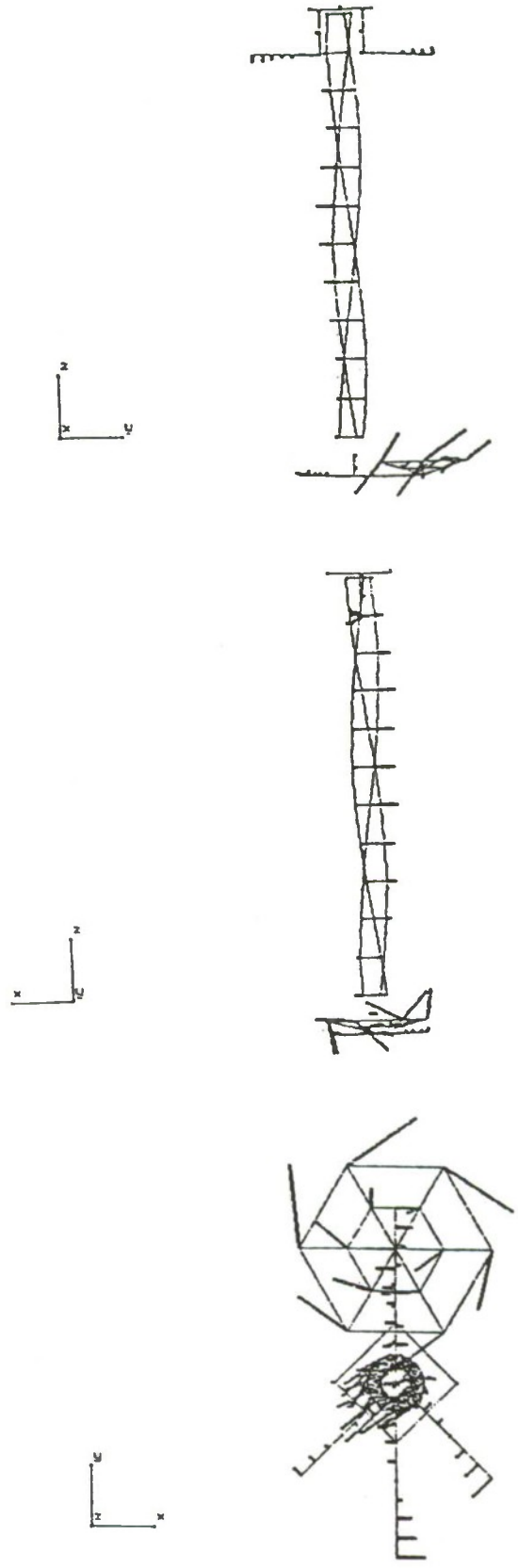
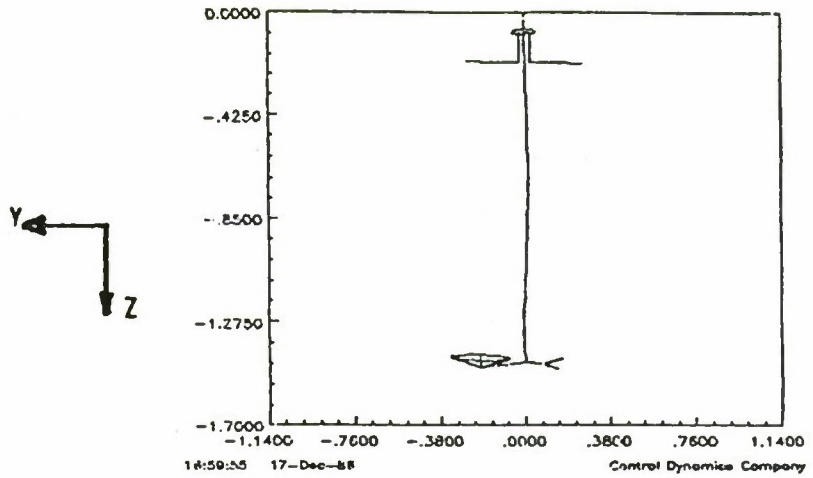
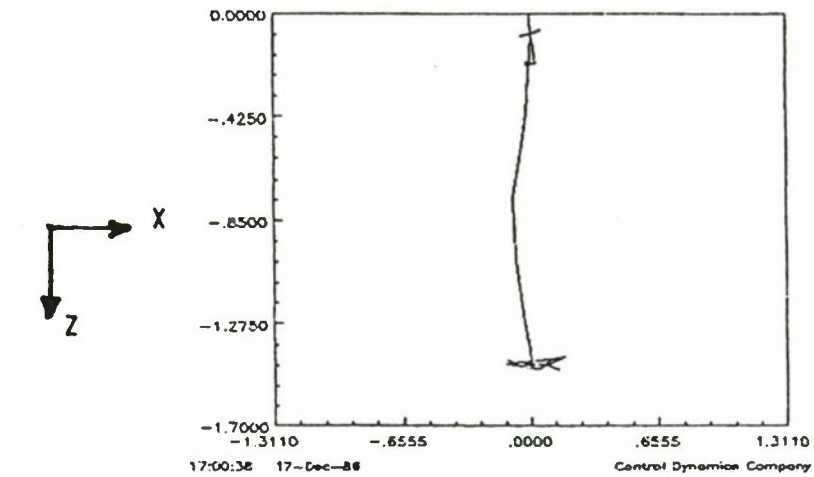


Figure 3.5-3A Experimental Mode, 2.000 Hz





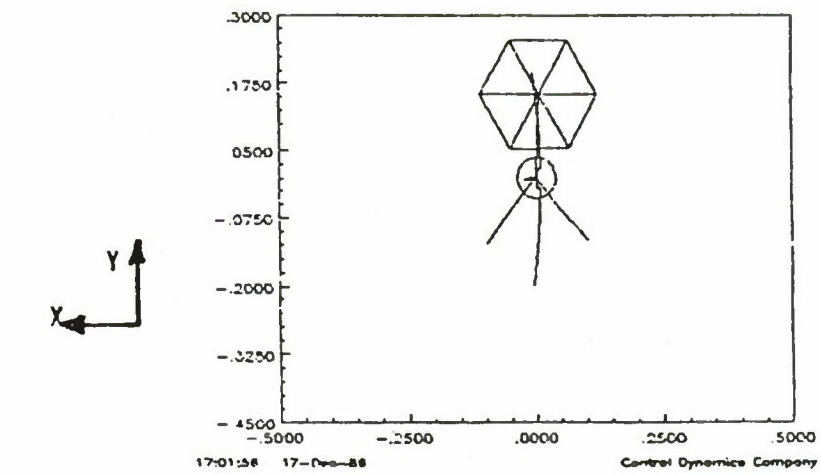
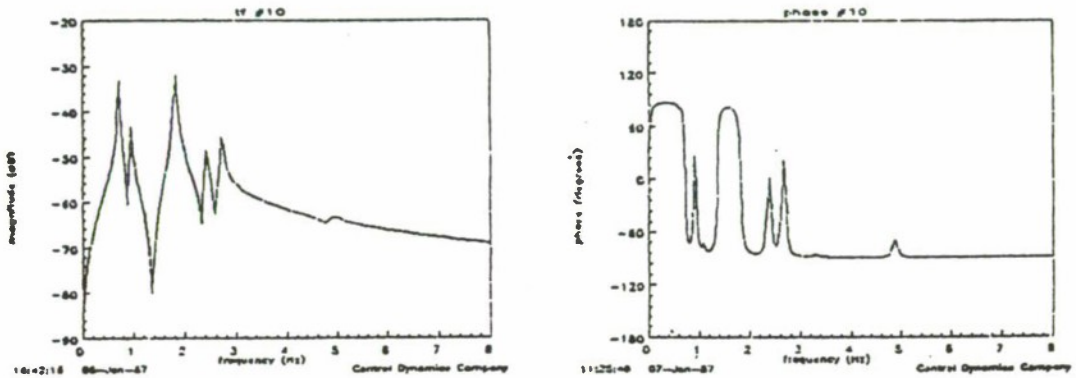
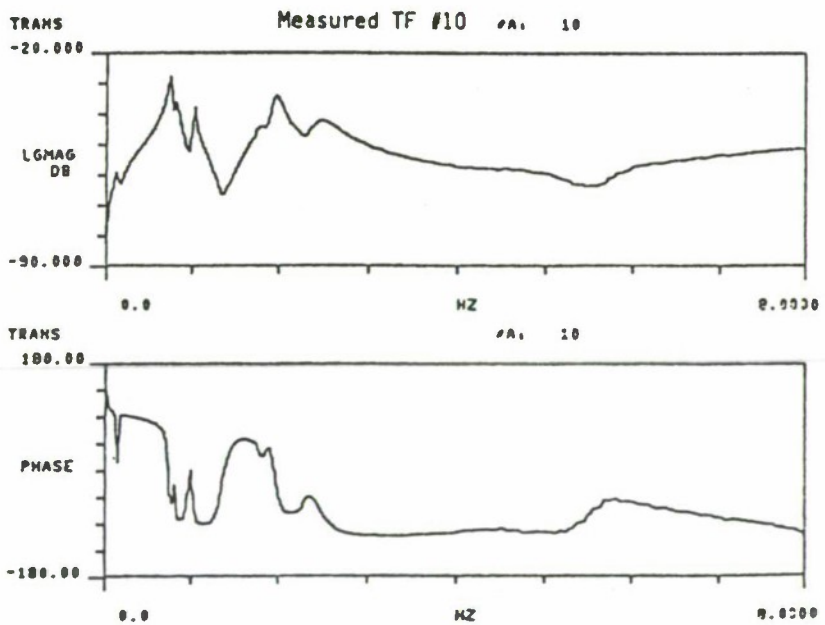


Figure 3.5-3B Analytical Mode 23, 2.20 Hz

AGS-Y to BASE GYRO-Y

Model TF #10



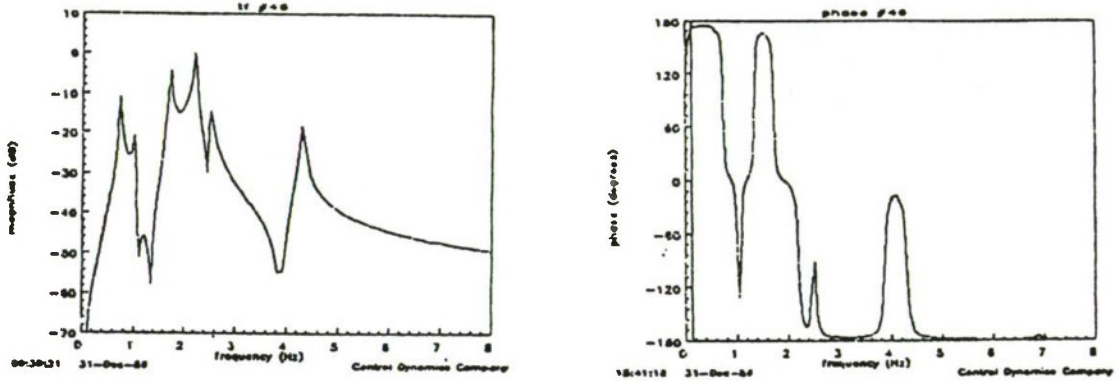


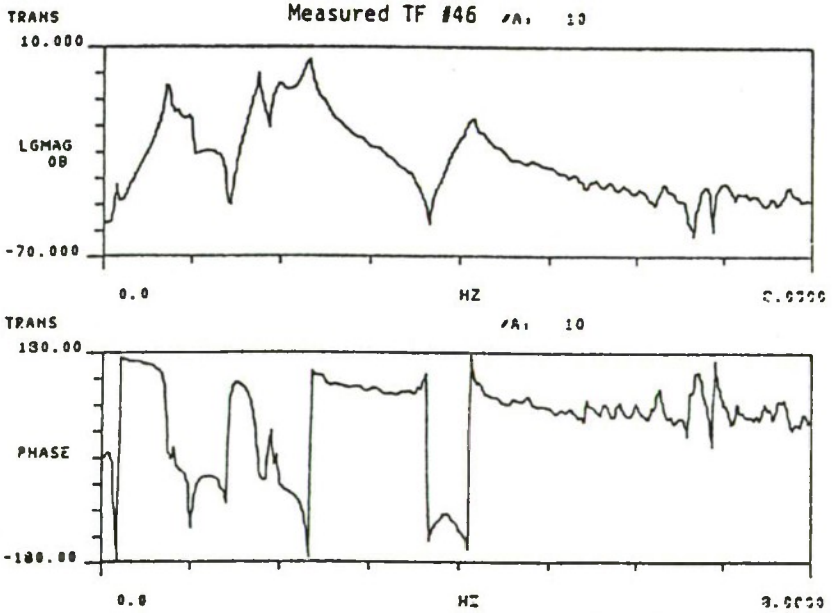
	Analytical	Experimental
0.75Hz	-33dB	-28dB
0.83Hz		-35dB
1.0 Hz	-44dB	-38dB
1.8 Hz	-32dB	-42dB
2.0 Hz	-48dB	-32dB
2.5 Hz	-45dB	-40dB

Figure 3.5-4 Transfer Function

AGS-Y to LMED1-X

Model TF #46





Measured TF #46

	Analytical	Experimental
0.75Hz	-10dB	-5dB
1.0 Hz	-21dB	-15dB
1.75Hz	-4dB	0dB
2.0 Hz	0dB	-5dB
2.3 Hz	-15dB	5dB
4.2 Hz	-18dB	-20dB

Figure 3.5-5 Transfer Function

experimental counterparts. The phases are difficult to compare as the experimental plots contain lags due to the computational delays in the computer system.

3.6 Control Model.

The control model has utilized all that has been learned in the previous configurations, especially the results from the preliminary model. The modal testing and transfer function testing have contributed a significant amount of knowledge about the structure which previously was not available. The following changes have been made to update the preliminary model to the control model form. The characteristics of the actual equipment were implemented: pointing gimbal assembly, mirrors, detector, and counterweights. The stiffness values for the BET and roll gimbal have been removed as the equipment is operational for control and disturbance purposes. Table 3.6-1 gives the frequencies and modeshape descriptions for the control model.

Line-Of-Sight (LOS) errors were calculated, for each mode, for the two mirrors and the detector. The LOS errors were calculated utilizing the structure's geometry (Figure 3.6-1.) and the modal gains for each frequency. The geometry relating the laser source, mirrors, and detector for a static condition is input and transformed from the laboratory reference frame to local detector and mirror frames. For the static case, this produces a 0.0 LOS error in the plane of the mirrors and detector. When the modal gains are included in the LOS equations, an X and Y error are calculated for each mirror and the detector. The detector local coordinate system is calculated to be parallel to the global system since the detector was originally in the horizontal plane and there are only small angle perturbations at the detector location in the analytical model. Again, these are the two LOS error components in the plane of a mirror or detector, and the values are the distance of the laser beam from the center point in meters.

This model has not been verified against experimental data, but Control Dynamics feels it is a good model based upon the preliminary model tuned against the modal test data and the transfer function data. For a more thorough explanation of the model, tests, and model results refer to the ACES Report on the Finite Element Model prepared by Control Dynamics.

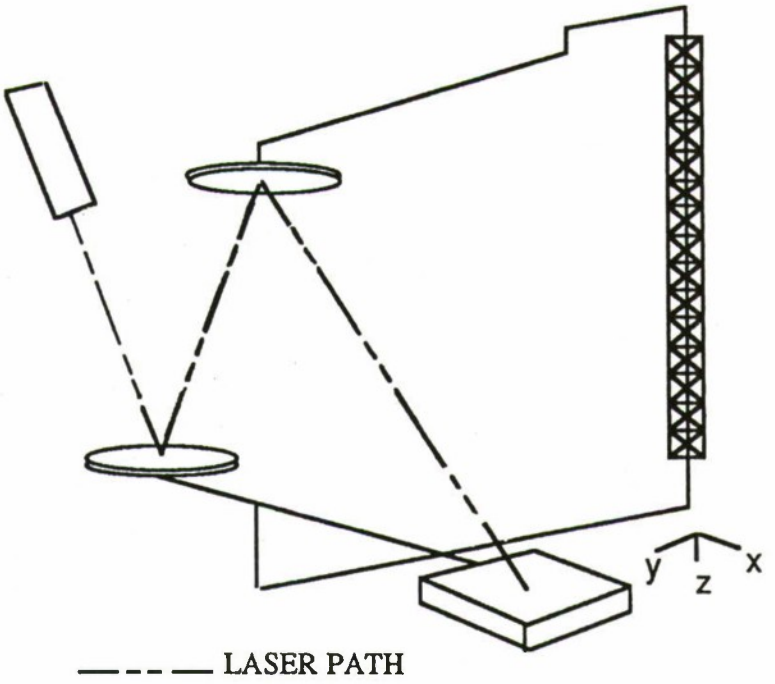


Figure 3.6-1. LOS Geometry

Observations Concerning the Control Model

The control system design model is composed of the dynamic model, generated through FEM techniques and refined with test data as described in Section 3.0, and additional information concerning actuators, sensors, and the physical laboratory system. Although all of this information is not necessarily used directly in the model, it is important for consideration in the design process.

The dynamic model as received by the controls engineer includes 43 modes and input/output gains for all actuator/sensor locations. The set of actuators and sensors and their locations were taken as given because of the impracticality of moving them around in the test facility. This is not so different from the constraints that are likely to be placed on a real spacecraft design where issues other than control are likely to have a great impact on hardware design. Obviously, model reduction and actuator/sensor choice are important parts of the design process, and, as such, are

included as part of each design technique application. This allows use of the model reduction process best suited to the peculiarities of each design technique.

Following are discussions of some areas of special interest to the control system designer, regardless of the design technique used.

Line of Sight Measurement

The line of sight (LOS) measurement is generated as shown in Figure 3.6-1. In this arrangement the laser source is fixed in the laboratory, which means that rigid body translation of the entire test fixture appears in LOS error. Therefore, rigid body translation is observable from the IMC system; however, rigid body translation is not controllable from any actuator(s) available to the control system. (All control actuators provide relative force or torque between structural components.) This, coupled with the fact that the dynamic model has two pure undamped rigid body modes in translation, leads to a dynamic model which is unstabilizable using the given set of control actuators and sensors.

In reality, the rigid body translational modes are stabilized by the BET. The BET model is included in the nonlinear simulation but is not included in the control system design models. For control system design in the time domain, the rigid body translational modes are simply removed from the model even though they appear to be important. But they are not ignored. The IMC system must be designed to reject them as a disturbance which is reasonable because they cannot affect stability but can affect performance in terms of the LOS error at the detector.

Table 3.6-1

Final ACES Model	
Mode	Frequency (Hz)
Rigid Body, Torsion + X-Bending	0.00
Rigid Body, Torsion + X-Bending	0.00
Rigid Body, Y-Bending	0.00
Torsion + Legs + Antenna + Arms + Gimbals	0.09
Y-Bending + Antenna + Gimbals + LMEDs	0.50
X-Bending + Antenna	0.59
Antenna	0.59
Torsion + Antenna	0.60
X-Bending + Legs + Antenna + Arms + Gimbals + LMEDs	0.69
X-Bending + Y Bending + Legs + Antenna	0.70
X-Bending + Legs + Antenna + LMEDs	0.71
Y-Bending + Legs + Antenna + LMEDs	0.92
Antenna	0.95
Antenna	0.95
X-Bending + Legs + Arms + Gimbals + LMEDs	0.96
X-Bending + Y-Bending + LMEDs	1.17
X-Bending + Y-Bending + LMEDs	1.18
X-Bending + Y-Bending + Legs + LMEDs	1.23
X-Bending + Y-Bending + Legs + LMEDs	1.24
Arms + Gimbals	1.25
Gimbals	1.51
X-Bending + Arms + Gimbals + LMEDs	1.67
Y-Bending + Legs + Antenna + Gimbals + LMEDs	1.76
Y-Bending + Legs + Antenna + Gimbals	1.85
Antenna	1.92
Antenna	1.93
X-Bending + Gimbals	2.08
Y-Bending + Antenna + Arms + Gimbals + LMEDs	2.18
X-Bending + Antenna + Gimbals	2.34
X-Bending + Legs + Antenna + Gimbals	2.58
Y-Bending + Antenna + LMEDs	2.67
Torsion + Arms + Gimbals	3.31
Antenna	3.31
Antenna	3.31
X-Bending + Y-Bending + Torsion + Legs + Antenna	4.58
Torsion + Antenna	4.71
Antenna	4.71
Torsion	4.71
Antenna	5.34
Y-Bending + Legs + Antenna	5.84
Y-Bending + Z + Legs	6.92
Torsion	8.77
Gimbal Arm	8.82

4.0 ACES SIMULATION

The purpose of the ACES FORTRAN program is to simulate the dynamic system consisting of the continuous plant, digital controller, actuation system, sensing system, base excitation system, image motion compensation system, and the computer algorithms associated with the ACES experiment. The ACES configuration of the LSS GTF experiment is described in Figure 4.0-1.

A graphical description of the LSS simulation is shown in Figure 4.0-2. The figure shows the meanings of several fundamental variables and the relationships between the components of the experiment. The variable definitions are provided in Table 4.0-1.

1. Base Excitation Table
2. 3 Axis Base Accelerometers
3. 3 Axis Gimbal System
4. 3 Axis Base Rate Gyros and Counterweight
5. 3 Axis Tip Accelerometers
6. 3 Axis Tip Rate Gyros
7. Optical Detector
8. Mirrors
9. Laser
10. 2 Axis Pointing Gimbal System
11. LMED System

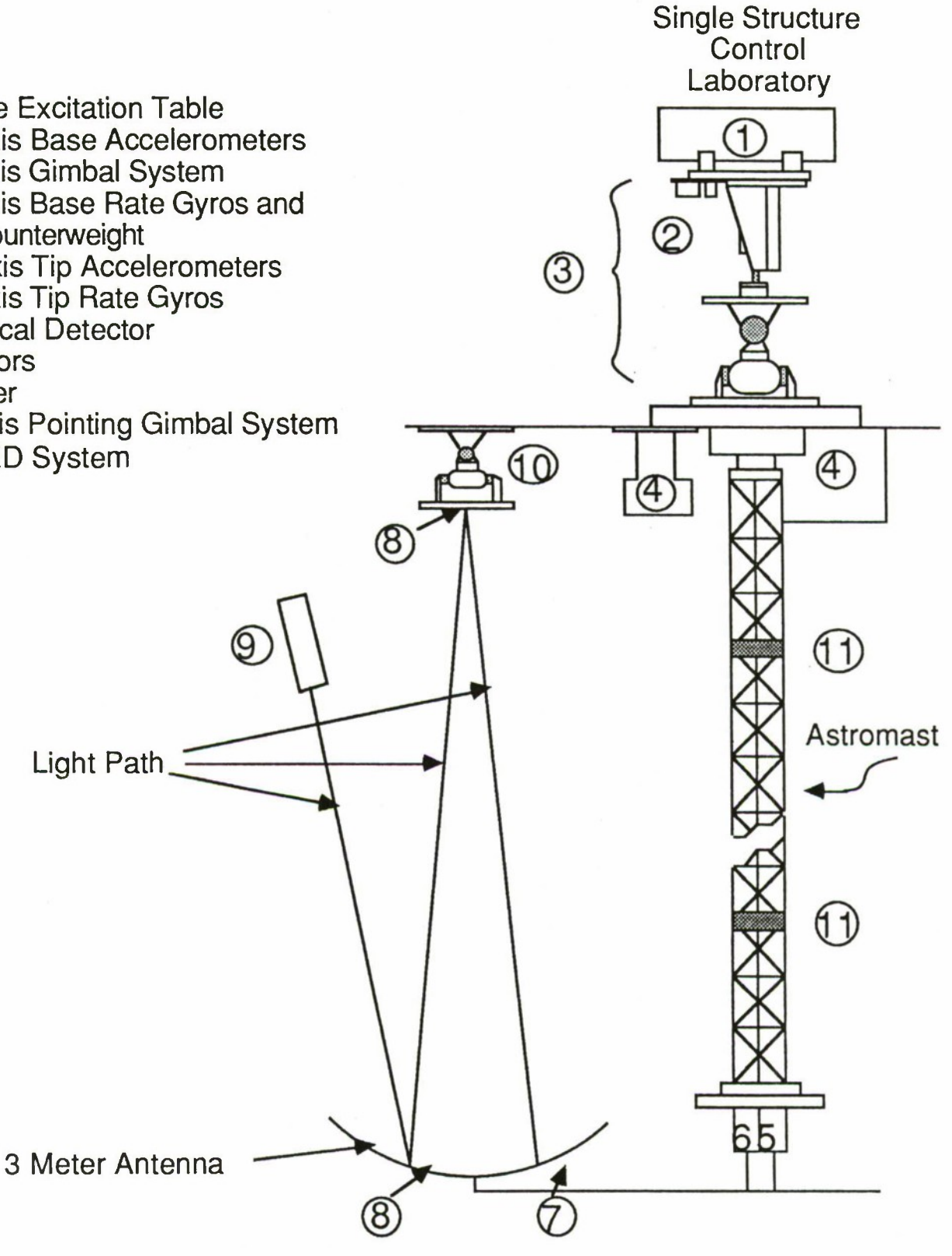


Figure 4.0-1. LSS GTF Experiment (ACES Configuration)

TABLE 4.0-1 VARIABLE DEFINITIONS OF SIMULATION BLOCK DIAGRAM

AGS	=	Advanced Gimbal System
$[BE]^T$,$[PE]^T$	=	instrument derived body (base, tip) to lab transformation matrix
BET	=	Base Excitation Table
Fbet	=	total force input to the BET
Fc	=	command force to LMEDs from controller
Fcl	=	force on beam applied by LMEDs
Gbet, GLMED	=	modal translational gain at BET, at LMEDs
Ggimbal, Gpg	=	modal rotational gain at gimbals, pointing gimbals
LOS	=	Line of Sight
LMED	=	Linear Momentum Exchange Device
LVDT	=	Linear Variable Displacement Transducer
$\eta,\dot{\eta},\ddot{\eta}$	=	modal displacement, velocity, acceleration
Pc, Pv	=	position, velocity BET command
Qb, Qp	=	base, tip quaternion (lab frame)
$Rb,\dot{R}b,\ddot{R}b$	=	position, velocity, acceleration at base (lab frame)
RCS	=	Reaction Control System
Rdet	=	detector LOS error (sensor frame)
Rl	=	acceleration of beam at LMED (lab frame)
Rpl	=	relative position of proof mass w.r.t. beam
$Rp, \dot{R}p,\ddot{R}p$	=	position, velocity, acceleration at tip (lab frame)
T, Ti	=	control time period, integration time period
Uc	=	control torque applied by gimbals
Ucg, Ucpg	=	command control torque to gimbals, pointing, gimbals
Ug	=	total torque input to gimbals
Upg	=	control torque applied by pointing gimbals
ZOH	=	zero order hold

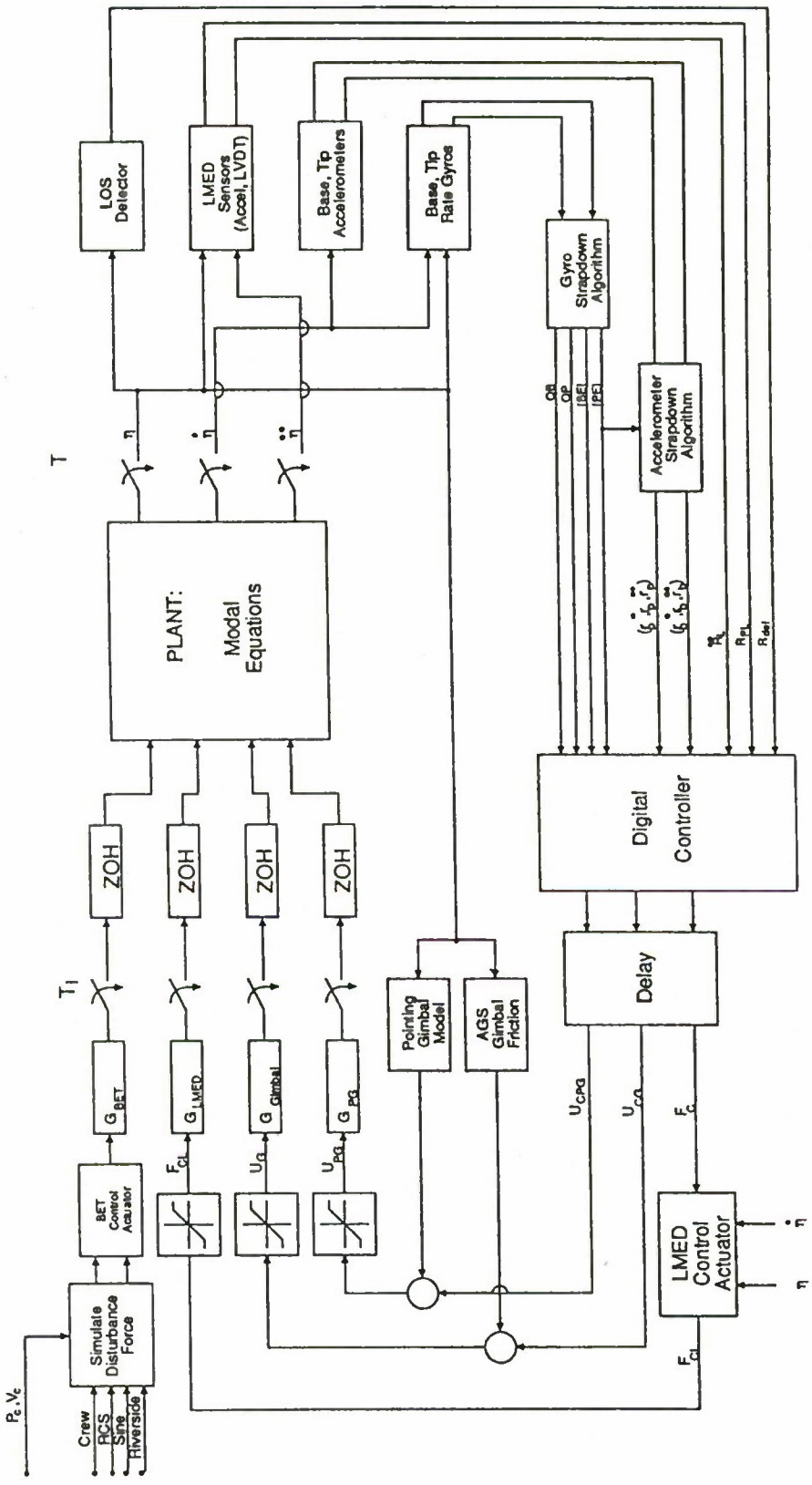


Figure 4.0-2. LSS Simulation Block Diagram.

System Dynamics

The system dynamics are described via a modal model and are defined by the modal frequencies, modal damping, and modal input and output gains. The dynamic equations of motion are described by the second order matrix equations below. The dynamics are simulated utilizing a fourth-order Runge-Kutta integration scheme. The forcing functions are the control torque inputs, the BET force inputs, and the LMED force inputs, each multiplied by the appropriate gain matrix.

$$\ddot{\eta} + 2\zeta\Omega\dot{\eta} + \Omega^2\eta = G_{gimbal}U_g + G_{bet}F_{bet} + G_{pg}U_{pg} + G_{LMED}F_{CL}$$

where

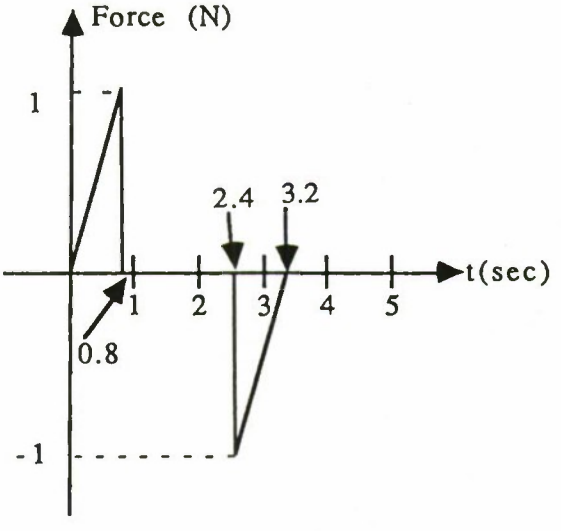
N	=	number of modes
ηi	=	modal coordinate of ith mode (i=1,...,N)
ζi	=	modal damping of ith mode (i=1,...,N)
Ωi	=	modal frequency of ith mode (i=1,...,N)
G_{gimbal}	=	control gimbal gain matrix (Nx3)
G_{bet}	=	BET disturbance gain matrix (Nx2)
G_{LMED}	=	LMED force gain matrix (Nx2)
G_{pg}	=	pointing gimbal gain matrix (Nx2)
ζ	=	diagonal matrix $(\zeta i)i=1,...,N$
Ω	=	diagonal matrix $(\Omega i)i=1,...,N$
U_g	=	gimbal torque input (3x1)
U_{pg}	=	pointing gimbal torque input (2x1)
F_{bet}	=	BET force input (2x1)
F_{c1}	=	LMED force input (4x1)

Base Excitation System

The base excitation system applies hydraulically generated forces to the base of the gimbals in order to provide two translational degrees of freedom in the horizontal plane. The BET disturbance force simulates the effects of either the crew motion, RCS (Reaction Control System) thruster firings, sinusoidal, or the Riverside disturbances on the structure.

The crew motion and thruster firing disturbances are modeled as force pulses and ramps applied for specified time periods as shown in Figure 4.0-3. An orbiter to GTF mass ratio of 100 is used before inputting the magnitude of disturbance into the simulation. The mass ratio division causes equal accelerations to be applied to the orbiter and the test structure.

Crew Motion Disturbance



RCS Thruster Firing Disturbance

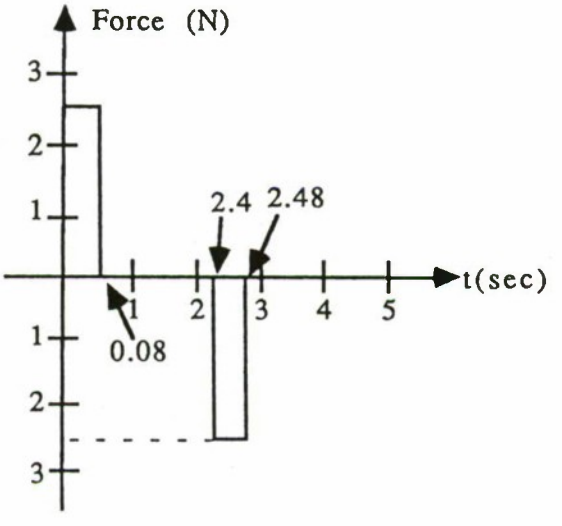


Figure 4.0-3. Crew and RCS Force Profiles.

The sinusoidal disturbance is implemented simply by applying a sine force to the BET, where the user specifies the amplitude, phase, and frequency of the sine wave.

The Riverside disturbance is defined by the one-sided PSD (Power Spectral Density) shown in Figure 4.0-4. The Riverside disturbance is approximated by the two low frequency sinusoids (8, 10 Hz). The high frequency component (20 Hz) of the disturbance is higher than the BET bandwidth and is not implementable at the facility; hence, it is not simulated in the program. The bandlimited noise is to be included in a future simulation update.

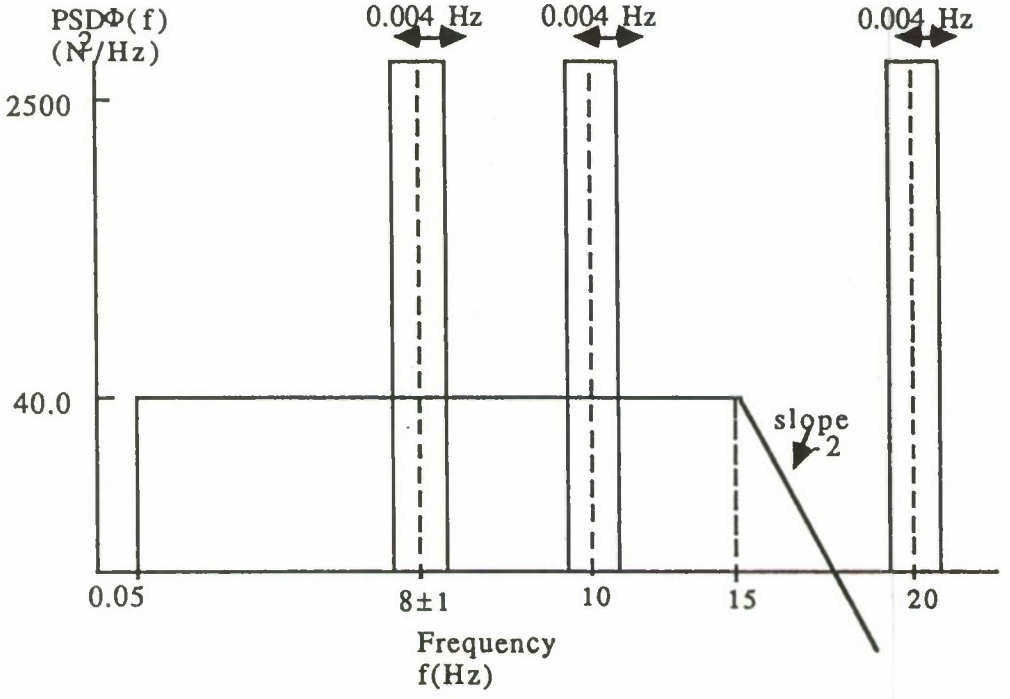


Figure 4.0-4. Riverside Disturbance PSD.

The disturbance force is applied through commanding specified position and velocity profiles to the BET actuator. The position and velocity commands corresponding to the crew, RCS, sine, and Riverside disturbances are derived by integrating the force profile and dividing by the accelerating mass. In addition, other disturbances may be applied through direct user definition of piecewise constant position and velocity commands.

The BET control actuator exerts a force to control the position and velocity of the BET which is dependent on the position and velocity errors and the user-defined error control gains.

Actuation System

The actuation system consists of the gimbal system, LMEDs, and the pointing gimbals. The gimbal system and LMEDs are described in this section, and the pointing gimbals are described in the IMC system section.

Gimbal System

The AGS is augmented with an azimuth torque motor to create a three-axis gimbal system. The gimbals apply the control torques to the base end of the Astromast. The torques physically achievable with each gimbal are defined by the user. The gimbal friction is incorporated using a sliding equilibrium friction model.

LMED System

The LMED system is a collocated sensor/actuator pair. The actuator applies a force to the structure and the sensor measures the acceleration of the structure. The LMED actuator consists of a linear permanent magnet motor, where the magnet serves as a proof mass. The force is applied to the structure as a reaction against the proof mass. The position of the proof mass with respect to the beam is measured by the LVDT (Linear Variable Displacement Transducer). The proof mass is constrained by a rubber bumper on each end of the travel shaft. In addition, a set of springs acts on the proof mass and provides a small centering force.

The simulation uses a simple spring-damper system to model the LMED actuator. The generation of the force applied to the beam is calculated by the following equation. Note that the first term (K1 Rpl) of the equation is not applied

by the simulation, but is applied by the structural model. Of course, the rubber stop terms are only applied if the proof mass hits the stop.

$$Fcl = K1\ Rpl + 2\,Z1\sqrt{K1\,M}\ \dot{R}_{pl} + K2\,(Rpl - D) + 2\,Z2\sqrt{K2\,M}\ \dot{R}_{pl} - Fc$$

where

F_{c1}	=	force applied by LMEDs on beam
R_{pl}	=	relative position of proof mass w.r.t. beam
K1, K2	=	spring constant of LMED, rubber stop
Z1, Z2	=	damping factor of LMED, rubber stop
D	=	distance factor of LMED, rubber stop
F_c	=	command force to LMED
M	=	mass of proof mass

The user has the capability to input the spring constants (K1, K2), damping values (Z1, Z2), maximum travel distance (Dmax), and mass of the proof mass (M). In addition, the user specifies the maximum Fcl which can be achieved by the LMEDs. Note that the frequencies of the proof mass and rubber stop are determined by the K1, K2, and M. Using nominal values, these are approximately

$$\omega_1 = \sqrt{K1/M} = 1.18 \text{ Hz}$$

$$\omega_2 = \sqrt{K2/M} = 13.6 \text{ Hz}$$

Sensing System

The measurement system is composed of two three-axis accelerometers, two three-axis rate gyros, two two-axis accelerometers, and two two-axis LVDTs, placed at various locations on the structure. One rate gyro package and one accelerometer package are each located at the ASTROMAST tip, one rate gyro package is positioned at the ASTROMAST base, and one accelerometer is placed on the base excitation table. The two two-axis accelerometers and LVDTs are collocated with the LMED packages on intermediate points along the ASTROMAST.

The physical limitations of each sensing device are user-inputs, such as dynamic range, biases, and scale factors. The base gyro measures small angular rates

very accurately, while the tip gyro measures large angular rates less accurately. The dynamic range of the base rate gyros is ± 1 deg/s and of the tip rate gyros is ± 40 deg/sec in each axis except roll, where it is 70 deg/s. The three-axis accelerometers are identical packages with each having the same dynamic range and resolution. The dynamic range of each tip and base accelerometer axis is ± 3 g's. The LMED accelerometers each have a dynamic range of ± 20g's. The travel range of each of the LVDTs is ±0.5 inches which is limited only by the LMED package size.

Figure 4.0-5 simulates the measurements of the tip and base accelerometers and rate gyro sensors in the sensor frame. The simulation also derives the transformation matrices (lab-to-body) for the base and tip body frames.

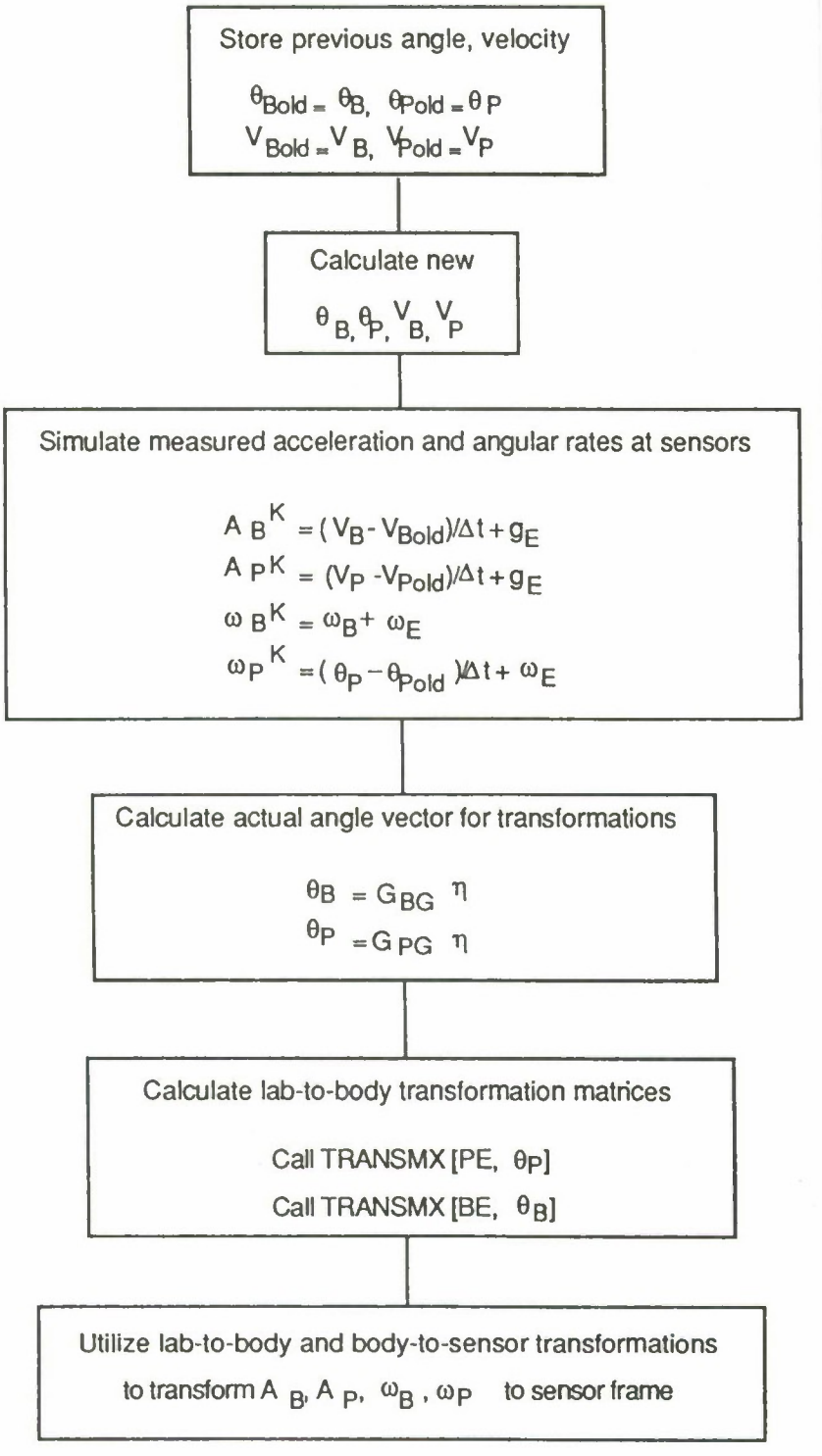


Figure 4.0-5. Simulate Tip, Base Sensors.

where

$\Theta_{B,P}$	=	angle of gyro at base (tip)
$V_{B,P}$	=	velocity at accelerometer at base (tip)
$\omega_{B,P}$	=	angular velocity at gyro at base (tip)
g_E	=	acceleration due to gravity
ω_E	=	angular velocity by gyro due to earth rate
G_{BG}, G_{PG}	=	rotational modal gain matrix at base, tip gyro
η	=	modal position
Δt	=	control time period

and "K" denotes simulated measured variables and "old" denotes the previous value of the variable.

Control System

The control system computes the torques to be applied to the gimbals and pointing gimbals, and the forces to be applied to the LMEDs. The inputs to the control system are the outputs from the sensors and the strapdown algorithm. The user is given the option of performing either open or closed loop testing by turning the controller off or on. The controller may be activated at any time during the simulation through use of the runtime input. The option of including a control delay (an integer number of integration steps) is provided.

Digital Controller

The controller is the most general form of digital MIMO controller. This algorithm has the flexibility to choose any vector of inputs and any vector of outputs. The form of the controller is determined by the discrete matrix state equations in equations below. The general controller is utilized to test the MESS (Model Error Sensitivity Suppression), HAC/LAC (High Authority Control/Low Authority Control), and the Positivity controllers prior to implementation.

$$X(k+1) = A\,X(k) + B\,Y(k)$$

$$U(k) = C\,X(k) + D\,Y(k)$$

where A, B, C, D = control matrices

X(k) = control state vector at time k
U(k) = control output vector at time k
Y(k) = control input vector at time k

The user defines the controller through specification of the input vector, output vector, control matrices, and initial conditions. The control parameters defined by the user include Ns, Ni, No, I(j), O(j), A, B, C, D, and X(0).

Ns = Number of controller states
Ni = Number of control inputs
No = Number of control outputs
I(j) = Specification of j-th element of input vector for j=1,..,Ni
O(j) = Specification of j-th element of output vector for j=1,..,No

The dimensions of the control matrices and vectors are user-defined through Ns, Ni, and No. The dimensions are as follows:

A(Ns,Ns), B(Ns,Ni), C(No,Ns), D(No,Ni)
X(Ns), Y(Ni), U(No)

Computer System

The strapdown algorithm tasks each simulate a function performed by the COSMEC/HP 9000 computer system at the Ground Test Facility. The objectives of the computer strapdown algorithm are to convert the sensor outputs to a common laboratory reference frame in common metric units and to remove the effects of the earth from the sensor outputs. In addition, the accelerometer strapdown algorithm converts the accelerometers output, a change in velocity over the time period, to an

acceleration. Similarly, the gyro strapdown algorithm converts the angular change to an equivalent angular velocity. The strapdown algorithm performs the following tasks:

(1) Converts gyro instrument outputs to changes in angles in the body frame, calculates the quaternions, and utilizes the quaternions to create earth (lab) to body transformation matrices (with subroutines GYROB, GYROP),

(2) Converts accelerometer instrument outputs to changes in velocity in the body frame, calculates the acceleration in body and lab frames, and computes the displacement, velocity, and acceleration in the lab frame (with subroutines ACCELB, ACCELP).

IMC System

The Image Motion Compensation (IMC) system consists of a laser, two mirrors, two pointing gimbals, a servo, and a detector. The objective of the analog control system is to maintain the laser beam in the center of the detector. The analog servo is being used for preliminary testing, but the digital loop capability has been added at the facility in order to implement the ACES controllers. The simulation models the digital loop option.

The simulation assumes the pointing gimbals are perfect command following gimbals. A pointing gimbal friction model will be incorporated. The simulation also assumes that the detector is a perfect sensor. This assumption will be modified to include the imperfect sensing characteristics of the detector.

The calculation of the LOS (Line Of Sight) errors for each mirror and for the detector is accomplished through use of the LOS gains provided by the structural model. These gains determine the position of the beam on the planes of the mirrors and detector. The LOS gains are not modal gains, but are a function of the modal gains. The LOS error is obtained in the sensor reference frame and not in the laboratory reference frame. The position and angle of each optical component is accounted for in the LOS gains. The physical limits of the mirrors and the detector

are determined by the user through input of the values of the radii of mirrors 1 and 2, and the values of the maximum and minimum detector limits.

The evaluation criteria of the IMC system include the number of hits, and the mean and standard deviation of the beam position on the detector. The presence of the beam within the physical ranges of each of the detector components is required for a detector hit. The sample mean and variance of the beam position on the detector (given a hit) is calculated using an unbiased estimator.

5.0 HIGH AUTHORITY CONTROL/LOW AUTHORITY CONTROL (HAC/LAC)

HAC/LAC is the LSS control system design technique developed by Lockheed Missiles and Space Corporation under the ACOSS program. As the beginning documentation for Control Dynamics' study of the HAC/LAC technique, references [1] and [2] were used. These are: [1] ACOSS-5 and [2] Low Authority Control Synthesis for Large Space Structures, J. N. Aubrun and G. Margulies, NASA Contractor Report 3495, September 1982.

5.1 Theory.

High Authority Control / Low Authority Control has as its cornerstone the separation of the control system design problem into two parts. The first part is High Authority Control (HAC) which is a high gain, low bandwidth controller, and the second part is Low Authority Control (LAC) which is a low gain, broad bandwidth control law. This separation of the control problem gives the designer a way in which to interject understanding and intuition into the control system design process. The greatest disadvantage to this approach is the robustness problem associated with a two part design procedure.

5.1.1 HAC Theory.

The HAC controller design is characterized by the following requirements and stipulations:

- Model includes well known modal characteristics (typically low frequency).

Since most Finite Element Models (FEM) are assumed to be accurate only for the lower frequency, and typically more fundamental, modes of behavior, the models lend themselves to this sort of interpretation. That is, certain modes are assumed to be well known and others are assumed to be less known and models composed of each set are easily obtainable given the complete FEM model with which to begin.

- Performance goals must be met by the HAC controller

The HAC controller is the high gain part of the control system and, as such, must provide for the performance oriented goals of the overall control system design. These goals may include such things as transient response requirements, disturbance rejection, and steady-state error criteria. If set point input following is required, then it must be designed in the HAC design step.

- Heavily damp modes within the HAC bandwidth

In addition to meeting performance goals, the HAC controller should greatly augment the damping of the structural modes within its bandwidth. If the controller design is for the purpose of structural damping, then any modes which require heavy damping must fall within the HAC bandwidth and be included in the HAC design.

- Actuators used in HAC design have high authority over characteristics to be controlled

The actuators used in the HAC control design, must have high authority, i.e., great controllability, over the structural and performance characteristics to be improved through the use of control. Saturation limits come into play also because they eventually define the limit of "high authority."

Actual design of the HAC control law is accomplished using LQG techniques. These are applicable through the use of model reduction and because the lower frequency modes are assumed to be well known. The LQG design is performed on a reduced order model given by

$$\dot{x} = A x + B u$$

$$y = C x + D u$$

where x is the state vector of dimension n, u is the control input vector of dimension m, and y is the measurement vector of dimension p. The A, B, C, and D matrices are constant coefficient matrices defining the linearized plant. This system may include filter states and states introduced to enhance disturbance rejection. (See [1].) The control law

$$u = K x$$

is then computed to optimize the quadratic performance index

$$J = \int_0^\infty (x^T Q x + u^T R u)\, dt$$

where Q is the state weighting matrix and R is the control weighting matrix. A Kalman filter design is then performed to estimate the unknown and unmeasurable system states.

An important part of the HAC problem is selection of the HAC design model. The HAC design model must include the system modes essential to performance as well as any modes which participate greatly in the actuator to sensor transfer function and therefore have a great effect on system stability. The selection of the model has an obvious impact on the success of the control system design.

The HAC controller has the same order as the HAC model, which gives cause for additional consideration in selection of the HAC model. The smallest model which adequately represents the important aspects of the system should be chosen. Typical model reduction schemes give no guarantee of system stability when the controller is used in conjunction with plant models other than the one for which it was designed, i.e., there are no guarantees of robustness. This is where LAC comes to the rescue.

5.1.2 LAC Theory.

The LAC controller design is intended to stabilize a system which has been destabilized by the effects of spillover from modes not included in the HAC design model. As stated above, the HAC design procedure provides no guarantees of stability when the HAC controller is combined with a more detailed model (more modes) than that for which it was designed. In general, it is expected that such a combination of plant and controller will be unstable.

LAC attempts to stabilize modes which have been driven unstable by augmenting the system damping. This can be viewed as increasing the damping of the structural modes. LAC uses simple gains in the feedback path together with collocated, consistent sensors and actuators to effect increased damping. Collocation indicates that the sensor/actuator pairs are physically located together, and consistcnt means that they are of corresponding types, i.e., translational sensors are paired with force actuators, rotational sensors are paired with torque actuators, etc. In addition, the sensors must measure rates.

The LAC procedure designs the feedback gain matrix, C, to minimize the cost functional

$$J(C) = \sum_{n} W_n [(d\lambda n)_p - (d\lambda n)_d]^2 + \sum_{a,r} C_{ar}^2$$

where

$(d\lambda n)_p$ - predicted root shift

$(d\lambda n)_d$ - desired root shift.

The solution is derived from the Jacobi Root Perturbation formula and is given by the following

$$\underline{d} = \left(S^T W S + I\right)^{-1} S^T W(\zeta\omega)$$

where $\underline{d}$ is a vector of the nonzero elements of C, S is the modal coefficient matrix, W is a diagonal weighting matrix, and $\zeta\omega$ is a vector of the desired root shifts.

This solution is general and implies no restrictions on the physical system; however, it requires the solution of a general eigenvector problem to find S. For the case where a modal system is assumed and the sensor and actuator bandwidths are assumed to be large, S becomes the real eigenvectors of the modal system, and the solution is straightforward.

The LAC controller as defined above has no dynamical order, i.e., it is simply a gain matrix. The size of the gain matrix is number of actuators by number of sensors, and the matrix may be full or certain elements may be specified to be zero. This is equivalent to disallowing certain feedback paths and can be very useful as an additional user input to the design procedure. Separation of controller size from number of modes used in the design model is an important feature of the design technique and allows the inclusion of more information in the design process without the penalty of large controller size.

The LAC process in all of its forms is derived for continuous systems only. Assuming the controller will be implemented digitally, some allowance must be made for the effects of sampling and computational delay on system stability.

One way to deal with the sampling problem is to include filters in the plant model which approximate the phase lag of sampling and delay. The filters would not be included in the controller implementation, but would cause the LAC design to account for sampling and delay in some sense. This process is complicated and approximate at best, and in addition dictates the use of the generalized LAC procedure which is more complicated in itself.

Another approach is to design the LAC controller as if the system were continuous and ideal but use very conservative design criteria, i.e., ask for small amounts of additional structural damping. With this approach, a post analysis of the sampled data system is required, but this is straightforward and not very computationally expensive.

5.1.3 HAC/LAC Combined Control.

Choice of the order of design of the HAC and LAC controllers is at the discretion of the designer. Because LAC is viewed as a means of correcting spillover problems, the HAC design is typically completed first. (Systems with no controller do not have spillover.) In this way a LAC controller is "helpful" to the HAC controller; however, it is not inconceivable that a LAC controller design could destabilize the HAC system. If the generalized LAC procedure (requiring complex eigenvector solutions) is used, the HAC controller may be included in the LAC "plant" assuming the HAC controller is continuous. For the digital HAC controller, some continuous approximation could be used with possible success.

In a straightforward application of HAC/LAC, the most reasonable approach is to perform the HAC design (in the digital domain if necessary) and then perform the LAC design without direct consideration of the HAC controller in the model. The HAC model modes should, however, be included in the LAC model. This approach is based on the inherent requirement that the LAC controller gains be small to satisfy the necessary Jacobi root perturbation requirements.

In any event, the HAC/LAC control system design should be subjected to a thorough linear post analysis including sampling and delay effects, sensor and actuator dynamics, and the effects of closure of both the HAC and LAC control loops simultaneously.

The comments in this section are only general guidelines of course, and any particular problem may require a variation on these ideas. Indeed, it is safe to say that most real world problems will require special application of any controller design technique with alterations to compensate for special considerations of the problem. HAC/LAC is no exception.

5.1.4 HAC/LAC Applied to ACES.

The overall approach to application of HAC/LAC to the ACES problem is one of prudent use of the control design technique features as applied to the peculiarities of the control problem at hand. The ACES problem has two aspects: performance, as embodied in the Image Motion Compensation (IMC) system, and structural damping, which is considered essential for control of lightly damped space structures even though it may not be required for performance directly. Such a case is that of a Large Space Structure which must undergo docking with another spacecraft and, therefore, should have some minimum structural damping so that the amount of energy stored in the structure is maintained below a specified level.

The two part requirement for ACES matches well with the two step control system design of HAC/LAC. The ACES design applies HAC to the IMC system to meet the performance requirements and then applies LAC to augment the structural damping. This facilitates the use of a very low order model for the HAC design and, therefore, a low order HAC controller. The LAC controller as defined above has no order, i.e., it is simply gain feedback. The LAC design then uses a collocated set of sensors and actuators to effect the required structural damping.

Some slight departures from HAC/LAC are embodied in this approach. The actual choice of sensors and actuators is used to solve some of the spillover problems, i.e., the HAC model needs only to include the dynamics necessary to model the IMC system. This is essentially a sixth order system comprised of three structural modes; however, they are not the three modes of lowest frequency in the structure. This is a departure from the use of lower frequency modes in the HAC model and higher frequency modes in the LAC model. It does not, however, violate the premise that the HAC model will be better known than the LAC model.

The following sections detail the above approach in application to the ACES model. The model selection process is explained, as is minimization of spillover through actuator/ sensor choice. The HAC and LAC design and post analysis processes are described and simulation results are presented. Finally, test results are shown to verify operation of the controller in the NASA LSS test facility.

5.2 Model Selection and Reduction.

Control system design actually begins with what is called the baseline model. This is the dynamic model generated through FEM techniques and refined with test data as described in Section 3. The model as received by the controls engineer includes 43 modes and input/output gains for all actuator/sensor locations. The set of actuators and sensors and their locations were taken as given because of the impracticality of moving them around in the test facility. This is not so different from the constraints that are likely to be placed on a real spacecraft design where issues other than control are likely to have a great impact on hardware design.

5.2.1 HAC Model Selection.

Choice of the HAC model is based on two important constraints. First, the size of the HAC model will dictate the size of the HAC control system, because the LQG design will result in a compensator of similar order to the plant used to perform the Kalman filter design. The other consideration is that of performance. Because the HAC design must provide for the performance of the resulting system, the HAC model must be of adequate fidelity to ensure the performance. These constraints impose opposite requirements upon the model, i.e., more fidelity requires greater order which drives up the HAC controller size.

For the ACES control problem a good compromise is possible because of the basic layout of the system and its requirements. The performance aspects of ACES are embodied in the IMC system and this is where the HAC design must be targeted. The IMC gimbal system as shown in Fig. 3.1-1 is modeled as a rigid body connected by a single degree of freedom hinge to the support arm and another rigid body connected to the first by a hinge orthogonal to the first hinge. In the presence of gravity, this system has two modes with frequencies fixed by the effective pendulum lengths in each axis. Since this is the minimal set of states which must be controlled to null error at the LOS sensor, a forth order model for the IMC system is the very least that could be expected to provide the performance requirement. In reality, the IMC gimbal motion is coupled to support arm bending motion which makes a two-mode model impossible.

The HAC model was chosen by examination of the frequency responses shown in Fig. 5.2-1. These responses are open loop from gimbal torque to LOS measurement in both axes and cross-axis. Because the LOS measurements are defined as displacement of the light spot at the detector, the "on-axis" input/output pairs are LOS x due to torque in y and LOS y due to torque in x. Figures 5.2-1a and 5.2-1b are the on-axis responses and examination of these together with the modal model for detail frequency values show that they are dominated by three structural modes. Examination of the shapes of these modes indicates that they incorporate the pendulum motion of the IMC gimbals and bending motion of the support arm. The LOS x on-axis transfer function of Fig. 5.2-1b is dominated by the pendulum mode of the inner gimbal which provides for its more decoupled nature and high gain. The LOS y on-axis transfer function includes two modes which are a combination of gimbal pendulum motion and support arm bending.

It is important to note that all of the transfer functions include a zero frequency rigid body mode generated by the rigid body translation of the entire structure at the BET. This motion is actually constrained by the BET control system and is of no concern to the HAC design except in that the apparent motion at the LOS sensor must be rejected by the HAC controller. In addition, the rigid body translation of the entire structure is not controllable from the IMC gimbal inputs. It appears in the transfer function because of numerical inaccuracies in the modeling process.

Consideration of Figures 5.2-1c and 5.2-1d, the cross-axis transfer functions of the IMC system, indicates that they include much more dynamical interaction than the on-axis transfer functions. However, the system is very decoupled as is indicated by the magnitude of the cross-axis terms. Because the closed loop behavior will be dominated by the on-axis (high gain) characteristics of the system, an accurate model of the cross-axis behavior is not required.

The HAC model (three modes) frequency responses for the IMC system are shown in Figures 5.2-2a through 5.2-2d. The dominant peaks of the on-axis transfer functions are well matched to the 43-mode model and the dc gain of each is matched ignoring the presence of the rigid body mode in the full order system.

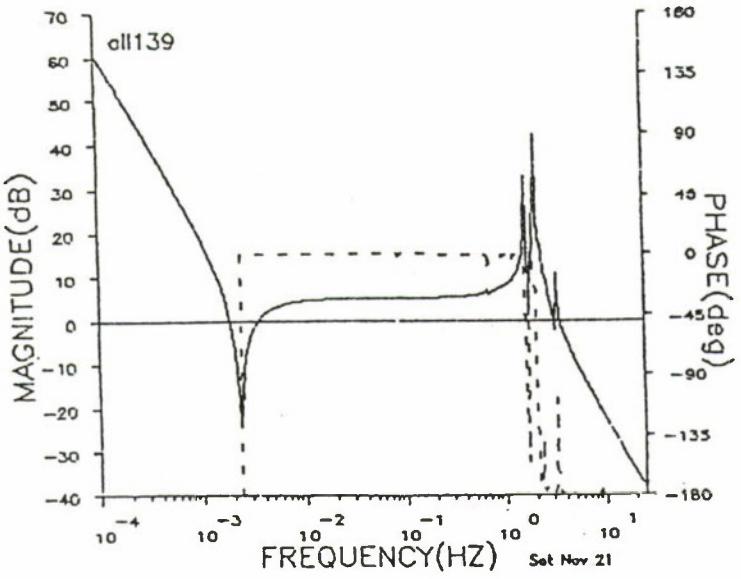


Figure 5.2-1a. Frequency Response from Pointing Gimbal Y to LOS X.

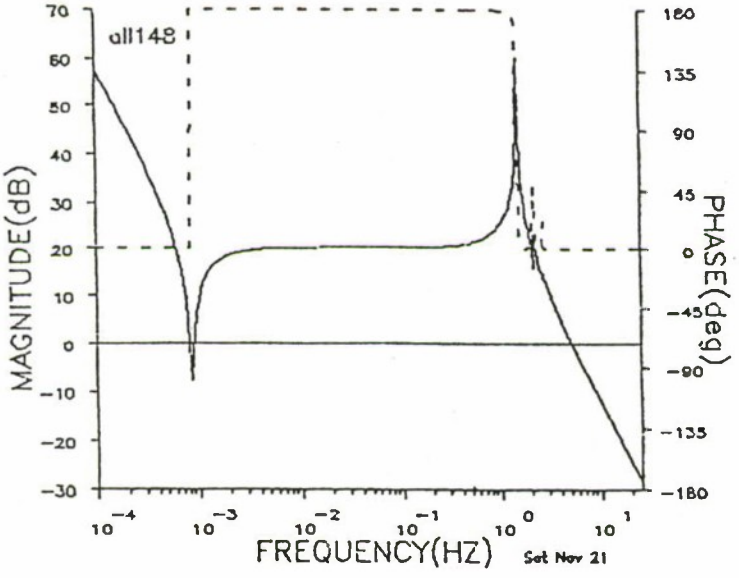


Figure 5.2-1b. Frequency Response from Pointing Gimbal X to LOS Y.

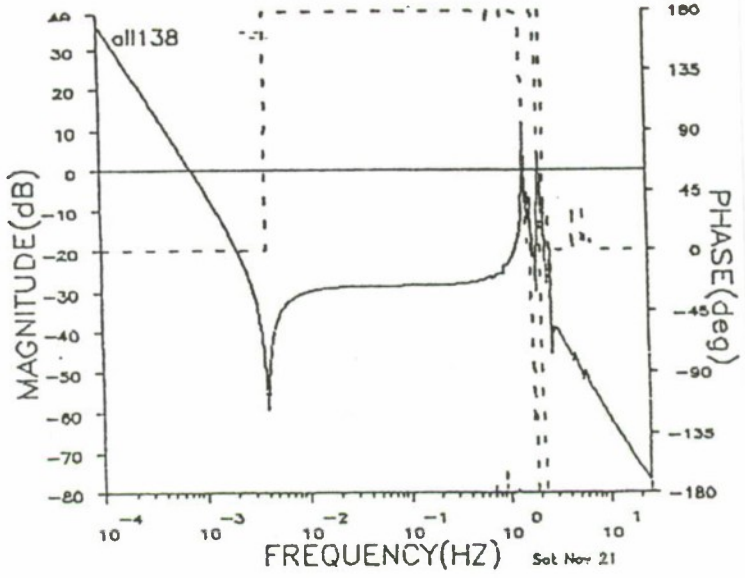


Figure 5.2-1c. Frequency Response from Pointing Gimbal X to LOS X.

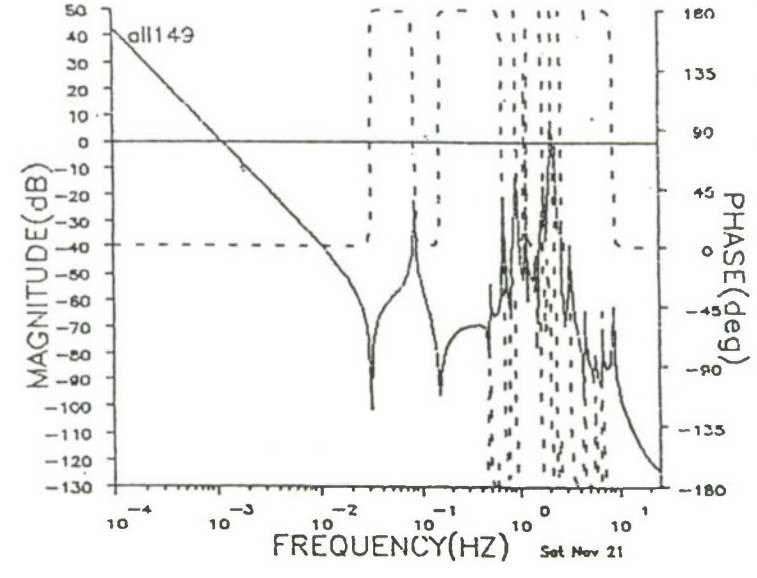


Figure 5.2-1d. Frequency Response from Pointing Gimbal Y to LOS Y.

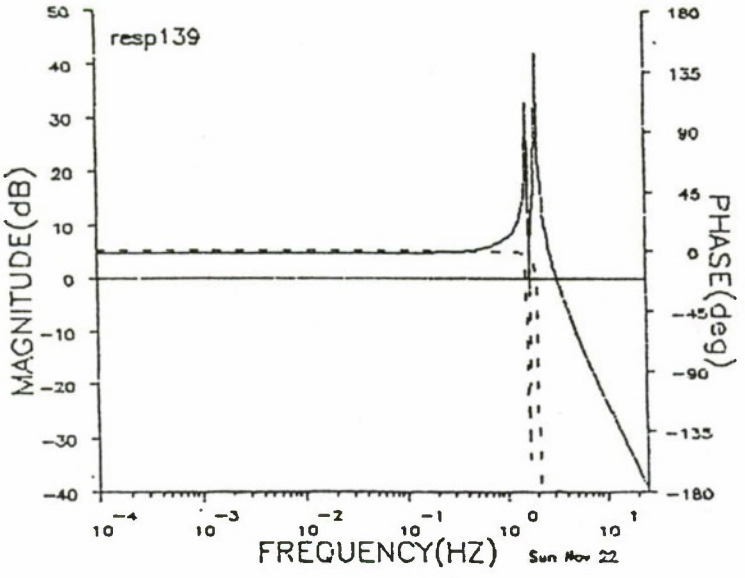


Figure 5.2-2a. Frequency Response from Pointing Gimbal X to LOS Y (3 Mode HAC Model)

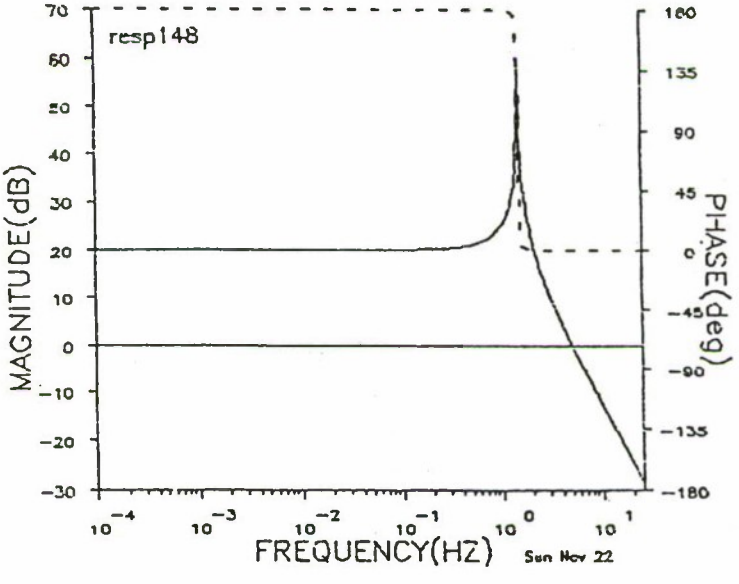


Figure 5.2-2b. Frequency Response from Pointing Gimbal X to LOS Y (3 Mode HAC Model).

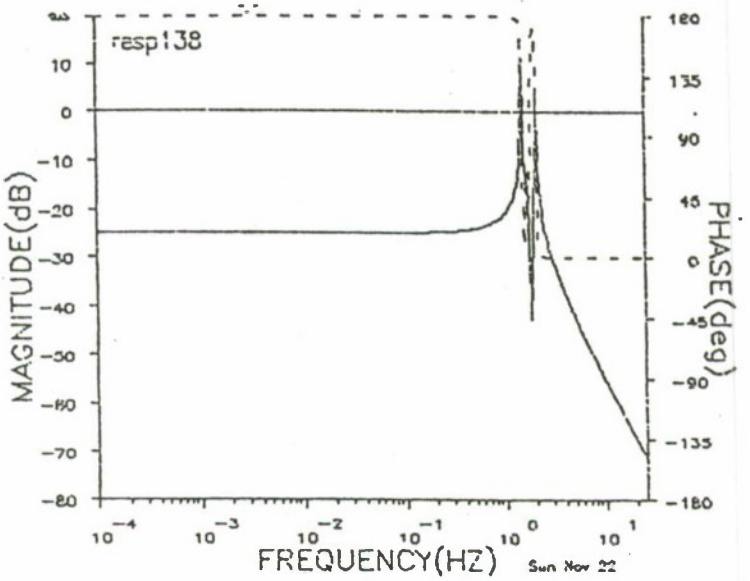


Figure 5.2-2c. Frequency Response from Pointing Gimbal X to LOS X (3 Mode HAC Model).

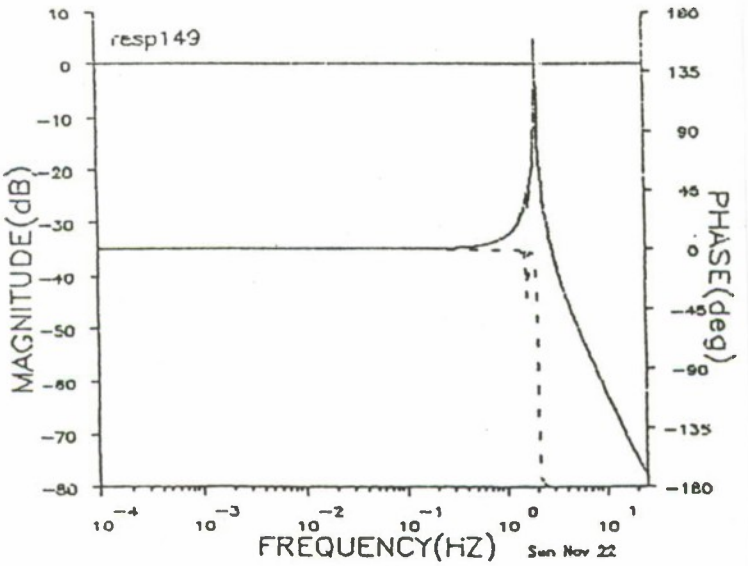


Figure 5.2-2d. Frequency Response from Pointing Gimbal Y to LOS Y (3 Mode HAC Model).

5.2.2 LAC Model Selection.

Choice of the LAC model hinges around the design technique as well as the objectives of the design. A collocated, consistent set of sensors and actuators is required if LAC is to exhibit its fullest robustness properties. In addition, the sensors must measure rates.

The only sensor/actuator pairs in the ACES configuration which strictly meet the requirements are the AGS gimbals and faceplate rate gyros. This set is almost exactly collocated because of the rigid nature of the AGS faceplate and gimbal hardware, and the axes of the gimbals and rate gyros are accurately aligned. In addition, the AGS torquers are wide bandwidth and respond all the way to dc on the low frequency end of the spectrum. The same is true for the rate gyros. An added attraction of the gimbal location is that most of the structural vibration can be sensed at this location. Figure 5.2-3 shows the three on-axis frequency responses of the AGS/Faceplate rate gyro system. Note the well behaved phase characteristic of these loops. The phase moves between positive and negative 90 degrees going through zero in between. For an infinite bandwidth sensor and actuator and a continuous controller, this system is theoretically stable for ANY negative feedback gain.

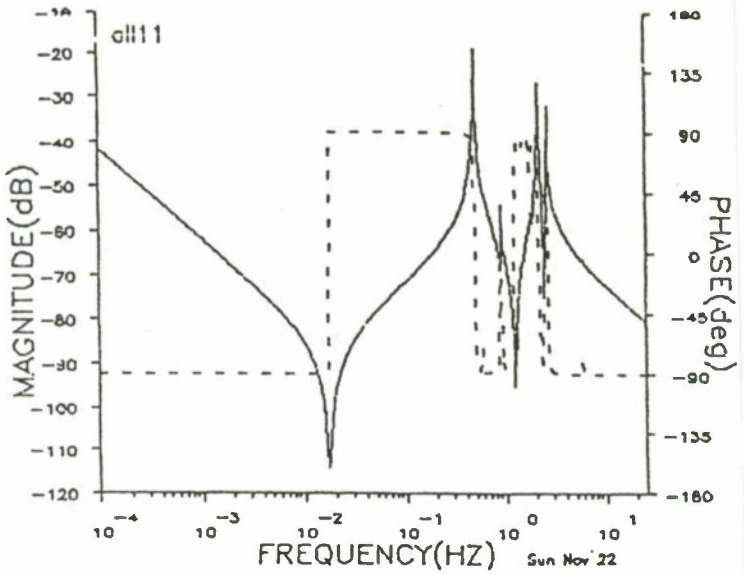


Figure 5.2-3a. Frequency Response from Gimbal X to Faceplate Gyro X.

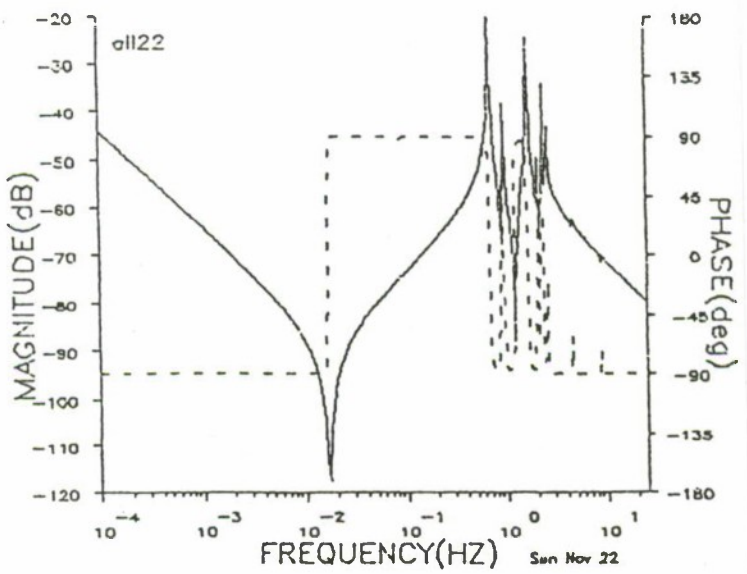


Figure 5.2-3b. Frequency Response from Gimbal Y to Faceplate Gyro Y.

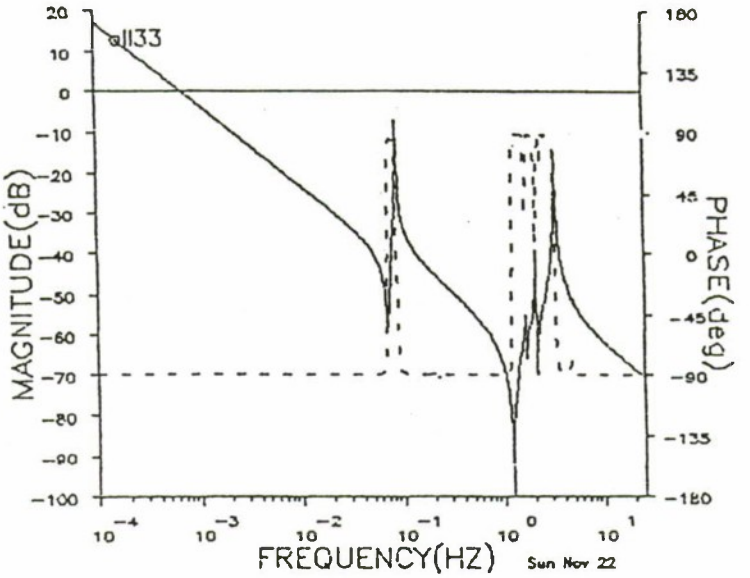


Figure 5.2-3c. Frequency Response from Gimbal Z to Faceplate Gyro Z.

The only other collocated consistent sensor/actuator pairs are the LMEDs and their collocated accelerometers. However, use of the LMEDs with the LAC design technique presents several unique problems.

A small, but obvious, consideration is that a rate measurement is required. It is reasonable to assume that the accelerometer outputs could be integrated to obtain translational rate measurements so this presents little difficulty.

Of much greater import is the noncollocated characteristic of the LMED sensor/actuator (S/A) pair. The LMED S/A pair is indeed physically collocated, but the centering spring on the LMED proof mass causes a distinct 180-degree phase shift in the input to output transfer function of each collocated LMED S/A pair. The proof mass together with the centering spring generate an "LMED mode" which sets the frequency of the phase shift. Figure 5.2-4 shows a typical LMED frequency response. In direct contrast to the AGS loops of Figure 5.2-3, the phase makes an abrupt shift of -180 degrees in the middle of the modal patch.

This phenomenon is NOT because of physical noncollocation but rather because the LMED is NOT a force actuator at low frequencies. To understand this physically, imagine that the LMED is commanded to provide a small constant force. After any transients have died, the centering spring is compressed so that it reacts with a force equal to the commanded force (provided by the motor) and the LMED provides a net force on the structure of zero. This is to say, the LMED has an effective lower frequency limit set by the proof mass and centering spring as well as an upper frequency limit set by the sensor bandwidth and motor electronics bandwidth.

All of this is, of course, no great surprise, as any proof mass type actuator has a low frequency operational limit dictated by the travel limits on the proof mass. If the centering springs were removed from the LMEDs, the linear model would exhibit perfectly collocated behavior, but the proof mass would probably hit the stops when the control system was implemented in the lab. If this low frequency limit is lower than the lowest frequency mode in the input to output transfer function, there is no problem as the actuator "acts like" an actuator over the range of interest. However, for the ACES problem the LMED modal frequency is among the frequencies of the bending modes which are to be damped. Not only is the LMED modal frequency within this modal "patch", the modal frequencies of the structure are highly uncertain in this frequency range. This causes extreme sensitvity problems for controller design. These sensitivity problems are not unique to LAC.

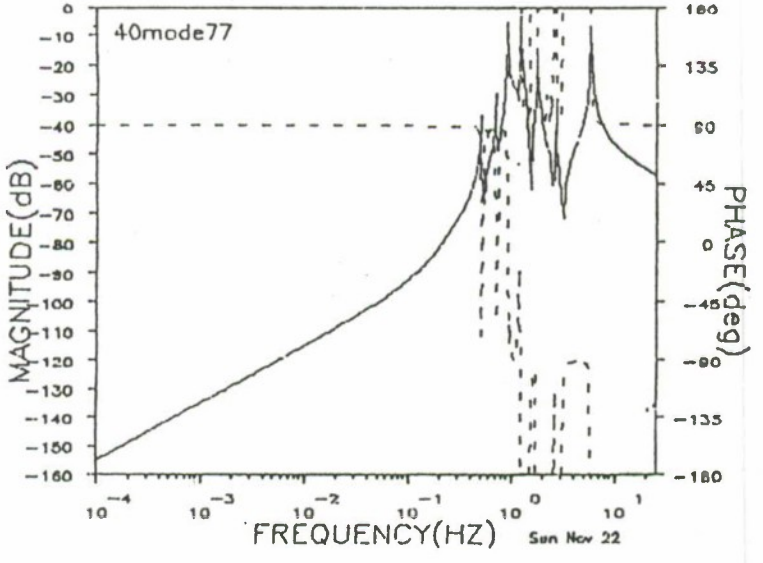


Figure 5.2-4. Typical LMED Frequency Response from LMED to LMED Accelerometer.

5.3 Design Process.

The design process for ACES is discussed in three parts. These are the HAC process, the LAC process, and HAC/LAC post analysis. The following sections address these three topics.

5.3.1 HAC Design.

Application of the HAC design process to the ACES problem requires extensive use of the computer and software. It should be remembered that even "small" LSS problems do not allow for manual handling of any data or any manual design steps. The design scenario is one of human interaction with design software. The efficiency of this interface is of paramount importance to successful completion of a controller design.

The HAC design may be performed in the continuous domain and then transformed to the digital domain for implementation. However, this approximation is dangerous, particularly for structural models which are always truncated and, therefore, have the potential for instability due to unmodeled high frequency modes. The greatest danger is presented by the phase lag due to the computational delay of one sample period. This phase lag may be approximated in the continuous design plant by inserting filters; however, design in the digital domain is the most straightforward way to deal with the digital nature of the control problem.

Although a continuous design was performed as a preliminary exercise to establish performance goals and validate the model and procedures, the HAC design for ACES was performed in the digital domain. This automatically includes two important effects: (1) phase lag effects of the zero order hold, and (2) phase lag effects of the computational delay. Inclusion of these effects addresses the HAC model from the robustness point of view. If they are not included, the design may be much too ambitious for the given physical constraints, i.e., sampling frequency and computational delay, because the design process does not "know" about the constraints. Design in the digital domain gives the LQG design process more information about the plant to be controlled.

As established in Section 5.2.1, the HAC controller must be capable of rejecting the dc disturbance due to rigid body translation of the entire structure at the BET. This is to say the IMC control loops must be of at least Type I, i.e., each channel contains one free integrator so that the error signal is integrated and must be driven to exactly zero to maintain stability.

The HAC model must be augmented to include the free integrators so that the resulting control system will be Type I in each axis. The HAC design model as presented to the LQG design process is shown in Figure 5.3-1. It includes the discretized sixth order HAC design model, two pure delays to represent the computational delay, and two first order integrators (trapezoidal). The resulting system has two inputs (torques) and four outputs (LOS errors and their integrals). The integrators must be included from the beginning, because the full-state feedback gain matrix must stabilize the states generated by the integrators as well as the plant dynamics and delays.

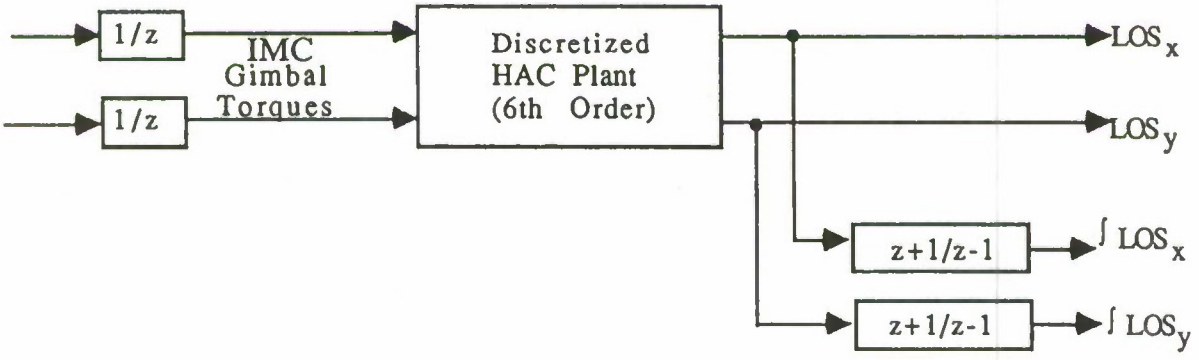


Figure 5.3-1. Discrete HAC Design Model.

The adjustable design parameters for the HAC feedback control gain design include the following:

Q - State weighting matrix (10 x 10)

R - Control input weighting matrix (2 x 2).

The adjustable design parameters for the Kalman Filter design include:

G - State weighting matrix (10 x 10)
H - Output weighting matrix (4 x 4).

These matrices define the set of numbers to be varied in iteration of the design. They are usually assumed to be diagonal and often of the form

$$A = \alpha I$$

where I is an identity matrix for simplicity.

Because LOS is the desired performance design parameter, it is of interest to include the influence of LOS directly in the choice of Q and/or R. An appropriate distribution of state weighting in terms of output measurements can be computed simply by defining an output weighting matrix Q' and requiring

$$Q = C^T Q' C$$

where C is the system output matrix. In this way Q' is chosen to directly penalize LOS error, and the penalty is distributed to the states for use in the design. This technique generated desirable transient performance with much less iteration than trial and error choices of Q.

The following steps are performed at the beginning of the design.

- Discretize the HAC model
- Augment the model with delays and integrators to form the LQR design model

The following steps are performed on each iteration of the controller design.

- Form state weighting matrix ($Q = C^T Q' C$)
- Compute the optimal feedback gain matrix (K)
- Compute the Kalman Filter gain matrix
    - Form the closed loop system with set point inputs using the design plant
- Compute the step response of the system

The closed loop plant with set points is configured as shown in Fig. 5.3-2.

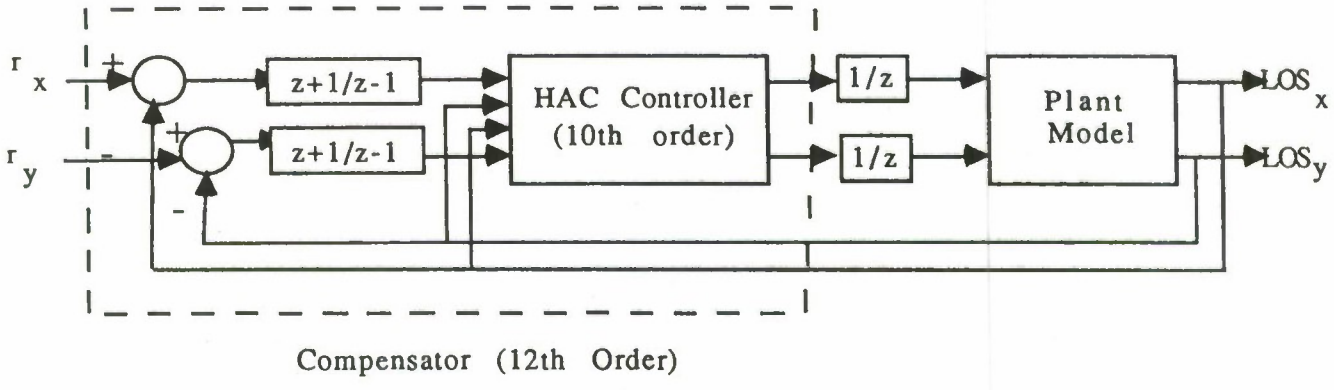


Figure 5.3-2. Closed Loop HAC System with Set Point Inputs.

The following steps are the first level of post analysis. They are performed after a suitable design is achieved with the steps above.

- Form the closed loop system with set points using the full order system
- Evaluate the system by computing:
    -- Step response
    -- Closed loop pole locations
    -- Closed loop frequency responses from command to measurement.

This post analysis may show the need to redesign the IMC controller for greater robustness, i.e., relax the performance requirements.

To give the reader a feel for the procedure, numerical values, and performance of the final HAC system, the following step by step account of the HAC procedure with actual numerical values and results is provided.

The 'output' weighting matrix for the HAC design is

$$Q' = \begin{bmatrix} 0.0 & 0.0 & 0.0 & 0.0 \\ 0.0 & 0.0 & 0.0 & 0.0 \\ 0.0 & 0.0 & 100.0 & 0.0 \\ 0.0 & 0.0 & 0.0 & 10.0 \end{bmatrix}$$

Only the integral outputs are penalized which places the control emphasis on steady state error performance.

The actual state weighting matrix is

$$Q = C^T Q' C = \begin{bmatrix} 0.0 & 0.0 & 0.0 & 0.0 & 0.0 & 0.0 & 0.0 & 0.0 & 0.0 & 0.0 \\ 0.0 & 0.0 & 0.0 & 0.0 & 0.0 & 0.0 & 0.0 & 0.0 & 0.0 & 0.0 \\ 0.0 & 0.0 & 0.0 & 0.0 & 0.0 & 0.0 & 0.0 & 0.0 & 0.0 & 0.0 \\ 0.0 & 0.0 & 0.0 & 0.0 & 0.0 & 0.0 & 0.0 & 0.0 & 0.0 & 0.0 \\ 0.0 & 0.0 & 0.0 & 0.0 & 0.0 & 0.0 & 0.0 & 0.0 & 0.0 & 0.0 \\ 0.0 & 0.0 & 0.0 & 0.0 & 0.0 & 0.0 & 0.0 & 0.0 & 0.0 & 0.0 \\ 0.0 & 0.0 & 0.0 & 0.0 & 0.0 & 0.0 & 100.0 & 0.0 & 100.0 & 0.0 \\ 0.0 & 0.0 & 0.0 & 0.0 & 0.0 & 0.0 & 0.0 & 10.0 & 0.0 & 10.0 \\ 0.0 & 0.0 & 0.0 & 0.0 & 0.0 & 0.0 & 100.0 & 0.0 & 100.0 & 0.0 \\ 0.0 & 0.0 & 0.0 & 0.0 & 0.0 & 0.0 & 0.0 & 10.0 & 0.0 & 10.0 \end{bmatrix}$$

The control weighting matrix is

$$R = \begin{bmatrix} 100.0 & 0.0 \\ 0.0 & 100.0 \end{bmatrix}$$

Application of the LQG design technique using Q' and R as weighting matrices and the HAC design plant as described above results in the following constant full state feedback gain matrix.

K =

row	col	1	2	3	4	5	6
1		-.2142E+03	-.7410E+01	-.7049E+00	-.1270E-02	-.2852E+01	-.4896E-01
2		-.8022E+00	-.6250E-01	.1511E+03	.5398E+01	.3150E+03	.1164E+02

	7	8	9	10
1	-.8080E-02	-.3539E+00	-.4000E-02	-.1752E+00
2	.1160E+01	-.4554E-02	.5740E+00	-.2254E-02

It is reassuring to note at this point that there are no extremely large values in the feedback gain matrix.

The next step is the design of the Kalman filter for estimation of the system states. The Kalman filter design proceeds with choice of the state and measurement weighting matrices. The state weighting matrix is

$$Q_{kal} = \begin{bmatrix} 9.0 & 0.0 & 0.0 & 0.0 & 0.0 & 0.0 & 0.0 & 0.0 & 0.0 & 0.0 \\ 0.0 & 9.0 & 0.0 & 0.0 & 0.0 & 0.0 & 0.0 & 0.0 & 0.0 & 0.0 \\ 0.0 & 0.0 & 9.0 & 0.0 & 0.0 & 0.0 & 0.0 & 0.0 & 0.0 & 0.0 \\ 0.0 & 0.0 & 0.0 & 9.0 & 0.0 & 0.0 & 0.0 & 0.0 & 0.0 & 0.0 \\ 0.0 & 0.0 & 0.0 & 0.0 & 9.0 & 0.0 & 0.0 & 0.0 & 0.0 & 0.0 \\ 0.0 & 0.0 & 0.0 & 0.0 & 0.0 & 9.0 & 0.0 & 0.0 & 0.0 & 0.0 \\ 0.0 & 0.0 & 0.0 & 0.0 & 0.0 & 0.0 & 9.0 & 0.0 & 0.0 & 0.0 \\ 0.0 & 0.0 & 0.0 & 0.0 & 0.0 & 0.0 & 0.0 & 9.0 & 0.0 & 0.0 \\ 0.0 & 0.0 & 0.0 & 0.0 & 0.0 & 0.0 & 0.0 & 0.0 & 9.0 & 0.0 \\ 0.0 & 0.0 & 0.0 & 0.0 & 0.0 & 0.0 & 0.0 & 0.0 & 0.0 & 9.0 \end{bmatrix}.$$

The measurement weighting matrix is

$$R_{kal} = \begin{bmatrix} 1.0 & 0.0 & 0.0 & 0.0 \\ 0.0 & 1.0 & 0.0 & 0.0 \\ 0.0 & 0.0 & 1.0 & 0.0 \\ 0.0 & 0.0 & 0.0 & 1.0 \end{bmatrix}.$$

Application of the steady state Kalman filter design algorithm to the HAC design plant using the weighting matrices shown results in the Kalman filter gain matrix

$$K_{kal} = \begin{bmatrix} -.7115E\text{-}04 & .5758E\text{-}02 & -.5925E\text{-}05 & .4368E\text{-}03 \\ -.1172E\text{-}04 & -.1797E\text{-}01 & .1121E\text{-}04 & -.2381E\text{-}02 \\ .2305E\text{-}02 & -.2645E\text{-}04 & -.1729E\text{-}04 & -.1631E\text{-}05 \\ -.1125E+00 & .2861E\text{-}03 & -.9346E\text{-}02 & .2824E\text{-}04 \\ .1124E\text{-}01 & -.3108E\text{-}04 & .8750E\text{-}03 & -.2328E\text{-}05 \\ -.8949E\text{-}03 & .8031E\text{-}04 & -.3454E\text{-}02 & .1577E\text{-}04 \\ .9472E+00 & -.1525E\text{-}04 & .7270E\text{-}01 & .6089E\text{-}05 \\ .4552E\text{-}03 & .9268E+00 & .4029E\text{-}05 & .7347E\text{-}01 \\ .1000E+01 & .1168E\text{-}06 & .1000E+01 & -.1435E\text{-}10 \\ .1168E\text{-}06 & .1000E+01 & -.1157E\text{-}10 & .1000E+01 \end{bmatrix}$$

This completes the actual HAC design process. At this point the HAC system as designed is ready for evaluation at the first level. A reasonable means of testing the performance of the system as designed is computation of a step response of the closed loop system. Because the system was designed in the z-domain, the step response may be computed by simply evaluating the matrix difference equation of the closed loop system.

A step response of the IMC system as designed, i.e., the design plant together with the controller, is shown in Fig. 5.3-3. Unit step inputs are applied to both position command inputs simultaneously. The response is nicely behaved with a rise time of about one second. Faster responses can be achieved but the with more ambitious choices of state weighting and lower control input weighting, but this is at the expense of robustness of the controller.

That the controller performs well on the plant for which it was designed is to be expected. Performance of the controller when closed with the full order plant is of interest because this checks for the effects of spillover. The step response of the closed loop IMC system with the full order (43 mode) plant is shown in Fig. 5.3-4. The system remains stable which is an indication of the minimal effects of spillover on this controller.

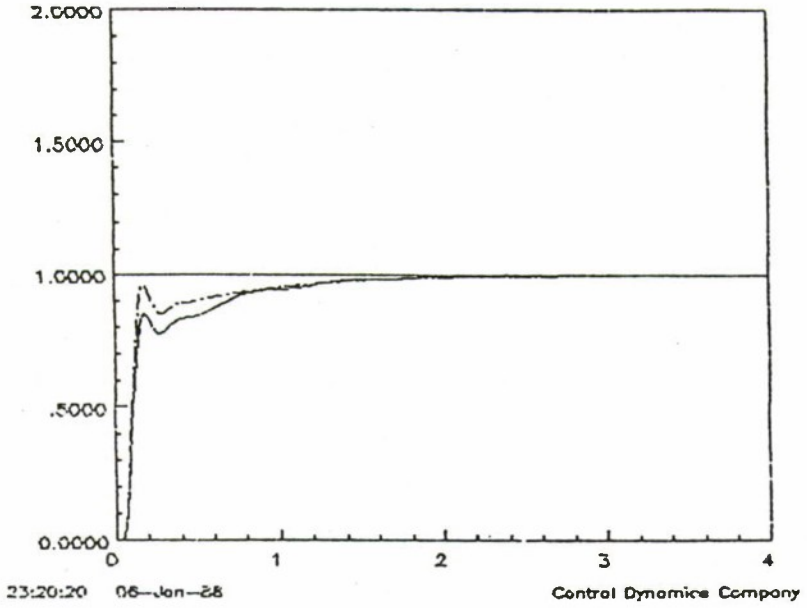


Figure 5.3-3. IMC System Responses from Design Plant.

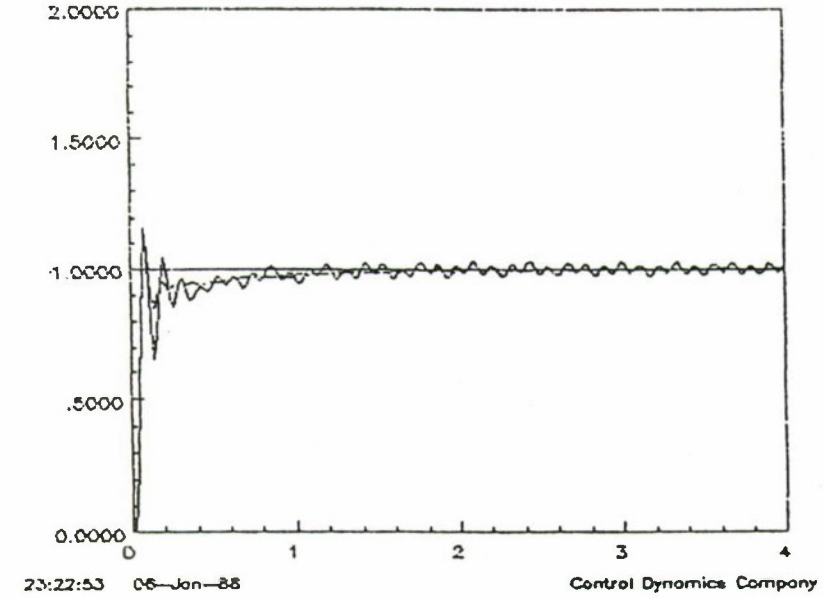


Figure 5.3-4. IMC System Step Responses from Full Order Plant.

5.3.2 LAC Design.

The LAC design process and post analysis include the following steps.

- Compute of the feedback gain matrix using the LAC plant.
- Form the continuous closed loop system using the gain matrix and the LAC plant and examine the poles.
- Form the continuous closed loop system using the gain matrix and the full order plant and examine the poles.
- Form the digital closed loop system with delays using the gain matrix and the full order plant and examine the poles.

The desired root shifts are given in Table 5.3-1. The desired root shifts amount to eight percent damping because with the simple approach used the structure is assumed to have no damping. The weights may seem large but they are appropriate when the size of the modal gains is considered.

TABLE 5.3-1. LAC CONTROLLER DESIGN DESIRED SHIFTS AND WEIGHTS

Desired Shift	Weighting
0.08	1.0d14
0.08	1.0d14
0.08	1.0d14
0.08	1.0d14
0.08	1.0d14
0.08	1.0d14
0.08	1.0d14
0.08	1.0d14
0.08	1.0d14
0.08	1.0d14
0.08	1.0d14

The LAC design input data is set to use only the control gains between the collocated sensor/actuator pairs. This means that no cross axis terms will be introduced because of the LAC controller design. The cross axis terms were tried but resulted in little performance improvement over using only the three on axis gains and definitely decreased the robustness of the design. The resulting control gain matrix is

$$C=\begin{bmatrix} 31.442477762924760 & 0.0 & 0.0 \\ 0.0 & 33.958538287082234 & 0.0 \\ 0.0 & 0.0 & 96.709233373053223 \end{bmatrix}.$$

It is reassuring at this point to see no extremely large (or small) values in this matrix. The off diagonal terms are zero, indicative of the design requiring no cross axis gains in the controller.

The LAC design plant is then closed with the gain matrix (all continuous because the design is in the continuous domain) and the poles of the resulting system computed as shown in Table 5.3-2. The system is more damped than when it started, but does not exhibit the eight percent damping desired by the design. At this point it is useful to remember that the design algorithm as used in this case is an approximation. To perform the LAC design and get exactly what is asked for, one must use the more complicated and computationally intensive general LAC algorithm for plants already having some damping. At any rate, some damping is achieved and is somewhat arbitrary based on the design input parameters: pole shifts and weightings. A more ambitious approach to damping was avoided because of concerns with the stability of the system once the sampling and computational delay lags were included.

TABLE 5.3-2. POLES OF CONTINUOUS LAC PLANT CLOSED WITH LAC CONTROLLER

real part	imaginary part	zeta	omega	freq(Hz)
-.1523424E+00	-.1677631E+02	+.9080429E-02	+.1677700E+02	+.2670137E+01
-.1523424E+00	+.1677631E+02	+.9080429E-02	+.1677700E+02	+.2670137E+01
-.1001880E+00	+.1622828E+02	+.6173548E-02	+.1622859E+02	+.2582854E+01
-.1001880E+00	-.1622828E+02	+.6173548E-02	+.1622859E+02	+.2582854E+01
-.1280300E+00	+.1470729E+02	+.8704878E-02	+.1470785E+02	+.2340822E+01
-.1280300E+00	-.1470729E+02	+.8704878E-02	+.1470785E+02	+.2340822E+01
-.1707258E+00	-.1367000E+02	+.1248811E-01	+.1367107E+02	+.2175813E+01
-.1707258E+00	+.1367000E+02	+.1248811E-01	+.1367107E+02	+.2175813E+01
-.1436067E+00	-.1306002E+02	+.1099524E-01	+.1306081E+02	+.2078687E+01
-.1436067E+00	+.1306002E+02	+.1099524E-01	+.1306081E+02	+.2078687E+01
-.7280672E-01	+.3140482E+01	+.2317706E-01	+.3141326E+01	+.4999564E+00
-.7280672E-01	-.3140482E+01	+.2317706E-01	+.3141326E+01	+.4999564E+00
-.1682123E+00	+.1050761E+02	+.1600656E-01	+.1050896E+02	+.1672549E+01
-.1682123E+00	-.1050761E+02	+.1600656E-01	+.1050896E+02	+.1672549E+01
-.3931782E-01	+.7855902E+01	+.5004814E-02	+.7856000E+01	+.1250318E+01
-.3931782E-01	-.7855902E+01	+.5004814E-02	+.7856000E+01	+.1250318E+01
-.9407463E-01	-.4345433E+01	+.2164401E-01	+.4346451E+01	+.6917576E+00
-.9407463E-01	+.4345433E+01	+.2164401E-01	+.4346451E+01	+.6917576E+00
-.3167742E-01	-.5779884E+01	+.5480550E-02	+.5779971E+01	+.9199088E+00
-.3167742E-01	+.5779884E+01	+.5480550E-02	+.5779971E+01	+.9199088E+00
-.4265733E-01	-.6047474E+01	+.7053567E-02	+.6047624E+01	+.9625071E+00
-.4265733E-01	+.6047474E+01	+.7053567E-02	+.6047624E+01	+.9625071E+00

The continuous closed loop system formed by the LAC controller and the full order plant is formed for inspection of the pole locations. The poles are shown in Table 5.3-3. The plant is assumed to have half a percent damping initially for realism. Note that the damping is augmented by the LAC controller and is not reduced in any case, which is to be expected for a system with collocation and infinite bandwidth sensors and actuators.

TABLE 5.3-3. POLES OF CONTINUOUS FULL ORDER PLANT CLOSED WITH LAC CONTROLLER.
(Plant had 0.5% Damping Initially.)

real part	imaginary part	zeta	omega	freq(Hz)
-.2756965E+00	+.5512931E+02	+.5000843E-02	+.5513000E+02	+.8774191E+01
-.2756965E+00	-.5512931E+02	+.5000843E-02	+.5513000E+02	+.8774191E+01
-.2779248E+00	+.5539929E+02	+.5016695E-02	+.5539999E+02	+.8817162E+01
-.2779248E+00	-.5539929E+02	+.5016695E-02	+.5539999E+02	+.8817162E+01
-.2172862E+00	-.4344946E+02	+.5000832E-02	+.4345000E+02	+.6915266E+01
-.2172862E+00	+.4344946E+02	+.5000832E-02	+.4345000E+02	+.6915266E+01
-.1838325E+00	+.3666953E+02	+.5013159E-02	+.3666999E+02	+.5836197E+01
-.1838325E+00	-.3666953E+02	+.5013159E-02	+.3666999E+02	+.5836197E+01
-.1681500E+00	-.3362958E+02	+.5000000E-02	+.3363000E+02	+.5352368E+01
-.1681500E+00	+.3362958E+02	+.5000000E-02	+.3363000E+02	+.5352368E+01
-.1459014E+00	+.2877952E+02	+.5069560E-02	+.2877989E+02	+.4580451E+01
-.1459014E+00	-.2877952E+02	+.5069560E-02	+.2877989E+02	+.4580451E+01
-.1539972E+00	+.2958804E+02	+.5204642E-02	+.2958844E+02	+.4709135E+01
-.1539972E+00	-.2958804E+02	+.5204642E-02	+.2958844E+02	+.4709135E+01
-.1479006E+00	-.2957963E+02	+.5000021E-02	+.2958000E+02	+.4707792E+01
-.1479006E+00	+.2957963E+02	+.5000021E-02	+.2958000E+02	+.4707792E+01
-.1479000E+00	-.2957963E+02	+.5000000E-02	+.2958000E+02	+.4707792E+01
-.1479000E+00	+.2957963E+02	+.5000000E-02	+.2958000E+02	+.4707792E+01
-.1927773E+01	-.2063655E+02	+.9301053E-01	+.2072640E+02	+.3298701E+01
-.1927773E+01	+.2063655E+02	+.9301053E-01	+.2072640E+02	+.3298701E+01
-.1039500E+00	+.2078974E+02	+.5000000E-02	+.2079000E+02	+.3308824E+01
-.1039500E+00	-.2078974E+02	+.5000000E-02	+.2079000E+02	+.3308824E+01
-.1039000E+00	+.2077974E+02	+.5000000E-02	+.2078000E+02	+.3307232E+01
-.1039000E+00	-.2077974E+02	+.5000000E-02	+.2078000E+02	+.3307232E+01
-.1523383E+00	-.1677627E+02	+.9080210E-02	+.1677696E+02	+.2670130E+01
-.1523383E+00	+.1677627E+02	+.9080210E-02	+.1677696E+02	+.2670130E+01
-.1001595E+00	-.1622847E+02	+.6171718E-02	+.1622878E+02	+.2582885E+01
-.1001595E+00	+.1622847E+02	+.6171718E-02	+.1622878E+02	+.2582885E+01
-.1279111E+00	-.1470848E+02	+.8696090E-02	+.1470904E+02	+.2341011E+01
-.1279111E+00	+.1470848E+02	+.8696090E-02	+.1470904E+02	+.2341011E+01
-.1707289E+00	-.1366993E+02	+.1248840E-01	+.1367100E+02	+.2175802E+01
-.1707289E+00	+.1366993E+02	+.1248840E-01	+.1367100E+02	+.2175802E+01
-.1418600E+00	+.1307153E+02	+.1085195E-01	+.1307230E+02	+.2080517E+01

real part	imaginary part	zeta	omega	freq(Hz)
-.1418600E+00	-.1307153E+02	+.1085195E-01	+.1307230E+02	+.2080517E+01
-.5957887E-01	-.1163990E+02	+.5118436E-02	+.1164005E+02	+.1852568E+01
-.5957887E-01	+.1163990E+02	+.5118436E-02	+.1164005E+02	+.1852568E+01
-.5759640E-01	+.1107971E+02	+.5198295E-02	+.1107986E+02	+.1763411E+01
-.5759640E-01	-.1107971E+02	+.5198295E-02	+.1107986E+02	+.1763411E+01
-.1682318E+00	+.1050831E+02	+.1600736E-01	+.1050965E+02	+.1672659E+01
-.1682318E+00	-.1050831E+02	+.1600736E-01	+.1050965E+02	+.1672659E+01
-.6045000E-01	-.1208985E+02	+.5000000E-02	+.1209000E+02	+.1924179E+01
-.6045000E-01	+.1208985E+02	+.5000000E-02	+.1209000E+02	+.1924179E+01
-.4738254E-01	+.9456882E+01	+.5010314E-02	+.9457001E+01	+.1505125E+01
-.4738254E-01	-.9456882E+01	+.5010314E-02	+.9457001E+01	+.1505125E+01
-.1182910E+00	+.5352883E+00	+.2157796E+00	+.5482028E+00	+.8724898E-01
-.1182910E+00	-.5352883E+00	+.2157796E+00	+.5482028E+00	+.8724898E-01
-.3690351E-01	+.7372908E+01	+.5005223E-02	+.7373000E+01	+.1173447E+01
-.3690351E-01	-.7372908E+01	+.5005223E-02	+.7373000E+01	+.1173447E+01
-.3694483E-01	+.7385908E+01	+.5002007E-02	+.7386000E+01	+.1175516E+01
-.3694483E-01	-.7385908E+01	+.5002007E-02	+.7386000E+01	+.1175516E+01
-.3872512E-01	-.7744903E+01	+.5000015E-02	+.7745000E+01	+.1232652E+01
-.3872512E-01	+.7744903E+01	+.5000015E-02	+.7745000E+01	+.1232652E+01
-.3896510E-01	-.7792903E+01	+.5000012E-02	+.7793000E+01	+.1240292E+01
-.3896510E-01	+.7792903E+01	+.5000012E-02	+.7793000E+01	+.1240292E+01
-.3931782E-01	+.7855902E+01	+.5004814E-02	+.7856000E+01	+.1250318E+01
-.3931782E-01	-.7855902E+01	+.5004814E-02	+.7856000E+01	+.1250318E+01
-.4265230E-01	-.6047398E+01	+.7052824E-02	+.6047549E+01	+.9624950E+00
-.4265230E-01	+.6047398E+01	+.7052824E-02	+.6047549E+01	+.9624950E+00
-.3167740E-01	-.5779876E+01	+.5480554E-02	+.5779963E+01	+.9199075E+00
-.3167740E-01	+.5779876E+01	+.5480554E-02	+.5779963E+01	+.9199075E+00
-.7281292E-01	-.3140541E+01	+.2317860E-01	+.3141385E+01	+.4999658E+00
-.7281292E-01	+.3140541E+01	+.2317860E-01	+.3141385E+01	+.4999658E+00
-.9894349E-01	-.4349723E+01	+.2274120E-01	+.4350848E+01	+.6924573E+00
-.9894349E-01	+.4349723E+01	+.2274120E-01	+.4350848E+01	+.6924573E+00
-.2539795E-01	-.4405749E+01	+.5764633E-02	+.4405822E+01	+.7012067E+00
-.2539795E-01	+.4405749E+01	+.5764633E-02	+.4405822E+01	+.7012067E+00
-.2259038E-01	-.4461731E+01	+.5063078E-02	+.4461788E+01	+.7101140E+00
-.2259038E-01	+.4461731E+01	+.5063078E-02	+.4461788E+01	+.7101140E+00
-.1901135E-01	+.3793958E+01	+.5010892E-02	+.3794006E+01	+.6038333E+00
-.1901135E-01	-.3793958E+01	+.5010892E-02	+.3794006E+01	+.6038333E+00
-.1938054E-01	+.3721053E+01	+.5208276E-02	+.3721104E+01	+.5922307E+00
-.1938054E-01	-.3721053E+01	+.5208276E-02	+.3721104E+01	+.5922307E+00
-.1919401E-01	+.3727896E+01	+.5148684E-02	+.3727945E+01	+.5933195E+00
-.1919401E-01	-.3727896E+01	+.5148684E-02	+.3727945E+01	+.5933195E+00
-.2976000E-01	-.5951926E+01	+.5000000E-02	+.5952000E+01	+.9472880E+00
-.2976000E-01	+.5951926E+01	+.5000000E-02	+.5952000E+01	+.9472880E+00
-.6045000E-01	+.1208985E+02	+.5000000E-02	+.1209000E+02	+.1924179E+01
-.6045000E-01	-.1208985E+02	+.5000000E-02	+.1209000E+02	+.1924179E+01
-.2976000E-01	+.5951926E+01	+.5000000E-02	+.5952000E+01	+.9472880E+00
-.2976000E-01	-.5951926E+01	+.5000000E-02	+.5952000E+01	+.9472880E+00

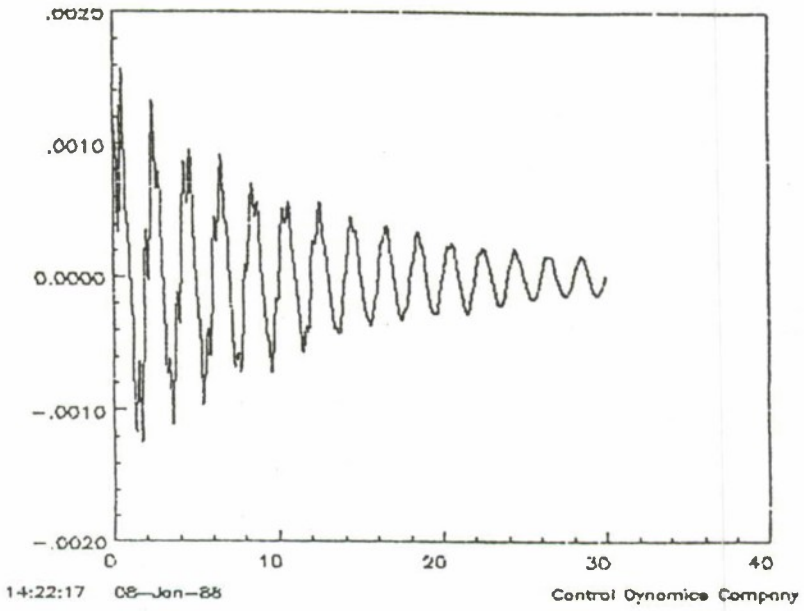
A more trying test of the controller is its closure with a digital plant of full order with the computational delay included. The poles of this system are shown in Table 5.3-4. The system is still solidly stable in this configuration.

TABLE 5.3-4. POLES OF DIGITAL FULL ORDER PLANT CLOSED WITH LAC CONTROLLER AND COMPUTATIONAL DELAY.

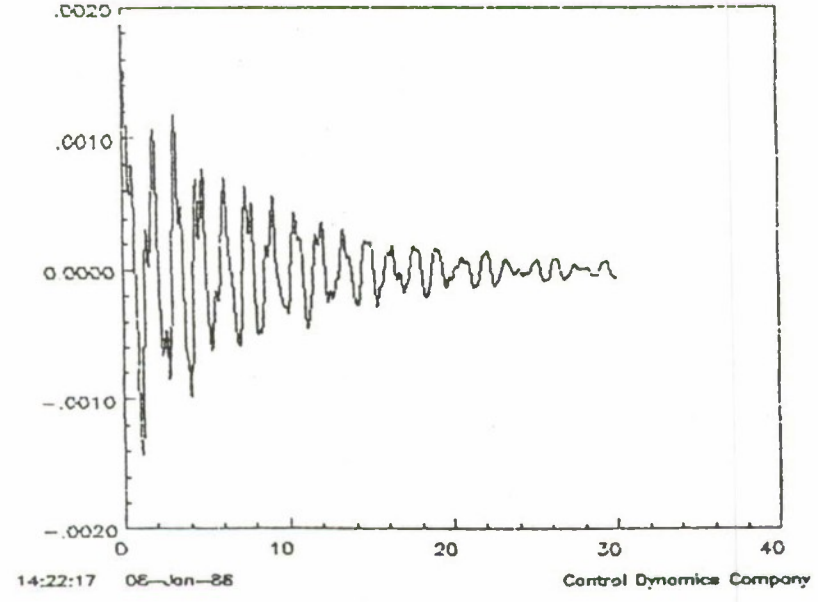
real part	imaginary part	zeta	omega	freq(Hz)
.4439826E+00	-.8898672E+00	-.4464484E+00	+.9944769E+00	+.1582755E+00
.4439826E+00	+.8898672E+00	-.4464484E+00	+.9944769E+00	+.1582755E+00
.4488078E+00	-.8874719E+00	-.4512888E+00	+.9945023E+00	+.1582796E+00
.4488078E+00	+.8874719E+00	-.4512888E+00	+.9945023E+00	+.1582796E+00
.9339036E-02	-.0000000E+00	-.1000000E+01	+.9339036E-02	+.1486350E-02
.1125147E-01	+.0000000E+00	-.1000000E+01	+.1125147E-01	+.1790724E-02
.8525804E-01	-.0000000E+00	-.1000000E+01	+.8525804E-01	+.1356921E-01
.6427991E+00	-.7603660E+00	-.6455983E+00	+.9956642E+00	+.1584645E+00
.6427991E+00	+.7603660E+00	-.6455983E+00	+.9956642E+00	+.1584645E+00
.7401807E+00	-.6669457E+00	-.7429032E+00	+.9963353E+00	+.1585713E+00
.7401807E+00	+.6669457E+00	-.7429032E+00	+.9963353E+00	+.1585713E+00
.7795835E+00	-.6209236E+00	-.7822097E+00	+.9966426E+00	+.1586202E+00
.7795835E+00	+.6209236E+00	-.7822097E+00	+.9966426E+00	+.1586202E+00
.8364184E+00	-.5427776E+00	-.8388533E+00	+.9970974E+00	+.1586926E+00
.8364184E+00	+.5427776E+00	-.8388533E+00	+.9970974E+00	+.1586926E+00
.8273341E+00	-.5562154E+00	-.8298869E+00	+.9969240E+00	+.1586650E+00
.8273341E+00	+.5562154E+00	-.8298869E+00	+.9969240E+00	+.1586650E+00
.8276019E+00	-.5560365E+00	-.8300536E+00	+.9970464E+00	+.1586845E+00
.8276019E+00	+.5560365E+00	-.8300536E+00	+.9970464E+00	+.1586845E+00
.8276019E+00	-.5560365E+00	-.8300536E+00	+.9970464E+00	+.1586845E+00
.8276019E+00	+.5560365E+00	-.8300536E+00	+.9970464E+00	+.1586845E+00
.8744589E+00	-.4093910E+00	-.9056625E+00	+.9655461E+00	+.1536711E+00
.8744589E+00	+.4093910E+00	-.9056625E+00	+.9655461E+00	+.1536711E+00
.9128957E+00	-.4030783E+00	-.9147956E+00	+.9979232E+00	+.1588240E+00
.9128957E+00	+.4030783E+00	-.9147956E+00	+.9979232E+00	+.1588240E+00
.9129772E+00	-.4028961E+00	-.9148763E+00	+.9979242E+00	+.1588242E+00
.9129772E+00	+.4028961E+00	-.9148763E+00	+.9979242E+00	+.1588242E+00
.9412433E+00	-.3289504E+00	-.9440098E+00	+.9970694E+00	+.1586881E+00
.9412433E+00	+.3289504E+00	-.9440098E+00	+.9970694E+00	+.1586881E+00
.9458521E+00	+.3184466E+00	-.9477283E+00	+.9980203E+00	+.1588395E+00
.9458521E+00	-.3184466E+00	-.9477283E+00	+.9980203E+00	+.1588395E+00
.9545409E+00	-.2896790E+00	-.9569063E+00	+.9975281E+00	+.1587612E+00
.9545409E+00	+.2896790E+00	-.9569063E+00	+.9975281E+00	+.1587612E+00
.9595224E+00	+.2699164E+00	-.9626377E+00	+.9967638E+00	+.1586395E+00
.9595224E+00	-.2699164E+00	-.9626377E+00	+.9967638E+00	+.1586395E+00
.9634074E+00	+.2582798E+00	-.9658918E+00	+.9974278E+00	+.1587452E+00
.9634074E+00	-.2582798E+00	-.9658918E+00	+.9974278E+00	+.1587452E+00

real part	imaginary part	zeta	omega	freq(Hz)
.9718661E+00	-.2304357E+00	-.9730226E+00	+.9988114E+00	+.1589654E+00
.9718661E+00	+.2304357E+00	-.9730226E+00	+.9988114E+00	+.1589654E+00
.9744224E+00	-.2195463E+00	-.9755451E+00	+.9988491E+00	+.1589714E+00
.9744224E+00	+.2195463E+00	-.9755451E+00	+.9988491E+00	+.1589714E+00
.9746503E+00	+.2086492E+00	-.9778444E+00	+.9967335E+00	+.1586347E+00
.9746503E+00	-.2086492E+00	-.9778444E+00	+.9967335E+00	+.1586347E+00
.9812364E+00	-.1878345E+00	-.9821666E+00	+.9990529E+00	+.1590038E+00
.9812364E+00	+.1878345E+00	-.9821666E+00	+.9990529E+00	+.1590038E+00
.9975636E+00	-.1071576E-01	-.9999423E+00	+.9976212E+00	+.1587760E+00
.9975636E+00	+.1071576E-01	-.9999423E+00	+.9976212E+00	+.1587760E+00
.9965707E+00	-.6278585E-01	-.9980213E+00	+.9985465E+00	+.1589232E+00
.9965707E+00	+.6278585E-01	-.9980213E+00	+.9985465E+00	+.1589232E+00
.9967435E+00	-.7577764E-01	-.9971226E+00	+.9996199E+00	+.1590941E+00
.9967435E+00	+.7577764E-01	-.9971226E+00	+.9996199E+00	+.1590941E+00
.9968388E+00	+.7446149E-01	-.9972218E+00	+.9996160E+00	+.1590935E+00
.9968388E+00	-.7446149E-01	-.9972218E+00	+.9996160E+00	+.1590935E+00
.9968460E+00	+.7432523E-01	-.9972319E+00	+.9996130E+00	+.1590930E+00
.9968460E+00	-.7432523E-01	-.9972319E+00	+.9996130E+00	+.1590930E+00
.9942530E+00	-.8692818E-01	-.9961997E+00	+.9980459E+00	+.1588436E+00
.9942530E+00	+.8692818E-01	-.9961997E+00	+.9980459E+00	+.1588436E+00
.9955705E+00	-.8907614E-01	-.9960212E+00	+.9995475E+00	+.1590826E+00
.9955705E+00	+.8907614E-01	-.9960212E+00	+.9995475E+00	+.1590826E+00
.9956052E+00	+.8795232E-01	-.9961207E+00	+.9994826E+00	+.1590722E+00
.9956052E+00	-.8795232E-01	-.9961207E+00	+.9994826E+00	+.1590722E+00
.9926963E+00	+.1152768E+00	-.9933249E+00	+.9993672E+00	+.1590539E+00
.9926963E+00	-.1152768E+00	-.9933249E+00	+.9993672E+00	+.1590539E+00
.9918431E+00	-.1205954E+00	-.9926892E+00	+.9991477E+00	+.1590189E+00
.9918431E+00	+.1205954E+00	-.9926892E+00	+.9991477E+00	+.1590189E+00
.9869060E+00	-.1563496E+00	-.9876823E+00	+.9992140E+00	+.1590295E+00
.9869060E+00	+.1563496E+00	-.9876823E+00	+.9992140E+00	+.1590295E+00
.9884179E+00	-.1468161E+00	-.9891477E+00	+.9992622E+00	+.1590371E+00
.9884179E+00	+.1468161E+00	-.9891477E+00	+.9992622E+00	+.1590371E+00
.9883789E+00	+.1470729E+00	-.9891095E+00	+.9992614E+00	+.1590370E+00
.9883789E+00	-.1470729E+00	-.9891095E+00	+.9992614E+00	+.1590370E+00
.9871091E+00	-.1551069E+00	-.9878787E+00	+.9992210E+00	+.1590306E+00
.9871091E+00	+.1551069E+00	-.9878787E+00	+.9992210E+00	+.1590306E+00
.9872623E+00	-.1541599E+00	-.9880273E+00	+.9992258E+00	+.1590314E+00
.9872623E+00	+.1541599E+00	-.9880273E+00	+.9992258E+00	+.1590314E+00
.9923325E+00	+.1186869E+00	-.9929233E+00	+.9994050E+00	+.1590599E+00
.9923325E+00	-.1186869E+00	-.9929233E+00	+.9994050E+00	+.1590599E+00
.9697361E+00	-.2391584E+00	-.9709093E+00	+.9987917E+00	+.1589623E+00
.9697361E+00	+.2391584E+00	-.9709093E+00	+.9987917E+00	+.1589623E+00
.9697361E+00	+.2391584E+00	-.9709093E+00	+.9987917E+00	+.1589623E+00
.9697361E+00	-.2391584E+00	-.9709093E+00	+.9987917E+00	+.1589623E+00
.9923325E+00	+.1186869E+00	-.9929233E+00	+.9994050E+00	+.1590599E+00
.9923325E+00	-.1186869E+00	-.9929233E+00	+.9994050E+00	+.1590599E+00

A check of the system performance in the time domain is provided by computing the step response of the full order digital LAC system and comparing it with the step response of the plant with half a percent damping. Fig.5.3-5 shows the rotational rate response at the AGS faceplate in each of the three axes to a simultaneous 'step' input in each axis. Fig. 5.3-6 shows the same response without the rate damping provided by the LAC controller. Comparison of the plots on a per axis basis shows considerable improvement in damping. This is deemed adequate in light of the fact that the HAC controller is robust to spillover of the structural modes into the IMC system, i.e., the LAC controller is not expected to stabilize the HAC design.

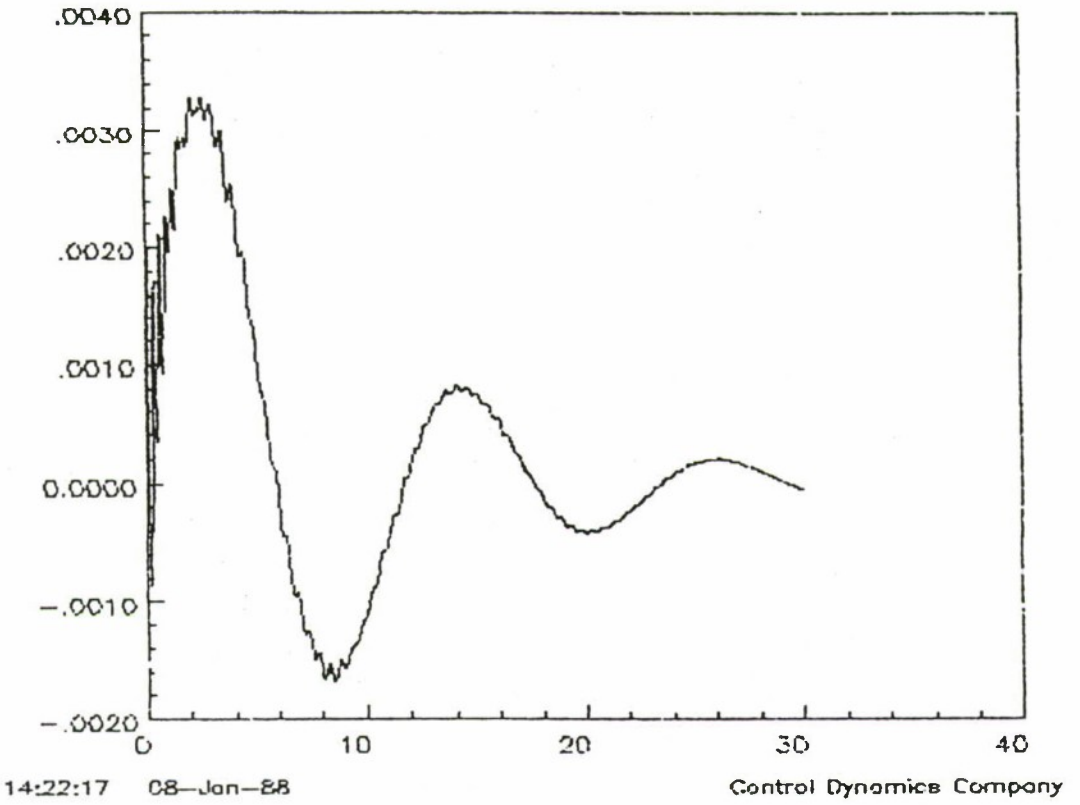


X-Axis



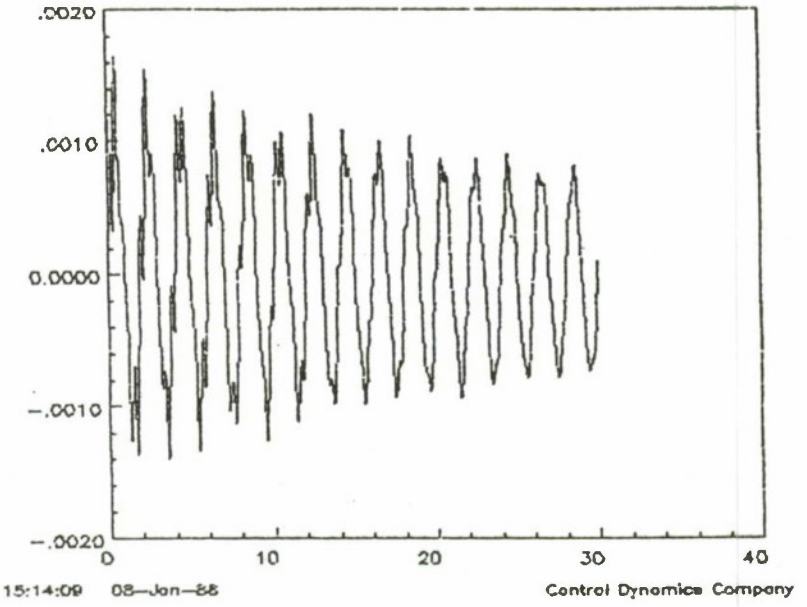
Y-Axis

Figure 5.3-5a. LAC Controller Faceplate Rate Responses to Step Inputs (X and Y Axes).

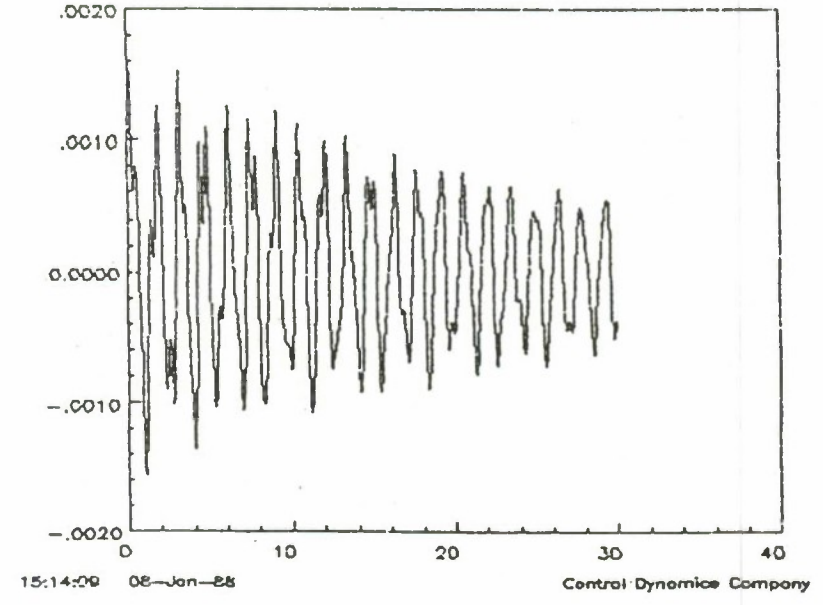


Z-Axis

Figure 5.3-5b. LAC Controller Faceplate Rate Response to Step Inputs (Z-Axis).

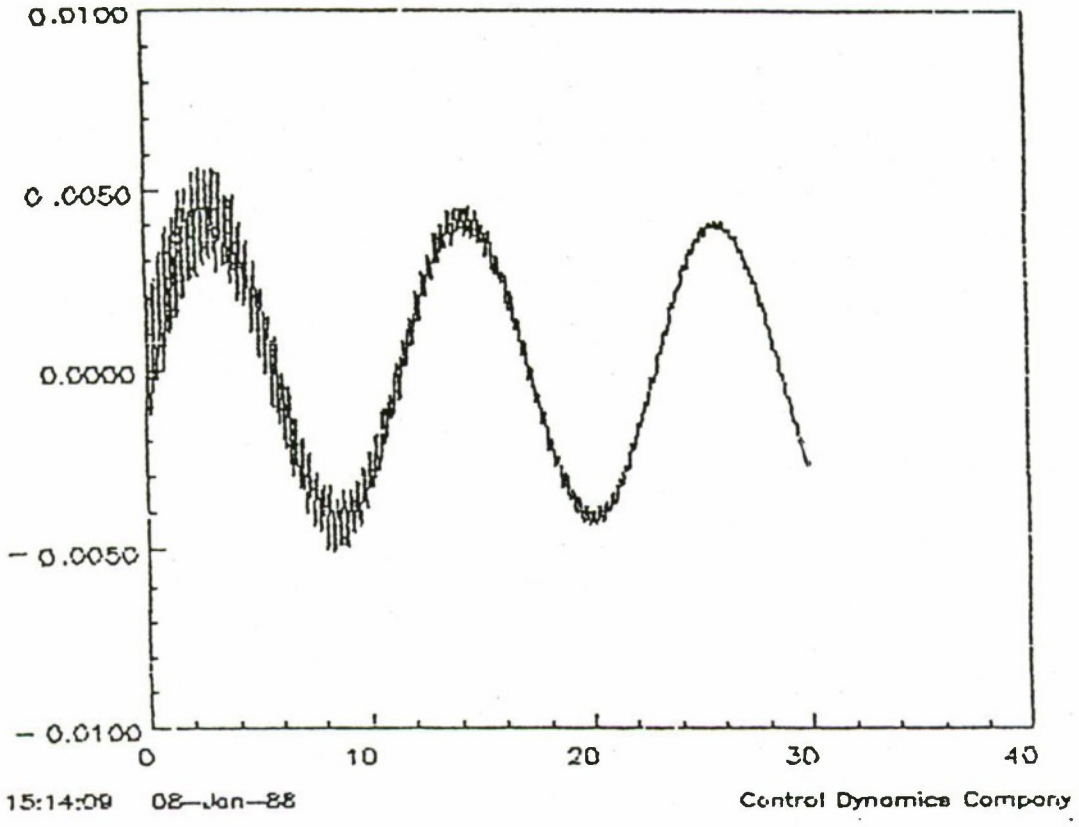


X-Axis



Y-Axis

Figure 5.3-6a. Open Loop Plant Faceplate Rate Responses to Step Inputs (X and Y Axes).



Z-Axis

Figure 5.3-6b. Open Loop Plant Faceplate Rate Responses to Step Inputs (Z-Axis).

5.4 Observations.

Before proceeding to the test results, several comments should be made regarding the design process and the expected results of the tests. It should be noted that HAC/LAC is not a design algorithm since the designer does not have a significant amount of freedom in achieving the design goals. In other words, HAC/LAC applied by different designers to different problems may lead to very different problem approaches.

The design process was easy to perform once the various issues of HAC goals, LAC goals, separate controller configuration, and LMED collocation were resolved. We expect that the controller will achieve significant performance gains in the hardware implementation unless the design assumptions are violated. The most critical of the design assumptions are the model fidelity in the IMC subsystem design and the assumption of relative isolation of the IMC components from the Astromast stabilization system.

5.5 Test Results.

The test sequence was carried out in the manner described in Section 2.2.1. The controller was subjected to the four disturbances described in Section 2.2.2. The following results illustrate that significant performance gains are precluded by the presence of unmodeled dominant LOS behavior and the very low level disturbances required to maintain the photodetector operation in a linear range.

The open loop faceplate angular rate response and the closed loop angular rates are shown in Figures 5.5-1 and 5.5-2, respectively, for the RCS disturbance applied in the x-axis. The angular rates are very low level, due to the constraints the detector places on the BET disturbance levels. The main problem with these disturbances is that the angular rates at the faceplate are used to achieve literally all of the stabilization of the Astromast structure. Since the low level signals at the faceplate effectively lead to periods of open loop Astromast control, the results at the detector are not surprising. The open loop and closed loop RCS detector responses are given in Figures 5.5-3 and 5.5-4 for the open loop

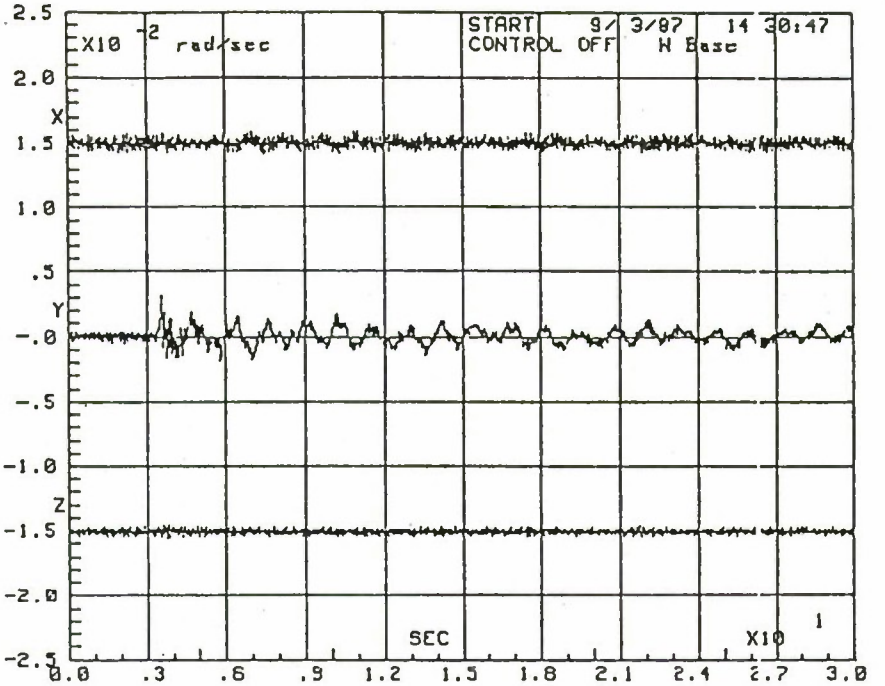


Figure 5.5-1. Open Loop Response at the Faceplate Gyros due to the RCS Disturbance.

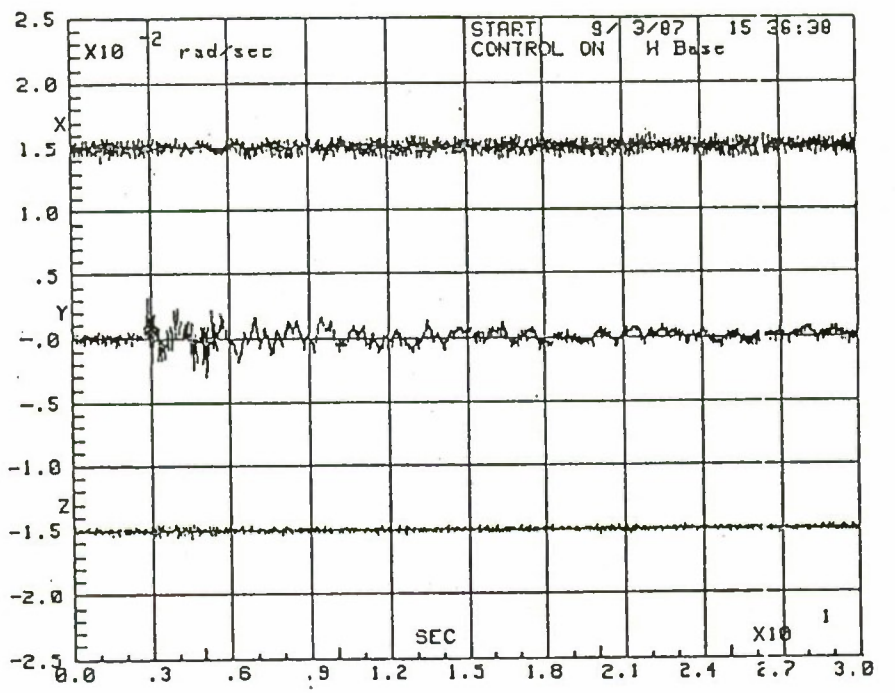


Figure 5.5-2. Closed Loop Gyro Response due to the RCS Disturbance.

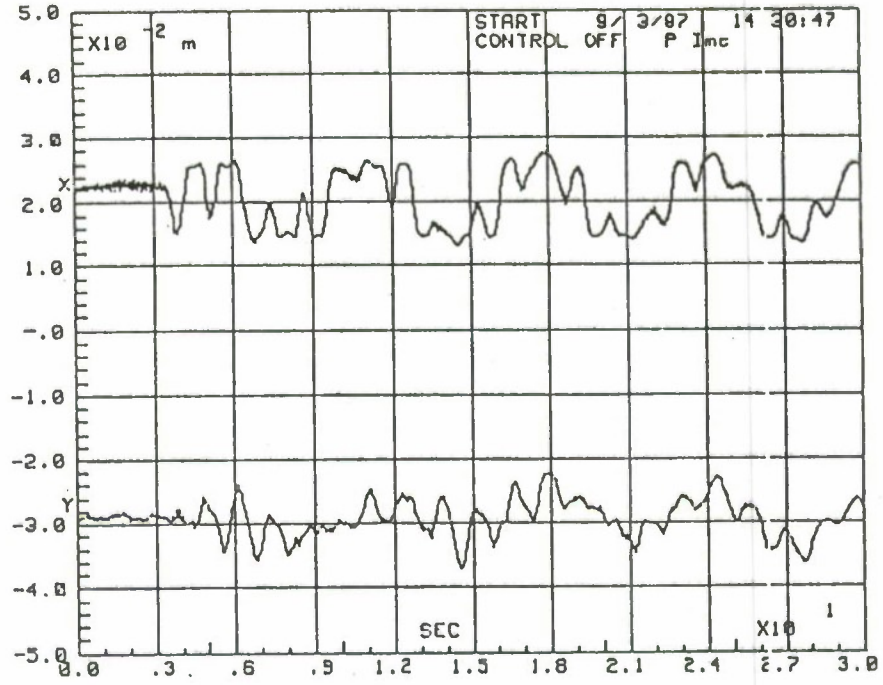


Figure 5.5-3. Open Loop Detector Response due to the RCS Disturbance.

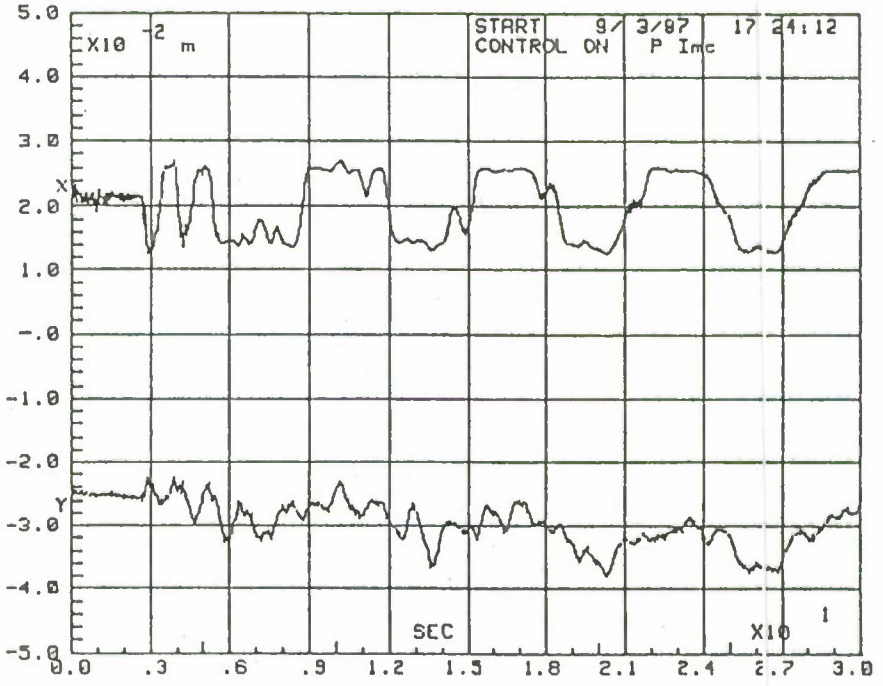


Figure 5.5-4. Closed Loop Detector Response due to the RCS Disturbance.

case. The open loop results are interesting for two reasons. First, the dominant behavior is at roughly 0.2 hertz, which is not predicted in the model. Second, the AGS hinge point pendulum behavior is also clearly evident. The closed loop results of Figure 5.5-4 indicate the effective damping or rejection of the pendulum behavior, but the 0.2-hertz unmodeled mode is unaffected. Since this mode lies within the bandwidth of the IMC system (2Hz) and the Astromast system, it is probably a "localized mode" at the antenna/detector mount assembly. This is consistent with the fact that the antenna behavior in the model is the most suspect.

The results of the crew motion tests effectively convey the same information as the RCS test results. The open loop and closed loop faceplate rate responses of Figures 5.5-5 and 5.5-6 indicate the presence of higher level rates for the crew motion disturbance. However, this is a transient phenomenon which does not persist after the removal of the disturbance, leading to the conclusion that much of the significant behavior at the faceplate is simply not excited. The open loop results of the crew motion disturbance applied along the BET Y-axis are shown in Figure 5.5-7, where again the dominant behavior is the superposition of the roughly 0.6-hertz pendulum behavior and the 0.2-hertz unmodeled mode. The closed loop results of Figure 5.5-8 again indicate a significant improvement as far as the pendulum behavior is concerned, but little or no improvement in the 0.2-hertz component.

The open loop and closed loop detector responses due to the Riverside disturbance are given in Figures 5.5-9 and 5.5-10, respectively. The open loop and closed loop faceplate rate responses are shown in Figures 5.5-11 and 5.5-12. Here again, there is very little improvement in the closed loop results. However, the reason for the lack of improvement is not the presence of the 0.2-hertz mode, which does not appear to be excited. The reason for the lack of improvement lies in the nature of the disturbance, which is persistent and has two relatively pure sinusoidal components. Effective rejection of the pure components would require an unreasonably high bandwidth IMC controller.

The results of the MSFC demonstration disturbance are given in the form of faceplate angular rates in Figure 5.5-13 for the open loop case and in Figure 5.5-14 for the closed loop case. Clearly, a significant degree of damping is achieved with the

controller. This disturbance illustrates the performance gains that are possible with significant signal levels at the faceplate.

The experimental test results for the HAC/LAC controller are summarized in Table 5.5-1. The mean and RMS detector errors are presented for the open and closed loop tests. Recall that each statistic is calculated by an average over five tests (see section 2.2.4). The requirement to remain in the linear region of operation is satisfied for the Crew, RCS, and Riverside disturbances. The results show that the HAC/LAC controller improves the detector mean in the X and Y axes. But the controller does nothing to improve the RMS detector errors (X and Y). The lack of RMS improvement for the Crew and RCS disturbances is explained by the unmodeled 0.2-hz mode which dominates the behavior of the detector response. If the 0.2-hz mode was modeled, the controller is likely to have added considerable damping to the mode. The lack of RMS improvement for the Riverside disturbance is not unexpected since the IMC bandwidth is less than 8 Hz.

The demonstration disturbance is utilized for the purpose of indicating the amount of vibration suppression of the beam provided by the HAC/LAC controller. Recall that the results of the demonstration disturbance do not meet the requirement to remain in the linear range. The detector error is not a very meaningful value for the demonstration disturbance; hence, the more meaningful variables of faceplate gyro settling time and detector percentage hits are provided. The test results indicate that the settling time is improved by 11 seconds in the X axis and by 32 seconds in the Y axis. The table also shows that the percentage of hits is increased from 51 percent to 67 percent. The demo disturbance was not as thoroughly examined as the crew, RCS or Riverside disturbances. The results of the demonstration tests were calculated with only one 80-second test run; thus, the results are not as representative of the average as the test results of the other disturbances.

TABLE 5.5-1. SUMMARY OF TEST RESULTS FOR HAC/LAC CONTROLLER

Disturbance	Quantity	Open Loop (mm)	Closed Loop (mm)	Improvement (dB)
Crew	Detector Mean (X)	2.2	0.13	24.9
	Detector Mean (Y)	1.1	0.31	11.2
	Detector RMS (X)	1.5	1.8	-1.3
	Detector RMS (X)	4.5	4.0	1.0
RCS	Mean (X)	0.87	0.04	26.1
	Mean (Y)	0.57	0.66	-1.3
	RMS (X)	4.5	4.4	0.1
	RMS (Y)	3.1	2.5	2.9
Riverside	Mean (X)	0.71	0.04	25.2
	Mean (Y)	1.3	0.30	12.6
	RMS (X)	2.5	2.2	1.0
	RMS (Y)	3.3	3.5	-0.5
Demo	*T_S Base Gyro (x)	35s	24s	11s
	T_S Base Gyro (y)	70s	38s	32s
	% Hits Detector	51%	67%	16%

*T_S = Settling time

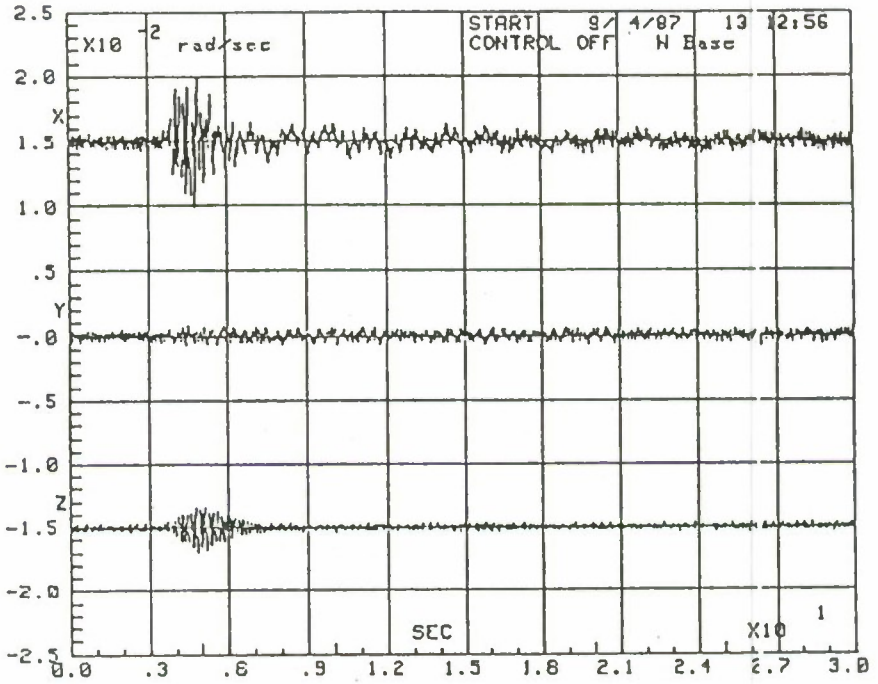


Figure 5.5-5. Open Loop Faceplate Gyro Response due to the Crew Motion Disturbance.

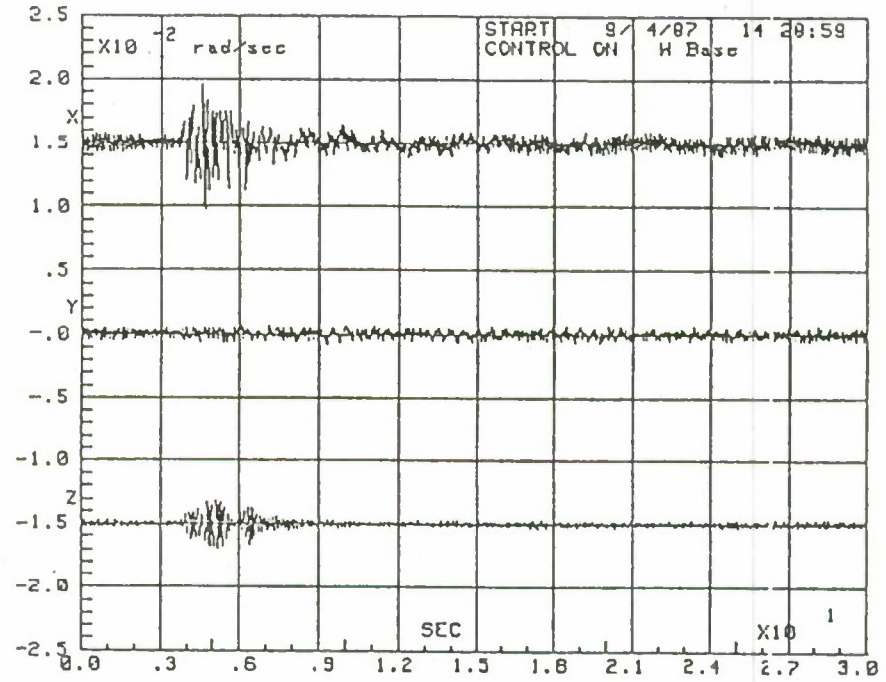


Figure 5.5-6. Closed Loop Faceplate Gyro Response due to the Crew Motion Disturbance.

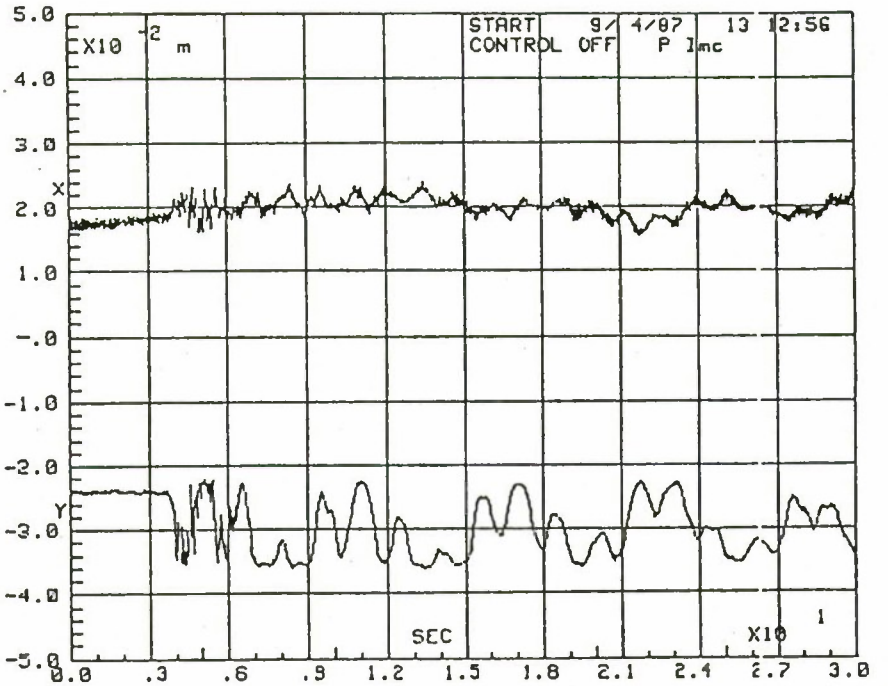


Figure 5.5-7. Open Loop Detector Response due to the Crew Motion Disturbance.

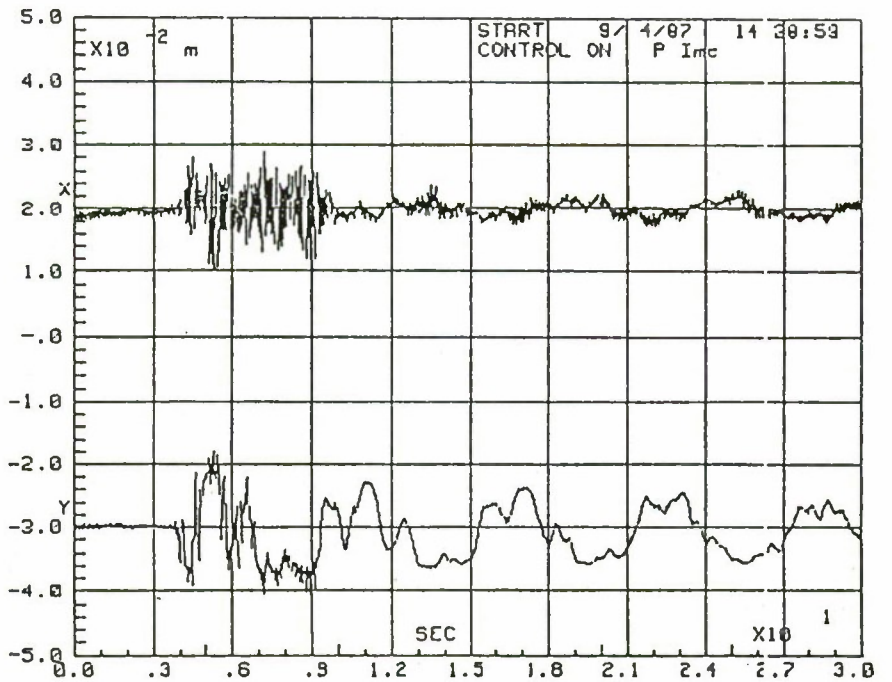


Figure 5.5-8. Closed Loop Detector Response due to the Crew Motion Disturbance.

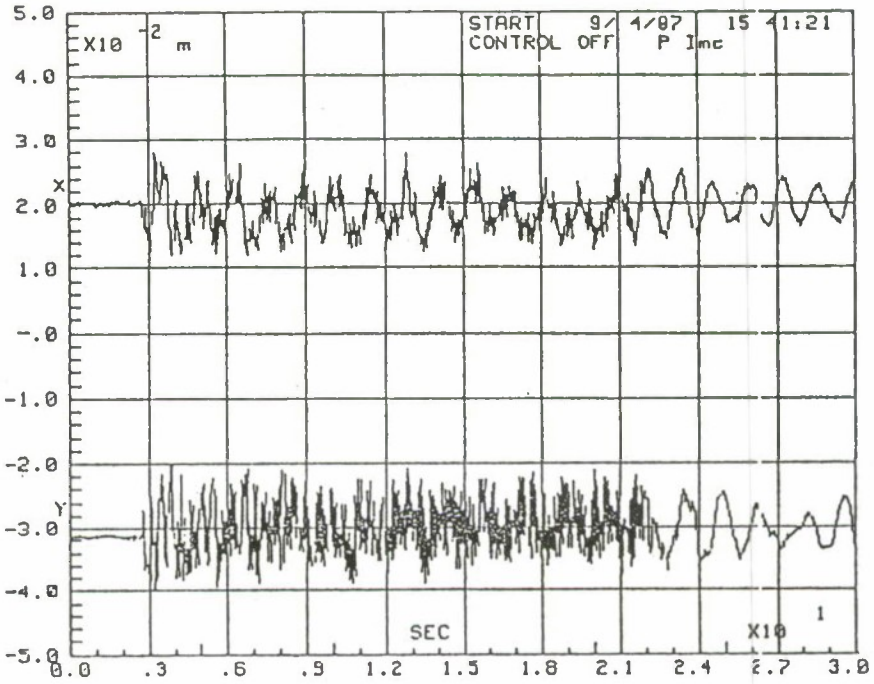


Figure 5.5-9. Open Loop Detector Response due to the Riverside Disturbance.

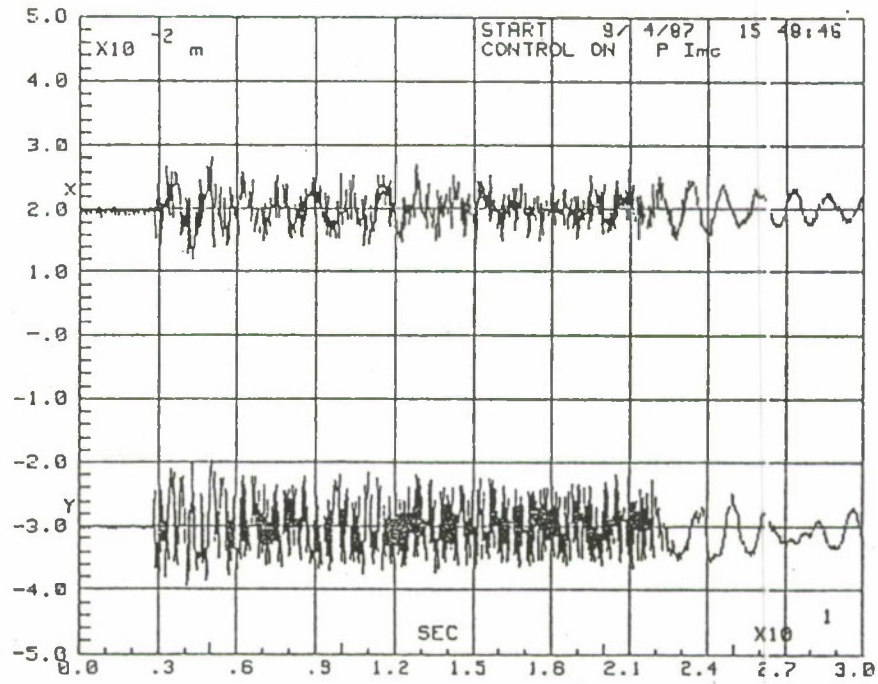


Figure 5.5-10. Closed Loop Detector Response due to the Riverside Disturbance.

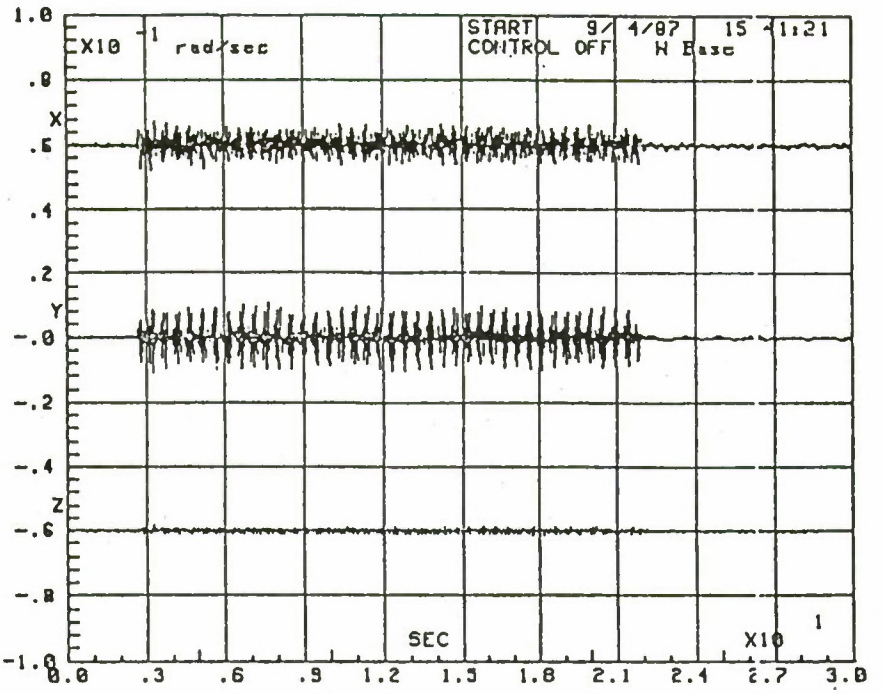


Figure 5.5-11. Open Loop Faceplace Gyro Response due to the Riverside Disturbance.

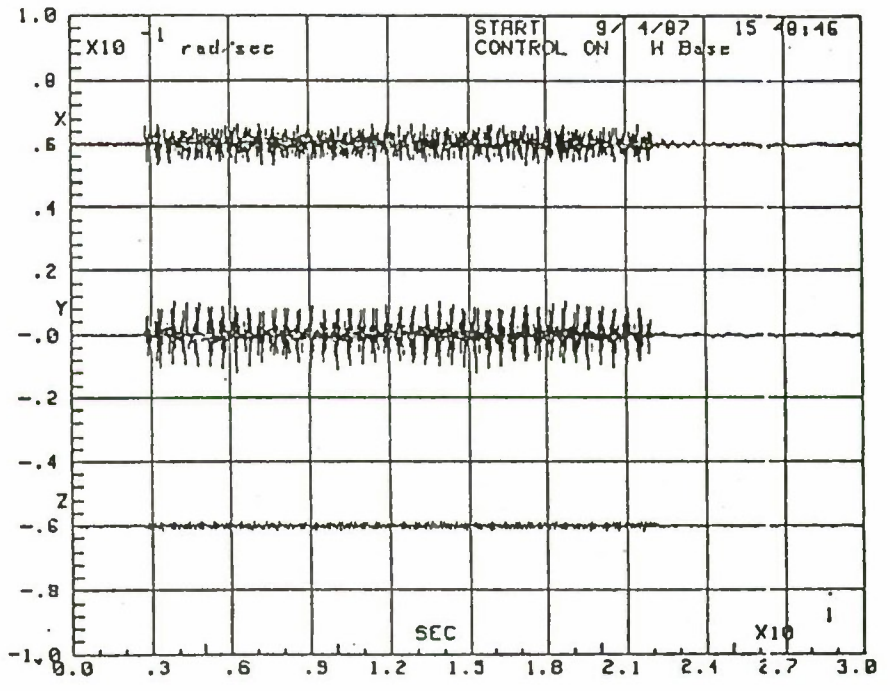


Figure 5.5-12. Closed Loop Faceplate Gyro Response due to the Riverside Disturbance.

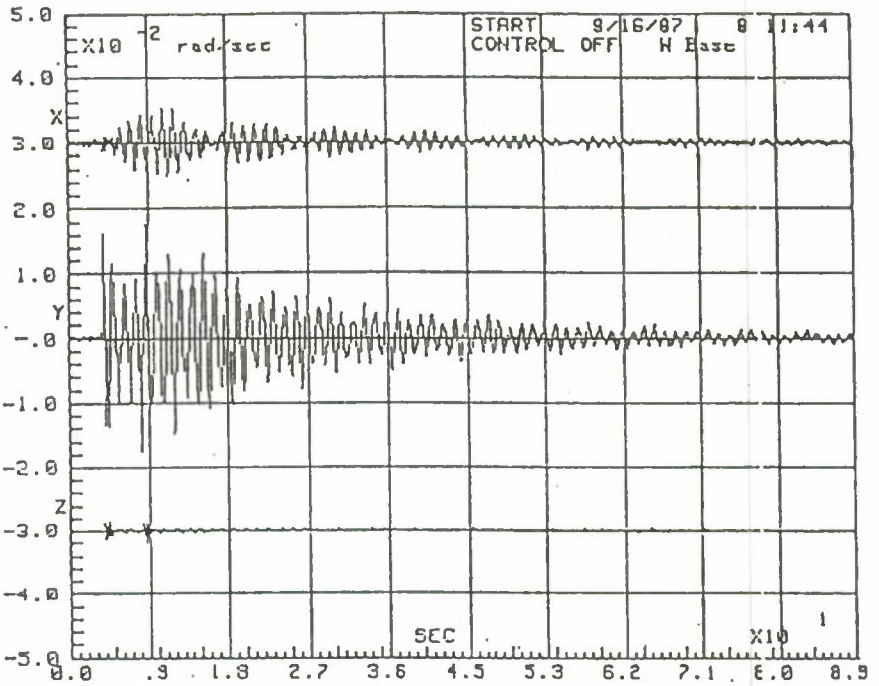


Figure 5.5-13. Open Loop Faceplate Gyro Response due to the Demonstration Disturbance.

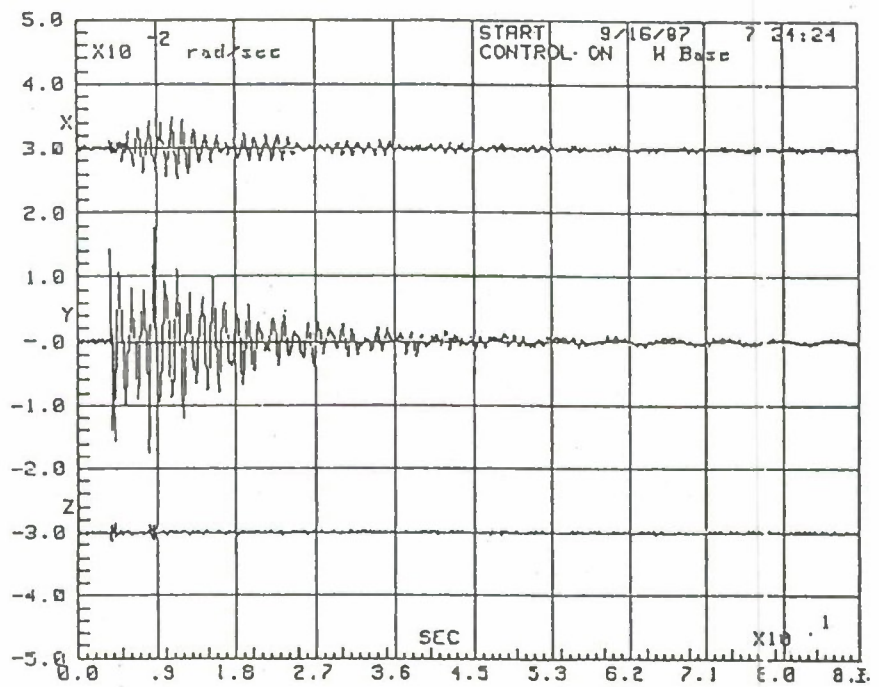


Figure 5.5-14. Closed Loop Faceplate Gyro Response due to the Demonstration Disturbance.

5.6 Conclusions

While the analytical design of the HAC/LAC controller can be termed a success, we must note that the performance of the controller in the hardware implementation is well below expectations. The major contributor to this is the effect of the unmodeled mode at 0.2 Hz which is probably due to unmodeled behavior at the antenna base. However, other contributors to the performance problem include the nonlinearity of the photodetector which causes extremely low signal levels at the AGS gyros and the noncollocated properties of the LMEDs.

Analytical problems also occurred which led to limitations on the achievable performance of the system, including the decision to omit the LMEDs from the LAC part of the design. Many of these problems are due to the fact that the LAC design process is limited to collocated sensor/actuator pairs and that, strictly speaking, HAC/LAC is most applicable to continuous time systems. The collocation limitation leads immediately to the omission of the LMEDs from the control design and the continuous time limitations leads to extreme conservatism in the LAC design. It should be noted that although the LMEDs could have been included in the HAC design, the expected sensitivity of the controller led to the decision to omit them entirely.

A summary of the advantages of HAC/LAC would have to include the capability to perform a conservative part of the design with LAC and the ability to obtain high performances via LQG (HAC) techniques. The disadvantages of HAC/LAC include the limitation of LAC to collocated sensor/actuator pairs, the sensitivity problems associated with LQG designs, and the limitation of the LAC technique to continuous time systems.

HAC/LAC can be used to effect the design of a control system for a large space structure as long as the designer fully realizes the fact that HAC/LAC is not actually a formal design process, but a collection of tools which can be helpful in the design.

6.0 POSITIVITY

Positivity, strictly speaking, is not an LSS control design technique. Rather, positivity is a system property that any particular system may or may not possess. Unfortunately, it has become common for many control theorists to speak of "design via positivity" and of "positivity design techniques." The approach of this effort is to advocate the use of positivity concepts to design controllers for systems with extremely "rough" models and to advocate the use of other methods as more information is gathered concerning the system model, so that system performance objectives can eventually be achieved. Of course, among the "other methods" one particular type may be more appropriate for a given application. The purpose of the work outlined in the following sections is to evaluate the appropriateness of the methods of ACOSS-14 [3] applied to the ACES configuration of the LSS GTF facility. These methods are commonly known as Positivity.

The portion of this report which deals with Positivity is divided into three sections. The first section is a brief summary of the theory and analytical methods pertinent to the ACES effort. The second section contains a brief description of the model reduction techniques used for the design. The third section describes the design process whereby the methods of ACOSS-14 are applied to the ACES configuration model. The final section contains the test results, along with observations and recommendations.

6.1 Theory.

The theory which is the basis of ACOSS-14 can be divided into two parts: (1) positivity concepts and (2) multivariable frequency domain concepts. Positivity concepts are those used when only a very rough model is available and multivariable frequency domain techniques are used as more information is gathered concerning the system model.

The fundamental system configuration is modeled in the frequency domain by the block diagram of Figure 6.1-1 where G(s) is the n by n transfer function matrix which represents the system model. At this point the system is assumed to have the

same number of inputs and outputs. This restriction will be removed in later discussions. H(s) is a square compensator, or controller, transfer function matrix whose elements may be chosen by the designer.

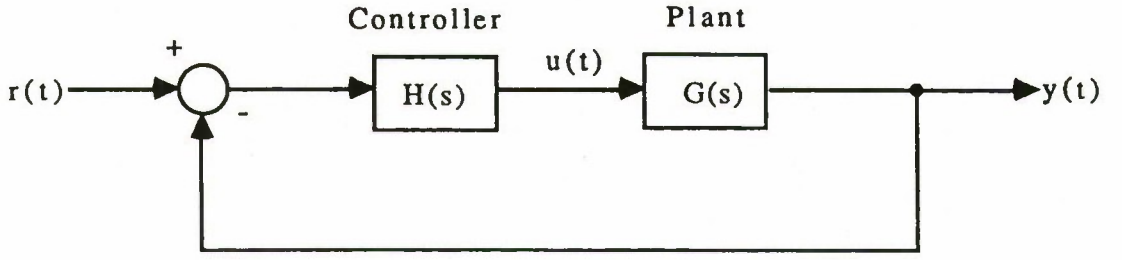


Figure 6.1-1. Block Diagram Representation Used to Illustrate Positivity.

The first step in discussing Positivity is the definition of a positive operator, or for the case of linear systems analysis, the definition of a positive system. The definition of a positive system can be approached via abstract notions of operators defined on extended Hilbert spaces. However, in the case of lumped parameter, linear, and time-invariant systems a simpler approach can be taken by defining the "positivity index."

The positivity index $\delta(\omega)$ is defined by

$$\delta(\omega) = \lambda_{min}\,(1/2\,[G(j\omega) + G^*(j\omega)]) \qquad 6\text{-}1$$

where ω is real and non-negative and $\lambda_{min}(.)$ denotes the minimum eigenvalue of (.).

For discrete systems the positivity index is defined by

$$\delta(\omega) = \lambda_{min}\,(1/2\,[G(z) + G^*(z)]) \qquad 6\text{-}2$$

where

$$z = e^{j\omega T} \text{ and } \omega \in [0, \pi/T). \qquad 6\text{-}3$$

The system represented by the transfer function matrix G(s) or G(z) is

strictly positive (real) if $\delta(\omega) > 0$ for all allowable ω,

positive (real) if $\delta(\omega) \geq 0$ for all allowable ω,

non-positive if $\delta(\omega) < 0$ for some ω.

The importance of the definition of positive systems (operators) is apparent when the Positivity Theorem is considered.

Positivity Theorem:

> The feedback system of Figure 6.1-1 is stable if both H and G are positive and at least one of them is strictly positive.

For the purposes of the positivity theorem, stability is in the sense of bounded outputs for bounded inputs.

The significance of the positivity theorem is, at first glance, limited to systems whose transfer function matrix is positive. However, the result can be generalized to nonpositive operators by utilizing operator embedding. The original motivation for considering the use of positivity concepts for LSS controller design seems to be the fact that an LSS with collocated ideal actuators and ideal rate sensors is, in fact, a positive system. For such a situation, any positive controller would yield a stable closed loop system in the configuration of Figure 6.1-1. Furthermore, the stability of such a system is independent of the model parameters. Unfortunately, in the presence of actuator or sensor dynamics an LSS is no longer positive, even if the sensors and actuators are collocated. In addition, if the overall system is sampled-data in nature, there is no guarantee that the system will be positive.

Operator embedding is, in theory, the answer to these limitations when using the positivity theorem for design purposes. Operator embedding is most easily visualized by considering the block diagram of Figure 6.1-2 where D is the embedding operator. The purpose of D is to force the new "plant" (the parallel combination feedback system of H and D) to be positive to guarantee stability via the Positivity Theorem. This places frequency-dependent constraints on H which are used in the design of the controller. Unfortunately, the constraints are in terms of the frequency dependent eigenvalues of H, a fact which poses a very difficult synthesis problem. The most common way of avoiding this difficulty is to arbitrarily assume that D is a matrix with real entries and derive the constraints on H via the Positivity Theorem. Further, if D is assumed to be a real constant

$$\delta_o = \min_{\omega} [\delta(\omega)] \qquad 6\text{-}4$$

then the positivity constraint obtained via embedding is that if H is a positive constant times an identity matrix then that constant must be less than the negative reciprocal of δ_0. More concisely, if

$$H = k\, I, \qquad 6\text{-}5$$

then

$$k < -1/\delta_0. \qquad 6\text{-}6$$

Since the above result simply specifies a way to gain stabilize the system, performance goals are impossible to achieve, in general.

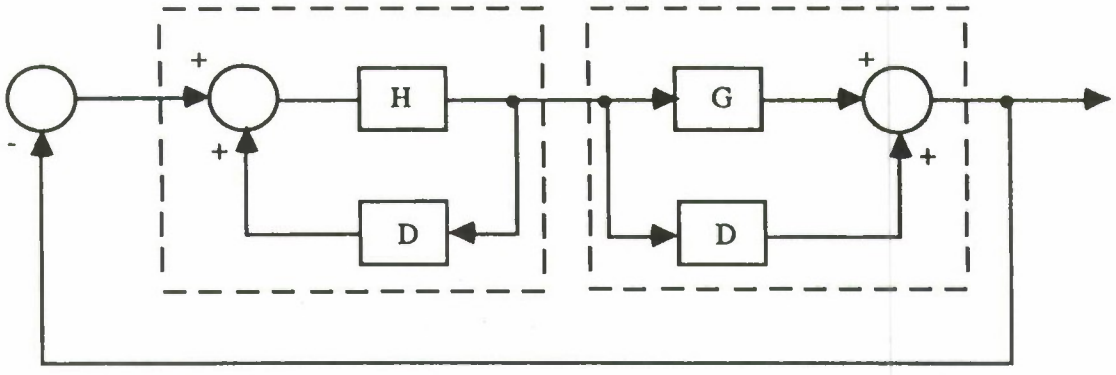


Figure 6.1-2. Operator Embedding Block Diagram.

Characteristic loci methods do not necessarily suffer from this limitation and, in the ACOSS documented results, are intended to aid in resolving the performance problems encountered when applying pure Positivity. In the documentation of Positivity, primarily the ACOSS reports, the suggestion is made to use characteristic loci to obtain performance and to use the positivity constraints to achieve robustness. Care must be taken when using such an approach, since systems exist for which the positivity constraints guarantee only marginal stability.

The characteristic loci methods are based on a dyadic expansion of the frequency dependent transfer function matrix. For example, let G(s) be given by

$$\begin{aligned} G(s) &= W(s)\ \mathrm{diag}[\lambda_i(s)]\ V(s) \\ &= W(s)\ \lambda(s)\ V(s). \end{aligned} \qquad 6\text{-}7$$

Then, with H(s) = I and the configuration of Figure 6.1-1, the closed loop transfer function matrix for a square system can be written

$$\begin{aligned} [I + G(s)]^{-1}\ G(s) &= [I + W(s)\ \lambda(s)\ V(s)]^{-1}\ W(s)\ \lambda(s)\ V(s) \\ &= [W\ V + W\ \lambda\ V]^{-1}\ W\ \lambda\ V \\ &= W\ [I+\lambda]^{-1}\ \lambda\ V, \end{aligned} \qquad 6\text{-}8$$

which is a dyadic expansion of the closed loop system with characteristic gains (eigenvalues) given by

$$\lambda_c = \lambda/[1+\lambda]. \qquad 6\text{-}9$$

The eigenvalues λ_c can be thought of as generalized transfer functions in the co-ordinates defined by the W and V matrices, which are composed of right and left eigenvectors of G(s). Now, G(s) can be modified at will to give the desired characteristic loci from Equation 6-9 as long as the modification is done in the co-ordinates defined by W(s) and V(s). Unfortunately, these transformations are frequency dependent algebraic functions which are not necessarily rational. Since any controller which is able to arbitrarily modify the characteristic gains must itself contain the transformations, the utility of Equation 6-9 is limited. Before presenting another approach to the problem of Equation 6-9, some consequences should be stated. The first of these is the Generalized Nyquist Criterion.

Generalized Nyquist Criterion

> The system of Figure 6.1-1 is stable if and only if the net sum of counterclockwise encirclements of the -1 + j0 points in the λ_i planes is equal to the number of open loop unstable poles.

Other consequences of Equation 6-9 are (1) that the closed loop system is roughly uncoupled at frequencies where the characteristic loci have large magnitudes (>>1), (2) that the system is also uncoupled at frequencies where the eigenvectors which compose W(s) are pairwise orthogonal, and (3) that if such decoupling occurs over an appropriately large frequency range, then performance can be inferred from scalar frequency responses.

Since there is no dependable way to design the compensator in the co-ordinates appropriate for use of Equation 6-9, a procedure known as generating an "approximately commutative" controller is usually used to approximate the co-ordinates of the dyadic expansion needed in Equation 6-9, but only at one particular frequency. The term "commutative" derives from the fact that the co-ordinates of

H(s) and G(s) are aligned if G(s) H(s) = G(s) H(s), i.e., H(s) and G(s) commute. The controller coordinates are only approximately those of the plant since the transformations which are used to replace W(s) and V(s) are by necessity matrices with real entries, whereas the entries of W(s) and V(s) are generally complex at a particular value of s. The approximately commutative controller has the form

$$K(s) = A\ \Gamma(s)\ B \qquad 6\text{-}10$$

where A and B are matrices of real entries and $\Gamma(s)$ is a diagonal matrix whose diagonal elements are rational functions of s. The approach is to find A and B which approximate the transformations W(s) and V(s) at a particular value of $s = j\omega$. The particular frequency chosen is referred to as the design frequency and is a frequency at which the characteristic loci of the resulting compensated plant are desired to be given by

$$\lambda comp_i(s) = \gamma_i(s)\ \lambda_i(s) \qquad 6\text{-}11$$

The approximate transformations A and B are obtained via a process known as frame alignment. Frame alignment is based on the fact that to approximate the transformations W(s) and V(s), the condition

$$K(s)\ G(s) = G(s)\ K(s) \qquad 6\text{-}12$$

must be approximately satisfied. Substitution of the dyadic expansions of K(s) and G(s) give

$$A\ \Gamma(s)\ B\ W(s)\ \lambda(s)\ V(s) = W(s)\ \lambda(s)\ V(s)\ A\ \Gamma(s)\ B \qquad 6\text{-}13$$

If A = W(s), B = V(s), B W(s) = I, and V(s) A = I, then Equation 6-13 is an identity and

$$K(s)\ G(s) = G(s)\ K(s) = W(s)\ \Gamma(s)\ \lambda(s)\ V(s) \qquad 6\text{-}14$$

so that Equation 6-9 can be used to predict the closed loop eigenvalues.

Of the four conditions listed which are sufficient to achieve the commutativity condition, only two are necessary, since the columns of W(s) are orthogonal to all but the corresponding rows of V(s). This means that the two conditions that are necessary for commutativity are

$$B\ W(s) = I \qquad 6\text{-}15$$

and

$$V(s)\ A = I. \qquad 6\text{-}16$$

The usual approach to this frame alignment is to choose A so that

$$\Phi_i = |(v_i, a_j)|^2 / \sum_j |(v_j, a_j)|^2 \quad \text{where } j \neq i \qquad 6\text{-}17$$

is maximum, where v_i is the ith row of V(s) at the design frequency and a_i is the ith column of A. After the n columns of A are chosen in this way, B can be chosen as

$$B = A^{-1}. \qquad 6\text{-}18$$

Again, it should be noted that there are two limitations on the use of the results of Equations 6-17 and 6-18. These are (1) Equations 6-15 and 6-16 are only approximately satisfied and (2) the commutativity conditions may be satisfied over only a very narrow range of frequencies.

The results up to this point have been based on the assumption that the transfer function matrix G(s) is square. In situations for which G(s) is not square, a square down procedure can be applied. For example, suppose the plant described by G(s) has n input and m outputs and further suppose that m > n, so that G(s) is m by n. A square down matrix filter L(s) can be defined which has m inputs and m outputs so that it has dimensions n by m and defines a new "plant" transfer function matrix

$$Gsquare(s) = L(s)\ G(s) \qquad 6\text{-}19$$

which is square and has dimensions n by n. Of course, some restrictions must be placed on L(s) so as to retain the nature of the control problem. This is usually done by choosing L(s) to be constant and such that the new (artificial) feedback signals adequately represent the control objectives. If some of the sensors and actuators are collocated, their collocated nature can be preserved by using a partial square down matrix, so that

$$L(s) = [I : F(s)]. \qquad 6\text{-}20$$

6.2 Model Selection and Reduction.

The Positivity design is begun by choosing a reduced order modal model from the set of 43 modes of the dynamic model. However, in contrast to the motivations for model reduction for FAMESS and HAC/LAC, the purpose of the model reduction process is not to ensure a lower order controller, but to minimize the computations required to generate the frequency response matrix needed in the Positivity design. Thirty-one of the available forty-three modes were selected for the Positivity design model based on the contribution of each mode to the elements of the transfer function matrix. The criterion used dictated that a mode be retained in the design model if its contribution to any of the elements of the transfer function matrix exceeded 6 decibels at any frequency up to half of the sampling frequency. All of the sensors and actuators are included in the model. Where available, pertinent sensor and actuator dynamics are included in the transfer function matrix model. Finally, the sampled-data version of the transfer function matrix is computed via a truncated series technique.

6.3 Design Process.

The feedback configuration originally assumed for the design process is that of Figure 6.3-1, where G(s) is the 14 by 9 continuous-time open loop plant transfer

function matrix, K is the 9 by 14 square down matrix, and $G_c(z)$ is the 9 by 9 compensator transfer function matrix. The constant square down matrix is chosen so that modes which are more significant at the LOS are emphasized in the new (artificial) outputs. This goal is realized by requiring that

$$K\,G(0) = R, \qquad 6\text{-}21$$

where

$$r_{ii} = \sum_{k=1}^{N} \Phi_k(a_i)\sqrt{\Phi_k^2(x) + \Phi_k^2(y)} \qquad 6\text{-}22$$

are the diagonal elements of R. Since G(0) is not square, the solution of Equation 6-21 is accomplished using a generalized inverse of G(0).

where

N = number of modes

$\Phi_k(a_i)$ = k^{th} modal gain at the i^{th} actuator

$\Phi_k(x)$ = k^{th} LOS gain at the x detector

$\Phi_k(y)$ = k^{th} LOS gain at the y detector

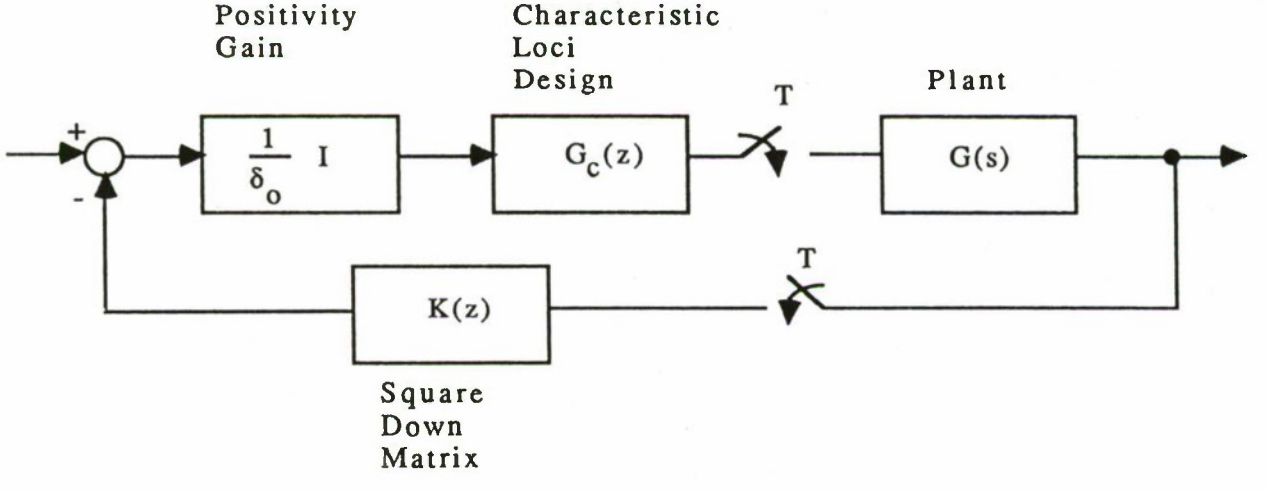


Figure 6.3-1. Positivity Controller Configuration.

During the actual design process we found that a full square down matrix using Equations 6-21 and 6-22 destroyed the collocation benefits of the AGS sensor/actuator pairs and that the resulting transfer matrix KG(s) needlessly complicated the transfer characteristics of the pointing gimbal/photodetector pairs. Therefore, two simplifications of the process were introduced:

(1) The IMC components were separated from the rest of the sensors and actuators, so as to preserve the decoupled nature of these components, which was discovered during development of the design model.

(2) A partial square down matrix was utilized in order to preserve the collocation properties of the AGS subsystem. In other words K was chosen to have the form

$$K = [\, I : L \,] \qquad 6\text{-}23$$

where L is found from the transfer matrix corresponding to the non-collocated sensors and actuators.

Also, in order to increase the collocation properties of the system, the LMED accelerometer outputs were compensated. The need for such compensation is apparent from Figure 6.3-2, which is the uncompensated transfer function from the LMED1 force input to the corresponding accelerometer output. The problem is the large phase shift between 1.0 and 2.0 hertz which is caused by the "mode" of the proof-mass/centering spring combination. The physical significance of the frequency of the phase shift is that below this frequency the centering spring acts as a force "balance" which results in zero net force acting on the structure at these frequencies. At frequencies above that of the phase shift, the LMED behaves properly as a collocated pair once rate measurements are derived from the accelerometer outputs. A possible fix is to gain stabilize the modes below and slightly above the troublesome frequency. However, such an approach limits the lowest usable frequency to roughly 4 hertz and would probably gain little in terms of

vibration suppression. Therefore, phase stabilization of the LMED outputs was used to provide the possibility of damping at lower frequencies. The compensated LMED transfer function is given in Figure 6.3-3. The phase lag at high frequencies is caused by the effects of sampling and computational delay. The compensator transfer functions for the LMED outputs are given by

$$L_C(z) = \left(\frac{0.07137009\, z^2 - 0.140926768\, z + .07115710245}{1.01240171\, z^2 - 1.999199979\, z + 0.988398506} \right) * \left(\frac{0.02z}{z-1} \right) \qquad 6\text{-}24$$

Since the LMED pairs are now approximately collocated (using the compensated outputs), the partial square down matrix can be easily modified to preserve the collocation properties of these pairs. The resulting "squared down" system transfer function matrix exhibits excellent collocation properties itself, as the LMED "rates" and the AGS angular rates appear to contribute most heavily to the elements of the transformed, or fictitious, outputs. This seems paradoxical at first glance, since the tip instruments are physically located much closer to the photodetector LOS measurement than are the remaining sensors. However, it should be remembered that the model is extremely complex and that while the antenna arm is highly flexible, as is the Astromast itself, the tip instruments are part of a fairly massive and rigid tip assembly.

The next step in the design process is the calculation of the dyadic expansion of the frequency response matrix. A representative example of a characteristic locus is that of Figure 6.3-4, where the locus compensation has been added in the form of a simple stage of lead at roughly 8 hertz for the purpose of extending the attainable bandwidth and a gain adjustment for the purpose of attaining a degree of modal damping. This indicates that if such compensation can be achieved in the "natural" coordinates of the system, then the vibratory LOS can be effectively stabilized. Unfortunately, the frame alignment process does not appear to be sufficient to accomplish such dramatic performance improvements.

Initially, the frame alignment was carried out at the design frequency for the first characteristic locus, which is roughly 8 hertz. Since this process produced a

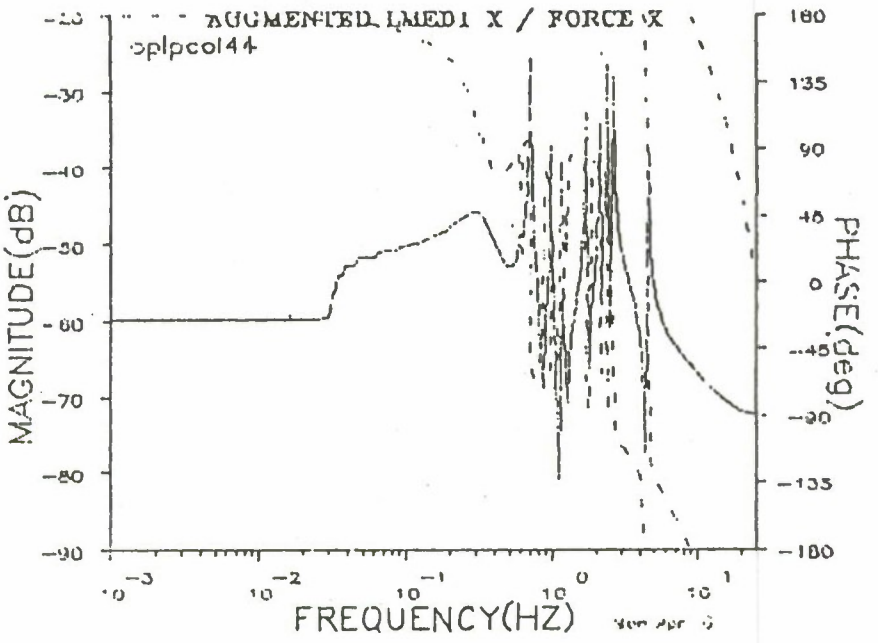


Figure 6.3-2. Transfer Function from LMED1 Force Input to LMED1 Accelerometer Output.

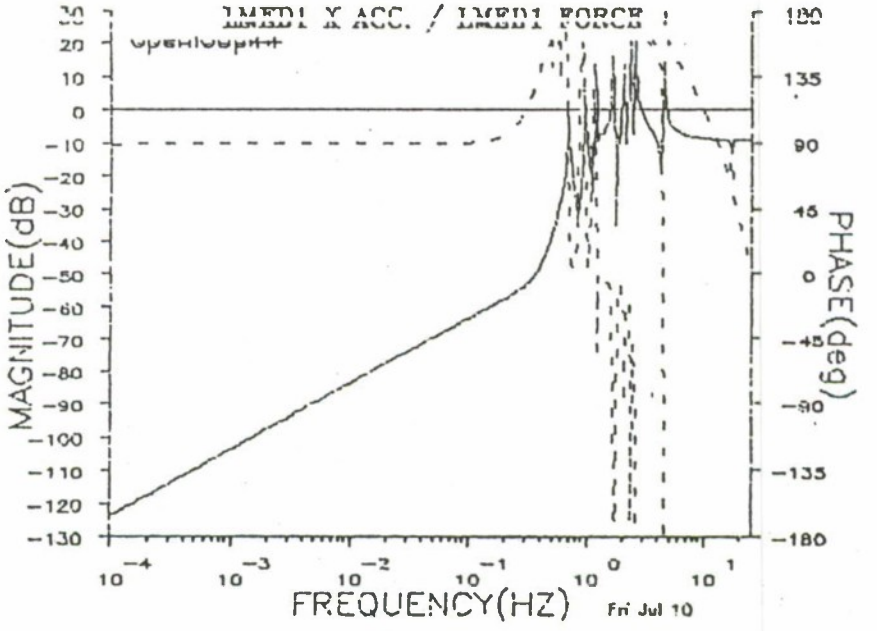


Figure 6.3-3. Compensated LMED Transfer Function.

precompensated system that was predicted to be unstable by application of the Generalized Nyquist Criterion, an investigation of the alignment process was performed. Since it was suspected that the complex behavior of the system transfer function matrix at 8 hertz was responsible for a poor approximation of the characteristic vectors by the alignment matrices, a relatively benign frequency was chosen for the purpose of investigating the alignment procedure. The results of the investigation are illustrated in Table 6.3-1, where the product of V(s)A is given at s=j2.0. This product should illustrate the pairwise orthogonality of the rows of V(s) with the columns of A by exhibiting strong diagonal dominance. Unfortunately, the calculated product does not exhibit this property. There are at least two possible causes for this situation. The first is that either the algorithm presented in MacFarlane, et al, is incorrect or the implementation is faulty. Since we found no published results to indicate the degree of alignment which might be expected in application of the alignment procedure and investigations detected no errors in the algorithm or the implementation, we concluded that the algorithm produced the best possible alignment at the chosen frequency. The second possibility is that the W(s) which is approximated by A at 2.0 rad/s is simply not appropriate for approximation by a real frame. Even in the case where W(s) and V(s) can be accurately approximated by real transformations at one particular frequency, complicated frequency dependence of W(s) and V(s) can cause the alignment to be lost at other points, even at frequencies very close to the aligned frequency. This can be seen clearly by considering the first element of the first characteristic vector, as shown in Figure 6.3-5. For this element, extremely rapid variations in direction occur over the frequency range from 0.2 hertz to 25 hertz.

A particular special case of perfect commutativity is when the controller is the identity matrix multiplied by a scalar transfer function. The limitation, of course, is that the same compensation must work for all n of the characteristic loci for the controller to be significantly beneficial. In the case of the ACES configuration, the collocation properties of the squared down system permit the use of such a controller, since destabilization is not a serious problem. Actually, much more freedom is gained by virtue of the collocation properties, since any reasonable constant gain diagonal controller can simultaneously provide stability and modal

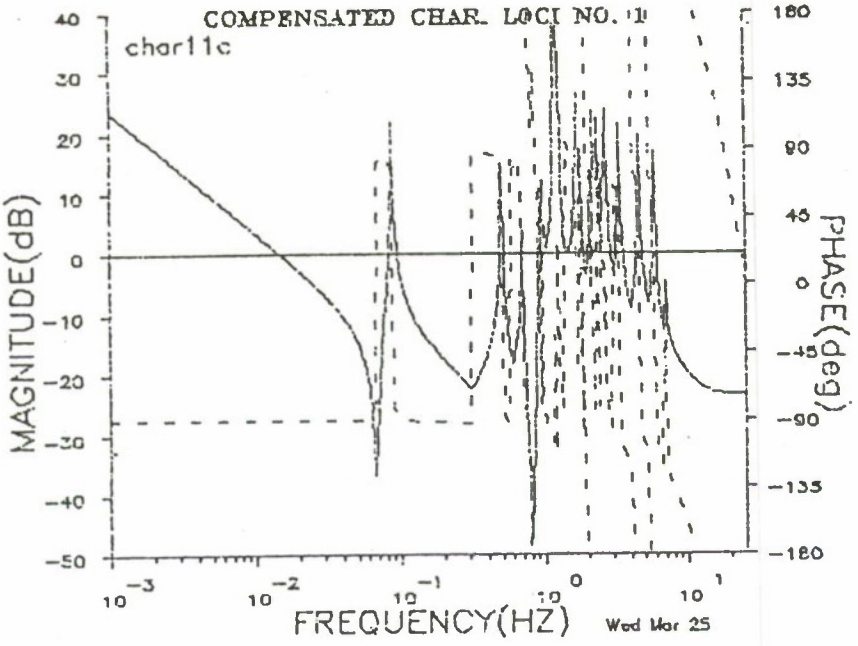


Figure 6.3-4. Magnitude and Phase of a Representative Plant Characteristic Locus (Compensated).

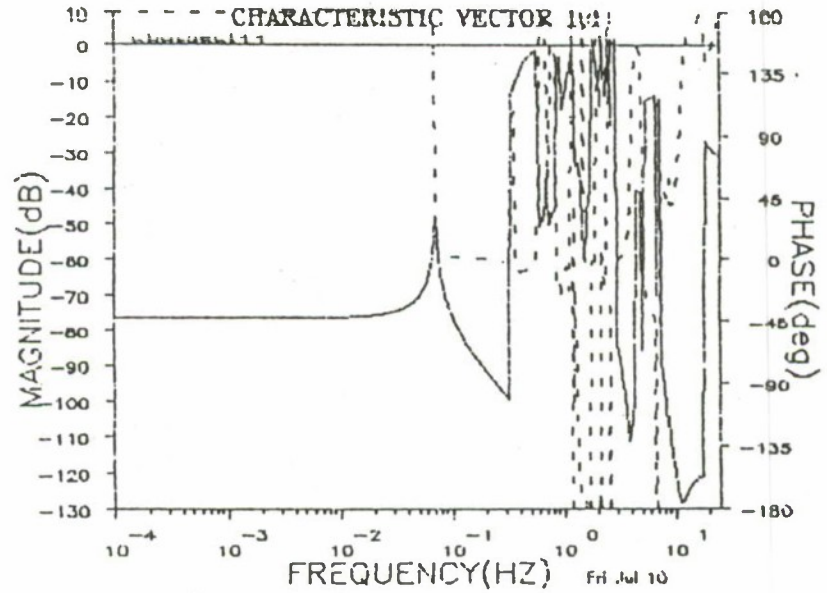


Figure 6.3-5. Element of Characteristic Vector.

TABLE 6.3-1. PRODUCT OF V(s) A at s = j 2.0

1		2	
.1466E+01	-.3519E+00	-.3177E+00	.1447E+00
-.1453E+00	-.1406E+00	.6669E+00	.7376E-02
.9410E-01	-.9506E-01	.1163E+01	-.7726E+00
.5374E+00	.2128E+00	.1160E-02	-.1938E+00
-.4263E+00	-.2191E+00	.9866E+00	.6750E+00
-.3582E+00	-.6508E+00	.1188E+00	.3549E+00
.8712E+00	.3793E-01	-.2713E+00	.2366E+00

3		4	
.6596E-01	-.1877E-01	.9773E-01	-.3614E-01
.1338E-02	.7268E-03	.1966E+00	-.1098E+00
-.7891E+00	-.1116E+00	-.1065E+00	.2239E+00
-.4944E-01	.2338E-01	.1035E+01	-.2546E+00
.2801E-01	.2665E-01	-.9940E-01	-.9121E-01
-.5652E-01	-.7223E-01	.5506E+00	.9598E+00
.3784E-01	.9782E-02	.4288E-01	.1805E-01

5		6	
.1071E+00	-.7405E-01	-.6183E-01	.2546E-01
.1797E+00	.1666E+00	-.1736E+00	.4307E-01
-.3412E+00	.4583E+00	.6512E-01	-.5465E-01
-.2523E-02	.2994E-01	.5370E-01	-.3860E-01
-.3694E+00	-.7190E+00	.8895E-01	.7292E-01
.2374E-01	.2399E-01	.6125E+00	-.1053E+01
-.2257E+00	.4153E+00	-.3175E-01	-.1574E-02

7	
.3268E+00	-.7744E-01
.8240E-02	-.2150E-01
-.1211E+00	-.7340E-01
.8279E-01	.5036E-01
-.5094E-01	-.3457E-01
-.1049E+00	-.1595E+00
.1789E+00	.3810E-01

damping. The final controller is designed in such a way, with single lead stages inserted in five of the seven forward paths to allow damping at higher frequencies than would normally be possible for a sampled data system. Since the lead stages actually upset the collocation properties, the Generalizcd Nyquist Criterion was uscd to verify the stability of the resulting closed loop system. The five lead stages, together with the LMED compensation and the accelerometer integrators yield a contoller for the Astromast subsystem which is 19th order. Representative closed loop transfer functions for the AGS gimbal/gyro pairs are given in Figures 6.3-6 and 6.3-7.

An interesting phenomenon is apparent in the frequency responses of the IMC shown in Figures 6.3-8 and 6.3-9. Due to the degree of modal damping attained with the Astromast components, the IMC frequency responses exhibit only the pendulum behavior associated with the two gimbals. Furthermore, the predominant diagonal characteristic of the IMC frequency response matrix is preserved. Hence the two dominant channels of the IMC subsystem are compensated separately, the only compensation required being integrators for forcing a type 1 system and lead devices for management of the crossover frequencies. The bandwidths of the resulting systems are both roughly 2.0 hertz. The combined controller (IMC and Astromast) is 23rd.

Results of a high fidelity simulation with an RCS input disturbance are given in Figure 6.3-10 for the open loop case and in Figure 6.3-11 for the closed loop case. Not only is a high degree of damping apparent, the IMC system effectively rejects the very low frequency behavior due to the Astromast first torsional mode and the AGS hinge point pendulum modes.

6.4 Test Results.

As is the case for all of the candidate controllers, the controller outlined in the previous section is subjected to a test cycle which includes four disturbances. These disturbances include the simulated reaction control system (RCS) thruster disturbance, the simulated crew motion disturbance, the "Riverside" disturbance, and

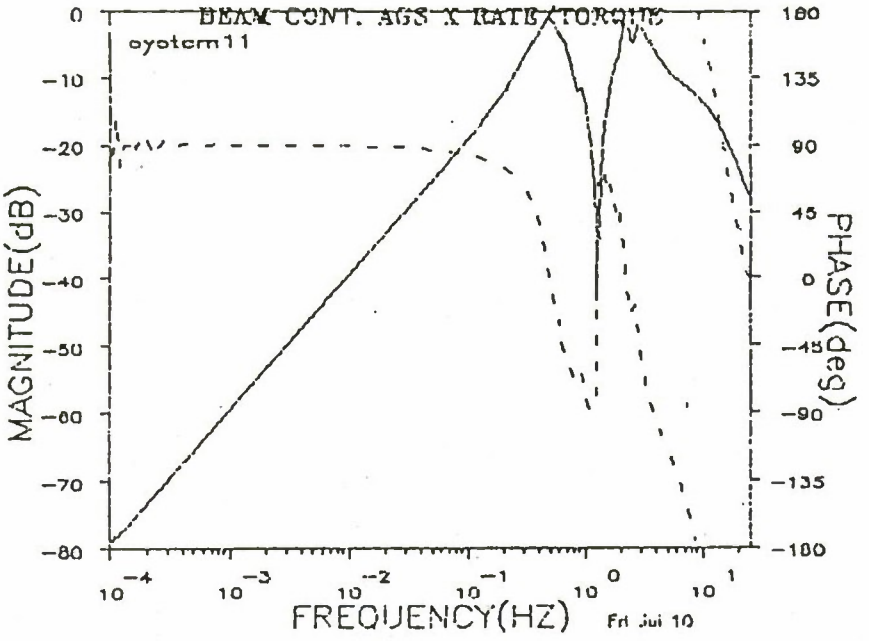


Figure 6.3-6. Transfer Function from Gimbal Torque X to Faceplate Gyro X.

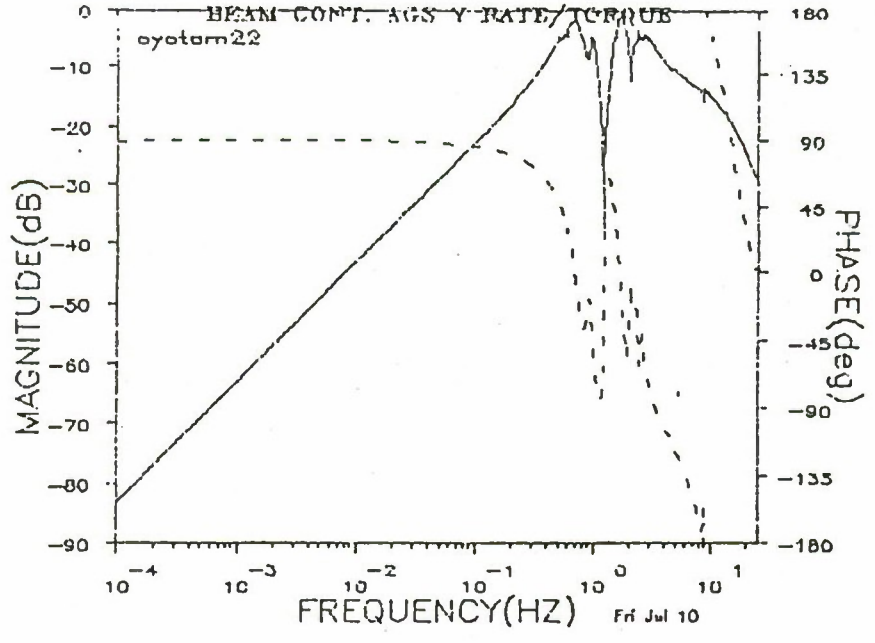


Figure 6.3-7. Transfer Function from Gimbal Torque Y to Faceplate Gyro Y.

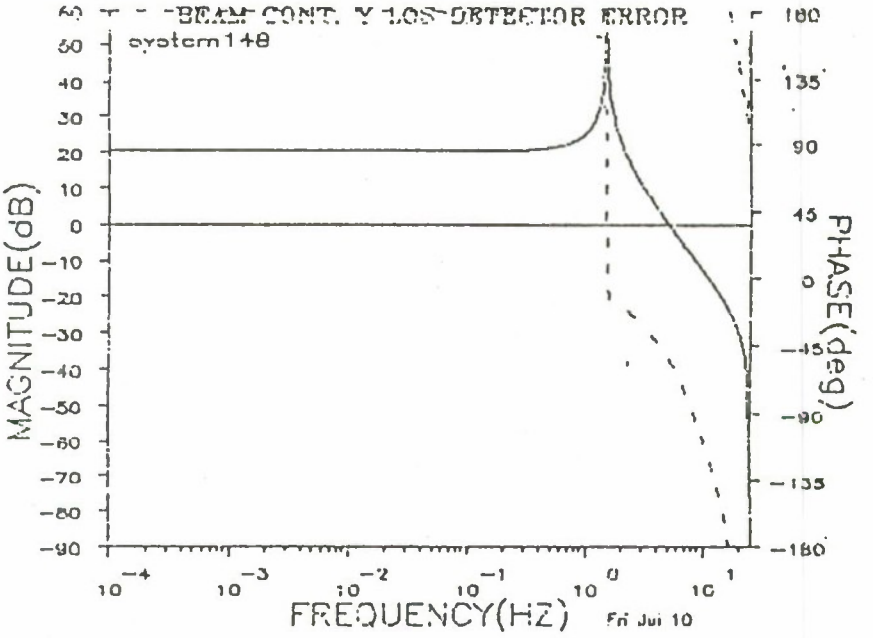


Figure 6.3-8. Frequency Response IMC X.

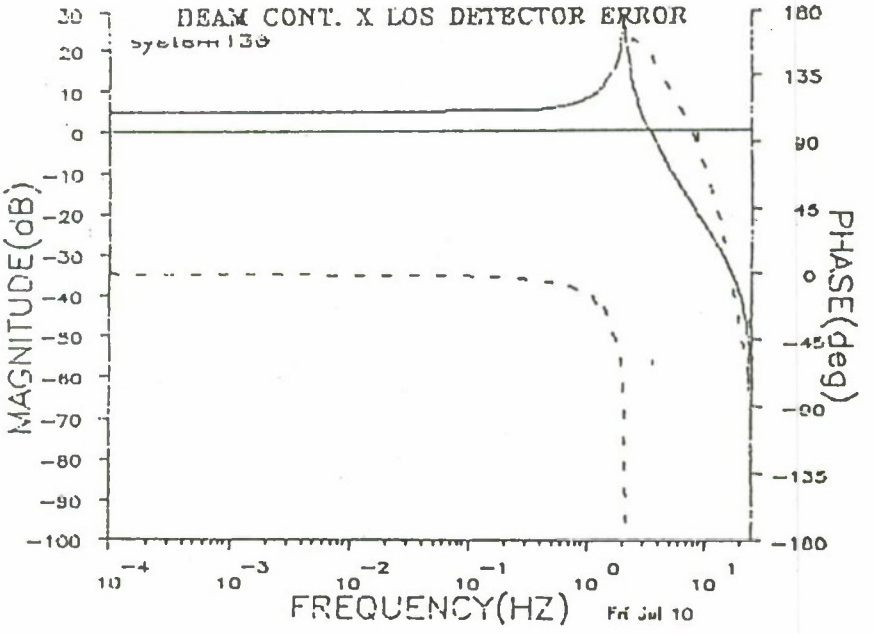


Figure 6.3-9. Frequency Response IMC Y.

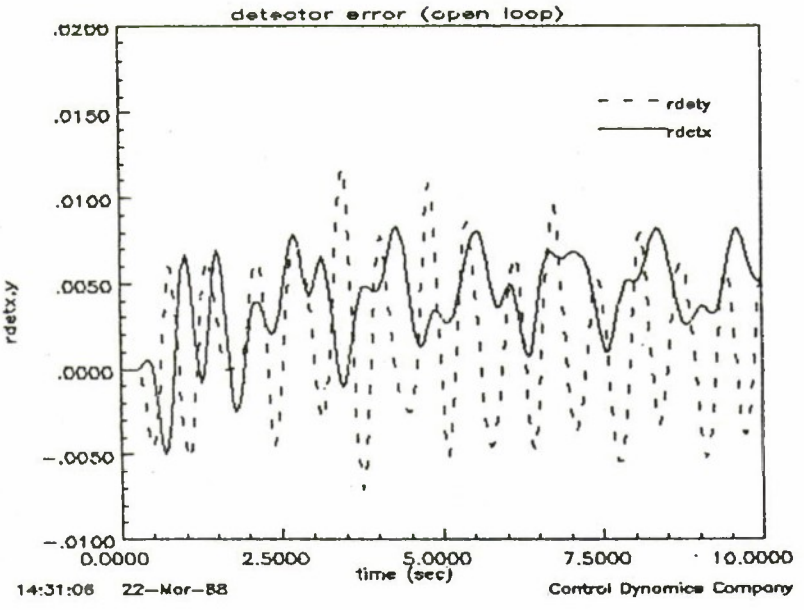


Figure 6.3-10. High Fidelity Simulation Response at Detector (m) due to the RCS Disturbance (Open Loop).

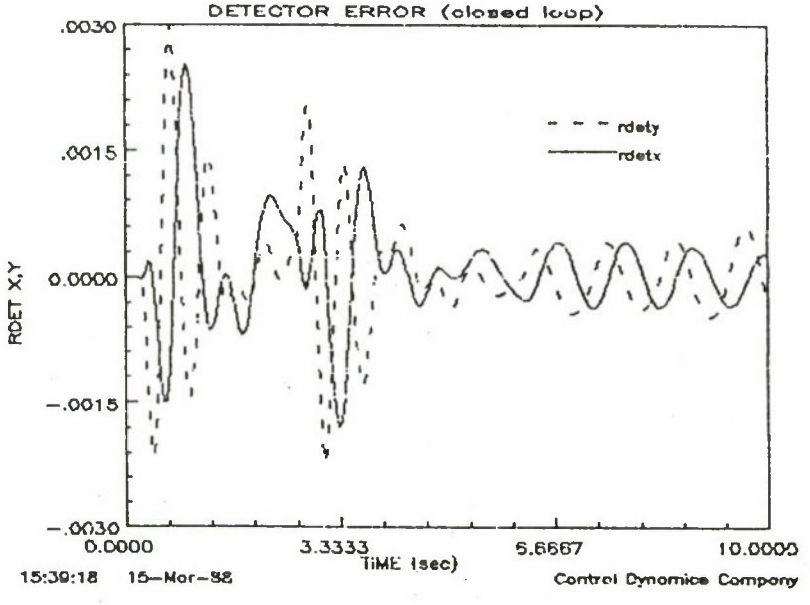


Figure 6.3-11. High Fidelity Simulation Response at Detector (m) due to the RCS Disturbance (Closed Loop).

a disturbance used by Marshall Space Flight Center for demonstration purposes. All but the last disturbance are designed to maintain the presence of the laser beam on the photodetector with no closed loop control active. The original intention was to maintain the beam presence with active control off in order to better evaluate the performance improvements incurred with each controller active. However, the results of the tests indicate that the resulting disturbance levels are so small that they do not provide an adequate measure of the performance of the controllers.

Initial tests with the full controller described in the previous section were unsuccessful, due to the sensitivity of the LMED post-compensation. For this reason, the implemented controller for which the test results follow is stripped of the LMED sensors and actuators.

The results of the open loop RCS tests are given in Figure 6.4-1 in the form of faceplate angular rates. The most revealing comment that can be made regarding these rates is that their magnitudes are very small compared to the range of the instruments. The closed loop results of Figure 6.4-2 exhibit little or no improvement over the open loop results. This can be attributed to the lack of significant signal levels at the faceplate gyros.

The open loop results of the crew motion disturbance are given in Figure 6.4-3 through Figure 6.4-6. The disturbance is applied in the y-axis direction only. Figures 6.4-3 and 6.4-4 are the open and closed loop faceplate gyro responses, respectively. In this case, some improvement is apparent in the x and z axes. The detector responses of Figures 6.4-5 and 6.4-6 are those of the open loop and closed loop, respectively. The open loop response of Figure 6.4-5 indicates that the dominant components of the response are at roughly 0.6 hertz and 0.2 hertz. While the first component can be identified with the AGS hinge point pendulum modes, there is no model mode corresponding to the 0.2 hertz mode. This unmodeled mode is the cause of the highly oscillatory response seen in the closed loop results of Figure 6.4-6. Clearly, without the unmodeled behavior the controller is capable of achieving significant LOS stabilization, as no other degrading components are apparent.

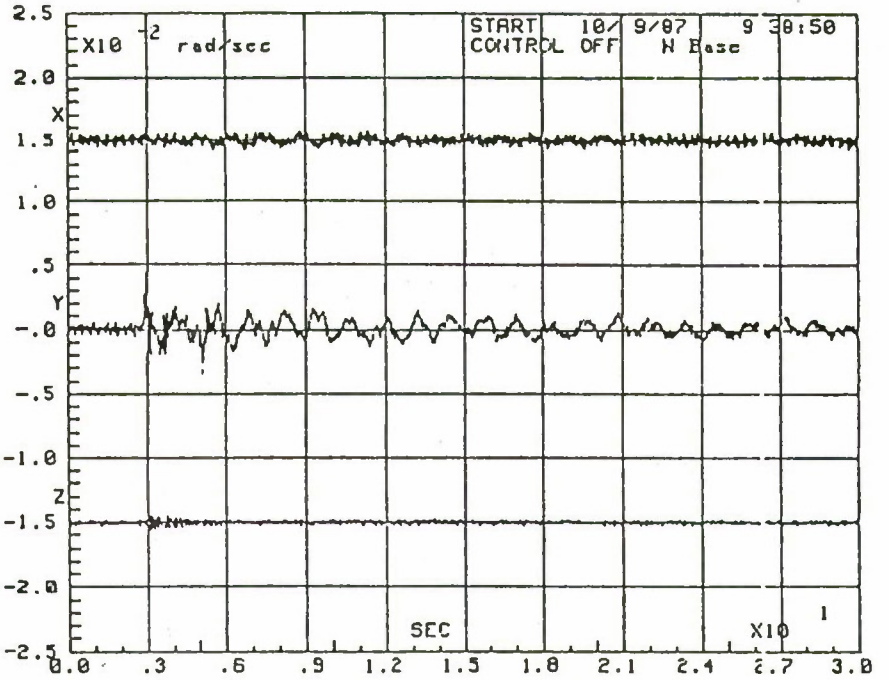


Figure 6.4-1. Open Loop Faceplate Angular Rate Response due to the RCS Disturbance.

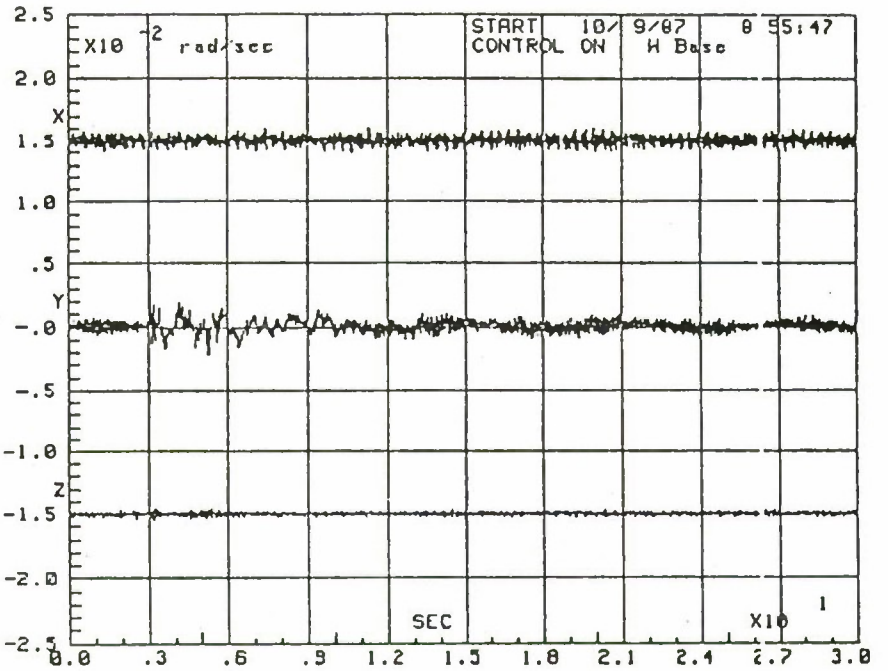


Figure 6.4-2. Closed Loop Faceplate Angular Rate Response due to the RCS Disturbance.

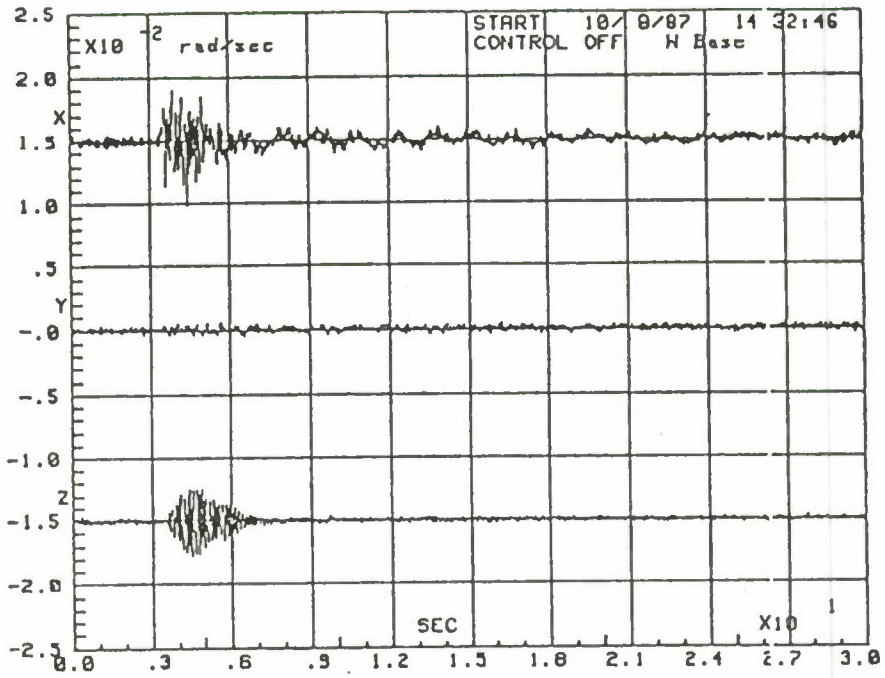


Figure 6.4-3. Open Loop Faceplate Angular Rate Response due to the Crew Motion Disturbance.

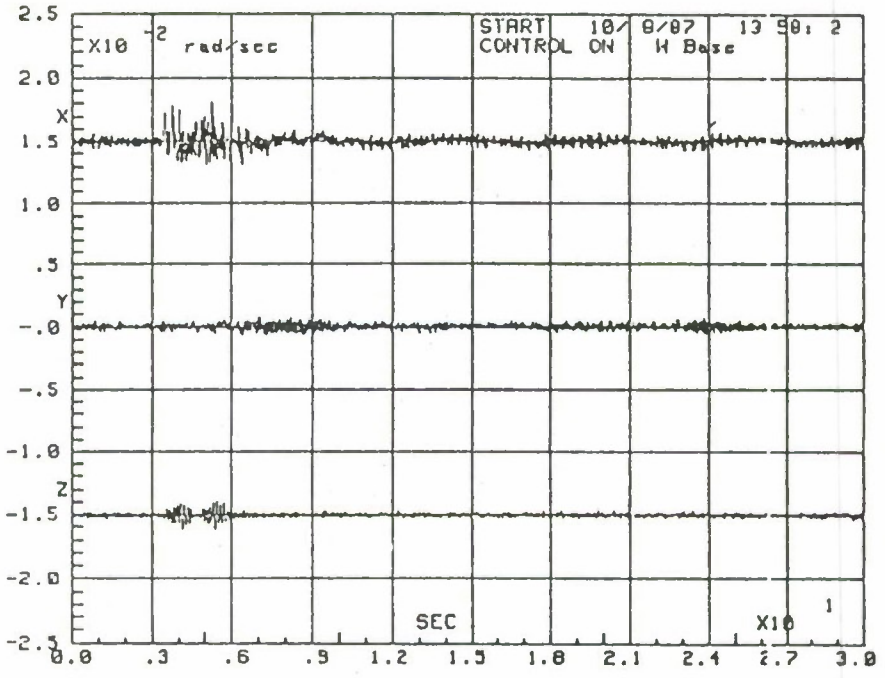


Figure 6.4-4. Closed Loop Faceplate Angular Rate Response due to the Crew Motion Disturbance.

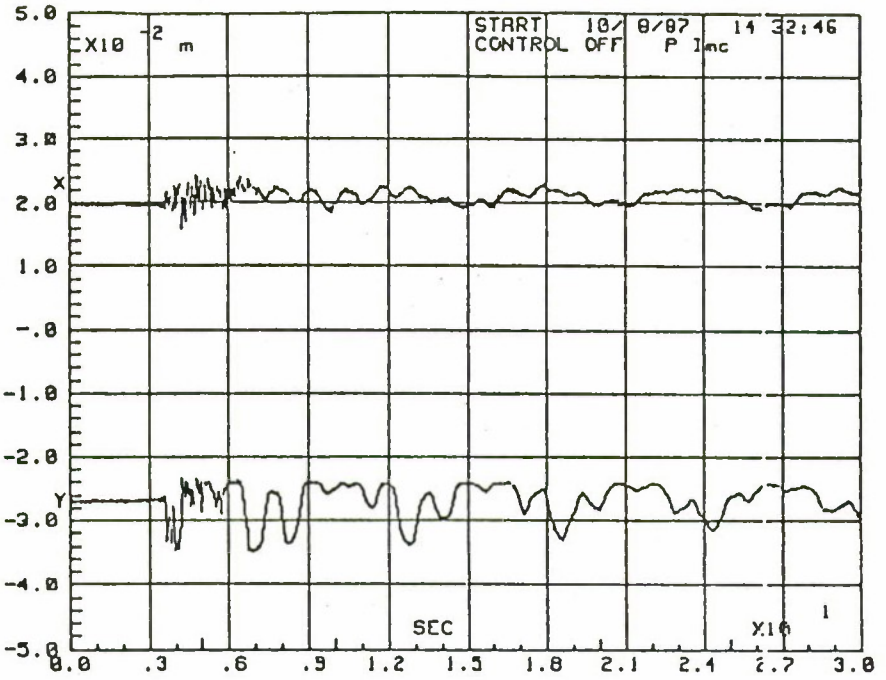


Figure 6.4-5. Open Loop Detector Response due to the Crew Motion Disturbance.

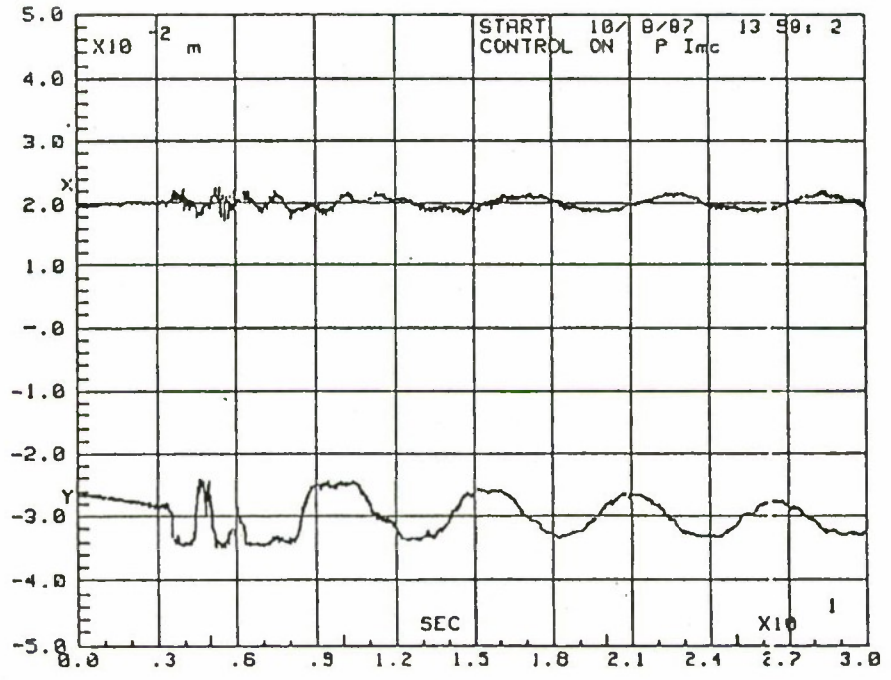


Figure 6.4-6. Closed Loop Detector Response due to the Crew Motion Disturbance.

The open loop results of the Riverside disturbance tests are given in Figure 6.4-7 as angular rates at the faceplate. Here the BET excitation occurs in both axes and is predominantly the two very narrow band components described in Section 2.2.2. Since the controller was not "tuned" to the Riverside disturbance, the most that can be expected from the closed loop results is a lack of degradation and the prevention of significant excitation of modes near the component frequencies. The open loop detector response is given by Figure 6.4-9, where it should be noted that the disturbance is removed at 22 seconds. Clearly, the pendulum behavior at the AGS hinge points has been excited. The closed loop results of the Riverside test are given in the form of faceplate angular rates in Figure 6.4-8, where apparently no improvement has resulted. However, the closed loop detector results of Figure 6.4-10 indicate a phenomenon not present in the RCS and crew motion results. In the previous tests, the unmodeled behavior at 0.2 hertz overshadowed the controller benefits at other frequencies. In the case of the Riverside tests, this 0.2 hertz mode is not heavily excited and the benefits of the controller are apparent after the disturbance is removed, at which time the pendulum modes are subject to significant damping.

The demonstration disturbance test results are given in Figure 6.4-11 for the open loop case and in Figure 6.4-12 for the closed loop case, both in the form of faceplate angular rates. The most outstanding fact is that significant damping of the dominant pendulum behavior is achieved in Figure 6.4-12. Since this effect is seen most clearly for tests in which relatively high angular rates occur, the lack of significant performance benefits for the RCS and crew motion disturbances is likely due to the fact that with small signal levels at the faceplate instruments, the AGS subsystem is essentially open loop.

The experimental test results for the Positivity controller are summarized in Table 6.4-1. The mean and RMS detector errors are presented for the open and closed loop tests. Each statistic is calculated using an average over five tests (see section 2.2.4). The requirement to remain in the linear region of operation is satisfied for the Crew, RCS, and Riverside disturbances. The results show that the Positivity controller improves the detector mean in the X and Y axes (i.e. it removes the dc bias). But, the controller does almost nothing to improve the RMS detector errors

(XandY).The lack of RMS improvement for the Crew and RCS disturbances is explained by the unmodeled 0.2-Hz mode which dominates the detector response. If the 0.2-Hz mode had been modeled, the controller most likely would have added significant damping to the mode. The lack of RMS improvement for the Riverside disturbance is expected because the 8-Hz and 10-Hz sinusoids are above the controller bandwidth.

The demonstration disturbance is utilized to evaluate the amount of vibration suppression of the laser beam provided by the Positivity controller. The demo disturbance causes the beam to miss the detector for a significant portion of the test (i.e., the detector is not operating in its linear range). The demo disturbance allows the base gyros to operate in a range with a larger SNR than was allowed in the Crew, RCS, or Riverside cases. Since the detector error is not a very meaningful value for the demo disturbance, the settling time of the base (i.e. faceplate) gyro and the percentage of detector hits are used to evaluate performance. The test results indicate the the settling time is improved by 20 seconds in the X axis and by 47 seconds in the Y axis. Table 6.4-1 also shows that the percentage of hits is increased from 66 to 89 percent. The results of the demo test were computed with one 80 sec test run; thus, averaging was not employed to increase the validity of the test results.

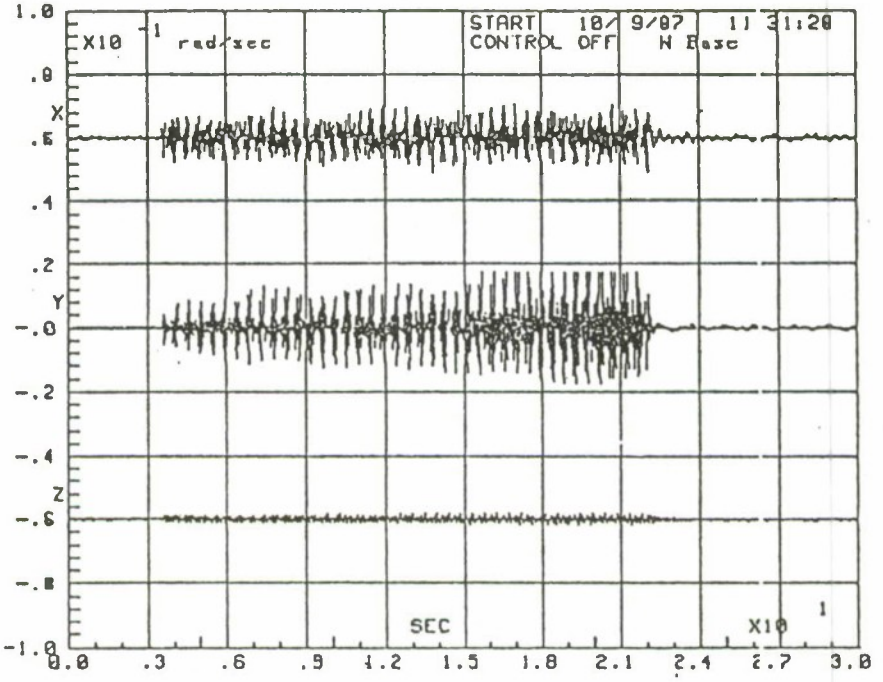


Figure 6.4-7. Open Loop Faceplate Angular Rate Response due to the Riverside Disturbance.

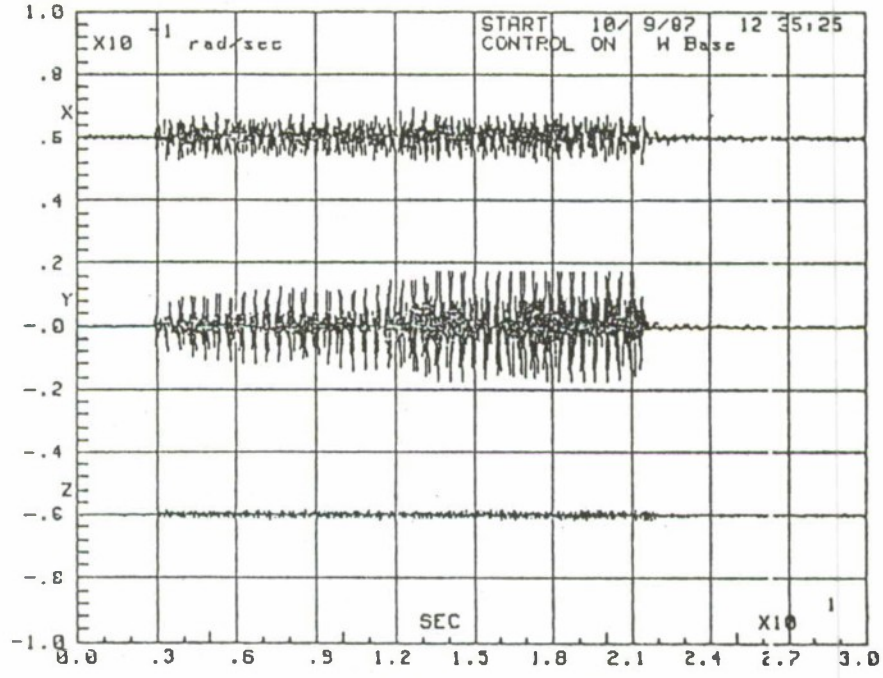


Figure 6.4-8. Closed Loop Faceplate Angular Rate Response due to the Riverside Disturbance.

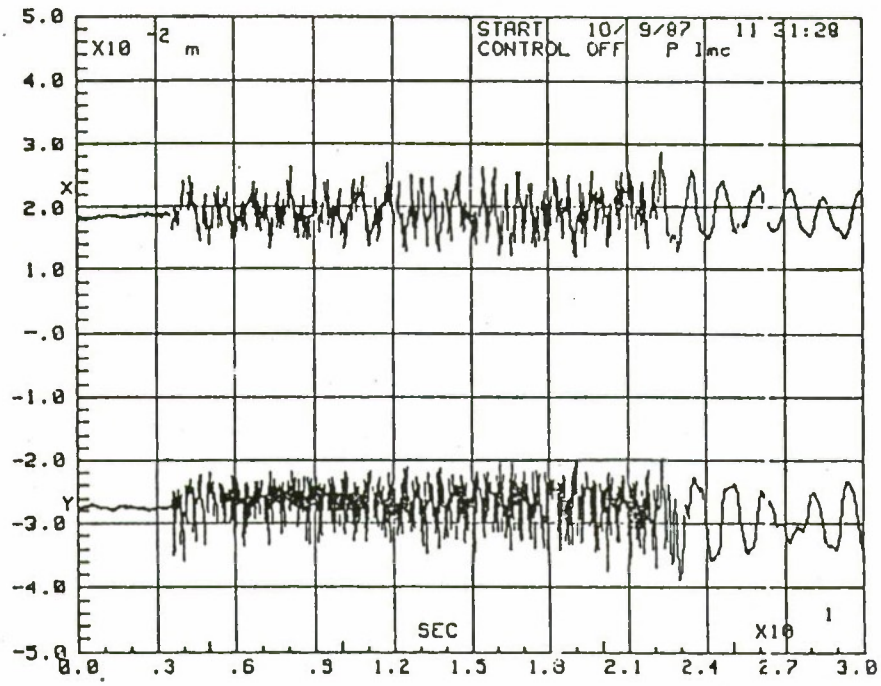


Figure 6.4-9. Open Loop Detector Response due to the Riverside Disturbance.

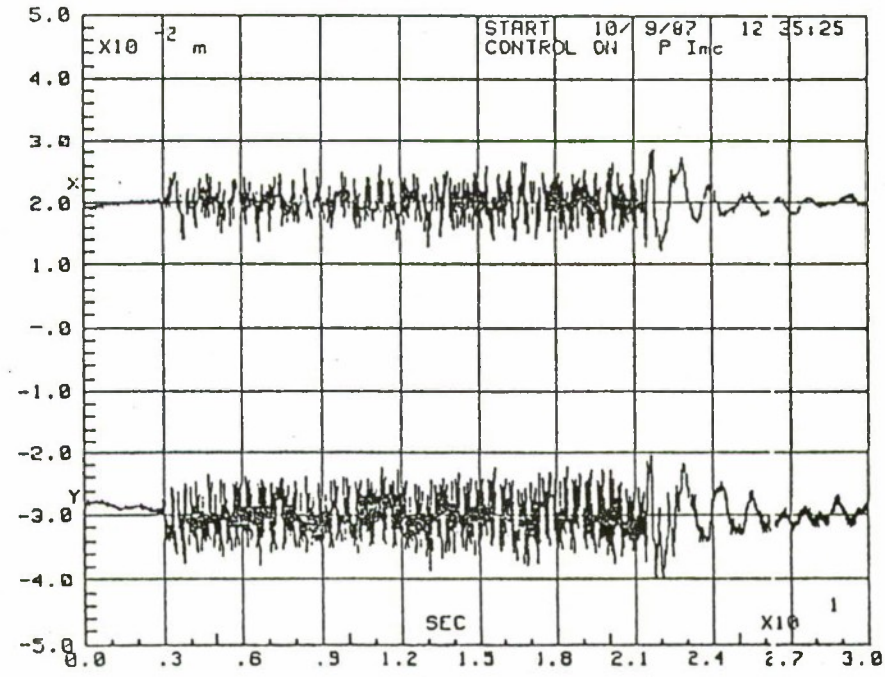


Figure 6.4-10. Closed Loop Detector Response due to the Riverside Disturbance.

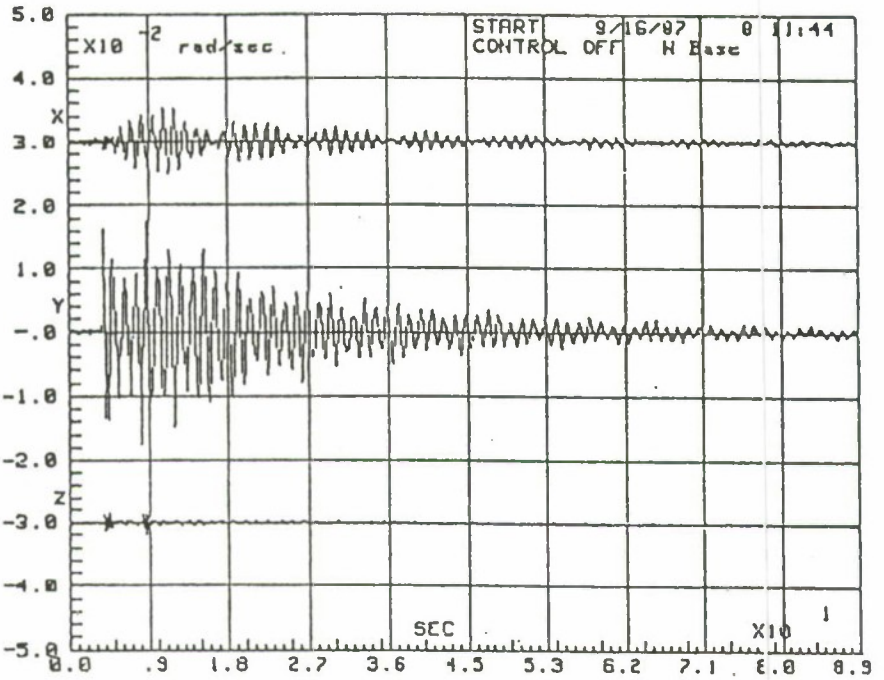


Figure 6.4-11. Open Loop Faceplate Angular Rate Response due to the Demonstration Disturbance.

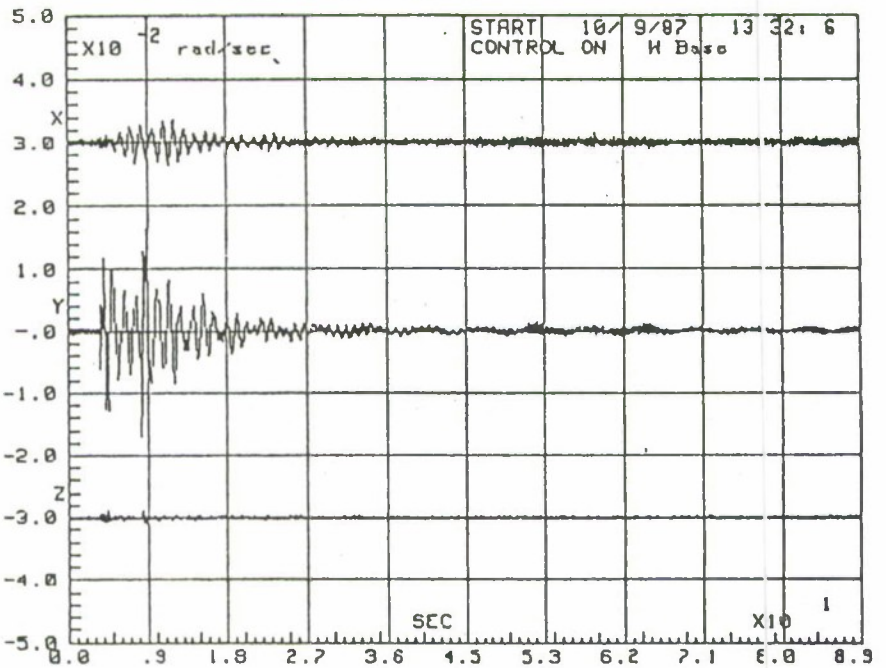


Figure 6.4-12. Closed Loop Faceplate Angular Rate Response due to the Demonstration Disturbance.

TABLE 6.4-1. SUMMARY OF TEST RESULTS FOR POSITIVITY CONTROLLER

Disturbance	Quantity	Open Loop (mm)	Closed Loop (mm)	Improvement (dB)
Crew	Detector Mean (X)	1.5	0.04	30.3
	Detector Mean (Y)	1.7	0.05	29.4
	Detector RMS (X)	1.2	0.96	1.7
	Detector RMS (Y)	3.1	3.0	0.5
RCS	Mean (X)	0.63	0.03	25.7
	Mean (Y)	2.5	0.13	25.7
	RMS (X)	3.8	2.3	4.3
	RMS (Y)	2.3	1.4	4.7
Riverside	Mean (X)	0.26	0.01	27.4
	Mean (Y)	1.9	0.03	35.7
	RMS (X)	2.7	2.5	0.8
	RMS (Y)	3.6	3.5	0.7
Demo	*T_s Base Gyro (X)	35s	15s	20s
	T_s Base Gyro (Y)	68s	21s	47s
	% Hits Detector	66%	89%	23%

*T_s = Settling time

6.5 Conclusions.

The results of the complete design of the controller using the positivity and characteristic loci methods are not encouraging. While it is possible to design a controller using these techniques, the techniques are rather awkward to use and do not seem to be directly applicable to the complicated models encountered in the ficld of LSS control. These facts may be due to the sketchy documentation available on the actual use of the methods. While the theory of positivity and its extensions give indications of the desirable frequency domain attributes of a particular system, there is almost no indication of how to achieve these goals. The exception is thc characteristic loci method, which is an extension of classical frequency domain compensation techniques to the multivariable case. However, even with characteristic loci there are significant gaps between knowledge of the goals of the controller and their actual achievement. The weak link in the characteristic loci method is undoubtedly the alignment procedure. Here again, the available documentation is slight. For example, no evaluation of the success of the various alignment procedures can be found.

The evaluation of the test results was difficult due to the limitations of thc available hardware. The most critical hardware problem was the limited range of the quadrant type photodetector, as this dictated extremely low-level disturbances. Another serious problem, which ultimately led to the elimination of the LMED actuators/sensors, is that the design frequency range of the LMED actuators is roughly five times that which is appropriate for the ACES configuration.

7.0 FILTER ACCOMMODATED MODEL ERROR SENSITIVITY SUPPRESSION (FAMESS)

FAMESS is an extension of Model Error Sensitivity Suppression (MESS) which was originally intended as a technique for reducing control and observation spillover problems often encountered in control system designs for large space structures [4]. These spillover effects are caused by the necessity of using a reduced order model for the controller design and are most apparent when such a controller destabilizes unmodeled dynamics of the actual system. MESS attempts to reduce both control and observation spillover by effectively decoupling the controller from the modes which have been omitted from the dynamic design model. However, the MESS procedure can constrain the control inputs to the plant so severely that the effectiveness of the controller is greatly reduced. Furthermore, the suppressed dynamics must be well known in order to apply the MESS procedures.

The filter accommodation part of the FAMESS design process is an attempt, via low pass filtering, to prevent destabilization of the inherently less well known high frequency modes of the system. A disadvantage of the filter accommodation approach is the additional order required by the inclusion of the output low pass filters.

The following sections include (1) a short description of the original FAMESS design procedure, (2) a description of the modifications necessary to implement the procedure in the MSFC facility, (3) a description of the model reduction and model selection processes, (4) the results of implementation in a high fidelity simulation and various observations on possible improvements in the design procedure, along with an assessment of the strengths and weaknesses of the FAMESS procedure.

7.1 Theory.

The FAMESS design procedure was originally developed for continuous-time linear systems and relied heavily on linear quadratic Guassian design procedures. The restriction to continuous-time systems is often considered by designers to be important, assuming that if the resulting controller is implemented in a sampled-data

system with a sampling rate much greater than the controller bandwidth, then the controller yields acceptable performance and robustness. This would probably be true, were it not for the fact that, because of computational and data input/output considerations, a full sample period pure delay exists in many systems, including the MSFC facility. The additional destabilizing phase lag due to the delay greatly decreases the achievable bandwidth of the controller when designed assuming a continuous-time plant with no delay. Consequently, a discrete-time LQG control design is carried out for the ACES configuration so that the sampled-data nature of the system and the delay are explicitly included in the design.

This section details first the FAMESS design procedure as originally developed for continuous-time systems with no delay. The modifications necessary to the theory in order to achieve a discrete time design are then presented.

7.1.1 Continuous-Time Theory.

The plant model is assumed to have the form

$$\begin{bmatrix} \dot{X}_c \\ \dot{X}_s \\ \dot{X}_r \end{bmatrix} = \begin{bmatrix} A_c & 0 & 0 \\ 0 & A_s & 0 \\ 0 & 0 & A_r \end{bmatrix} \begin{bmatrix} X_c \\ X_s \\ X_r \end{bmatrix} + \begin{bmatrix} B_c \\ B_s \\ B_r \end{bmatrix} u$$

$$y = [C_c C_s C_r] \begin{bmatrix} X_c \\ X_s \\ X_r \end{bmatrix}$$

u - control vector

X_C - controlled states of the system

X_S - suppressed system states

X_r - residual system states.

y - output vector.

The controlled system states (or modes) are assumed to strongly influence system performance, the suppressed modes are assumed to have little effect on system

performance, and the residual modes are assumed to be modes which would not normally be included in a control system design model due to their uncertain nature.

The quadratic performance index is

$$J = \int_0^\infty (X_c^T Q_{cr} X_c + X_s^T Q_{sr} X_s + u^T R u)\, dt.$$

The fundamental approach of the MESS philosophy is to prevent the excitation by the controller of the suppressed modes while simultaneously achieving the performance requirements via the controlled modes. The effect is to decouple the controller from the suppressed part of the system. Stated still another way, the goal of MESS is to eliminate the "spillover" to the suppressed states. The control spillover term is given by $B_S\ u$ and the observation spillover term is given by $C_S\ X_S$. The control spillover term can be penalized via the performance index in either of two ways: (1) Internal Driver Minimization or (2) Forced Singular Perturbation.

Internal driver minimization directly penalizes the spillover term $B_S\ u$ by including it in the performance index as

$$J = \int_0^\infty [X_c^T Q_{cr} X_c + u^T R u + (B_S u)^T Q_{sr} (B_S u)]\, dt$$

or

$$J = \int_0^\infty [X_c^T Q_{cr} X_c + u^T (R + B_s^T Q_{sr} B_S)\, u]\, dt.$$

It is important to note that the $X_S^T Q_{SR} X_S$ term has been omitted. The most important consequence is that feedback of the suppressed states is not required,

implying that these states do not require estimation. This fact, combined with a similar result for the state estimator design, leads to a controller of the same dynamical order as the controlled system, i.e., a reduced order controller. Also, the solution of the MESS feedback gain matrix can be obtained by standard software for solving the matrix Algebraic Riccati Equation (ARE). The resulting control law, assuming full controlled state availability, is

$$u = - F X_C.$$

The control law designed via the modified control weighting matrix deserves comment. First, if only one control input exists, the constraint forced by the B_S u weighting is also a constraint on the controlled mode internal driver B_C u. Second, even if multiple actuators exist, general control authority will be constrained unless B_S u does not imply B_C u = 0. However, in the case of multiple actuators the constraint simply leads to a preferred control vector direction so that the projection of the control vector u onto the rows of B_S u is reduced.

The estimator design takes advantage of the duality between the optimal control problem and the estimation problem. The estimator has the form

$$\dot{\hat{X}}_c = A_c\hat{X}_c + B_c u + G(y - C\hat{X}_c).$$

Expressing the estimator in terms of the estimation error $X_e = X_c - \hat{X}_c$ gives

$$\dot{X}_e = (A_C - GC_C) X_e.$$

The error "system" response is dictated by the eigenvalues of $A_C - GC_C$, which are the same as the eigenvalues of $A_C^T - C_C^T G^T$. In other words, the feedback system

$$\dot{Z} = A_C^T Z + C_C^T r,$$

$$r = - G^T Z$$

has effectively the same response as the error dynamics. Also, since it is cast in the form of a feedback system, the estimator feedback gain can be calculated via optimal control techniques with a performance index given by

$$J = \int_0^\infty (Z^T Q_{CO} Z + r^T R_O r)\, dt.$$

For the estimator design, the internal driver is $Cs^T r$, which leads to the modification

$$J = \int_0^\infty [Z^T Q_{CO} Z + r^T (R_O + C_S Q_{SO} C_S^T) r]\, dt.$$

Again, the solution for G^T can be found via standard software.

Forced Singular Perturbation penalizes spillover in a slightly more indirect manner. The quadratic performance index is first written

$$J = \int_0^\infty (X_C^T Q_{Cr} X_C + X_S^T Q_{Sr} X_S + u^T R_r u)\, dt$$

with the constraints

$$\dot{X}_C = A_C X_C + B_C u$$

$$\dot{X}_S = A_S X_S + B_S u.$$

The singular perturbation constraint

$$\dot{X}_S = 0 = A_S X_S + B_S u$$

can be solved to yield

$$X_S = -A_S^{-1} B_S u,$$

which is then used to modify the performance criterion as

$$J = \int_0^\infty [X_C^T Q_{cr} X_C + u^T(R_r + B_S^T A_S^{-T} Q_{sr} A_S^{-1} B_S)u] dt.$$

Of course, the forced singular perturbation approach is simply a special case of the internal driver minimization approach.

An almost identical procedure is followed to yield the modification to the estimator "dual" performance index:

$$J = \int_0^\infty [X_C^T Q_{co} X_C + r^T(R_o + C_S A_S^{-1} Q_{so} A_S^{-T} C_S^T)r] dt.$$

An alpha shift technique can also be used to guarantee controlled mode damping factors. The approach is to first employ an alpha shift on the open loop matrix A_C:

$$A_C' = A_C + aI, \; a>0.$$

When the modified A_C' is used in place of A_C when finding the state feedback gain matrix F, the closed loop eigenvalues will have real parts less than zero. In other words, if l is a solution to

$$\det [lI - A_C - aI + BF],$$

then

$$\text{Re } (l) < 0,$$

assuming that the original controlled system is stabilizable. The desirable properties of the alpha shift derive from the fact that if l is an eigenvalue of A_C + aI - BF, then l-a is an eigenvalue of A_C - BF; and since a>o and l<o, then

$$\mathrm{Re}\,(l + a) < -a,$$

so that the resulting eigenvalues of the nominal closed loop system all lie to the left of the line Re(s) < -a in the s-plane. However, this is not true for the suppressed modes. In fact, the alpha shift will be detrimental to modal suppression unless perfect suppression can be achieved without the alpha shift.

The alpha shift can also be used in the estimator dual control problem to guarantee a minimum damping factor for the estimator. However, for the estimator it is usual to use an alpha which is roughly 10 percent larger than the alpha for the regulator design. A comment on the use of a control law/estimator design is in order. The approach of (1) designing a control law based on full state availability, (2) designing an estimator to reconstruct the states from available measurements and (3) implementing the combination as a controller, or compensator, is based on the separation principle of optimal control. The separation principle states that the resulting closed loop eigenvalues are a combination of those of the regulator design and those of the estimator design. The separation principle, while valid for the overall system, does <u>not</u> imply that the compensator eigenvalues are any combination of the regulator and estimator design eigenvalues. This is an important fact that must be remembered in any LQG based design, such as MESS.

Filter Accommodation (FA) is a method of forcing a strong low-pass characteristic for the controller designs. The motivation for attempting to achieve a low pass controller is that of reducing, or eliminating, the spillover to high frequency residual modes since, in general, an LQG based design results in a high bandwidth controller. Furthermore, it is difficult, using the standard LQG approach, to identify how the design parameters affect the controller bandwidth.

The approach of FA is to cascade low pass filters with each of the system outputs. The result is a design model with a strong low pass characteristic and a desired corner frequency. If a full state feedback design is carried out on the new design model with no constraints on the design parameters, the resulting closed loop system has, in general, low pass characteristics which are no better than the original system without the filters. The underlying problem with this approach is the feedback of the filter states. The approach of FA is to constrain the design problem so that the feedback of the filter states is eliminated.

Before examining the FA design equations, it is worthwhile to note that the problem of high controller bandwidth is also crucial when working with non-ideal sensors and actuators since the LQG design process may actually attempt to "increase the bandwidth" of these devices to achieve the minimization of the performance index. Since there are practical reasons (noise, uncertain high frequency sensor/actuator characteristics) for avoiding such a situation, various schemes such as FA have a direct impact on all LQG based designs.

The FA approach involves adding a minor loop to the system which enforces the constraint of zero filter state feedback. Figure 7.1-1 illustrates the interconnections required by the additional loop.

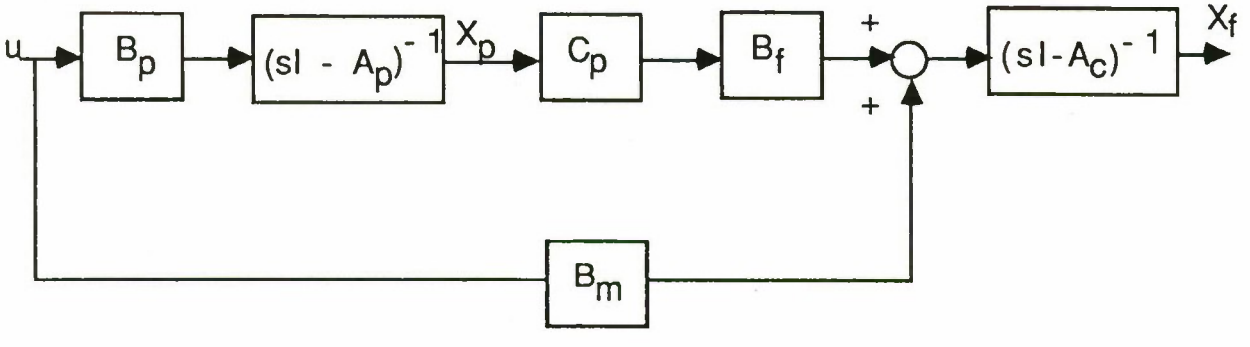


Figure 7.1-1 Design Model for Filter Accommodation Regulator Design.

The matrix B_m is artificially introduced to aid in the solution of the constrained design equations. The resulting state equations are

$$\begin{bmatrix} \dot{X}_p \\ \dot{X}_f \end{bmatrix} = \begin{bmatrix} A_p & 0 \\ B_f C_p & A_f \end{bmatrix} \begin{bmatrix} X_p \\ X_f \end{bmatrix} + \begin{bmatrix} B_p \\ B_m \end{bmatrix} u$$

which can be written in more compact notation as

$$\begin{bmatrix} \dot{X}_1 \\ \dot{X}_2 \end{bmatrix} = \begin{bmatrix} A_{11} & 0 \\ A_{21} & A_{22} \end{bmatrix} \begin{bmatrix} X_1 \\ X_2 \end{bmatrix} + \begin{bmatrix} B_{11} \\ B_{21} \end{bmatrix} u$$

where $A_{11} = A_p$, $A_{21} = B_f C_p$, $A_{22} = A_f$, $B_{11} = B_p$, and $B_{21} = B_m$.

Now the problem is to minimize

$$J = \int_0^\infty (X^T Q X + u^T R u)\, dt$$

where

$$Q = \begin{bmatrix} Q_{11} & Q_{12} \\ Q_{21} & Q_{22} \end{bmatrix},$$

to obtain the feedback control

$$U = KX = [K_1 \quad K_2] \begin{bmatrix} X_1 \\ X_2 \end{bmatrix}$$

subject to

$$K_2 = 0.$$

In other words, the problem is to find the optimal feedback control law such that the filter states are not fed back. The solution has the form

$$u = -R^{-1} B^T P X$$

where

$$B^T = [B_{11}^T \quad B_{21}^T],$$

$$P = \begin{bmatrix} P_{11} & P_{12} \\ P_{12} & P_{22} \end{bmatrix},$$

and

$$X = \begin{bmatrix} X_1 \\ X_2 \end{bmatrix}$$

The requirement of zero feedback of X_2 yields the constraint

$$B_{11}^T P_{12} + B_{21}^T P_{22} = 0$$

which, when carried through in an expansion of the Riccati equation in P yields the three equations to solve for the elements of P:

Modified Riccati Equation

$$(A_{11}^T P_{11} + A_{21}^T P_{12}^T) + (P_{11} A_{11} + P_{12} A_{21})$$

$$-(P_{11} B_{11} R^{-1} B_{11}^T P_{11} + P_{11} B_{11} R^{-1} B_{21}^T P_{12}^T)$$

$$+ P_{12} B_{21} R^{-1} B_{11}^T P_{11} - P_{12} B_{21} R^{-1} B_{21}^T P_{12}^T) = 0$$

Sylvester Equation

$$A_{11}^T P_{12} + P_{12} A_{22} + A_{21}^T P_{22} + Q_{12} = 0$$

Liapunov Equation

$$A_{22}^T P_{22} + P_{22} A_{22} + Q_{22} = 0$$

In the original FA procedure B_{21}, Q_{12}, and Q_{22} are free parameters and B_{21} is chosen to satisfy

$$B_{21}^T = -B_{11}^T P_{12} P_{22}^{-1}.$$

Q_{12} and Q_{22} are chosen at the designer's discretion with the constraints that the overall optimal control problem is well posed and that the three design equations possess solutions. The Liapunov equation is solved first for P_{22}, the Sylvester's equation is next solved for P_{12}, and the Riccati equation is solved for P_{11}. At that point the solution to the original optimal control problem is solved with zero feedback of the filter states.

An alternative approach is suggested by investigating the situation in which

$$Q_{12} = 0$$

and

$$Q_{22} = 0.$$

The first requirement causes no problem since the original problem is still meaningful. The second requirement is another matter, but if the open loop system is stable and controllable, the closed loop system will also be stable and controllable. Furthermore, there is no overriding practical reason that the filter states should appear in the performance index, in view of the facts that they are not the desired quantities to be controlled and that the designer has full a priori control over the filter dynamics.

The new requirements on Q_{12} and Q_{22} now give the mathematically trivial solutions for P_{12} and P_{22}:

$$P_{12} = 0,$$

and

$$P_{22} = 0.$$

Also, the modified Riccati equation reduces to that which would have existed had the filters been ignored completely,

$$A_{11}^T P_{11} + P_{11} A_{11} - P_{11} B_{11} R^{-1} P_{11} + Q_{11} = 0$$

and

$$B_{21} = 0.$$

There is some danger in forcing $Q_{12} = 0$ and $Q_{22} = 0$. This danger is that of assuming that X_1 (or X_p) are available for feedback, when actually only estimates are available. Care must be taken when designing the estimator so that the filters are included in the estimator model, to ensure that the correct estimates are used in the control law.

The preceding very specific solutions to the FA design equations should not be misinterpreted as the only logical approach to the FA design equations since there are systems and design procedures for which these simplifications do not apply.

7.1.2 Discrete - Time Theory.

The motivation for implementing a FAMESS controller designed using discrete-time counterparts of the continuous-time techniques deserves some explanation. The decision to use discrete-time techniques is, of course, in part motivated by the fact that the hardware implementation is sampled-data in nature. However, this fact alone probably would not be sufficient reason to modify the existing techniques, since the system sampling rate (50 Hz) is high compared to the frequency of many of the dominant known modes (from 0.5 Hz to less than a 2.0 Hz for the first 15 significant modes). The problem with implementing a continuous-time design is that

other destabilizing effects are present in the system. Probably the most severe of these effects is the inherent delay associated with data I/O and computation of the controller commands. In the case of the LSS GTF this delay is a full sampling period, which contributes 36 degrees of phase lag at 5.0 Hz. Less severe, but certainly causes of concern, are the destabilizing effects of unmodeled sensor and actuator dynamics.

Of course, each of these effects can be handled, at least approximately, by including models of the delay and the sensor/actuator dynamics. There are several reasons for not approaching the problem in such a way. First, the inclusion of sensor/actuator and delay models can contribute to an "order explosion" for the resulting controllers since each additional modeled effect contributes directly to the dynamical order of the resulting controller. Second, it is not a simple matter to incorporate the resulting design models into the MESS design procedure. Finally, it is much easier to deal with the pure delay in a discrete-time approach.

The basic MESS design approach is easily extended to the discrete-time case, where now the performance index is

$$J = \sum_{k=o}^{\infty} X_c^T(k)\, Q_{cr}\, X_c(k) + u^T(k)\, R\, u\,(k)$$

and the discrete-time state space model is of the form

$$\begin{bmatrix} X_c\,(k+1) \\ X_s\,(k+1) \\ X_r\,(k+1) \end{bmatrix} = \begin{bmatrix} A_c & 0 & 0 \\ 0 & A_s & 0 \\ 0 & 0 & A_r \end{bmatrix} \begin{bmatrix} X_c\,(k) \\ X_s\,(k) \\ X_r\,(k) \end{bmatrix} + \begin{bmatrix} B_c \\ B_s \\ B_r \end{bmatrix} u(k).$$

The singular perturbation approach to MESS is not strictly applicable to the discrete-time case. However, internal driver minimization is identical for the discrete case. The performance index is modified to give

$$J = \sum_{k=o}^{\infty} X_c^T(k)\, Q_{cr}\, X_c(k) + u^T(k)(R_r + B_s^T A_s^{-T} Q_{sr} A_s^{-1} B_s)\, u(k)$$

and the control law which minimizes J has the form

$$u(k) = -F\, X_c(k)$$

and can be found via standard software for solving the discrete algebraic Riccati equation.

As for the continuous-time case, the estimator design is performed by solving a so-called dual optimal control problem. The estimator has the form

$$\hat{X}_c(k+1) = A_c \hat{X}_c(k) + B_c u(k) + G\,[Y(k) - C_c \hat{X}_c(k)].$$

The feedback system

$$Z(k+1) = A_c^T Z(k) + C_c^T r(k)$$

$$r(k) = -\,G^T Z(k)$$

has effectively the same form of response as the error dynamics. The estimator feedback gain is calculated by minimizing the performance index given by

$$J = \sum_{k=o}^{\infty} Z^T(k)\, Q_{co} Z(k) + r^T(k)\, R_o r(k).$$

The internal driver of this system is $C_S{}^T(k)$, leading to the modified performance index

$$J = \sum_{k=o}^{\infty} Z^T(k)\, Q_{co} Z(k) + r^T(k)(R_o + C_s A_s^{-1} Q_{so} A_s^{-T} C_s^T) r(k).$$

The effect of modifying the performance index is to penalize use of the suppressed system internal drivers $B_S\, u(k)$ and $C_S{}^T\ r(k)$, effectively decoupling the controller from the suppressed system.

Since one of the major reasons for utilizing the discrete time approach is to allow inclusion of the pure delay inherent in the system, an analysis of the effect of including the delays on the MESS procedure is in order. The delay states, which are here modeled at the system inputs, modify the design model to give

$$X_c(k+1) = A_c X_c(k) + B_c X_D(k)$$

$$X_s(k+1) = A_s X_s(k) + B_s X_D(k)$$

$$X_D(k+1) = u(k)$$

$$y(k) = C_c X_c(k) + C_s X_s(k)$$

The suppressed state internal driver is now $B_S\ X_D(k)$ and the performance index is now

$$J = \sum_{k=o}^{\infty} X_c^T(k)\, Q_{cr} X_c(k) + X_D^T(k)\, Q_{Dr} X_D(k) + u^T(k)\, R_r\, u(k).$$

The internal driver weighting is now $B_S{}^T\ A_S{}^{-T}\ Q_{Sr}\ A_S{}^{-1}\ B_S$ leading to the modified performance index

$$J = \sum_{k=o}^{\infty} X_c^T(k)\, Q_{cr} X_c(k) + X_D^T(k)(Q_{Dr} + B_s^T A_s^{-T} Q_{sr} A_s^{-1} B_s)\, X_D(k) + u^T(k)\, R_r\, u(k).$$

The performance index for the estimator dual control design is unaffected by the inclusion of delays at the inputs.

An alpha sealing can be used for discrete-time designs to guarantee minimum damping for the controlled modes. For the discrete case the system model for the design is modified as

$$A' = e^{\alpha T} A_c$$

$$B' = e^{\alpha T} B_c$$

The optimal feedback law is

$$u(k) = -F X_c(k)$$

which will result in the eigenvalues of the modified closed loop system satisfying

$$| \lambda[e^{\alpha T}(A_c - B_c F)] | < 1$$

which is equivalent to

$$e^{\alpha T} | \lambda (A_c - B_c F) | < 1$$

or

$$| \lambda (A_c - B_c F) | < e^{-\alpha T}.$$

Then the eigenvalues of the actual closed loop system lie inside a circle of radius e^{-aT} center at the origin in the Z-plane. Thus, any amount of damping can be

specified by choosing a exactly as if choosing a minimum damping factor for a continuous-time design. Again, the alpha scaling must be used with care, since it can prevent suppressed mode weighting from having any effect in the design of F. In other words, any interpretation of the alpha-shift line as a stability margin is unjustified in view of the model reduction.

Filter accommodation has not been extended to the discrete-time case. For the ACES effort, this fact is of little importance, as the computational burden of dedicated low pass filters at each output is unacceptable.

7.2 Model Selection and Reduction.

The first step in the controller design process for any complex system is that of model reduction. The model reduction technique must retain, in the reduced order model, sufficient fidelity to (1) enable the design to achieve acceptable performance and (2) ensure that all stability-related issues can be addressed during the design process. In the case of LQG-based design methods, such as MESS, the reduced order model must also fit within the order constraints of the controller. For the ACES hardware configuration this is a critical issue. The following sections outline an evolution of the design model, an evolution which is dictated by the conflicting requirements of stability, performance, and controller order.

7.2.1 Decentralized Approach.

Two separate models are chosen for the control system design, since the system can be naturally separated into a vibration suppression system and a pointing stabilization system. The concept of decentralization with MESS is used to choose the design models so that their separate controller designs can be implemented without destabilization.

The pointing stabilization portion of the problem involves the image motion compensation (IMC) system alone. The design approach involves realizing a regulator control system which possesses sufficient bandwidth to reject disturbances introduced at the detector via structural vibrations of the Astromast, gimbal arm, and antenna arm.

The vibration suppression system is intended to provide a relatively benign environment for the pointing stabilization system. This is achieved via stabilization of the detector motion induced by the BET excitation.

Since the two controllers, called the IMC and Astromast controllers, are designed separately, with no explicit knowledge of the other's affect on the system, decentralized MESS techniques are used to ensure that the interaction of the controllers is not destabilizing. This "decoupling" of the controllers is accomplished via the choice of the design models. First, the controlled modes are selected for each controller. Second, the suppressed modes are identified for each controller design model. At this point, some of the controlled modes can appear in both design models. This is undesirable, since both controllers will attempt to exercise great authority over the common controlled nodes. The effect of designing each controller independently can then be instability or poor performance.

Of course, one way to avoid the possibility of instability is to use only one large design model. However, there are practical computational and reliability reasons for using decentralized controllers. A more attractive solution, and one which presents the advantage of the separate controllers, is that of decentralization by MESS. This decentralization is accomplished by assigning the common controlled modes to one controller as controlled modes and to the other as suppressed modes. Naturally, this approach will be more effective if the number of common controlled modes is small, as is the case for the ACES model. Of course, the suppression of the common controlled modes can constrain the achievable performance of the closed loop system.

7.2.2 IMC Design Model.

The basic approach to model reduction is via the frequency domain. A mode normally is selected as significant to the design process if its contribution at any

frequency to any combination of input/output transfer functions is greater than a specified tolerance (e.g., 6.0dB). However, this criterion applied to the ACES configuration control model leads to the selection of 36 modes from a total of 43. In a straightforward LQG design, this would lead to a 72 order controller.

The philosophy used for the MESS design, while aided by the above mentioned selection criterion, takes a quite different approach. The idea is to first limit the number of controlled modes retained in the design model to fit within the estimated computational limitations. The input/output pairs are also limited to those pertinent to the particular decentralized controller for which the model is chosen. The tolerance is then relaxed until the number of significant modes fits within the order constraint dictated by the computational limitations. The overall effect is to rank the modes according to their contributions to the LOS.

Other properties of the system can give the designer information regarding which input/output pairs need be examined. For the IMC controller, two transfer characteristics dominate the four possible channels. These dominant channels are (1) the X gimbal torque to Y detector and (2) the Y gimbal torque to X detector. The separation between the channels is greater than 30 dB, leading to the decision to neglect the two relatively insignificant input/output pairs in the modal selection process. The channel separation is clear from examination of Figures 7.2-1 through 7.2-4. Modal selection on the two significant input/output pairs yields three significant modes at 1.51 Hz, 1.67 Hz, and 2.08 Hz. The first of these is primarily the pendulum motion of the inner pointing gimbal. The latter two involve both outer gimbal and gimbal arm bending motion. These three modes are designated as the IMC controlled modes.

The suppressed modes for the IMC include all of the remaining modes of the full control model. This approach is completely consistent with the standard MESS procedure, since any of the suppressed modes may have zero weighting, thus designating them as residual modes. In the case of the IMC controller, the large number of suppressed modes is unlikely to cause severe constraints on the control because of the high degree of isolation from much of the structural behavior of the Astromast.

The control design model for the IMC is completed by adding delay states to model the inherent system delay and by adding integrators at the outputs to improve steady state error characteristics.

7.3 Design Process and Simulation Results.

The following sections describe the design process encountered in evolving the design which was actually implemented in the MSFC facility. Since the IMC and MAST controllers are designed separately, they are described in separate sections. Also, several major redesigns were necessary to fit the controller within the computational limitations. Therefore, each major redesign is described in a separate section.

7.3.1 Original IMC Design.

The IMC design involves a two input (the pointing gimbal torques), two output (the two photodetector outputs) system with three modes, two delay-modeling states, and two states which are output integrations whose purpose is to provide zero steady state error to constant photodetector disturbances. The approach to the resulting LQG design is to suppress the remaining modes while at the same time controlling the three modes and providing sufficient bandwidth to treat the disturbances at the sensors (which are introduced via structural vibrations of the MAST and are not significantly controllable at the IMC gimbals) as output-additive. Dealing with the MAST vibrations as additive output disturbances leads to a fairly simple method of rejection: that of keeping the "loop gain" of the IMC control system as high as is practical over the frequency range of the dominant MAST vibrational modes observed at the detector. Fortunately, high bandwidth designs are typical of the LQG methodology used in the FAMESS approach.

Of course, there are limitations on the achievable bandwidth, namely sensor and actuator bandwidth, sensor induced noise, and control model accuracy. Shortly, it will be seen that the limitation in the case of the ACES design is mainly that of model accuracy.

The IMC design is accomplished via the MESS procedure combined with an output regulation weighting approach. In other words, the controlled state weighting matrix has the form $C^T Q_c C$, so that the state weighting for the individual states is "distributed" according to their contribution to the photodetector output (LOS error). The initial step of the design iteration process is to assign unity weighting to the outputs and also to the control penalty term in the performance index. Unity diagonal weighting is also assigned to the weighting matrices of the dual estimator design. Initially, the alpha shift is chosen as $\alpha_c = 0.1$ and $\alpha_e = 0.11$.

The design iteration process proceeded from this stage with several short investigations into the effect of varying the various design parameters. The design evaluation at this point was based on overall performance of the controller in a linear simulation with all 43 evaluation model modes, as the high fidelity simulation was not operational.

The first investigation step involved the investigation of the effect of increasing the weighting of one of the photodetector outputs, after it was noticed that the y-axis detector output was roughly a factor of 3 greater than that of the x-axis detector output. Increasing the y-axis output weighting by a factor of 100 achieved the desired balance in the closed loop detector outputs.

The second step was to investigate the effect of increasing the alpha-shift. It was hoped that there would be a corresponding increase in the observed bandwidth of the system, resulting in the rejection of output disturbance caused by MAST vibrational effects. This attempt to achieve increased bandwidth met with limited success, as significant increases in the values of α_c and α_e soon caused sufficient spillover to destabilize the closed loop systems. This destabilizing effect was not diminished by a subsequent increase in the spillover weighting matrix Q_s for the regulator and estimator suppressed states. As has been mentioned, the α shift is a guaranteed effect, no matter what matrix Q_s may be. The unavoidable conclusion was that the controlled modes could not be moved by a significant amount without destabilization.

The final steps in the IMC design iteration process occurred after the high fidelity simulation became operationa. The motivation for a redesign was overwhelming, since the IMC controller/simulation combination was initially unstable. Since there were no significant differences in the simulations (it was determined that nonlinear effects were not responsible) an investigation of the input/output properties of the controller was performed. We found that the controller itself possessed an extremely lightly damped mode at approximately 9 Hz. The occurrence of this undesirable controller bahavior is probably best explained by considering the effects of modal suppression via constraining the control effort. Note that at this step of the design process, significant modal suppression has been introduced for all modes other than the IMC controlled modes.

The ACES model contains 43 modes, spaced in frequency by as little as 0.01 Hz and ranging from 0.09 Hz to roughly 8.82 Hz. By suppressing the great majority of these modes, the design process is almost certain to place controller modes outside the modal frequency range to prevent spillover within. This illustrates a fundamental limitation of MESS; namely, that with a limited number of sensors and actuators simultaneous control and suppression can be difficult to achieve with a reasonably robust controller.

There are at least two methods of ensuring that the lightly damped controller modes do not appear. The first is to reduce the suppressed mode weighting in the design parameter set. The other is to force the design to be conservative by increasing the control weighting. Of the two options, the former probably lends more freedom to the designer, since only some of the modes may need decreased suppression. However, it is not clear how to make the selection.

Thus, the latter method was used to prevent the unreasonable design constraint of simulation control and suppression. The final design parameters are given in Table 7.3-1. The simulated open loop RCS disturbance response and the response with the final IMC is given in Figure 7.3-1.

TABLE 7.3-1. FINAL IMC CONTROLLER DESIGN PARAMETERS

Design Parameter	Value
Q_R	diag [100.0 1.0]
Q_o	1.0 I_{10}
R_R	500.0 I_2
R_o	50.0 I_2
Q_{rs}	100.0 I_{74}
Q_{os}	100.0 I_{74}
α_c, α_e	0.0

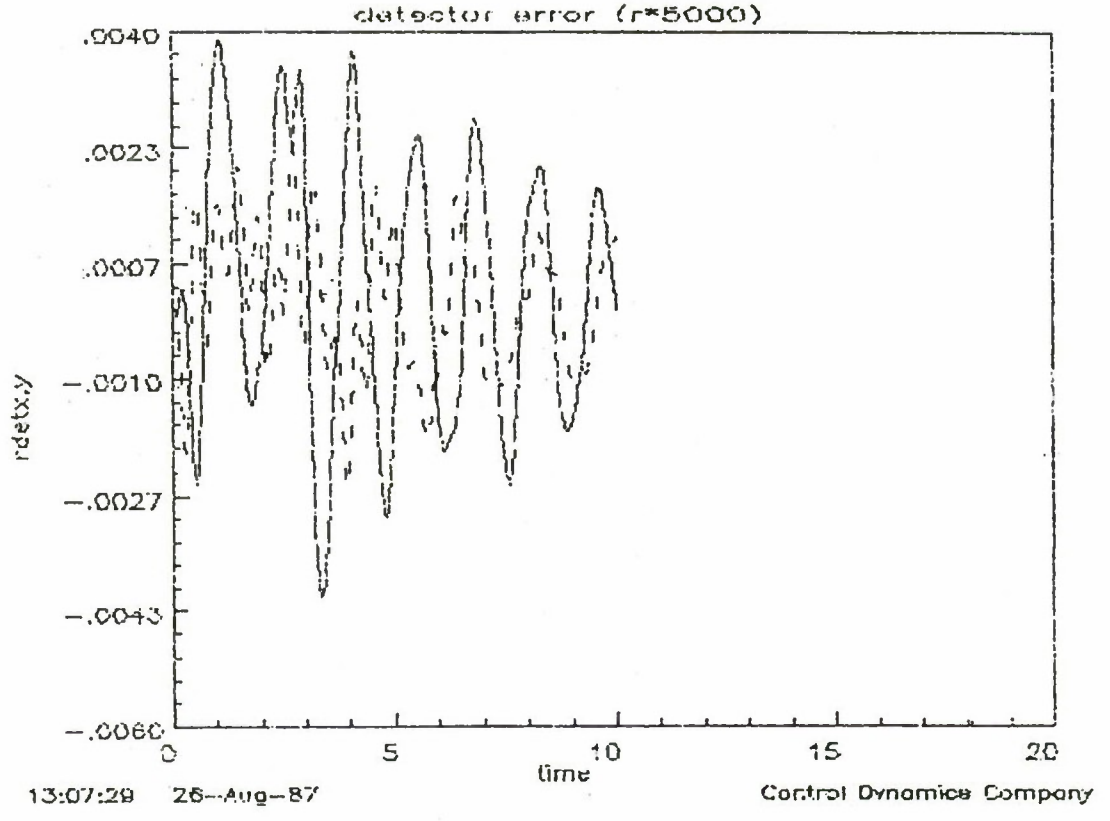


Figure 7.3-1. Detector Response with Final Controller to Simulated RCS Disturbance.

All design iterations were based on consideration of the controller's various responses to the simulated RCS disturbance. The justification for not using the response of the system to crew and Riverside disturbances is based on several facts. The first of these is that the overall disturbance profile is not amenable to the design of optimal estimators based on statistical characteristics of the disturbances, since the overall disturbance profile is not stationary. Another reason to use the RCS disturbance exclusively is that it is relatively easy to determine the short-comings of candidate controllers in terms of modal suppression, modal damping, and steady-state error properties. A final reason for relying on the RCS disturbance is that, with obvious differences, the RCS is, at the very least, a fair approximation to an impulse input. This is beneficial in that most, if not all, modes are strongly excited.

While it is true that relying exclusively on the RCS disturbance can lead to controllers that are tuned to a particular input, it is by no means clear that any reasonable alternative exists within the FAMESS framework.

7.3.2 MAST Controller Design Process.

The design of the MAST controller was executed in several stages, just as was done for the IMC controller. However, the motivations for the MAST controller re-designs were distinctly different in several cases. In fact, with the exception of an investigating iteration process intended to determine the usefulness of alpha-shift techniques, the major redesign effort centered on the attempt to reduce the controller order so that the controllers fit within the computational limitations of the facility. The various controller designs are described in subsequent sections.

7.3.2.1 Original MAST Controller Design.

The original design of the MAST controller involved several steps. The initial design parameters were chosen to be unity scaled identify matrices, with the exception of the suppressed state weighting matrices, which were initially zero matrices, and α_c and α_e which were 0.1 and 0.11, respectively.

Since the MAST and IMC controllers are intended to operate concurrently, all MAST simulations included both controllers. It is important to note that the design model for the MAST controller design did not include the IMC controller. As a consequence, it was possible to evaluate spillover effects between the two controllers.

The initial design with the nominal values of the design parameters was not stable due to spillover effects. Attempts to stabilize the system by increasing the suppressed state weighting were not successful. As with the IMC design the major contributor to the spillover appeared to be the alpha-shift technique since setting $\alpha_c = \alpha_e = 0$ immediately led to a stable design. Subsequent investigations showed that for any significant α_c and α_e, spillover effects were devastating to the stability of the closed loop system. For this reason, the values of α_c and α_e were set to zero in all designs.

The next step in the design of the original MAST controller was that of increasing the suppressed mode weighting so that the closed loop response appeared to exhibit no significant spillover. This was difficult to ascertain, since the system response with no spillover was unknown, although the undesirable effects on stability could have been verified via eigenvalue studies. For the situation at hand, it was sufficient to increase the suppressed mode weighting across the board, hence an investigation of the effects of spillover on each particular mode was not performed.

The next step in the design process was to increase the controlled mode weighting uniformly, i.e., by scaling the initial identity matrix weighting, as is indicated in ACOSS 1. However, we found that uniformly increasing the weighting had much the same effect as the alpha shift in that spillover was unacceptable. Therefore, individual modes were "targeted" according to their apparent contribution to the detector response. This was executed for each significant mode in sequence. An interesting finding during the process of increasing the controlled mode weighting was that there appeared to be a "point" beyond which increased weighting did not significantly contribute to improving the response of the system, with the exception that eventually the system became unstable due to spillover.

Another important aspect of the MAST design is the effect of the LMED actuators and sensors on the performance and stability of the system. During the process of "targeting" the various controlled modes we noted that several modes that were primarily controllable/observable at the LMED locations were contributing to spillover problems and significantly limiting the achievable performance of the overally system. Attempts to reduce the spillover via increased suppression met with limited success. The probable cause of this anomalous bahaviour is that the LMED locations are intended to provide control over the largest number of modes possible. Effectively, this "forces" the LMED part of the controller to spill over to suppressed modes. The problem should have been helped by increased suppressed mode weighting, but the other control actuators were constrained too heavily to result in any performance improvement. Eventually, the problem was solved by directly penalizing the LMED control effort. Note that MESS suppresses the known model error due to the "model reduction" and not the unknown model inaccuracies.

An important lesson can be learned from the experience with LMEDs. Simply stated, "more controllable modes" is much the same as "more spillover" and "more sensitivity." In hindsight, it is clear that by placing the LMEDs to optimize the number of controllable/observable modes, the effect is in direct opposition to the hoped-for effects of the controller, which are to decouple the suppressed modes from the controller (and hence the LMED sensor/actuator pairs). The problem is compounded in the case of the ACES configuration, where the model has 15 modes between the frequencies of 0.9 Hz and 2.0 Hz, which is precisely the range of frequencies over which the LMEDs are the most effective. Also, since the LMED proof-mass motion is involved in at least eight of the modes in this frequency range, the LMEDs cannot be considered ideal collocated sensor/actuator pairs. Hence, the controller must perform the nontrivial task of stabilizing the closed loop behavior in this frequency range. While this is easily accomplished for a perfect model with no suppressed modes, the resulting controller (and hance the closed loop system) is very sensitive to model inaccuracies, which in the FAMESS approach are partially due to the separation of the modes into the suppressed and controlled classifications. Stating the problem in another way, it is clear that closed-loop control using the LMED pairs must be "gain stable." Unfortunately, little or no performance benefits can be realized with such controllers. However, the foregoing discussion explains the result obtained via simulation investigations; namely, that

the LMED control effect must be heavily weighted, or penalized, in order to achieve acceptable spillover characteristics.

It should be clearly understood that the problem encountered with the ACES configuration LMED pairs is not an indictment of either the LMEDs or the FAMESS design tcchnique. Two circumstances contributed to the situation: (1) the LMEDs cannot be approximated by ideal collocated sensor-actuator pairs in the frequency range of interest and (2) the modes of the system are extremely closely spaced in this range. The absence of either situation would likely lead to the effective use of the LMEDs.

Also, in a morc realistic situation, the LMED locations could be changcd to alleviate the problem of "too many" closely spaced modes. Another alternative is to customize the design of proof-mass actuators to ensure that over some frequency range, these devices are approximately ideal.

Thc final design parameters of the original MAST controller are contained in Tablcs 7.3-2, 7.2-3, and 7.3-4.

Table 7.3-5 contains various particulars such as MAST controller order, total controller order, and sensors and actuators used. Figure 7.3-2 is the detector error response to the simulated RCS input with both the IMC controller and the MAST controller operating. Clearly, the detector error is significantly reduced compared to Figure 7.3-1 which is the detector error response with no MAST controller opcrational.

TABLE 7.3-2. DESIGN PARAMETERS FOR THE ORIGINAL MAST CONTROLLER DESIGN (Q_R, R_R)

Design Parameters	Value	
Q_R	Mode 4	2.5×10^3*
	Mode 5	2.5×10^3
	Mode 6	2.5×10^2
	Mode 9	1.0×10^3
	Mode 10	1.0×10^3
	Mode 12	1.0
	Mode 15	1.0
	Mode 16	1.0
	Mode 17	1.0
	Mode 19	1.0
	Mode 23	1.0
	Mode 24	1.0
	Mode 28	1.0
R_R	AGS-X	1.0
	AGS-Y	1.0
	AGS-Z	1.0
	LMED1-X	1.0×10^6
	LMED1-Y	1.0×10^6
	LMED2-X	1.0×10^6
	LMED2-Y	1.0×10^6

*The two state variables associated with each mode are weighted equally.

TABLE 7.3-3. DESIGN PARAMETERS FOR THE ORIGINAL MAST CONTROLLER DESIGN (Q_o, R_o)

Design Parameters	Value	
Q_o	Mode 4	5.0×10^3
	Mode 5	5.0×10^3
	Mode 6	5.0×10^2
	Mode 9	2.0×10^3
	Mode 10	2.0×10^3
	Mode 12	1.0
	Mode 15	1.0
	Mode 16	1.0
	Mode 17	1.0
	Mode 19	1.0
	Mode 23	1.0
	Mode 24	1.0
	Mode 28	1.0
R_o	Faceplate $\dot{\Theta}_x$	1.0
	Faceplate $\dot{\Theta}_y$	1.0
	Faceplate $\dot{\Theta}_z$	1.0
	LMED1 $\ddot{x}$	1.0
	LMED1 $\ddot{y}$	1.0
	LMED2 $\ddot{x}$	1.0
	LMED2 $\ddot{y}$	1.0
	Tip $\dot{\Theta}_x$	1.0
	Tip $\dot{\Theta}_y$	1.0
	Tip $\dot{\Theta}_z$	1.0
	Tip $\ddot{x}$	1.0
	Tip $\ddot{y}$	1.0

TABLE 7.3-4. DESIGN PARAMETERS FOR THE ORIGINAL MAST CONTROLLER DESIGN (Q_{rs}, Q_{os}, α_c, α_e)

Design Parameters	Value
Q_{rs}	$1.0 \times 10^5 \times I$
Q_{os}	$2.0 \times 10^5 \times I$
α_c	0.0
α_e	0.0

TABLE 7.3-5. ATTRIBUTES OF THE COMBINED IMC/MAST CONTROLLER

CONTROLLER ATTRIBUTES	
MAST Controller Order	33
IMC Controller Order	12
Total Controller Order	45
IMC Actuators	2
IMC Sensors	2
MAST Actuators	7
MAST Sensors	12
Total Actuators	9
Total Sensors	14

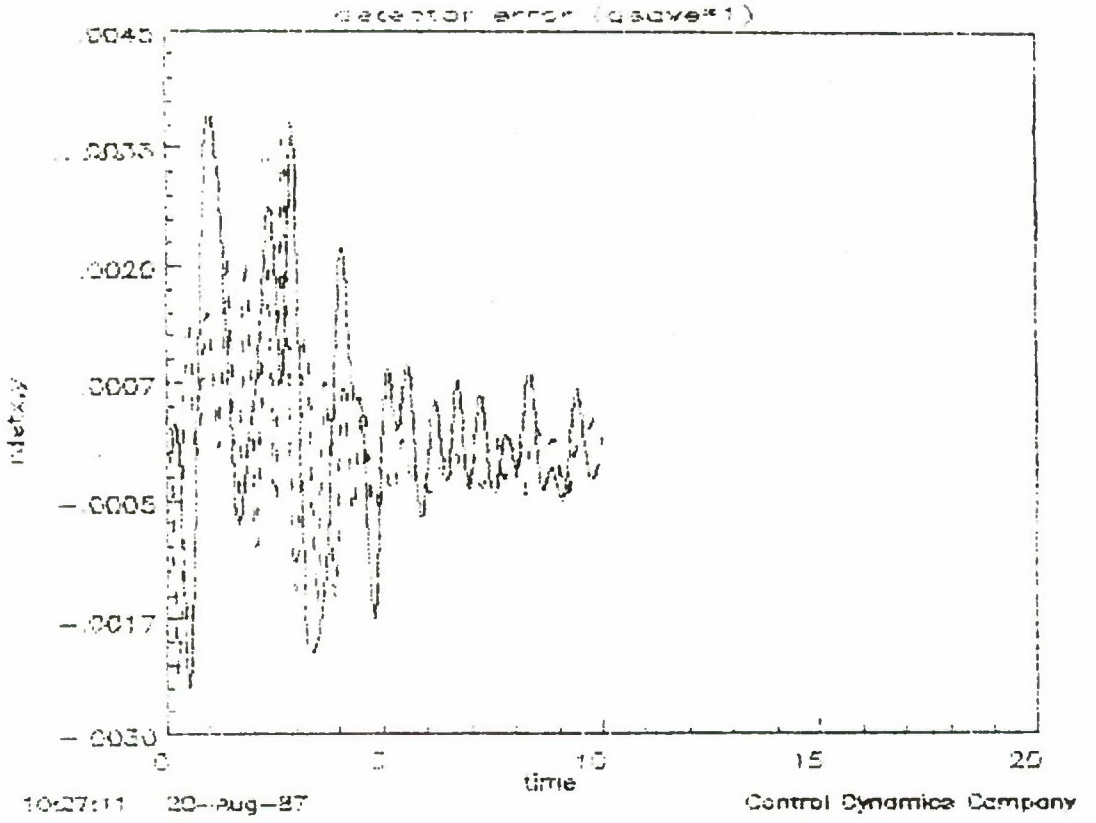


Figure 7.3-2. Detector Error Response for the Combined IMC/MAST Controller (Original MAST Controller).

7.3.2.2 Final MAST Controller Design.

The original expectation of computational capacity for the ACES configuration indicated that a general 30th order controller with no simplifying structure could be implemented. However, the lack of a planned floating point processor caused these estimates to be revised downward. In particular, rough estimates of processor capability indicated that the original MAST/IMC combined controller would exceed the capacity of the processor by a factor of three. The attempts to reduce the computational burden of the FAMESS controller centered on the MAST controller, since the IMC controller contained the bare minimum required for system stabilization.

The first step in the redesign of the MAST controller was that of omitting the eight controlled modes of the design model which were slightly weighted due to spillover problems. The performance degradation was slightly with the resulting design; however, this controller also exceeded the computational limitation.

It is interesting to note that the controller dynamical order is reduced from 45 to 29 by omitting the eight modes. However, a major portion of the computational burden is due not to the order of controller, but to the large number of sensors and actuators. Since the order of the controller could not be reduced significantly, the decision was made to delete the LMED sensor/actuator pairs from the MAST controller design. Unfortunately, the resulting controller remained too "large" for the available facility hardware, although the simulated performance of this controller indicated that the removal of the LMED pairs as possible input/output pairs would have resulted in virtually no degradation of performance.

At this point in the redesign, the actuator/sensor complement was still of a highly noncollocated nature, as the tip instruments are spacially separated from any actuators. The solution to the dilemma of whether (1) to omit the tip instrument package, thereby gaining the benefits of collocation afforded by the AGS gimbal/faceplate gyro pairs, but also to some extent losing the desired complexity of

the ACES design or (2) to delete the faceplate rate gyros, thereby sacrificing collocation, was solved by the simple fact that the deletion of the tip instruments contribute more to the computational burden than do the faceplate gyros.

The deletion of the tip instruments contributed to a significant degradation in the simulated response of the system. Therefore, the design parameters were adjusted by repeating the mode "targeting" process described previously. The design parameters for the final MAST controller are given in Table 7.3-6. A summary of the pertinent controller attributes is that of Table 7.3-7. The simulated RCS detector error response is that of Figure 7.3-3. Comparison with Figure 7.3-2 indicates that the performance of the final controller is roughly comparable to that of the more complex original controller. However, in Figure 7.3-3 a mode with moderate damping at roughly 0.6 Hz can be seen. This mode is probably a pendulum mode which, with the deletion of the tip instruments, is only slightly observable at the faceplate.

TABLE 7.3-6. DESIGN PARAMETERS FOR THE FINAL MAST CONTROLLER DESIGN

Design Parameters	Value	
Q_R	Mode 4	2.5×10^3
	Mode 5	2.5×10^3
	Mode 6	6.25×10^3
	Mode 9	20.0×10^3
	Mode 10	1.0×10^3
R_R	AGS-X	1.0
	AGS-Y	1.0
	AGS-Z	1.0
Q_o	Mode 4	5.0×10^3
	Mode 5	5.0×10^3
	Mode 6	1.25×10^3
	Mode 9	40.0×10^3
	Mode 10	4.0×10^3
R_o	Faceplate $\dot{\Theta}_x$	1.0
	Faceplate $\dot{\Theta}_y$	1.0
	Faceplate $\dot{\Theta}_z$	1.0
Q_{rs}		$1.0 \times 10^5 \times I$
Q_{os}		$2.0 \times 10^5 \times I$
α_c		0.0
α_e		0.0

TABLE 7.3-7. ATTRIBUTES OF THE COMBINED IMC/MAST CONTROLLER (FINAL MAST DESIGN)

CONTROLLER ATTRIBUTES	
MAST Controller Order	13
IMC Controller Order	12
Total Controller Order	25
IMC Actuators	2
IMC Sensors	2
MAST Actuators	3
MAST Sensors	3
Total Actuators	5
Total Sensors	5

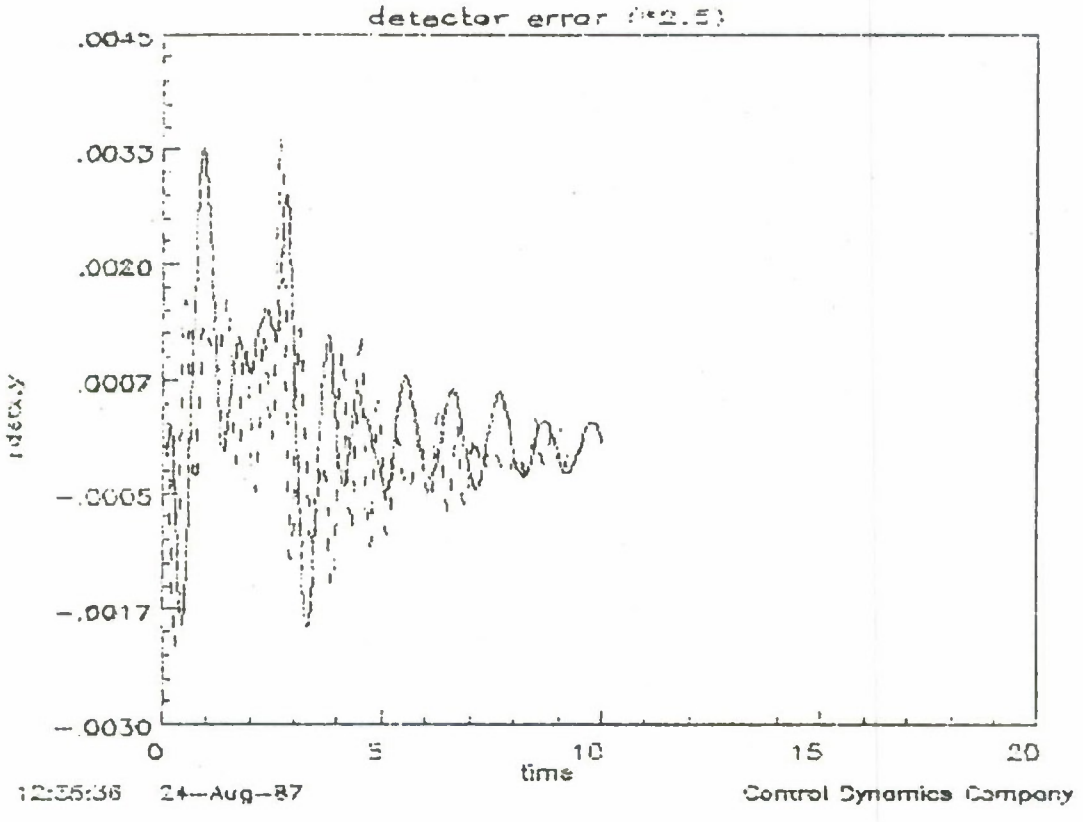


Figure 7.3-3. Detector Error Response for the Combined IMC/MAST Controller (Final MAST Controller).

7.4 Test Results.

Although the FAMESS controller was designed based on the RCS disturbance alone, the test cycle included each of the three disturbances described in Section 2.2. The methods of data acquisition and reduction are described in detail in Section 2.2.

The first part of the test cycle for the FAMESS controller was that of investigating the ability of the controller to zero small initial offsets of the laser beam from the center of the photodetector. The first results of these tests are given in Figure 7.4-1, where a very undesirable phenomenon is evident. The settling time to the non-zero effects is roughly 20s. This effect is not due to a bandwidth limitation, but is probably due to the excitation of an unmodeled mode at roughly 0.25 Hz. The desirable approach to this effect is to perform testing to determine the precise frequency of the unmodeled mode; however, program time constraints prevented further refinement of the design model. Therefore, the decision was made to reduce the gain of each IMC channel by a factor of two. The results are given in Figure 7.4-2, where the settling time is roughly 6 seconds. Another phenomenon is now clearly evident from the fact that the beam position is roughly constant for the first 2 seconds of operation. This effect is undoubtedly due to the nonlinearity of the four-quadrant detector.

The test cycle proceeded with the simulated crew motion disturbance. The open loop results are given in Figures 7.4-3 and 7.4-4, where in Figure 7.4-4 the beam error exhibits predominant behavior at roughly 0.5 Hz in the X channel and a more complicated response consisting possibly of modes at 0.5 Hz and 0.2 Hz in the Y channel. The 0.5-Hz behavior is probably due to pendulum motion about the ASG X and Y gimbals. However, the 0.2-Hz mode has not been modeled and can cause both stability and performance problems.

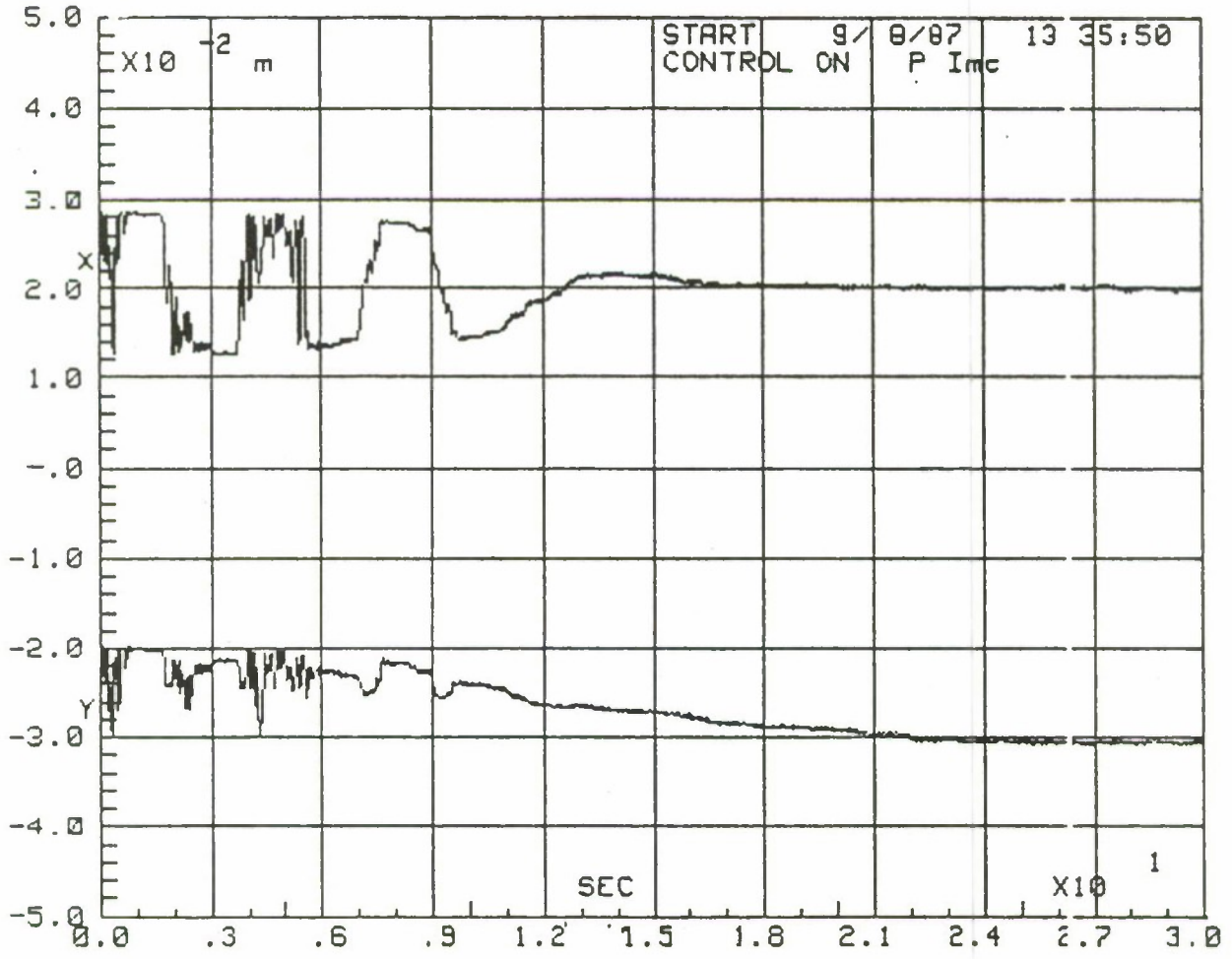


Figure 7.4-1. Detector Error Offset Response with FAMESS IMC Controller Only.

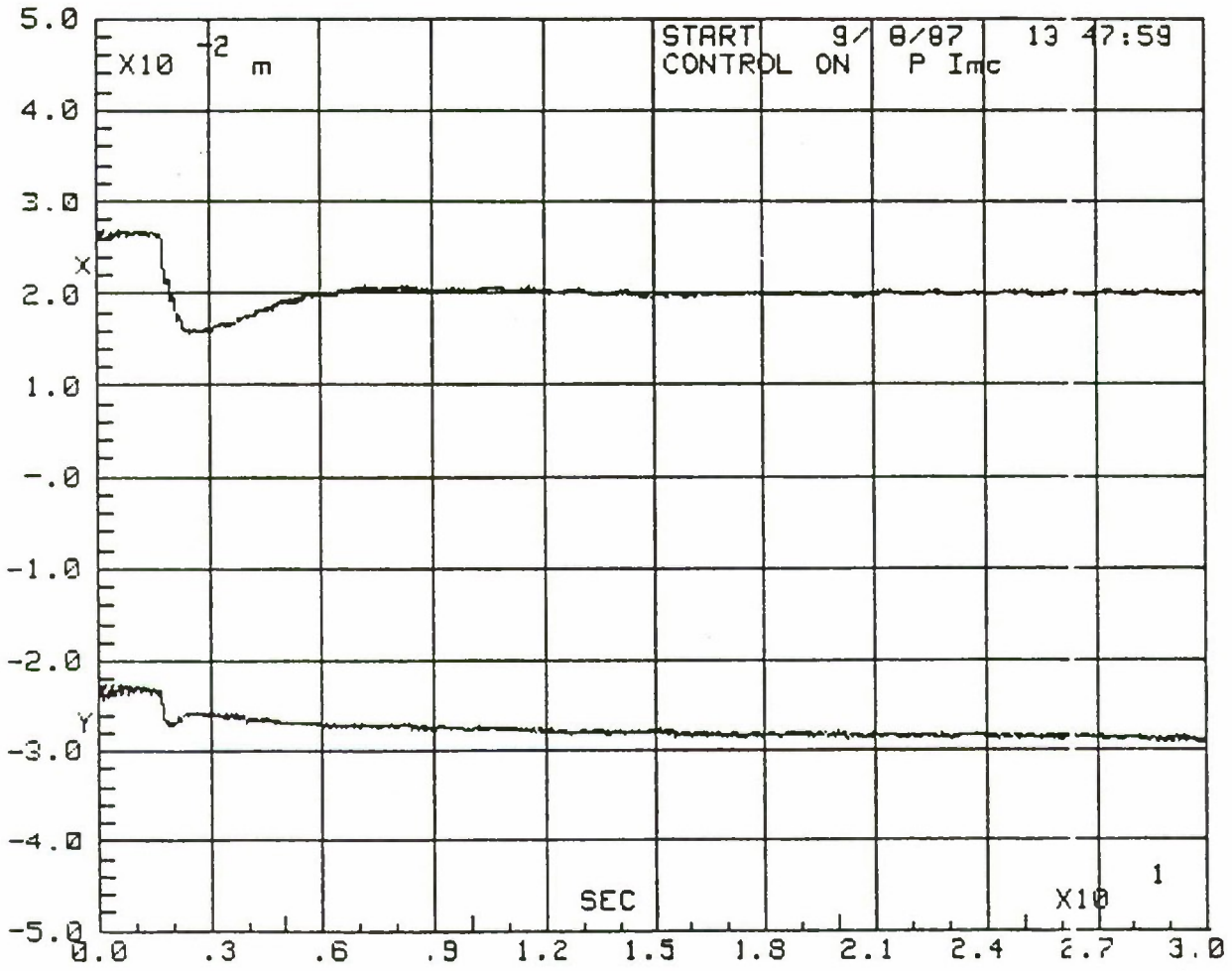


Figure 7.4-2. Detector Error Response with FAMESS IMC Controller Only (Gains Reduced by 6 dB).

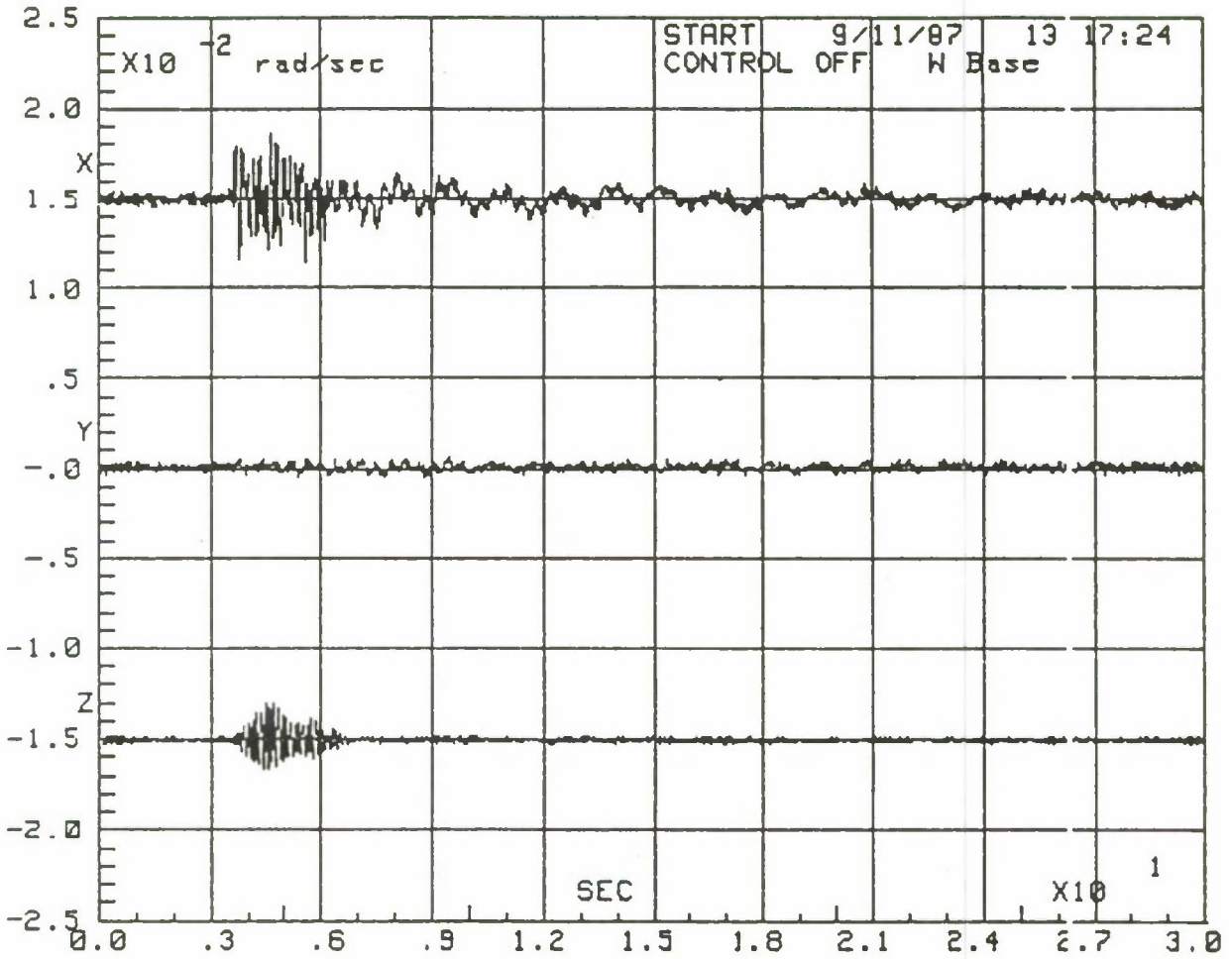


Figure 7.4-3. Open Loop Response at the Faceplate Gyros Due to the Crew Motion Disturbance.

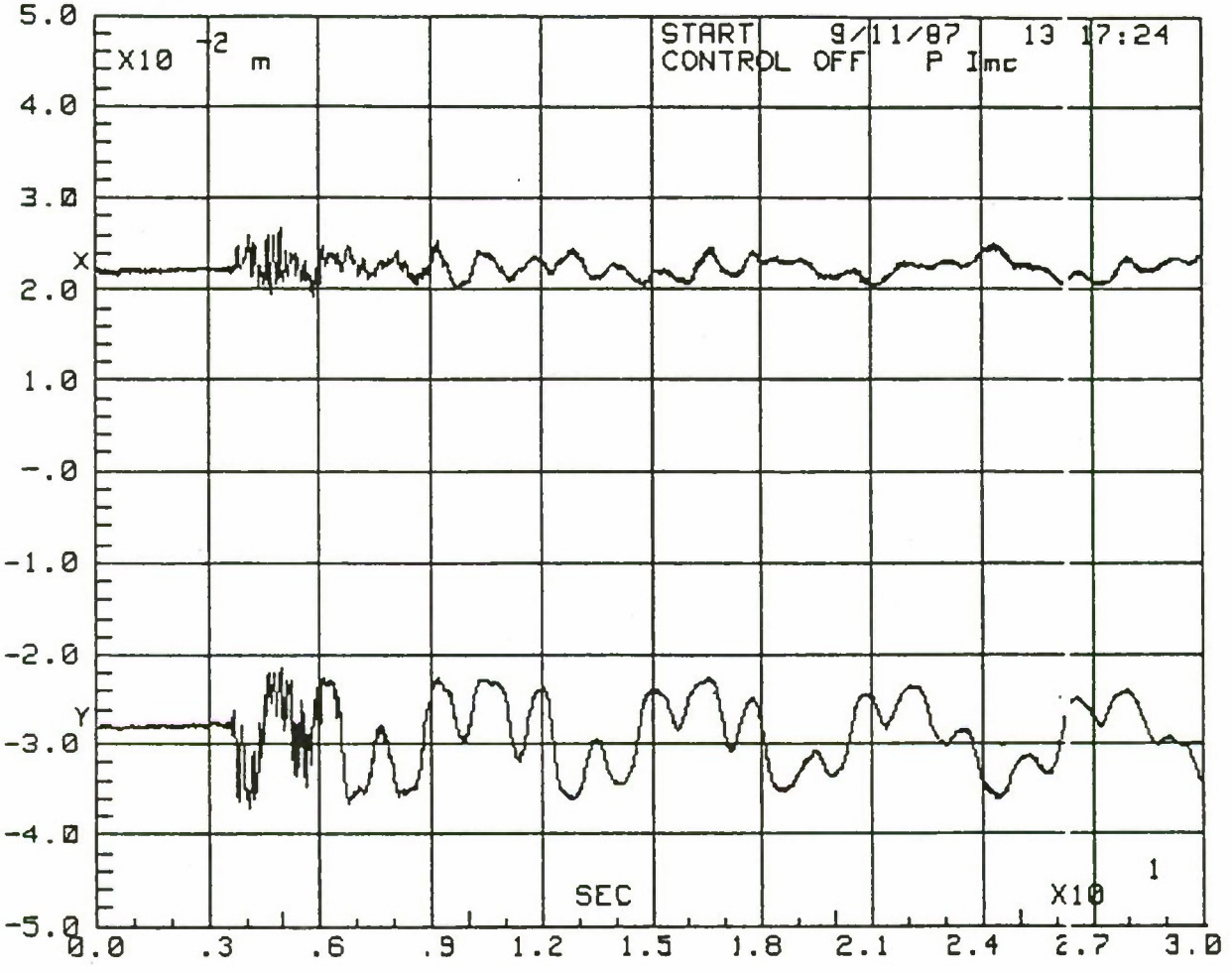


Figure 7.4-4. Open Loop Detector Response Due to the Crew Motion Disturbance.

The results of the first closed loop test with the crew motion disturbance are given in Figures 7.4-5 and 7.4-6. The gyro response is slightly improved, but effectively the same as the open loop. However, the closed loop response at the photodetector is much degraded over the open loop response, mainly due to a 5.8-Hz mode in the X channel and a 0.2-Hz mode in the Ychannel. As mentioned previously, the 0.2-Hz mode is not contained in the design model. The situation is actually the same for the 5.8-Hz mode; although a 5.8-Hz mode is contained in the design model, it is not subject to destabilization since the only actuator/sensor pairs with dual authority over the model 5.8-Hz mode are the AGS gimbal/faceplate gyro, which are collocated. Therefore, the decision was made to decrease the MAST controller gains in each loop so as to decrease the spillover to the unmodeled 5.8-Hz mode. The results of a retest are given in Figure 7.4-7, where the 5.8-Hz mode is no longer apparent. However, the response is not significantly improved over the open loop response of Figure 7.4-4. This is mainly due to the effect of the unmodeled mode at 0.2-Hz.

The open loop RCS disturbance response due to an X channel BET input is given in Figures 7.4-8 and 7.4-9. Again, the predominant response at the detector is the 0.2-Hz unmodeled mode. It should be pointed out that this mode must involve the IMC gimbals, since such a low frequency structural disturbance would be rejected if it appeared only at the detector. Because of this the closed loop results of Figures 7.4-10 and 7.4-11 are not unexpected. As for the crew motion disturbance, there is little or no improvement of the closed loop response over the open loop.

The open loop Riverside disturbance response is given in Figures 7.4-12 and 7.4-13. Since the Riverside disturbance is dominated by a persistent 8-Hz excitation, the major effect in the open loop response is that of an 8-Hz component. It is interesting to note that with the disturbance removed at 21 seconds, the 8-Hz behavior does not persist. This is most likely due to the 8-Hz that is excited. Of course, this is not a consequence of the controller, so that the 8-Hz component does not provide a rigorous test of the controller. A more suitable disturbance would have included a dominant component at one of the controlled mode frequencies.

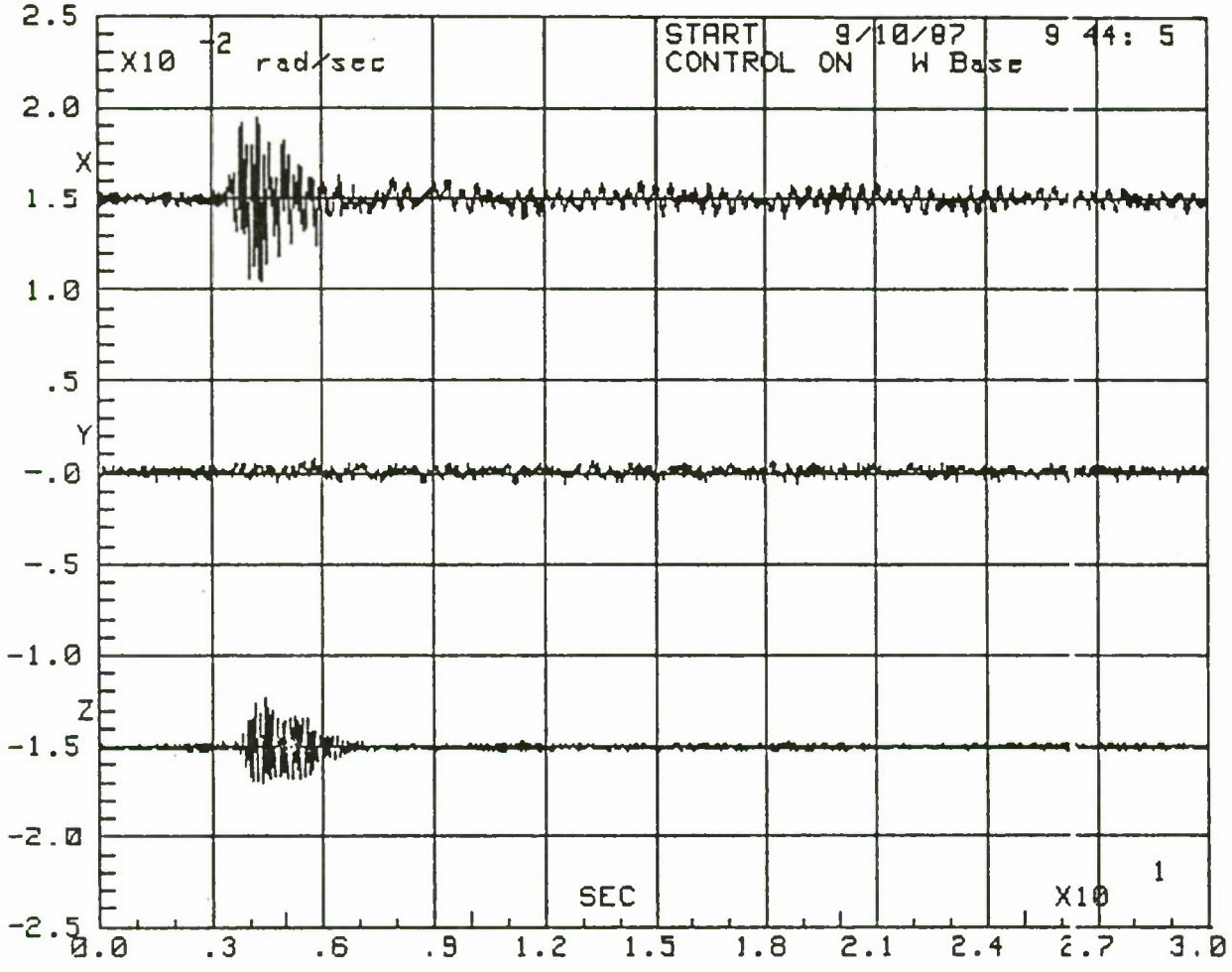


Figure 7.4-5. Closed Loop Faceplate Gyro Response Due to Crew Motion Disturbance.

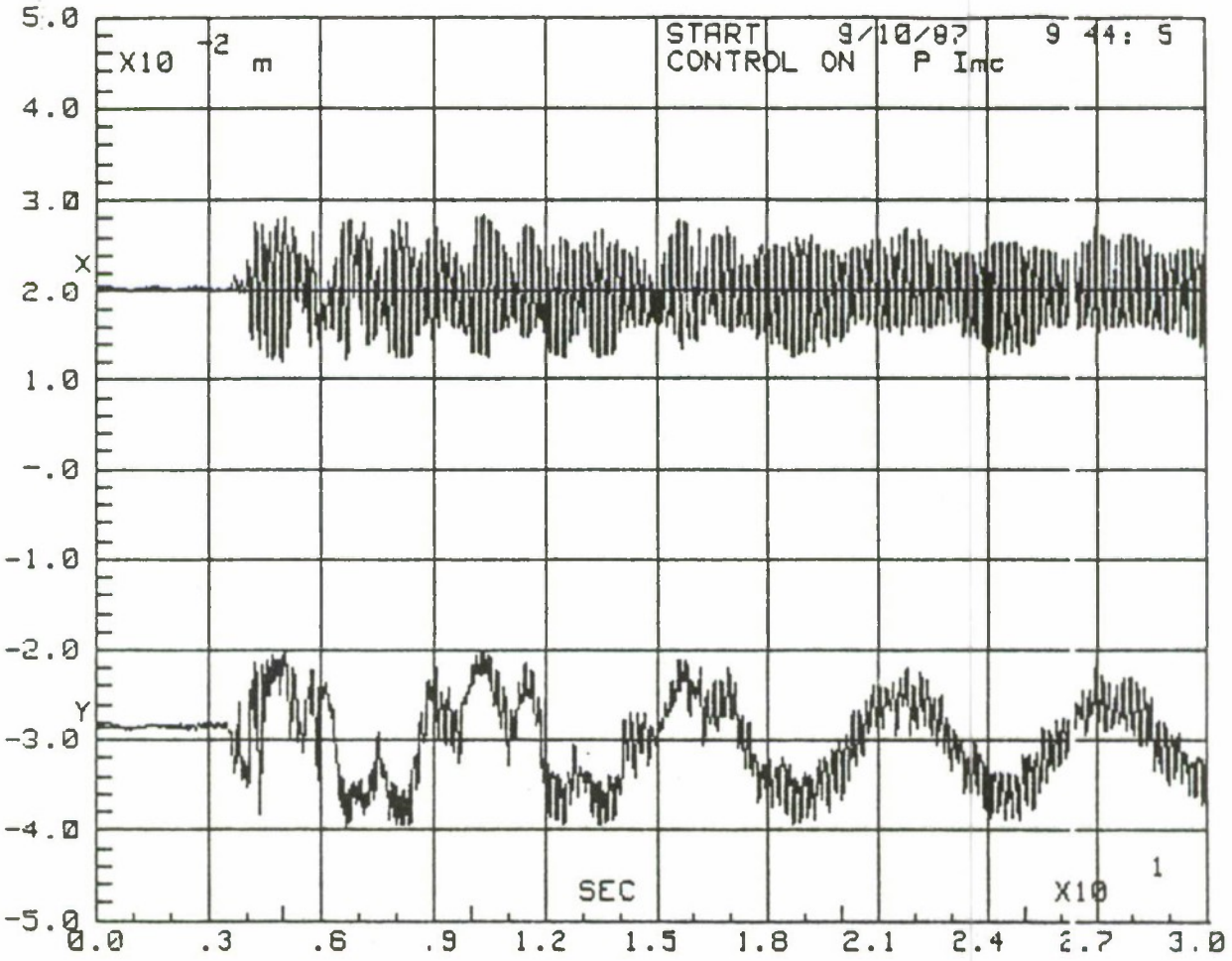


Figure 7.4-6. Closed Loop Detector Response Due to Crew Motion Disturbance.

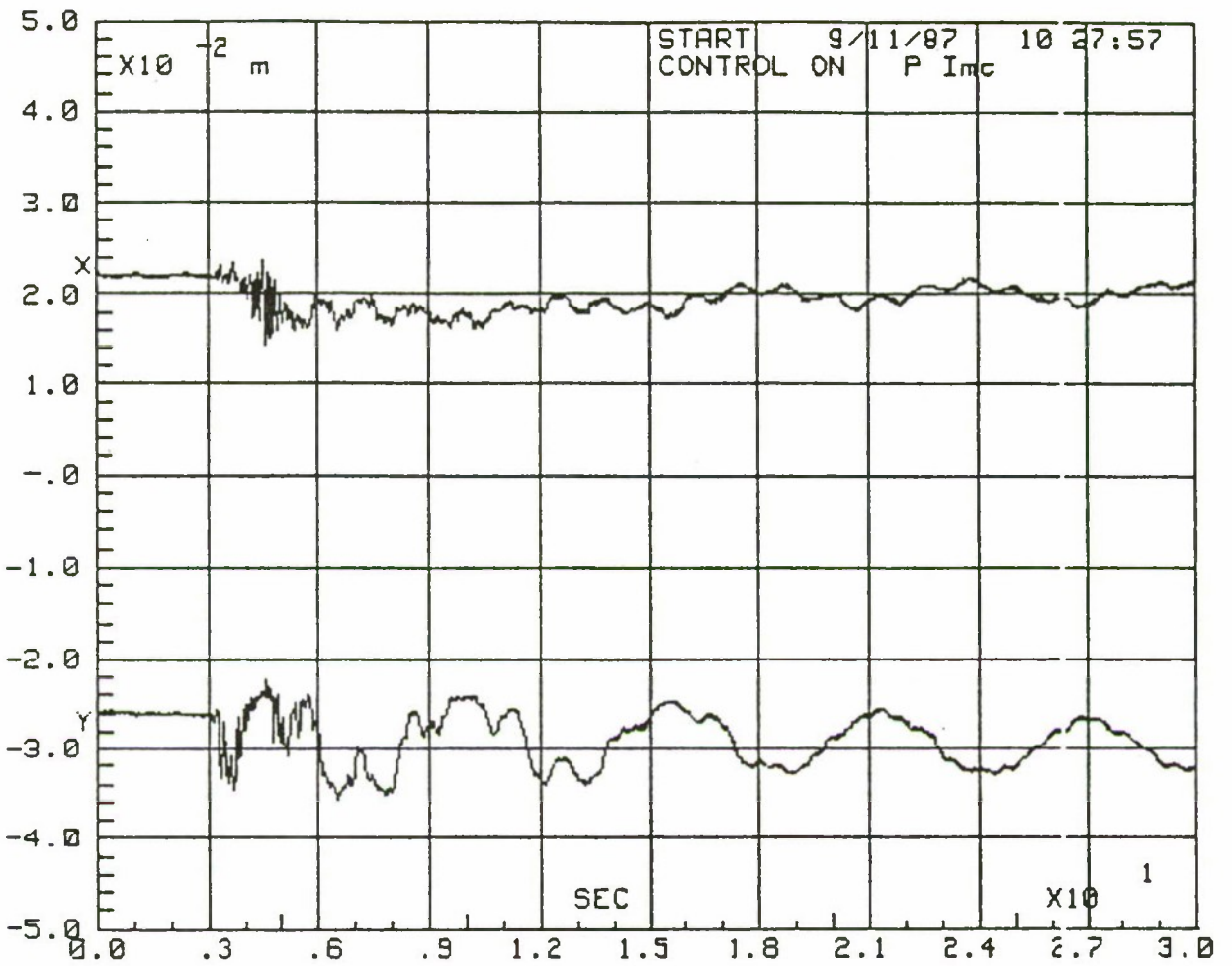


Figure 7.4-7. Closed Loop Detector Error Response Due to Crew Motion Disturbance (Pointing Gimbal Gains Reduced).

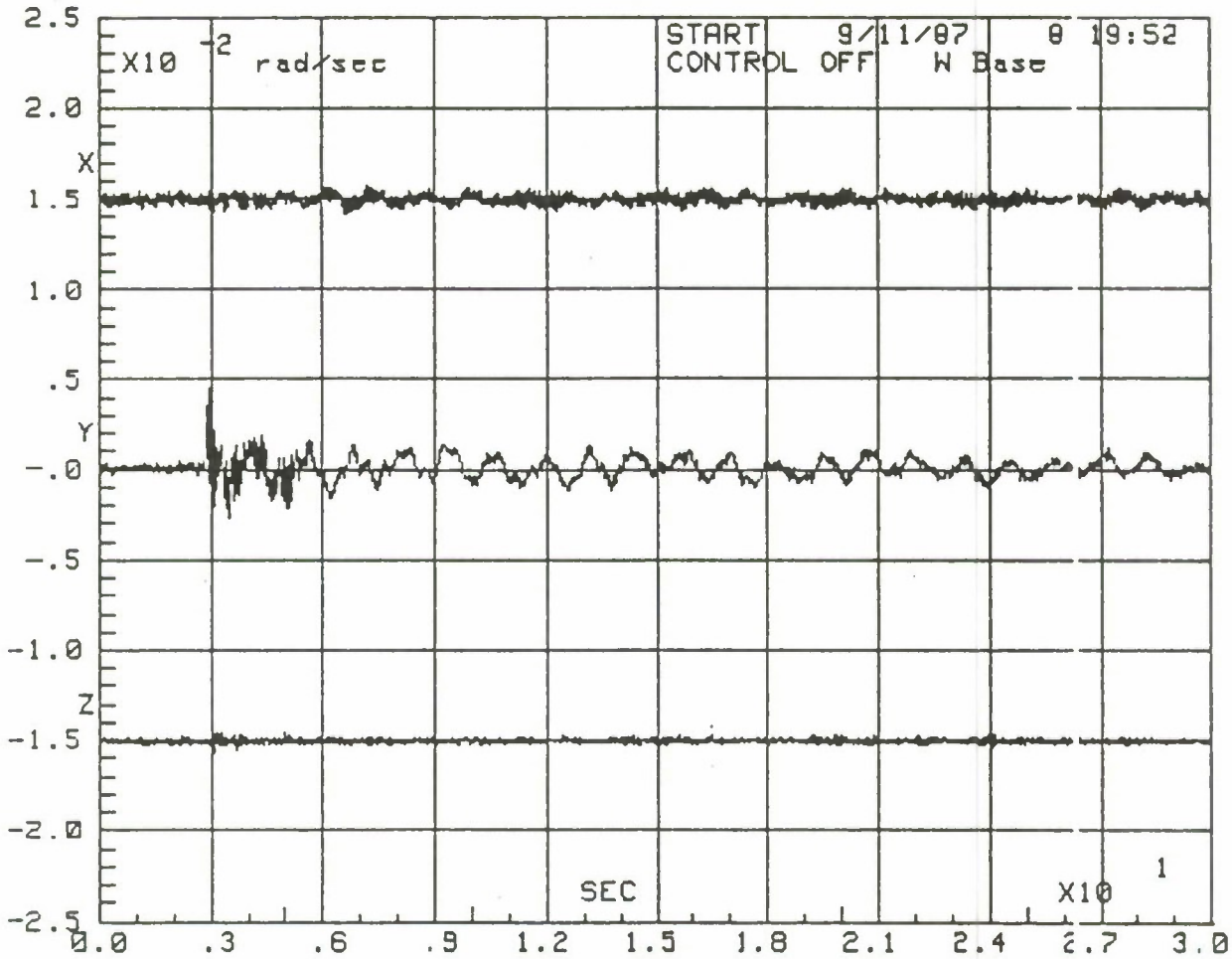


Figure 7.4-8. Open Loop Gyro Response Due to the RCS Disturbance.

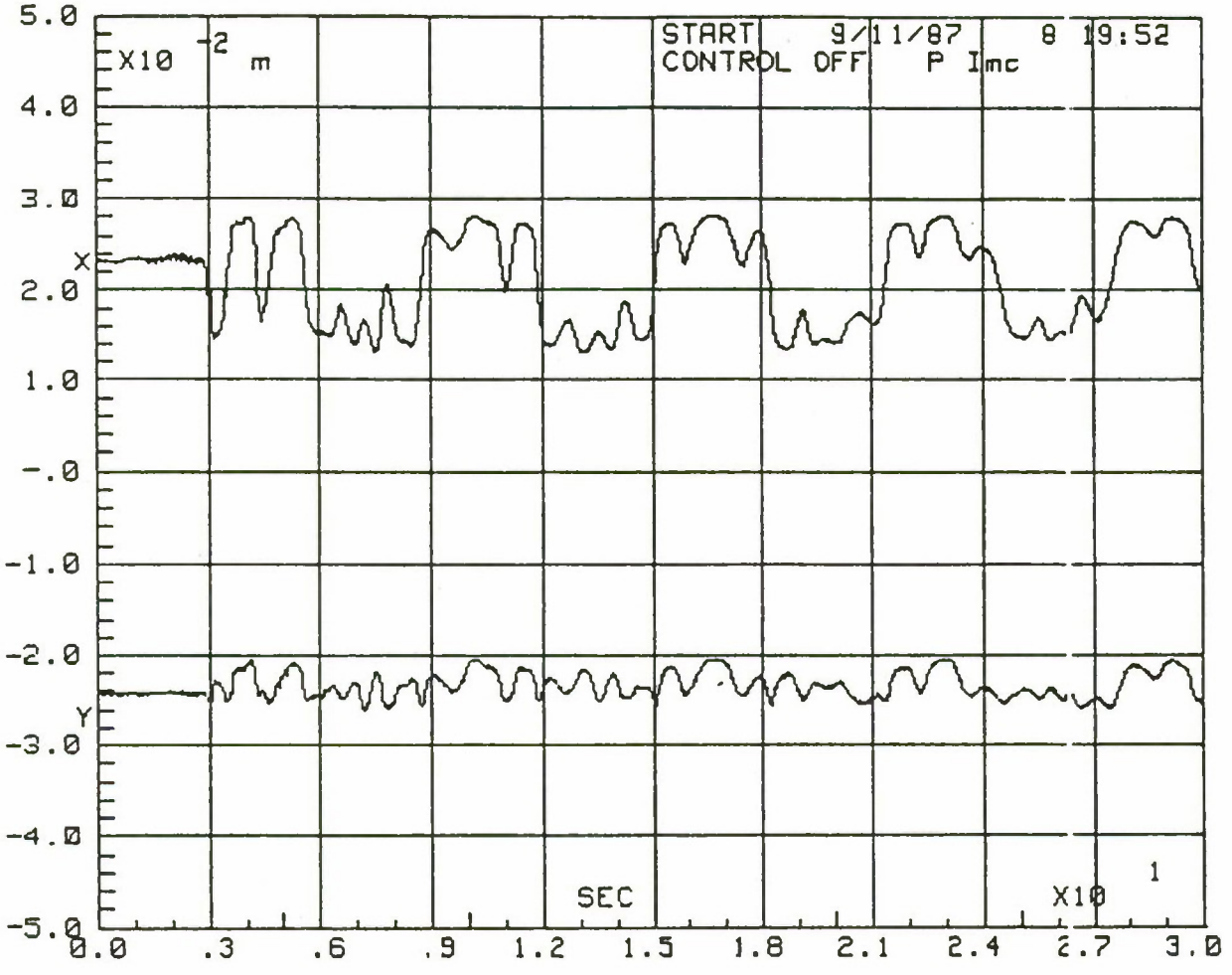


Figure 7.4-9. Open Loop Detector Response Due to the RCS Disturbance.

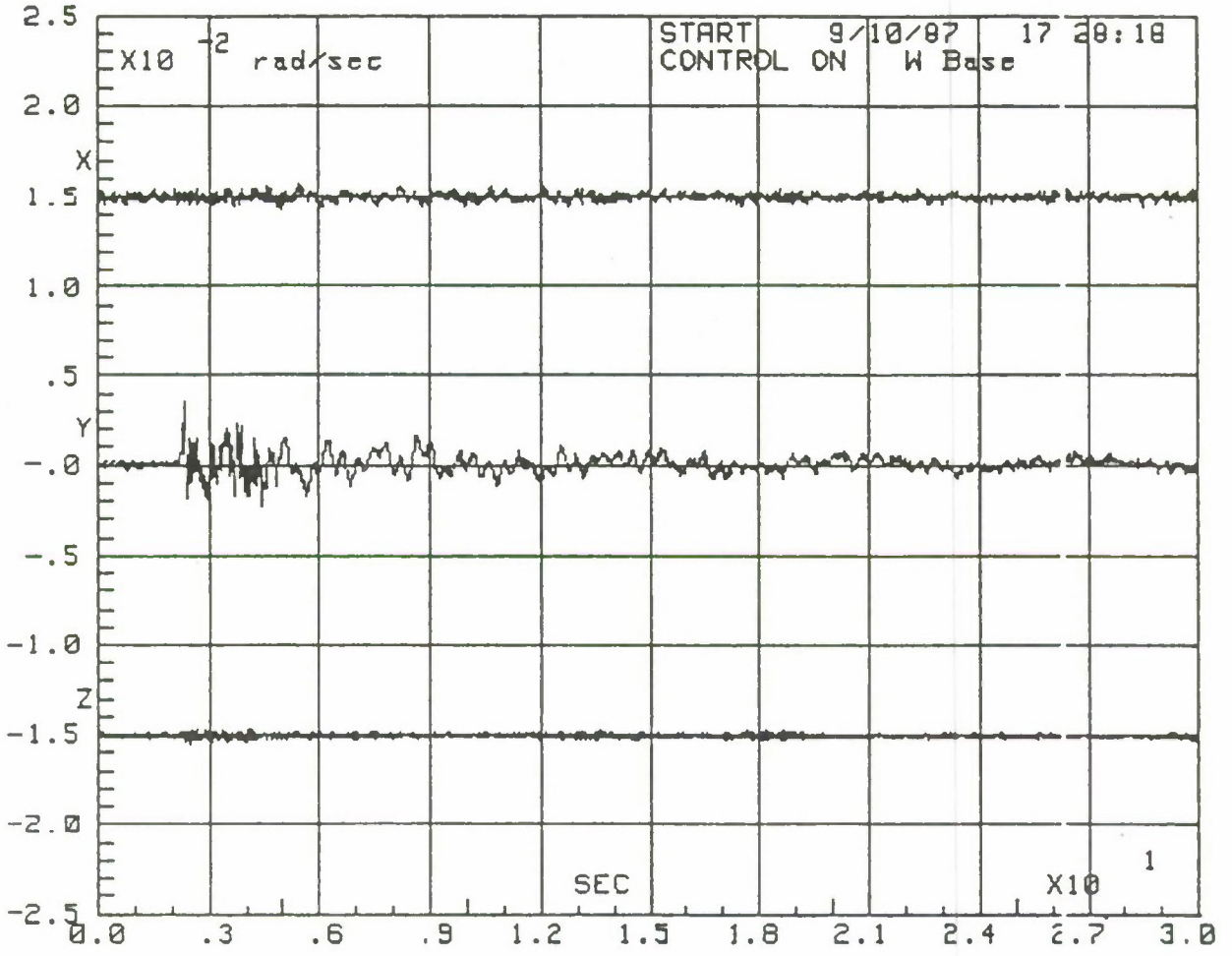


Figure 7.4-10. Closed Loop Faceplate Gyro Response Due to the RCS Disturbance.

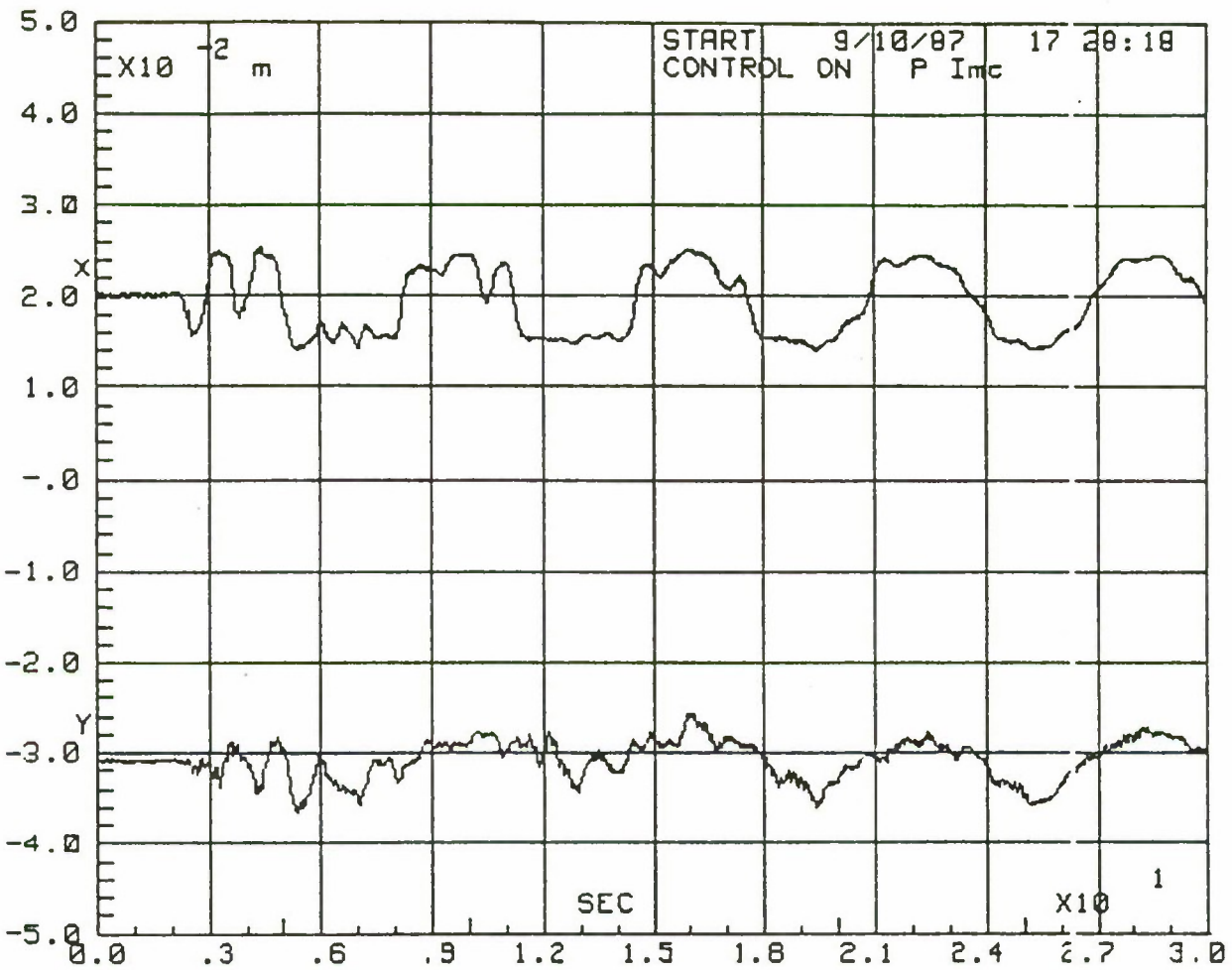


Figure 7.4-11. Closed Loop Detector Response Due to the RCS Disturbance.

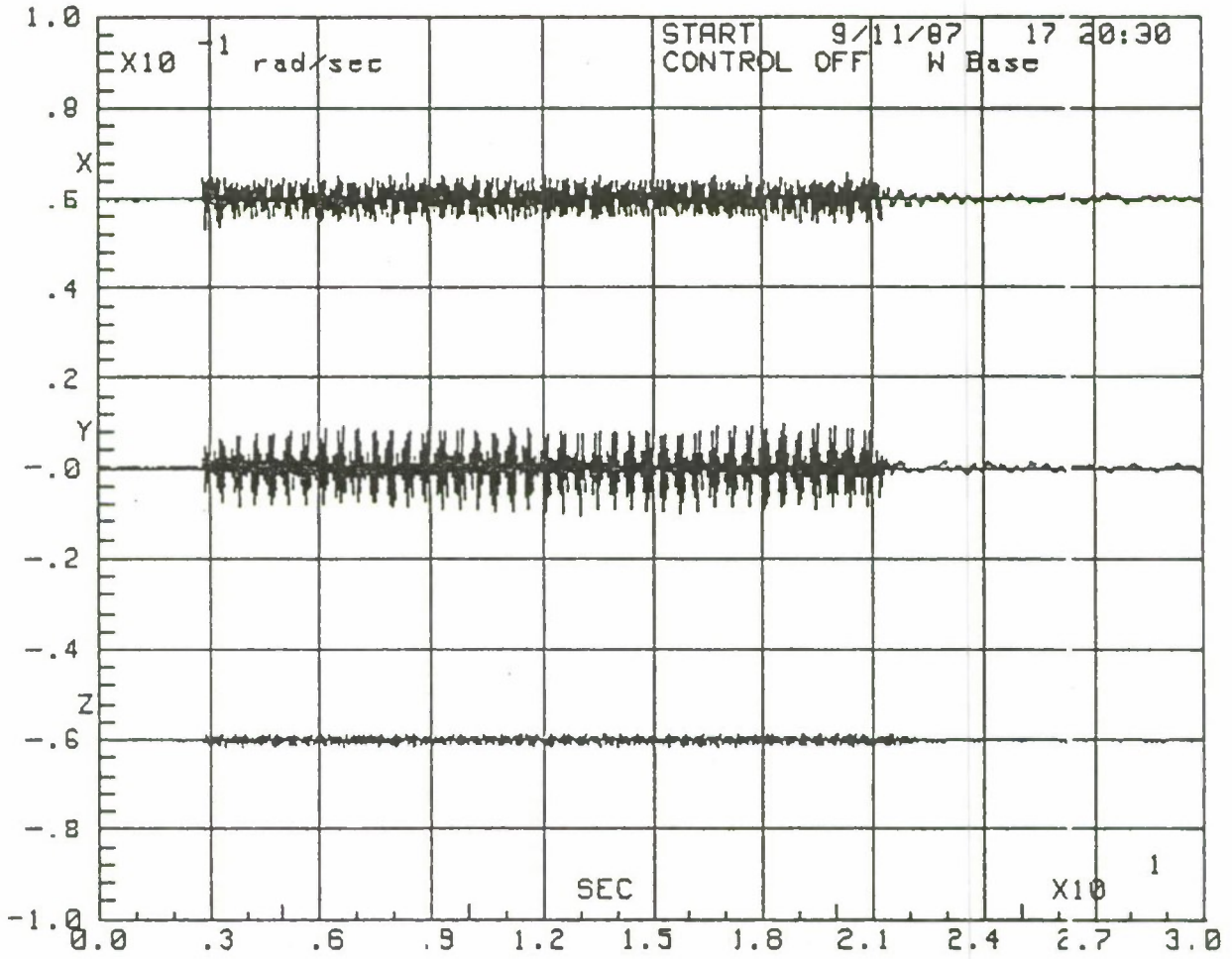


Figure 7.4-12. Open Loop Gyro Response Due to the Riverside Disturbance.

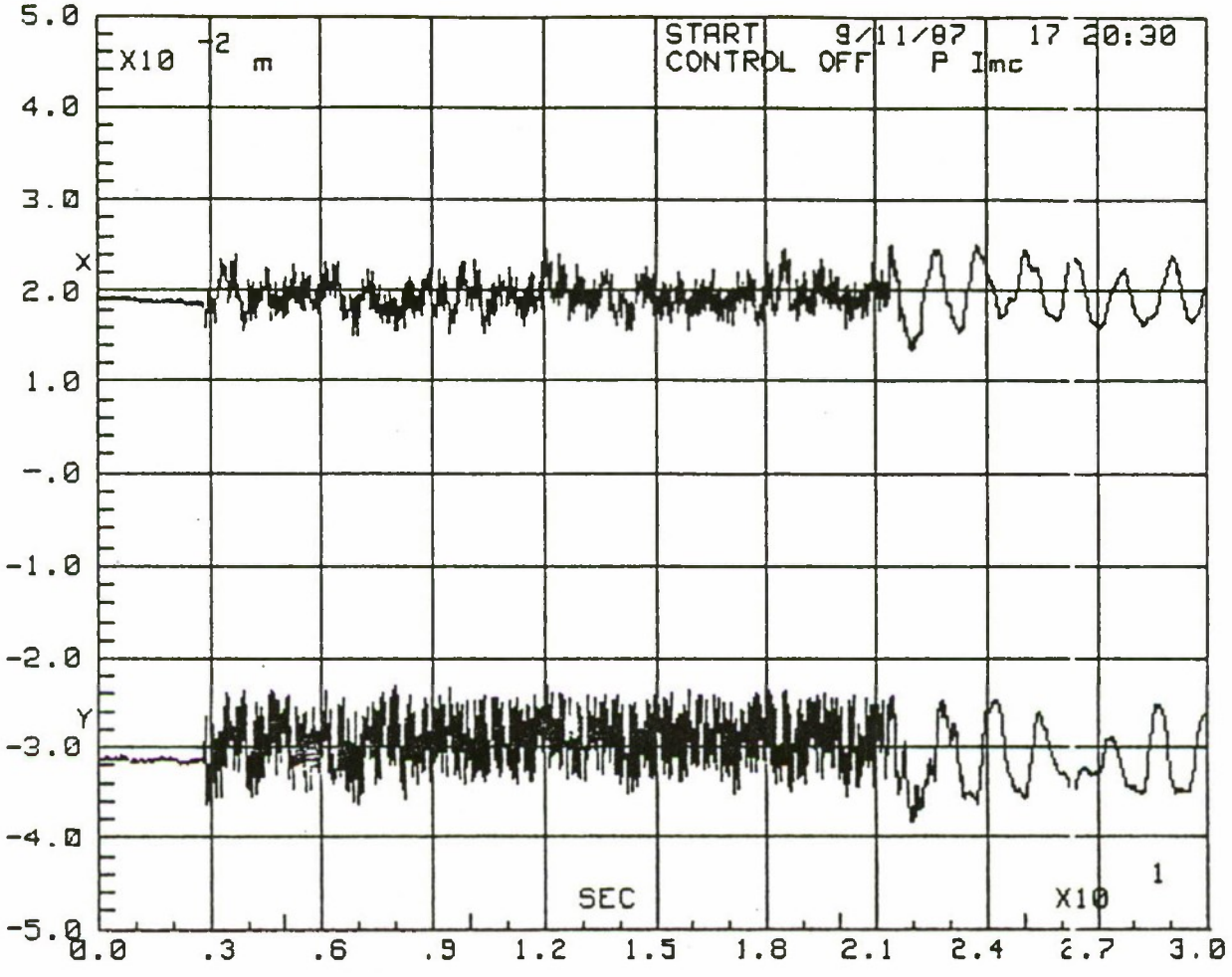


Figure 7.4-13. Open Loop Detector Response Due to the Riverside Disturbance.

The closed loop results for the Riverside disturbance are given in Figures 7.4-14 and 7.4-15. Compared to the open loop results, the closed loop responses are roughly equivalent, with the exception that the closed loop response is significantly more damped after the removal of the disturbance at 21 seconds.

Another disturbance which is used for demonstration purposes at MSFC was included in the test cycle. The disturbance is similar to the RCS disturbance with larger force magnitudes. The open loop response to the demonstration disturbance is given in Figure 7.4-16 for the faceplate gyros and in Figure 7.4-17 for the detector channels. The loss of the detector signal is evident in Figure 7.4-17 from the signal dropout. However, Figure 7.4-18 is a binary signal which indicates the absence (low) or presence (high) of the laser beam on the detector and indicates that after 80 seconds the beam has not settled on the detector.

The closed loop results are those of Figures 7.4-19, 7.4-20 and 7.4-21, which are the gyro, detector, and beam presence responses, respectively. The improvement over the open loop results is most apparent in Figure 7.4-21, where the beam presence is persistent after roughly 40 seconds, a fact which is certainly due to the increased damping provided by the MAST controller.

The experimental test results for the FAMESS controller are summarized in Table 7.4-1. The mean and RMS detector errors are presented for the open and closed loop tests. Recall that each statistic is calculated by an average over five tests (see section 2.2.4). The requirement to remain in the linear region of operation is satisfied for the Crew, RCS, and Riverside disturbances. The results show that the FAMESS controller improves the detector mean in the X and Y axes. But, the controller does not improve the RMS detector errors (X and Y). The lack of RMS improvement for the crew and RCS disturbances is explained by the unmodeled dominant 0.2-Hz mode in the detector response. If this mode had been contained in the control design model, it would almost certainly have received significant damping, with a corresponding performance improvement. The lack of RMS improvement for the Riverside disturbance is expected since the dominant 8-Hz component is above the IMC controller bandwidth.

The demonstration disturbance is utilized for the purpose of testing the amount of vibration suppression of the beam provided by the FAMESS controller. The demo disturbance causes the beam to miss the detector during the test. Of course, the misses imply that the laser beam is not always in the linear region of the detector. The beam controller is not limited to operation in a range with a very low SNR (as is the case with the other disturbances). The faceplate gyro settling time and the detector percentage of hits are the variables used to evaluate the beam controller performance. The test results indicate that the settling time is improved by 12 seconds in the X axis and by 43 seconds in the Y axis. Table 7.4-1 also shows that the percentage of hits is increased from 56 percent to 73 pecent. The results of the demo tests were calculated with one 80-second test run. Averaging was not used to improve the reliability of the test results.

TABLE 7.4-1. SUMMARY OF TEST RESULTS FOR THE FAMESS CONTROLLER

Disturbance	Quantity	Open Loop (mm)	Closed Loop (mm)	Improvement (dB)
Crew	Detector Mean (X)	1.6	0.5	4.1
	Detector Mean (Y)	2.4	1.2	6.0
	Detector RMS (X)	1.2	1.6	-2.5
	Detector RMS (X)	3.1	3.1	0.0
RCS	Mean (X)	0.81	0.4	6.0
	Mean (Y)	5.7	0.99	15.2
	RMS (X)	4.6	3.5	2.5
	RMS (Y)	1.6	1.9	-1.7
Riverside	Mean (X)	2.3	0.24	21.0
	Mean (Y)	1.1	0.42	8.4
	RMS (X)	2.0	2.2	-0.5
	RMS (Y)	3.8	3.2	1.4
Demo	*T_S Base Gyro (x)	35.0s	23.0s	12.0s
	T_S Base Gyro (y)	70.0s	27.0s	43.0s
	% Hits Detector	56.0%	73.0%	17.0%

*T_S = Settling time

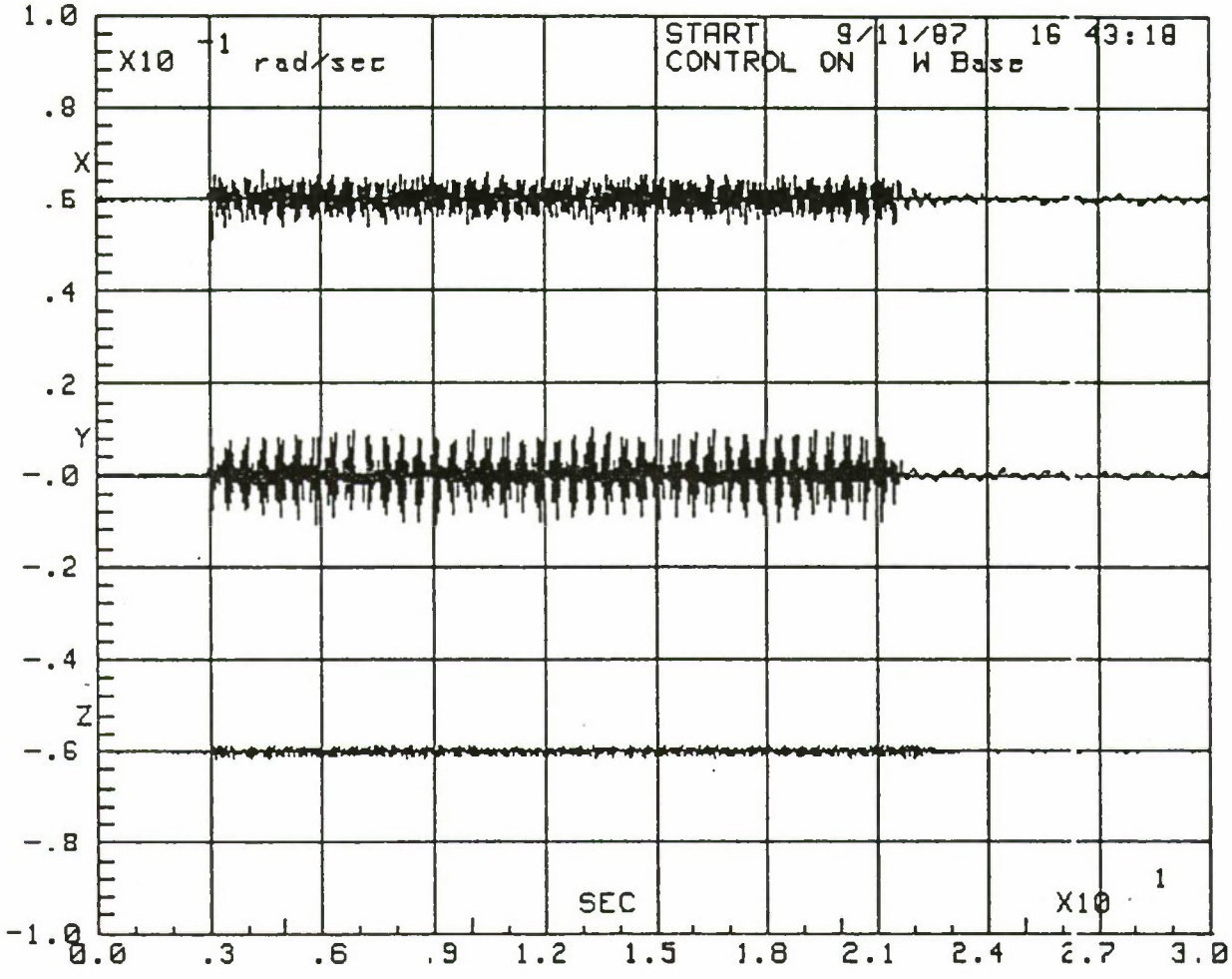


Figure 7.4-14. Closed Loop Gyro Response Due to the Riverside Disturbance.

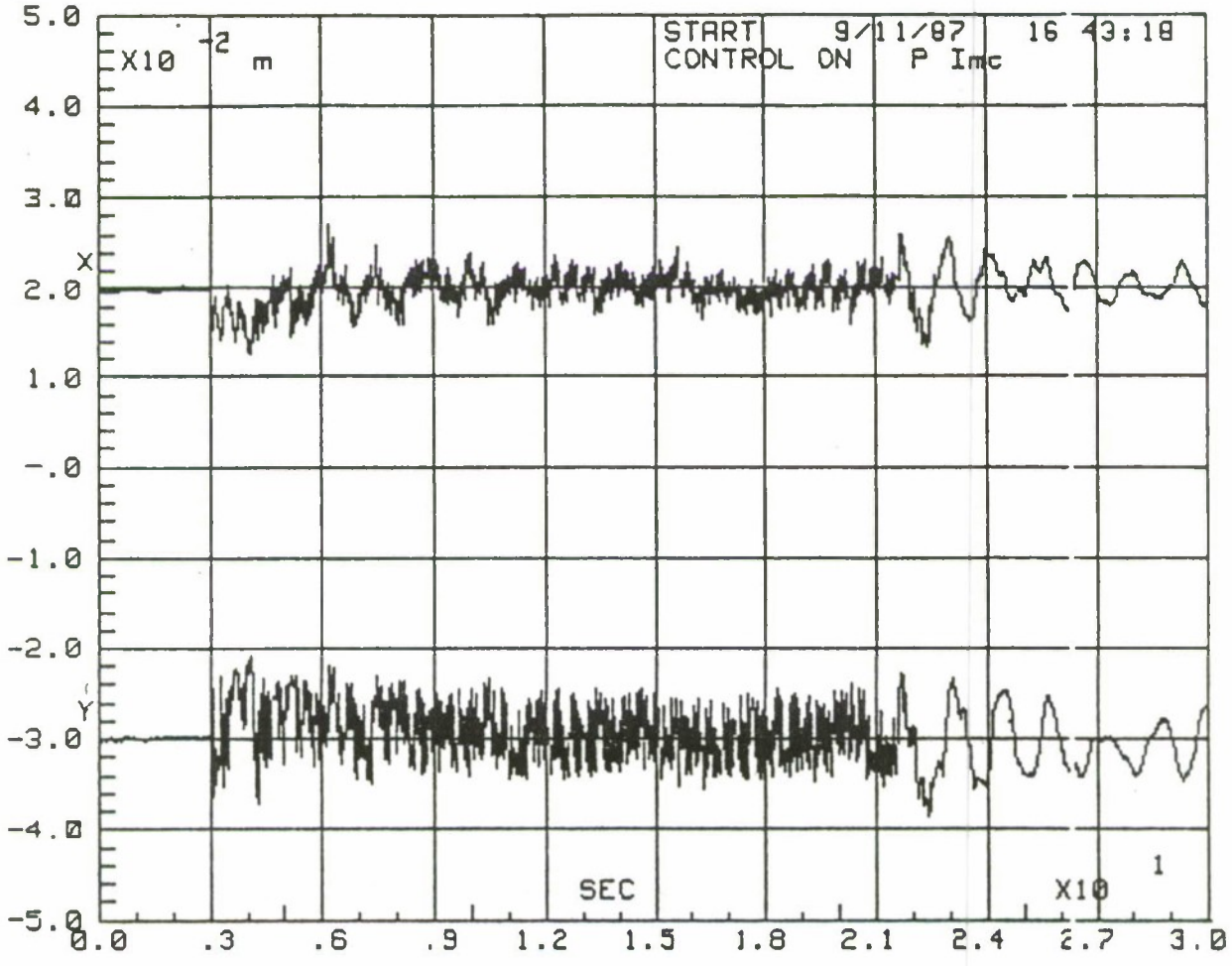


Figure 7.4-15. Closed Loop Detector Response Due to the Riverside Disturbance.

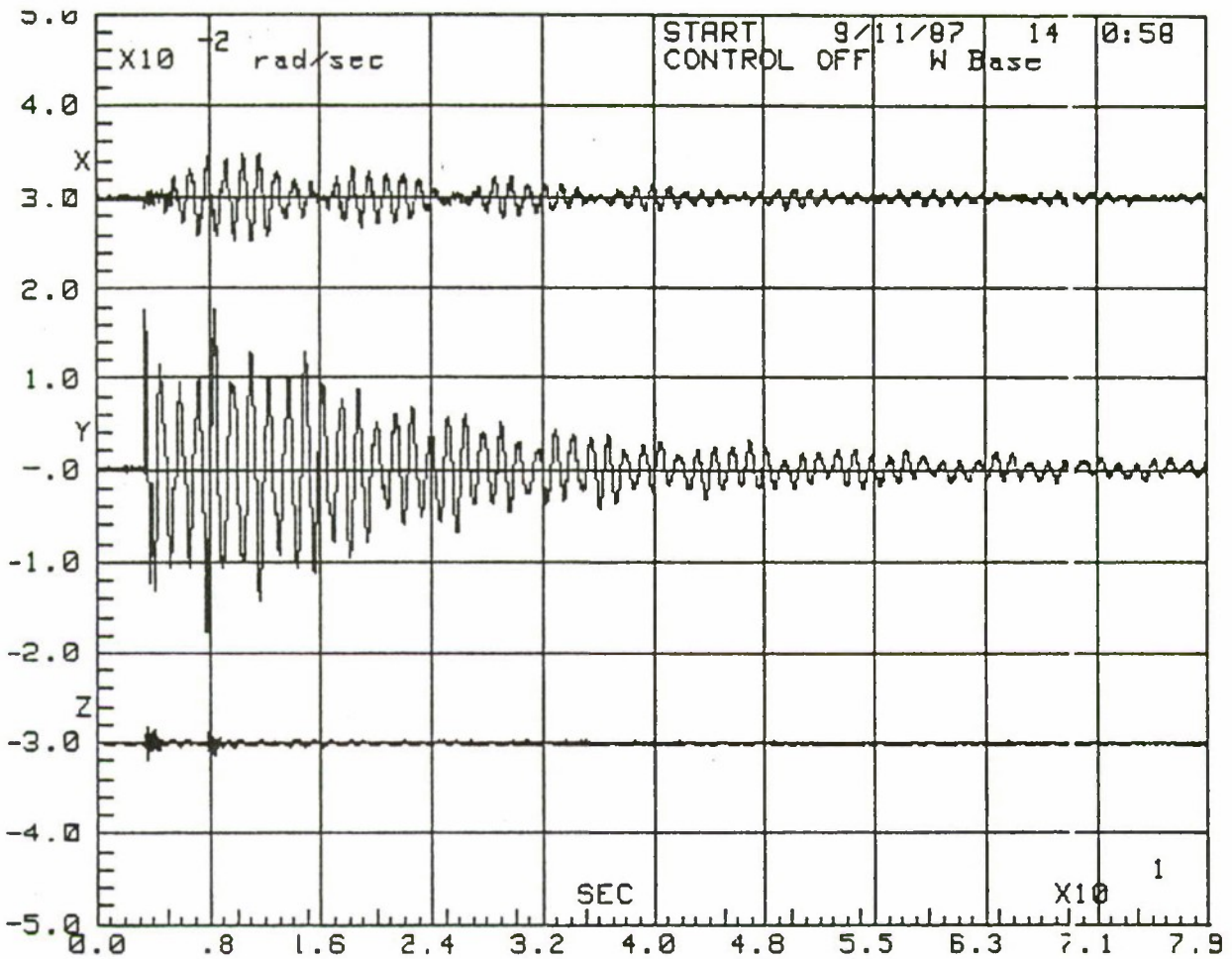


Figure 7.4-16. Open Loop Gyro Response Due to the Demonstration Disturbance.

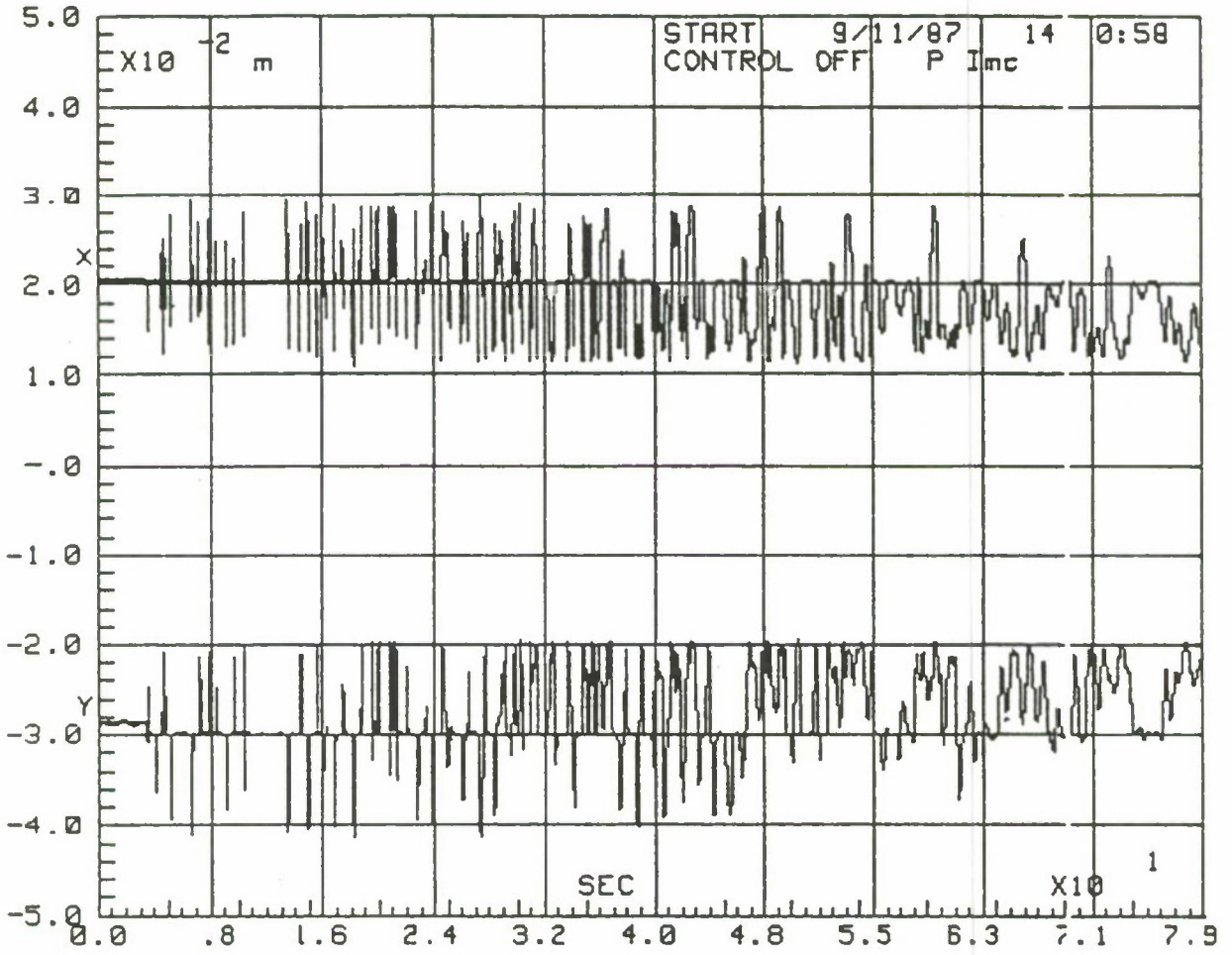


Figure 7.4-17. Open Loop Detector Response Due to the Demonstration Disturbance.

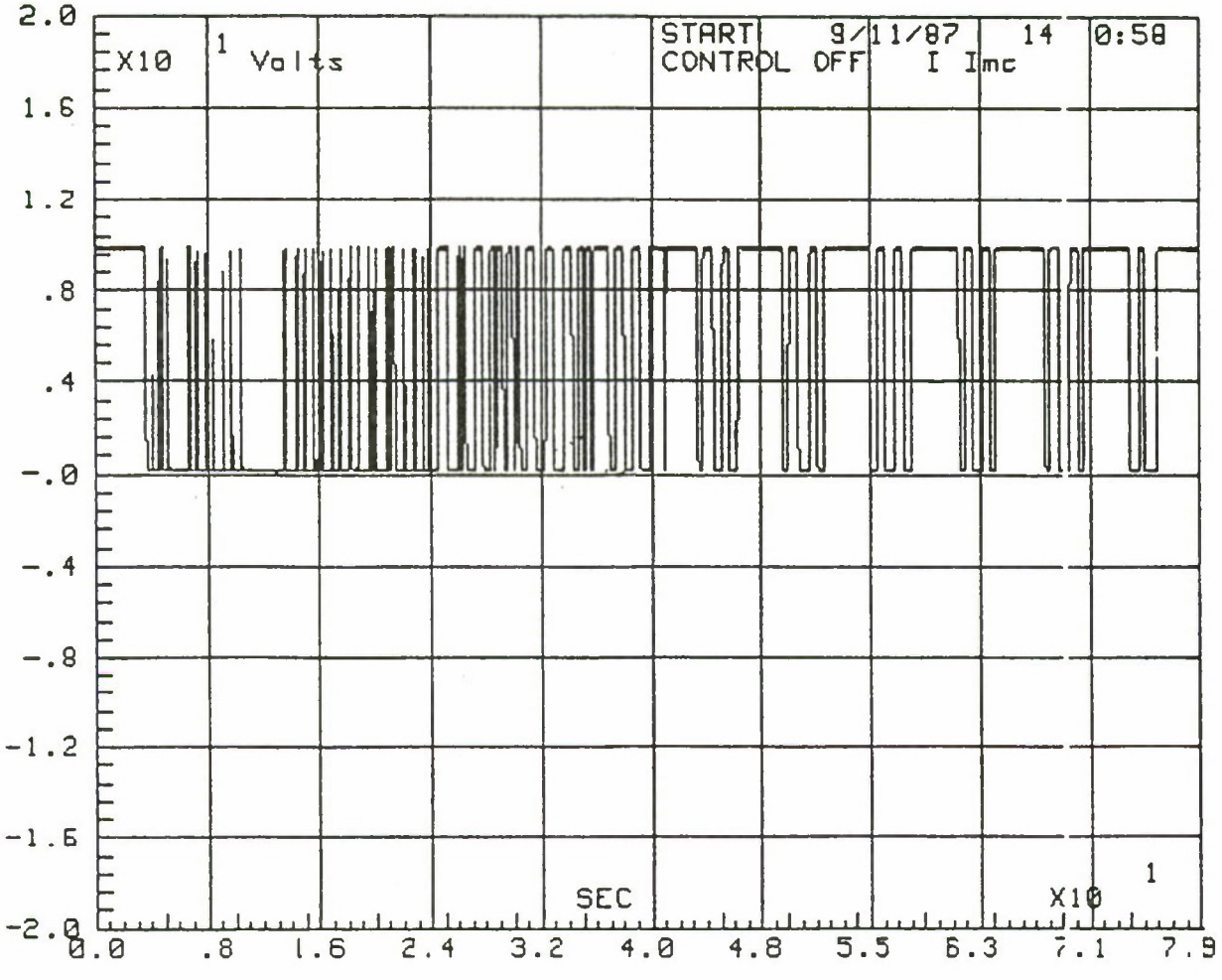


Figure 7.4-18. Open Loop Laser Beam Detector Presence Due to the Demonstration Disturbance.

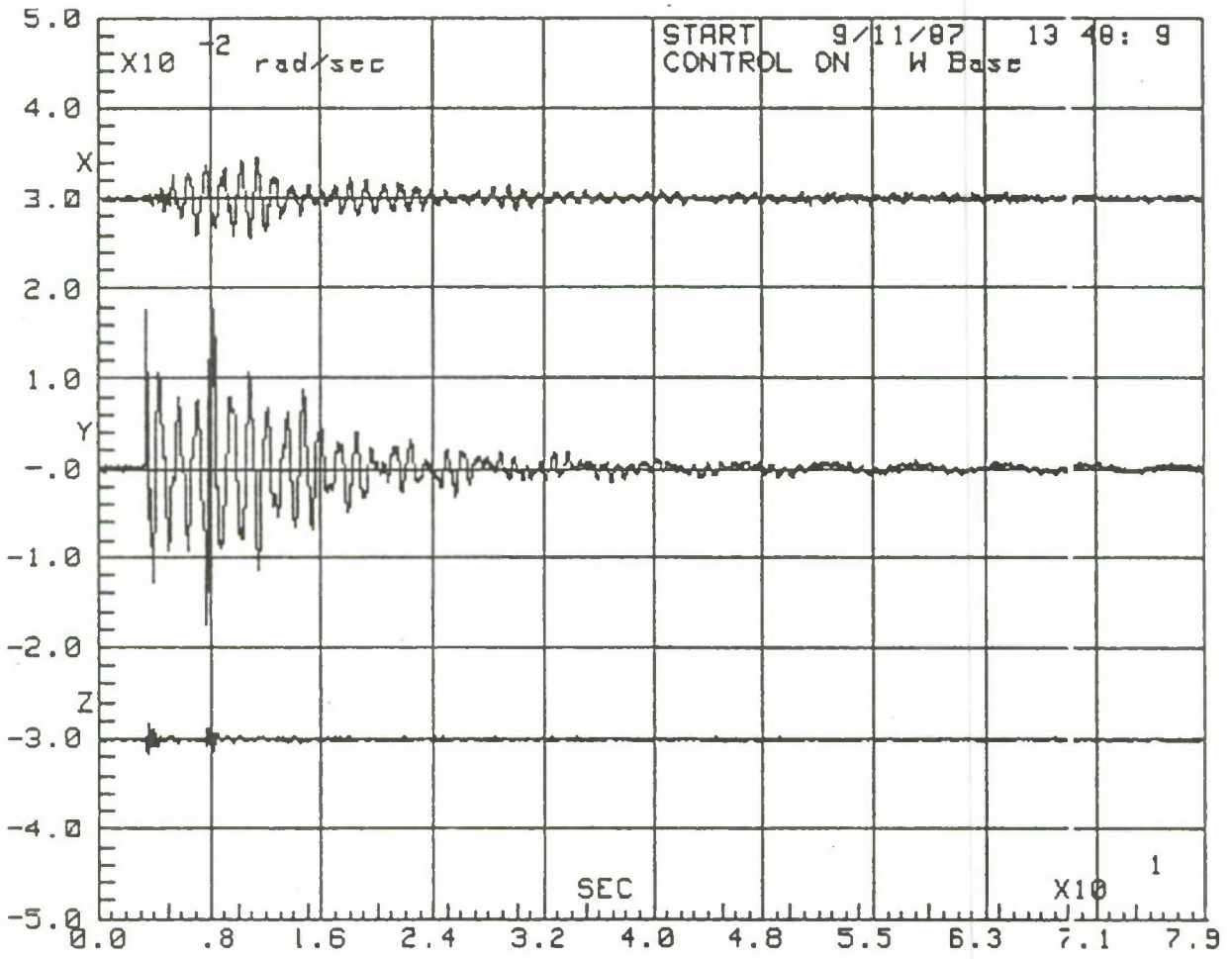


Figure 7.4-19. Closed Loop Gyro Response Due to the Demonstration Disturbance.

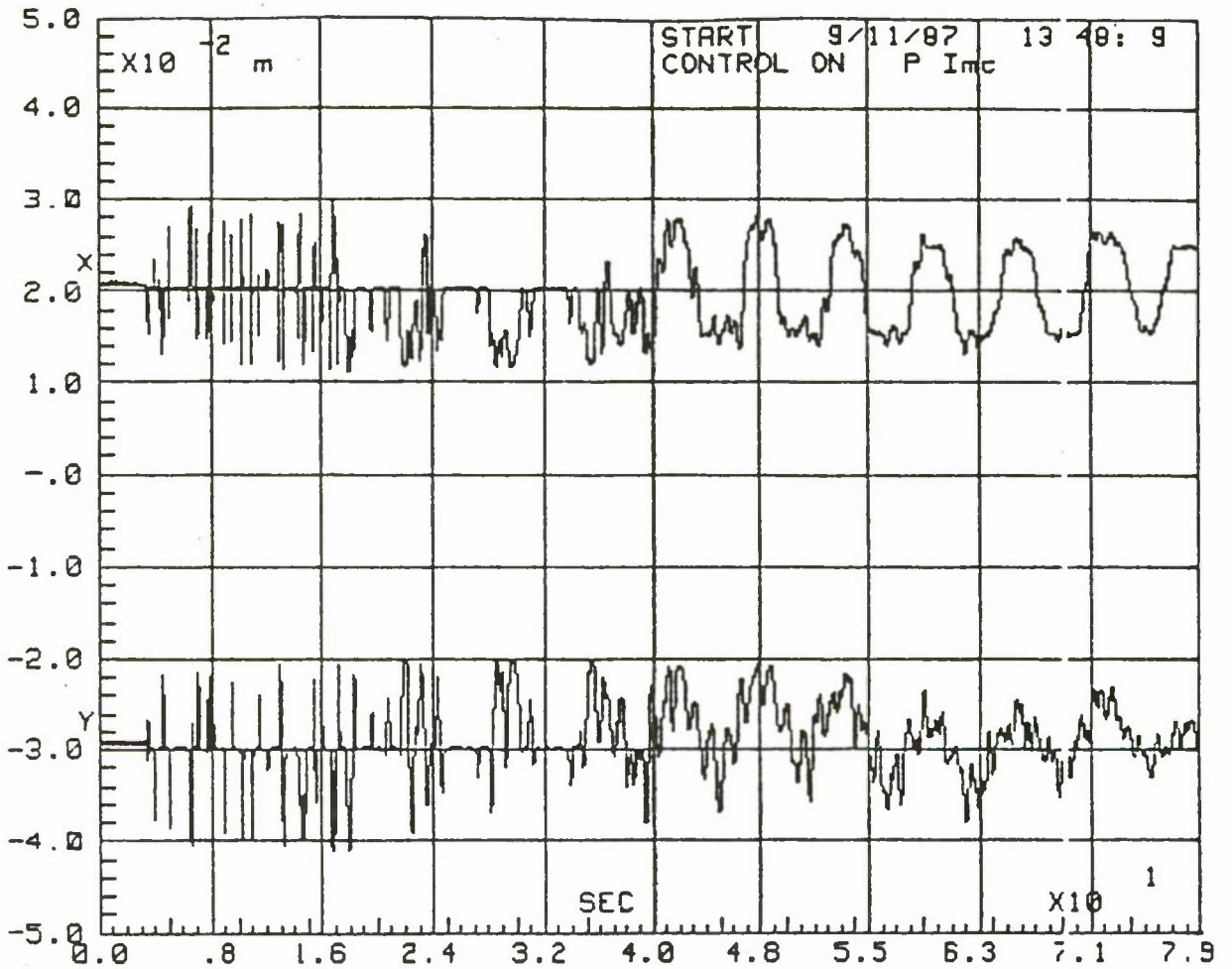


Figure 7.4-20. Closed Loop Detector Response Due to the Demonstration Disturbance.

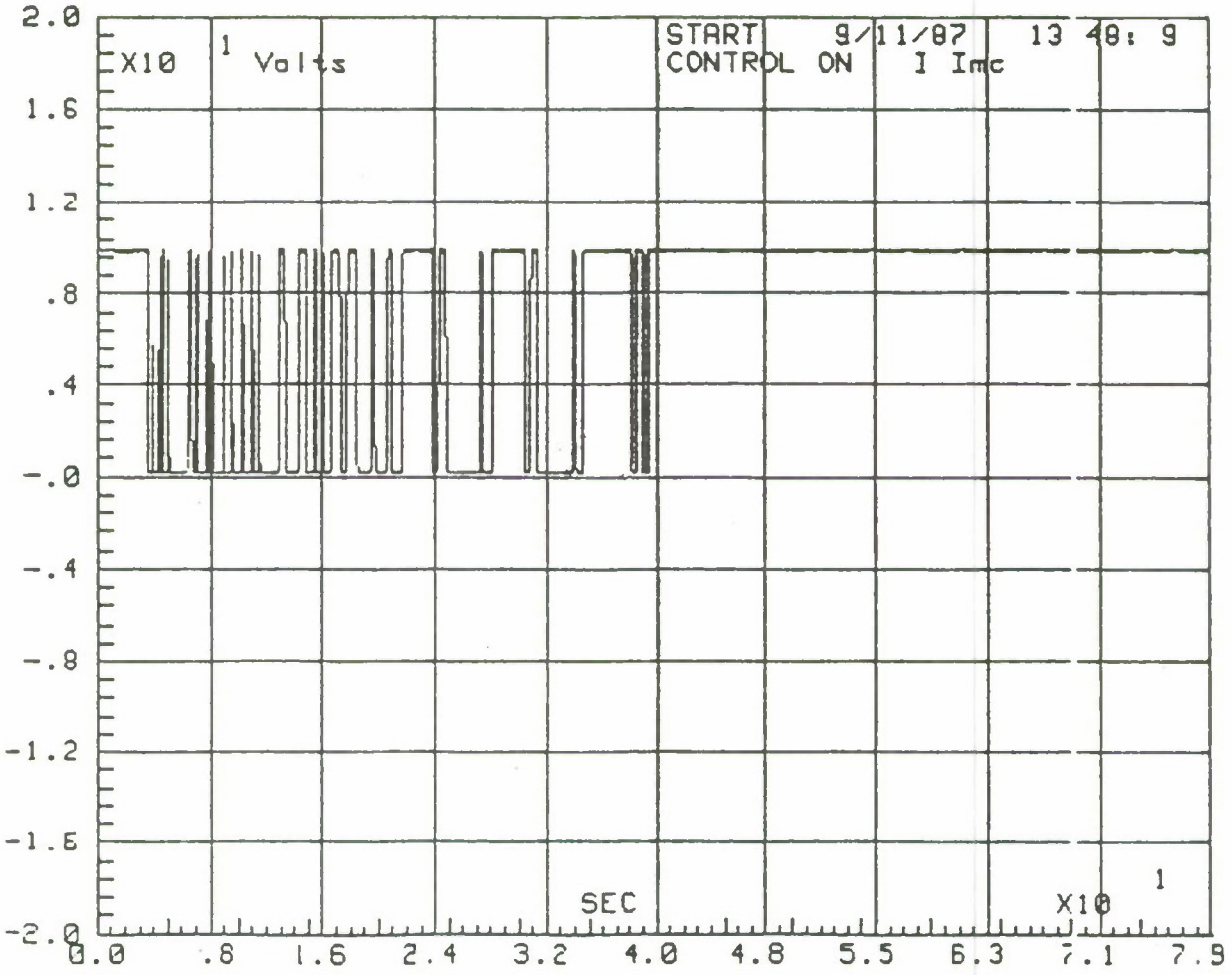


Figure 7.4-21. Closed Loop Laser Beam Presence Due to the Demonstration Disturbance.

7.5 Conclusions.

Many observations can be made regarding the FAMESS theory, its application to the ACES configuration, and the results of the actual testing. In almost every case, suggested improvements can be justified, either to the FAMESS design technique or to the MSFC facility hardware. The following discussion is presented in two parts: (1) observations and critical issues and (2) recommendations.

7.5.1 Observations and Critical Issues.

The observations on the application of the FAMESS design technique to the MSFC facility involves both design technique issues and facility hardware issues.

Computational Limits

As mentioned in Section 7.3, the computational limitations of the MSFC facility placed serious limitations on the achievable complexity of the FAMESS controller. While this was originally considered to be almost fatal to the evaluation of the FAMESS controller, the test results indicated that the performance limitations are not so much due to the limited-order controller as to other effects.

Unmodeled Dynamics

The most serious performance related problem encountered in this test program was the effect of unmodeled modes. Since the control design model did not contain these modes (particularly the 0.2-Hz behavior noted in Section 7.4) the designed controller provided little attenuation at the photodetectors (LOS). However, it is relevant to note that in no case was an unmodeled mode completely destabilized.

LMED Restrictions

Probably the most disappointing outcome of the design process was the discovery that the LMED pairs require gain stabilization. As discussed in Section 7.3, this was because (1) the LMEDs are coupled to a majority of the MAST

significant modes whose desirable control strategies are conflicting, (2) the LMEDs do not form approximately ideal collocated sensor/actuator pairs over the range of frequencies of interest and (3) the significant modes are extremely closely spaced at the chosen LMED locations, causing an extremely sensitive design problem. In the favor of the FAMESS technique, the LMED problem was discovered fairly early in the design process. This fact prevented a "last ditch" redesign during the test cycle. The early discovery of the problem can certainly be attributed to the model reduction inherent in the FAMESS design procedure.

Alpha Shift

The alpha shift techniques proved to be useless for the ACES design due to the drastic, but necessary, model order reduction. Alpha shift techniques are often hailed as providing guaranteed stability margins but what is seldom mentioned is the fact that this is completely false when significant model error is present. During the ACES design process, we found that the alpha shift forced undesirable spillover leading to instability and degraded performance.

Collocated Control Restrictions

Since the MESS technique contributes to the constraint of control effort in the "directions" corresponding to the suppressed modes, care should be taken to remove the suppressed mode weighting when near-perfect sensor/actuator collocation is achieved. This approach is necessary to ensure that the advantages of collocation can be realized, since spillover is not a major problem with collocated control.

Low Disturbance Levels

Problems with the resolution of the different sensors became apparent during the early stages of testing. We found that disturbance levels low enough to maintain the laser beam on the LOS detector were too small to appear significantly at the faceplate gyros. This is likely an important cause of the lack of closed loop performance improvement, since the gyro channels are essentially open loop during much of the test time interval.

Control Effort Constraints

A fundamental part of the (FA)MESS design procedure is that of constraining the control "directions" for the purpose of the suppressed modes. Clearly, this is the major advantage of FAMESS over more traditional LQG based techniques. However, for an LSS, the MESS procedure can lead to severely constrained control efforts, to the point that few of the benefits of closed loop control can be realized. Rather than an indictment of the technique, this should be considered an advantage since the inability to achieve performance improvement leads the designer to more realistic closed loop expectations and specifications.

7.5.2 Recommendations.

While it is felt that the FAMESS technique is a viable LSS control design technique and that the MSFC LSS/GTV facility is an effective control verification tool, several modifications should be made to both the facility and the FAMESS design process before a complete evaluation of the effectiveness of FAMESS can be made.

Facility Computational Capacity

Efforts are presently underway to increase the computational capacity of the LSS/GTV facility. These efforts are mainly oriented toward increasing the floating point operation capacity of the control computer. Although the completion of the present effort will significantly enhance the utility of the facility, it is believed that additional capacity will be required for future, more complex, control designs. Therefore, significant resources should be committed to ensure that the computational and data acquisition capacity of the facility accurately reflect the expected capacities of future flight hardware.

LMED Design

As pointed out in Section 7.3, a major reason for the exclusion of the LMED sensor/actuator pairs was their nonideal nature in the frequency range of interest. This was mainly due to the fact that the LMED actuators were originally designed to

operate in a frequency range above 5.0 Hz. Before the LMEDs can be predictably used in the ACES configuration they will either have to be modified to lower their 1.2 Hz characteristic frequency or relocated so that the lower frequency modes of the ACES configuration do not interact with the LMED proof mass.

Preliminary Transfer Function Testing

Due to program schedule constraints, it was not possible to perform transfer functions model verification with the full hardware complement of the ACES configuration. This situation led to the omission of the 0.2-Hz mode which is dominant at the LOS detector. We felt that due to the limitations of present structural modeling techniques, it is necessary to obtain experimental model verification to achieve significant performance improvements.

Photodetector

The disturbances possible with the ACES configuration were severely limited by the characteristics of the LOS error photodetector. Because of its quadrant construction, the linear dynamic range of the detector was limited by the bandwidth of the laser source to roughly ± 1 cm, corresponding to roughly 200 m rad. A larger detector without quadrature construction could easily increase the dynamic range by a factor of 10 with a corresponding increase in disturbance levels, leading to much greater gyro effectiveness.

8.0. MEETINGS WITH DEVELOPERS OF ACES TECHNIQUES

Introduction

On 13-16 July 1987, a trip was made to the sites of the originators of the controls techniques being assessed in the ACES Program. The primary purpose of the trip was to solicit their comments and/or criticisms. The secondary purpose was to describe the NASA/MSFC test facilities and the cooperative efforts by the USAF and NASA/MSFC.

The ACES Program personnel who participated in this trip were:

Mr. Jerome Pearson, USAF Wright Aeronautical Lab;

Capt. Robert Hunt, USAF Weapons Lab;

Dr. Henry B. Waites, NASA/MSFC;

Dr. Sherman M. Seltzer, Control Dynamics Company;

Dr. R. Dennis Irwin, Control Dynamics Company.

The sites visited were Lockheed/Palo Alto Lab (13 July), General Dynamics/San Diego (14 July), Lockheed/Sunnyvale (15 July A.M.), Lawrence Livermore National Lab (15 July P.M.) and TRW/ El Segundo (16 July).

The following agenda was followed at each site:

• Introduction	Mr. Pearson
• Description of SDIO & AFWL Participation	Capt. Hunt
• Description of NASA Participation	Dr. Waites

- ACES & DARPA/ACOSS Background — Dr. Seltzer
- Dctailcd Dcscription of ACES Techniques — Dr. Irwin
- Discussion — All

The three controls techniques under investigation within the ACES Program are termed High Authority/Low Authority Control (HAC/LAC), Filter Accommodated Model Error Sensitivity Suppression (FAMESS), and Positivity.

High Authority/Low Authority Control (HAC/LAC)

This technique results primarily from the efforts of Dr. Jean-Noel Aubrun of Lockheed Research Lab in Palo Alto, California. Dr. Aubrun approved of Control Dynamics' interpretation of HAC/LAC and the implementation approach. He rccommended considering applying "HAC" again -- after applying the "HAC/LAC" sequencc -- i.e., as an iteration. Dr. Aubrun also recommended that Control Dynamics consider using "HAC" on the NASA/MSFC Astromast as a vibration controllcr.

Filter Accommodated Model Error Sensitivity Suppression (FAMESS)

The FAMESS technique is primarily the result of Dr. John Sesak while he was with General Dynamics (hc prescntly is with Lockheed). Because of the possiblc "split" bctween the companies, the ACES Program personnel visited both.

At General Dynamics in San Diego, the team mct with Dr. Art Halc and several associatcs. When Control Dynamics stated that the implementation of FAMESS did not use the "Filter Accommodation" portion of FAMESS due to the computational constraints, he took strong exception. Dr. Hale recommended we should always use Filter Accommodation with FAMESS. Dr. Hale also stated that the design proccss should bc carried out without regard to implementation issues. Even more surprising, thc cntirc General Dynamics contingent said wc should <u>nevcr</u> design a systcm digitally. Rathcr, dcsign the systcm in the continuous domain first and then

apply Tustin's approximation to "digitize" the result. Needless to say, we were fascinated and spellbound with this design approach!

The ACES Program personnel visited Dr. Sesak (and associates) at Lockheed in Sunnyvale. Refreshingly, Dr. Sesak gave his complete approval of Control Dynamics' interpretation of FAMESS and the Control Dynamics implementation. It is interesting that Dr. Sesak has discarded "Filter Accommodation" for the same reasons as Control Dynamics. Further, Dr. Sesak strongly supports the concept of performing the original design in the digital (rather than continuous-time) domain.

Positivity

The Positivity technique is the work of Dr. Ralph Iwens at TRW/El Segundo. The ACES Program personnel met with a number of TRW controls engineers, including Doctors Iwens, Joanne Maguire, and Al Fleming. TRW would like to look at the "Alignment Matrices" to see if we can better separate the two ("AGS" and "LMED") controllers. TRW expressed curiosity concerning the robustness properties of the ACES test article. They are in agreement with the Control Dynamics implementation approach. Capt. Hunt agreed to supply TRW with descriptions of the HAC/LAC and FAMESS techniques for use in the JOSE contract.

Lawrence Livermore National Laboratory (LLNL)

The meeting with LLNL personnel was coordinated by Dr. Ray McClure. LLNL directs and evaluates new Directed Energy Weapons (DEW) Acquisition, Tracking, and Pointing (ATP) techniques for SDIO (funded through AFWL). These techniques are being studied by five universities. They are assessed by a national committee of experts (Capt. Hunt and Dr. Seltzer are members). It appears that the controls efforts at LLNL are fast disappearing. Other areas of potential common interest were discussed (oriented strongly toward Precision Engineering Program (PEP)).

Conclusions

The trip objectives were achieved i.e., the comments of the developers of the three control techniques being investigated in the ACES Program were obtained in frank and extensive discussions. With the exception of General Dynamics (whose disagreement was countered by Dr. Sesak), there was full agreement with Control Dynamics' interpretation and implementation approach.

As a result of the foregoing, Control Dynamics was directed to:

(1) proceed with the assessment of the three techniques on a high fidelity computer simulation;

(2) install the three techniques on the NASA test facility; and

(3) assess the techniques on the NASA hardware.

9.0 CONCLUSIONS

The goals of the ACES program were to design, test, and evaluate three controllers for the ACES configuration at the MSFC facility. The main evaluation criterion was the reduction of LOS error due to three specified disturbances. However, during the test cycle it became apparent that the performance benefits based on the LOS criterion alone were not sufficient to allow a definitive evaluation and comparison of the three controllers. Although the LOS results are contained in tabular form in previous sections, the evaluations contained in this section are based on qualitative considerations. Indeed, as the program progressed it became clear that the main benefit of the ACES program was its contribution to the maturity of LSS control system design in general and to the maturity of the three design techniques in particular.

The conclusions, observations, and recommendations contained in this section are organized roughly in the order that the particular issues were encountered.

9.1 Technique Theory.

Significant parts of the theory of HAC/LAC and FAMESS are contained in the literature and lore of LQG design. This background can be expected to exist in any organization undertaking the design of high performance control systems for large space structures. The major exception in the case of HAC/LAC is the low authority control portion of the technique, which is relatively easy to understand and implement. The major unique aspect of FAMESS is the filter accommodation technique.

Positivity is the least familiar of the three techniques to practicing engineers. However, its main component, the characteristic loci technique, is not difficult to comprehend once the parallels to classical scalar frequency domain techniques are outlined.

9.2 Software.

Although, strictly speaking, there is a wealth of software available for effecting the calculations necessary for each of the design "algorithms," especially the LQG portions of HAC/LAC and FAMESS, the time required to implement a software system for use in a design iteration process should not be neglected. A well tested, commercially available, and highly flexible control design software system is almost a necessity when undertaking controller designs using these three techniques. Even with the availability of such a package, some code development is mandatory; such development can be done in the package's higher level language or in more primitive languages such as Fortran.

Although each of the techniques requires some amount of software development, this task is not particularly difficult for any of the techniques when building from a good existing package. However, acquiring the capability to dependably effect these designs without such a package is a formidable task.

9.3 Model Fidelity.

Concisely stated, each of the techniques requires an excellent model in order to dependably obtain excellent performance in hardware implementation. This statement is supported in full by the results of the hardware testing. The 0.2-Hertz unmodeled mode almost completely invalidates the planned quantitative LOS evaluation criterion since (1) the LOS error is predominantly due to this mode and (2) none of the three controllers significantly improved its behavior. Unmodeled low frequency modes are especially hazardous because they typically lie within the controller bandwidth and are thereby prime candidates for spillover destabilization.

9.4 Technique Applicability.

Each of the three techniques is capable of yielding controller designs for high order systems. FAMESS appears to be the most general of the techniques, although filter accommodation can lead to extremely high order controllers. HAC/LAC suffers

from no outstanding limitations except that the LAC design requires collocation for at least some of the sensors and actuators. An undesirable situation may present itself if the spillover modes that LAC is intended to stabilize are not observable and/or controllable via the LAC hardware. This situation did not occur during the ACES program. Positivity is appropriate for certain high order systems but may not be suitable for lightly damped systems such as large space structures due to possible problems with frame alignment. However, the characteristic loci methods should not be ruled out as a design option until, and unless, the alignment problems are investigated more systematically.

9.5 Design Process Complexity.

With a suitable software system in place for each of these techniques, the design process is not unduly difficult or tedious. None of the techniques yields a satisfactory controller without a significant amount of iteration, as should be expected when working with very complex systems. The weighting matrix schemes used in FAMESS should probably be used also in HAC/LAC designs since those schemes systematize the design iteration process.

9.6 Hardware Limitations.

The limited dynamic range of the photodetector is the most critical hardware issue in regard to the achievable performance of the control systems. In order for the photodetector operation to be kept within its linear range, disturbances are so small that other instruments operate at or below their resolution threshold. The obvious solution to the detector problem is to use a photodetector with a much greater dynamic range.

The LMEDS are a problem for which no easy solution exists. The presence of gravity dictates the use of proof-mass centering springs, which limit the low frequency characteristics of the LMEDs as force actuators. In the case of the ACES configuration, the springs probably cannot be softened without eliminating the centering action.

9.7 Summary.

Each of the design techniques can be used to design controllers for large space structures which prevent destabilization of unmodeled modes. However, the prevention of destabilization is much easier to achieve than the realization of high performance. This fact is quantifiable in terms of a tradeoff between achievable performance and "robustness" and leads to the sensible conclusion that control designers faced with achieving stringent performance specifications must in turn be able to specify acceptable tolerances on model error or accept more realistic performance.

Software is a nontrivial aspect as regards the amount of effort required to use these design techniques. Although the component parts of the software required to effect the actual detailed calculations may exist beforehand, the truly important aspect of the software question is the time required to gather these components into a flexible and easily used design system.

The applicability of the three techniques to high order control system design is unquestionable. However, the applicability of positivity and characteristic loci to the more particular case of large space structure control is unresolved. It should be noted that this conclusion may be highly dependent on the particular algorithms and approaches used in applying characteristic loci to the ACES problem.

Of the three techniques, FAMESS appears to be the most systematic and dependable and possesses more of the representative characteristics of an algorithm rather than a technique in the intermediate stages of development. Again, this conclusion is user and application dependent.

REFERENCES

[1] Aubrun, Jean N., et al, ACOSS Five (Active Control of Space Structures) Phase 1A, LMSC-D811889 under ARPA Order 3654, March 1982.

[2] Aubrun, J. N., and Margulies G., Low Authority Control Synthesis for Large Space Structures, NASA Contractor Report 3495, Langley Research Center, Va., September 1982.

[3] Benhabib, Robert J., et al, ACOSS Fourteen (Active Control of Space Structures), RADC-TR-83-51, Rome Air Development Center, Griffiss Air Force Base, NY, March 1983.

[4] Sesak, John R., ACOSS Seven (Active Control of Space Structures), RADC-TR-81-241, Rome Air Development Center, Griffiss Air Force Base, NY, September 1981.

Acronyms

ACES	=	Active Control Technique Evaluation for Spacccraft
ACOSS	=	Active Control of Space Structures
AFWAL	=	Air Force Wright Aeronautical Laboratories
AFWL	=	Air Force Weapons Laboratory
AGS	=	Advanced Gimbal System
ARE	=	Algebraic Riccati Equation
ASCOT	=	Advanced Structural Control Techniques
ATM	=	Apollo Telescope Mount
BET	=	Base Excitation Table
CL	=	Closed Loop
CPU	=	Central Processor Unit
DARPA	=	Defense Advanced Research Projects Agcncy
DOD	=	Department of Defense
DOF	=	Degrees of Freedom
FA	=	Filter Accommodation
FAMESS	=	Filter Accommodated Model Error Sensitivity Suppression
FEM	=	Finite Element Modcl
GTF	=	Ground Test Facility
HAC/LAC	=	High Authority Control/Low Authority Control
HPIB	=	Hewlett Packard Interface Bus
IMC	=	Image Motion Compensation
IMCS	=	Image Motion Compensation System
I/O	=	Input/Output
JPL	=	Jet Propulsion Lab
KARS	=	Kearfott Attitude Reference Systcm
LLNL	=	Lawrence Livermore National Laboratory
LMED	=	Linear Momentum Exchange Device
LOS	=	Line Of Sight
LQG	=	Linear Quadratic Gaussian
LQR	=	Linear Quadratic Regulator
LSS	=	Large Space Structures
LSS GTF	=	Large Space Structures Ground Test Facility
LTA	=	Load Test Anncx
LVDT	=	Linear Variable Displacement Transducer

MESS	=	Model Error Sensitivity Suppression
MIMO	=	Multi-Input Multi-Output
MSFC	=	Marshall Space Flight Center
NASA	=	National Aeronautics and Space Administration
OL	=	Open Loop
PI	=	Performance Index
PSD	=	Power Spectral Density
RADC	=	Rome Air Development Center
RCS	=	Reaction Control System
RMS	=	Root Mean Square
RSS	=	Root Sum Square
S/A	=	Sensor/Actuator
SD	=	Standard Deviation
SDIO	=	Strategic Defense Initiative Office
SNR	=	Signal-to-Noise Ratio
TF	=	Transfer Function
VCOSS	=	Vibration Control Of Space Structures
ZOH	=	Zero Order Hold